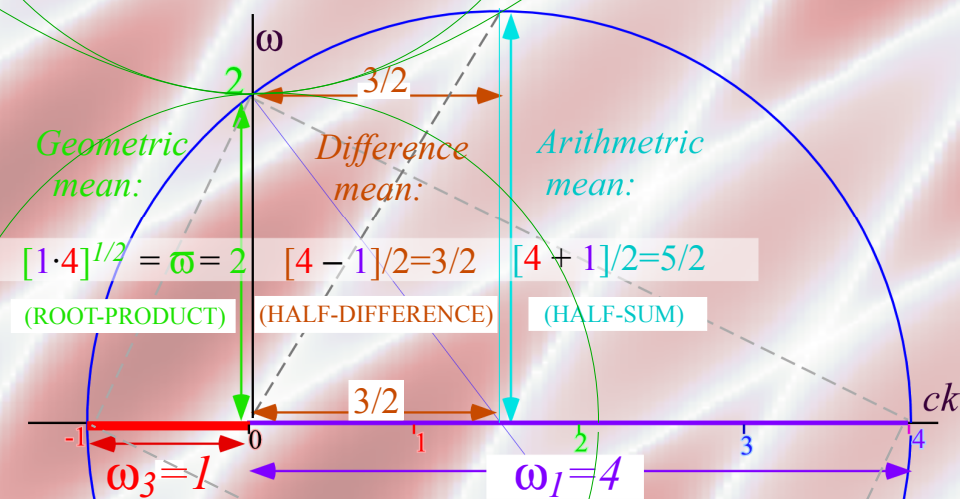# MODERN PHYSICS

and its

Classical Foundations

A Geometric Introduction to Analysis
of
Quantum Momentum, Energy, and Action

Unit 2. Relativity and Quantum Theory

Geometric mean:

Difference mean:

Arithmetic mean:

$$[1 \cdot 4]^{1/2} = \varpi = 2 \qquad [4-1]/2 = 3/2 \qquad [4+1]/2 = 5/2$$

(ROOT-PRODUCT)   (HALF-DIFFERENCE)   (HALF-SUM)
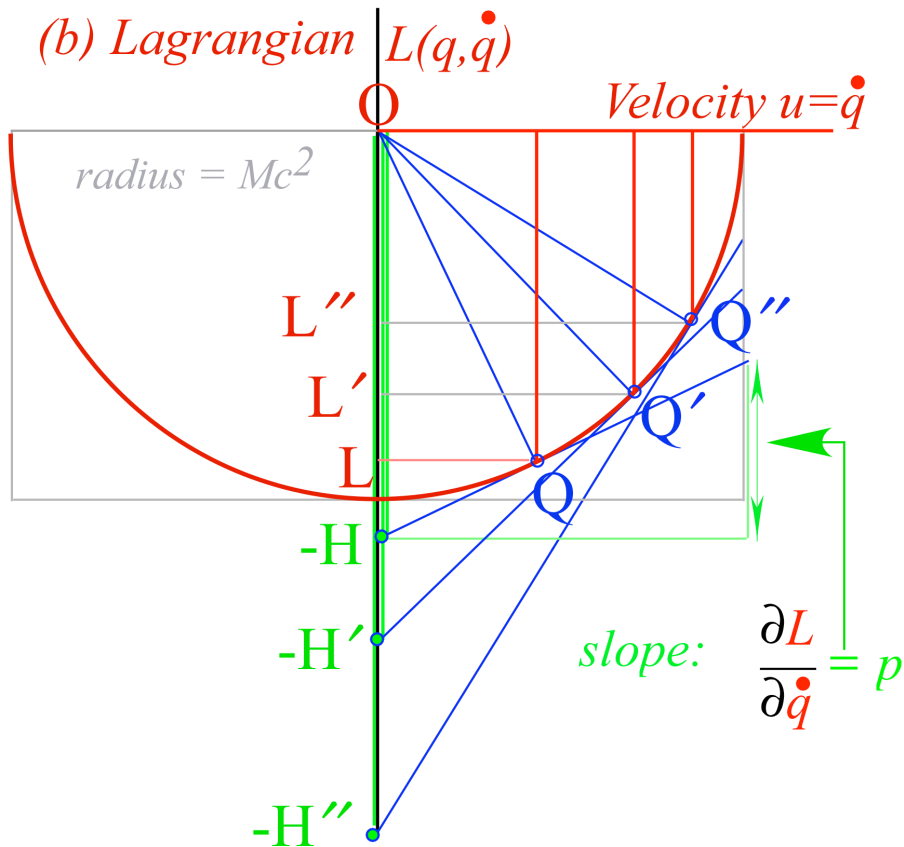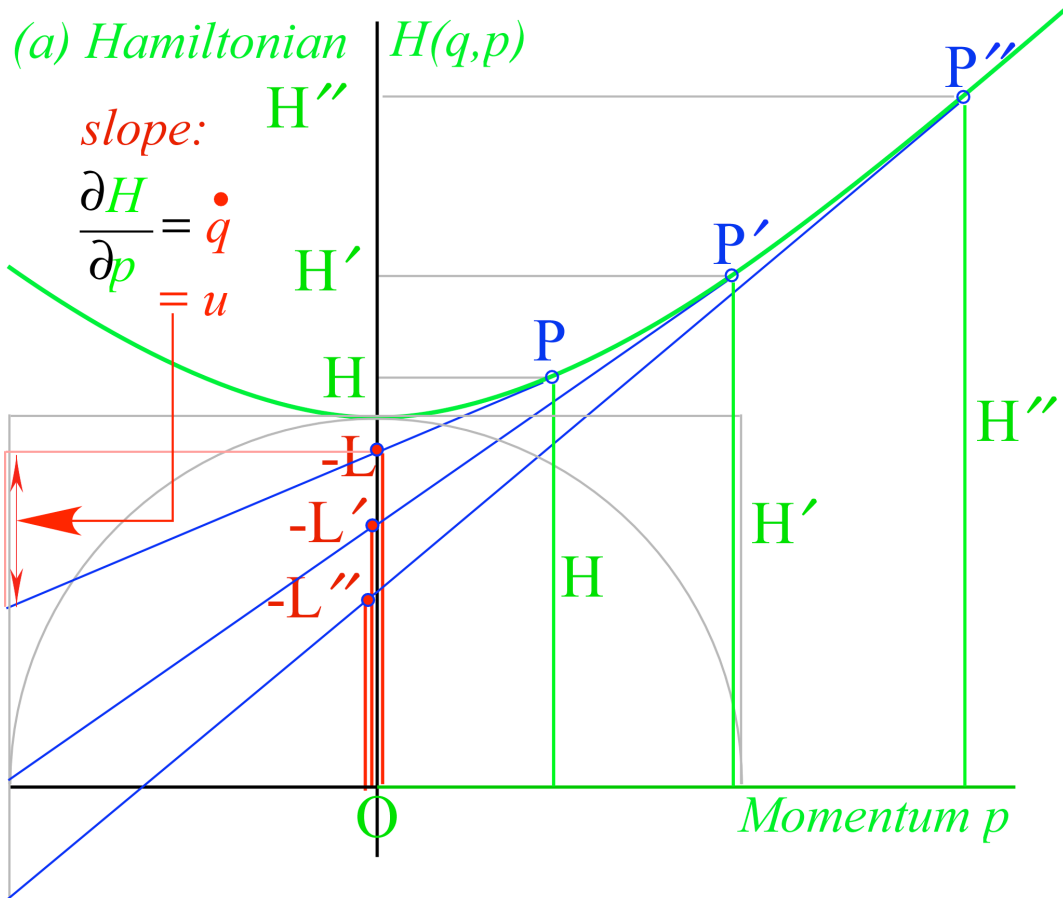
$\omega_3 = 1$

$\omega_1 = 4$

Department of Physics - University of Arkansas - Fayetteville

Hardware and Software by

HARTER *-Soft*

Elegant Educational Tools Since 2001

(a) Hamiltonian $H(q,p)$

H″

slope:

$$\frac{\partial H}{\partial p} = \dot{q}$$
$$= u$$

H′

H

P″

P′

P

-L

-L′

-L″

H″

H′

H

O   Momentum p

(b) Lagrangian $L(q,\dot{q})$

O   Velocity u=$\dot{q}$

radius = Mc^2

L″

L′

L

Q″

Q′

Q

-H

-H′

slope: $\frac{\partial L}{\partial \dot{q}} = p$

-H″

Legendre contact transformation for relativistic mechanics

Unit 2. Relativity and Quantum Theory

Chapter 0. Introducing phasor arrays and wave functions

In Unit 1 we reviewed classical foundations that set the stage for modern physics of *spacetime relativity* and *quantum wave mechanics* to be introduced here. We will use a wave based geometric approach in order to better understand special relativity (SR) and quantum mechanics (QM). In fact we will show that these two pillars of modern physics really belong to *the same subject*!

SR and QM have been treated in separate texts as different and even inimical subjects. (SR is most often found in E&M texts.) Advanced quantum field theory treatments do force an SR-QM unity but in a mathematical way lacking lucidity or physical intuition. The present development seeks to improve the situation at a fundamental level using detailed geometry and algebra of optical wave interference.

Plan of attack: Relativity of pairs

Our plan of attack in Unit 2 for relativity and quantum theory has similar philosophy to that of Unit 1 for classical Newtonian mechanics and Unit 3 for resonance. The idea is to develop the axioms, rules, or laws of physics using *relativity of elementary pairs*. (It's an *Occam-razor* approach!)

Unit 1 derives rules of classical mechanics using pairs of cars, super-balls, and phasors. Unit 3 uses phasor pairs again to derive rules of coupled pendulum resonance. Here in Unit 2 we use pairs of interfering light waves to derive SR-QM rules. Geometry is particularly important to lightwave-pairs since their wave *phase* is so extremely sensitive to *relative* position and velocity.

Geometry of complex ψ-clock phasor plots of oscillator functions was introduced in Fig. 1.10.5. A row of ψ-clock phasors will be used to represent a *plane lightwave function* $\psi_{k,\omega}(x,t)$.

$$\psi_{k,\omega}(x,t) = Ae^{i(k \cdot x - \omega \cdot t)} = A\cos(k \cdot x - \omega \cdot t) + iA\sin(k \cdot x - \omega \cdot t) \qquad (0.1)$$

A row of ψ-clock phasors with (k=-2) resembles a line of 12-hr clocks of world time zones in Fig. 0.1(a). A row of ψ-clock phasors with (k=-1) resembles a line of 24-hr clocks of world time zones in Fig. 0.1(b). A "Midnight wave" sweeps East-to-West around the world each day marking where clock hour-hands pass their highest point of 12:00 for 12-hr clocks or 24:00 for 24-hour clocks. 12-hour clocks reach high points twice a day, at 12:00AM (Midnight crest) and again at 12:00PM (Noon crest) as their two-crested wave moves East-to-West in Fig. 0.1(a). A wave crest has zero-phase *(k·x-ω·t=0)* so its space-time path is a line *(x=(ω/k)·t)* with slope or *phase velocity* *(c=ω/k)*. The 12-hr clock *angular frequency* is given as ω_{12}=4π/24hr=π/6 *per hr* while 24-hr clocks are half that. (ω_{24}=2π/24hr=π/12 *per hr*) The 12-hr clock *wavevector* is given as k_{12}=-2 rotations per Earth circumference (k_{12}=-2·2π/2π$R_\oplus$=-2/$R_\oplus$) while 24-hr clocks are half this. (k_{24}=-1·2π/2π$R_\oplus$=-1/$R_\oplus$) Phase velocity (ω_{24}/k_{24}=-2π$R_\oplus$/24 =ω_{12}/k_{12}) is the same for both 12hr and 24hr clocks, namely, one *clockwise(-)* Earth circumference 2π$R_\oplus$ every 24 hours.

(a) 12-hr clocks

A 12-hr world-time analogy for the ψ-clock wave function $\psi = e^{i(k \cdot x - \omega \cdot t)}$ (wavevector $k=-2$ in units of $1/R_{Earth}$)

ψ-clock wave function
$$\psi = e^{i(k \cdot x - \omega \cdot t)} = \cos(k \cdot x - \omega \cdot t) + i \sin(k \cdot x - \omega \cdot t)$$

(b) 24-hr clocks

A 24-hr world-time analogy for the ψ-clock wave function $\psi = e^{i(k \cdot x - \omega \cdot t)}$ (wavevector $k=-1$ in units of $1/R_{Earth}$)

ψ-clock wave function
$$\psi = e^{i(k \cdot x - \omega \cdot t)} = \cos(k \cdot x - \omega \cdot t) + i \sin(k \cdot x - \omega \cdot t)$$
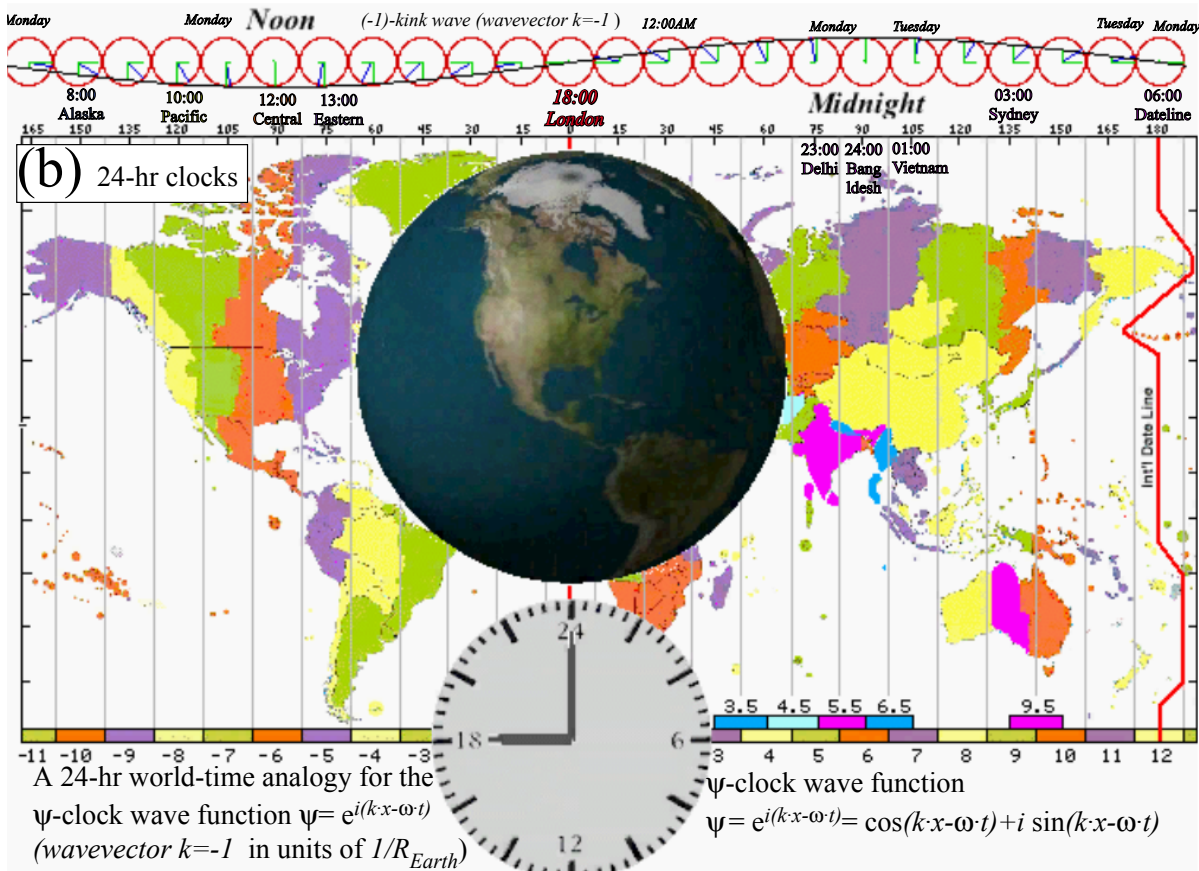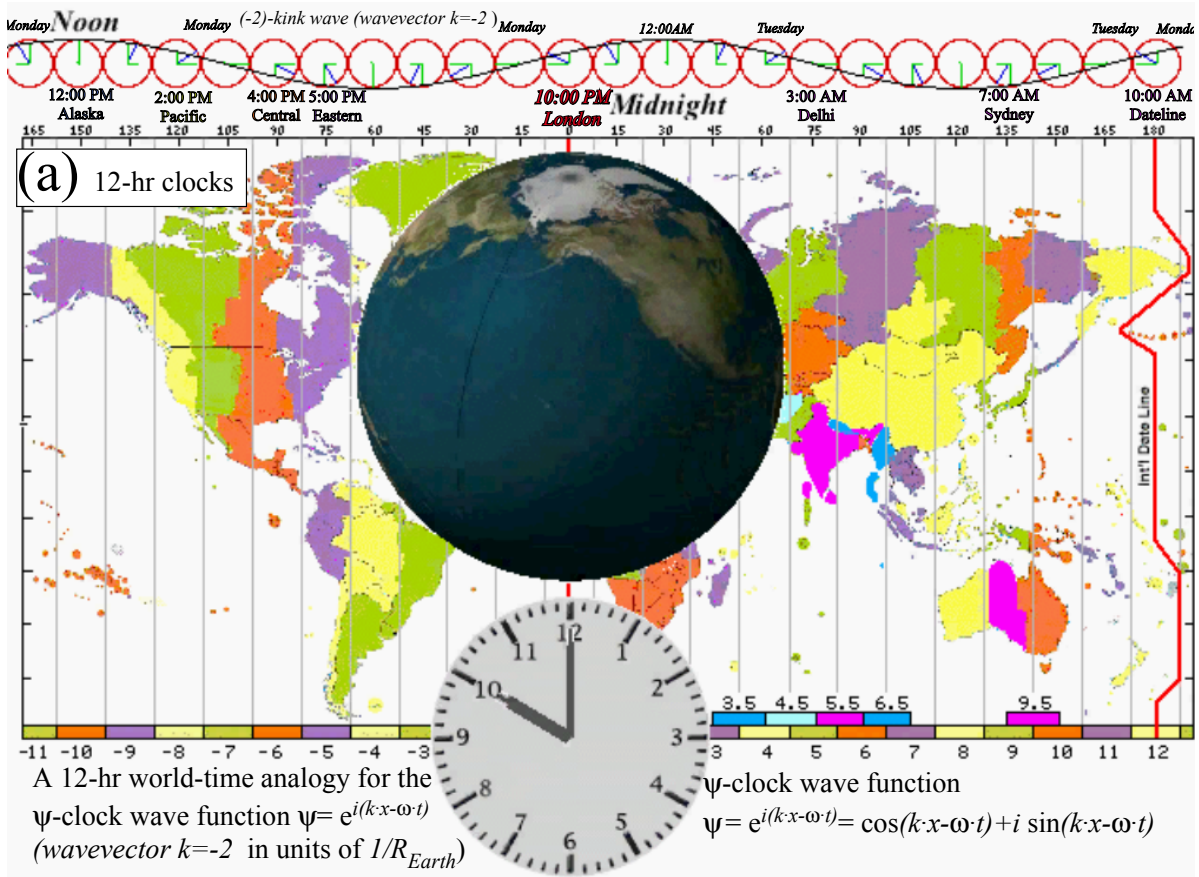
Fig. 0.1 World clocks. For animation see website: www.uark.edu/ua/pirelli/php/clocks_desc.php

Equatorial clock phase velocity is pretty fast; about *25,000 miles per day, 1,042mi/hr, or 0.3 mi/sec.* However, lightwave speed $c_\gamma=186,000mi/sec.$ or *7 Earth round trips per sec.* surely beats that. Still it's a useful analogy where 12hr and 24hr clock phase velocity ω/k, like lightspeed c_γ, doesn't vary with ω or k.

Some tricks for wave analysis

The world-clock analogy provides a familiar context for wave phasors. Still the concept of waves whiffling through fixed rows of clocks can be confusing particularly for two or more waves. Some clever bookkeeping tricks help us study complex waves and dynamics of their *(k·x-ω·t)*-phases. *Trick-1* lets waves make their own space-time *(x,ct)*-coordinates with their real zeros or "roots." *Trick-2* projects these root-coordinates into per-space-time *(ck,ω)*-coordinates of frequency vs. wavevector that are reciprocal lattices of wave-period vs. wavelength lattices in space-time. *Trick-3* factors complex sums of interfering waves to locate zeros or "root" lines. *Trick-3* makes *Trick-1* and *Trick-2* practical so we start with it.

Trick-3: Factoring a wave pair

A sum or difference of complex waves e^{ia}=cos$a$+$i$sin$a$ and e^{ib}=cos$b$+$i$sin$b$ are factored as shown below.

$$\psi_+ = e^{ia} + e^{ib}$$
$$= e^{i\frac{a+b}{2}}\left(e^{i\frac{a-b}{2}} + e^{-i\frac{a-b}{2}}\right) \quad (0.2a)$$
$$= 2e^{i\frac{a+b}{2}}\cos\frac{a-b}{2}$$

$$\psi_- = e^{ia} - e^{ib}$$
$$= e^{i\frac{a+b}{2}}\left(e^{i\frac{a-b}{2}} - e^{-i\frac{a-b}{2}}\right) \quad (0.2a)$$
$$= 2ie^{i\frac{a+b}{2}}\sin\frac{a-b}{2}$$

These hold for all phase arguments $a=(k_a x-\omega_a t)$ or $b=(k_b x-\omega_b t)$ and constituent frequency-time $\omega_{a,b}t$ and wavevector-space $k_{a,b}x$ terms. The real cosine or sine factor in (0.2) is the wave's *modulus* or *group envelope* shown by the outside envelope or "skin" in the Fig. 0.2 below. The complex exponential factor is the wave's *argument* or *phase carrier* whose amplitude is *modulated* by the group factor.
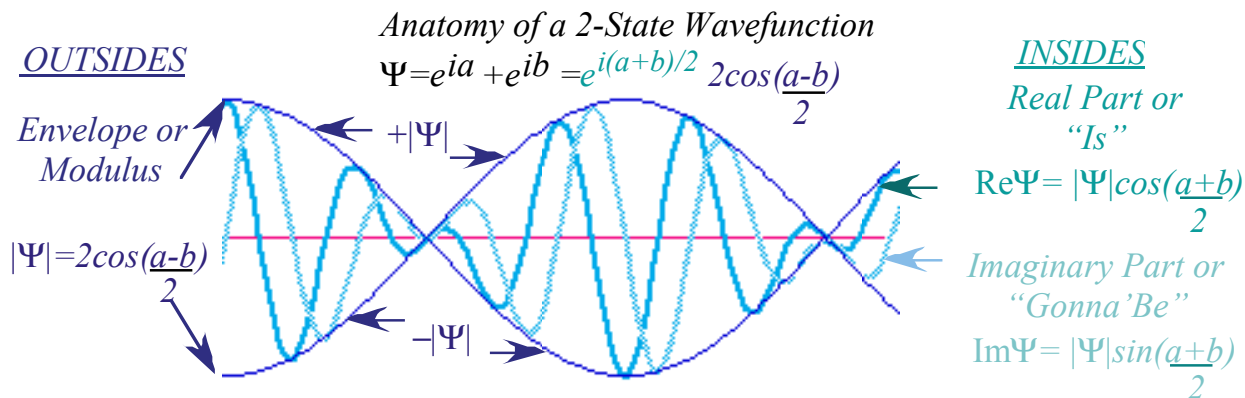
Fig. 0.2 Snapshot of sum of two waves showing group (MOD) factor enveloping phase (ARG) factor.

The group *(MOD)* factor survives in product $\psi^*\psi$ for intensity but the phase *(ARG)* part $e^{i(a+b)/2}$ of ψ cancels the $e^{-i(a+b)/2}$ of ψ^*. Intensity $|\psi|^2$ or MOD are "real survivor" functions of phase *half-difference (a-b)/2* only.

$$MOD(\psi_\pm) = |\psi_\pm| = \sqrt{\psi_\pm^*\psi_\pm} = \begin{cases} \cos\left(\dfrac{a-b}{2}\right) = \cos\left(\dfrac{k_a-k_b}{2}x - \dfrac{\omega_a-\omega_b}{2}t\right) & \text{for } \psi_+ \\[2mm] \sin\left(\dfrac{a-b}{2}\right) = \sin\left(\dfrac{k_a-k_b}{2}x - \dfrac{\omega_a-\omega_b}{2}t\right) & \text{for } \psi_- \end{cases} \qquad (0.3a)$$

Group wave speed V_{group} is the ratio ω_{group}/k_{group} of *group frequency* ω_{group} and *group wavevector* k_{group}.

$$\omega_{group} = \frac{\omega_a-\omega_b}{2} \quad (0.3b) \qquad\qquad k_{group} = \frac{k_a-k_b}{2} \quad (0.3b) \qquad\qquad V_{group} = \frac{\omega_{group}}{k_{group}} = \frac{\omega_a-\omega}{k_a-k_b} \quad (0.3c)$$

The phase *(ARG)* wave factor $e^{i(a+b)/2}$ is a function only of phase *average (a+b)/2* or *overall phase*.

$$ARG(\psi_\pm) = ATN\frac{\operatorname{Im}\psi_\pm}{\operatorname{Re}\psi_\pm} = \begin{cases} \left(\dfrac{a+b}{2}\right) = \left(\dfrac{a+b}{2}x - \dfrac{\omega_a+\omega_b}{2}t\right) & \text{for } \psi_+ \\[2mm] \left(\dfrac{a+b}{2}+\dfrac{\pi}{2}\right) = \left(\dfrac{a+b}{2}x - \dfrac{\omega_a+\omega_b}{2}t\right) & \text{for } \psi_- \end{cases} \qquad (0.4a)$$

Phase wave speed V_{phase} is the ratio ω_{phase}/k_{phase} of *phase frequency* ω_{phase} and *phase wavevector* k_{phase}.

$$\omega_{phase} = \frac{\omega_a+\omega_b}{2} \quad (0.4b) \qquad\qquad k_{phase} = \frac{k_a+k_b}{2} \quad (0.4b) \qquad\qquad V_{phase} = \frac{\omega_{phase}}{k_{phase}} = \frac{\omega_a+\omega_b}{k_a+k_b} \quad (0.4c)$$

These both govern real *(*Re ψ*)* and imaginary *(*Im ψ*)* "carrier" parts that are internal "wave guts" shown in Fig. 0.2. (One might imagine a boa constrictor having swallowed its prey live.) Internal phase "guts" may oscillate extremely rapidly and be difficult or impossible to measure directly.

   Amplitude-Modulation (*AM*) radio waves use group waves to send a *signal* riding on (or "in") the phase *carrier* wave whose frequency is assigned by the Federal Communications Commission (FCC) in the *100kHz* to *MHz* range while group signal frequency is in the audible range of 50Hz to 1kHz. Group and phase velocities would be the same speed of light value $c\sim3.0\cdot10^8 m/s.$ in a vacuum. However, both may vary considerably in the ionosphere, and thus it is possible for AM waves to reflect therefrom and be detected the world around. 100MHz FM is too fast to reflect and must rely on line-of-sight transmission.

Trick-1 Wave-zero space-time coordinate lattices
Any pair of waves whose speeds are different can be made to trace a coordinate grid or lattice in space-time using its wave function's real zeros or "roots." If the amplitudes of the pair are equal, as is the case for wave pair in (0.2a) or (0.2b), the resulting real zeros trace a pair of overlapping rows of equally spaced parallel lines that solve the following wave-zero equation based on (0.2a), (0.3a), and (0.4a).

$$0 = \operatorname{Re}\psi_+ = \operatorname{Re} e^{i\frac{a+b}{2}}\cos\frac{a-b}{2} = \cos\frac{a+b}{2}\cos\frac{a-b}{2}$$
$$= \cos\left(\frac{k_a+k_b}{2}x - \frac{\omega_a+\omega_b}{2}t\right)\cos\left(\frac{k_a-k_b}{2}x - \frac{\omega_a-\omega_b}{2}t\right) \qquad (0.5a)$$
$$= \cos\left(k_{phase}x - \omega_{phase}t\right)\cos\left(k_{group}x - \omega_{group}t\right)$$

Intersections of these lines form a lattice of space-time *(x_{m,n} , t_{m,n})*-points solving the following.

$$k_{phase}x - \omega_{phase}t = m(\pi / 2) \qquad m = \pm 1, \pm 3, ...$$
$$k_{group}x - \omega_{group}t = n(\pi / 2) \qquad n = \pm 1, \pm 3, ... \qquad (0.5b)$$

The following matrix form (0.5c) of equations (0.5b) have solutions (0.5d) for vector $\mathbf{X}_{m,n} = (x_{m,n}, t_{m,n})$.

$$\begin{pmatrix} k_{phase} & -\omega_{phase} \\ k_{group} & -\omega_{group} \end{pmatrix}\begin{pmatrix} x \\ t \end{pmatrix} = \begin{pmatrix} m \\ n \end{pmatrix}\frac{\pi}{2} \quad (0.5c) \qquad \begin{pmatrix} x_{m,n} \\ t_{m,n} \end{pmatrix} = \frac{\begin{pmatrix} \omega_{group} & -\omega_{phase} \\ k_{group} & -k_{phase} \end{pmatrix}}{\left| \omega_{group}k_{phase} - \omega_{phase}k_{group} \right|}\begin{pmatrix} m \\ n \end{pmatrix}\frac{\pi}{2} \quad (0.5d)$$

Space-time vector notation provides a convenient way to display results in (0.5e) and figures below.

$$\begin{pmatrix} x_{m,n} \\ t_{m,n} \end{pmatrix} = \mathbf{X}_{m,n} = \left[m\mathbf{K}_{group} - n\mathbf{K}_{phase} \right]s_{gp} \text{ where: } s_{gp} = \frac{\pi}{2\left| \mathbf{K}_{group} \times \mathbf{K}_{phase} \right|} \qquad (0.5e)$$

Base vectors of $\mathbf{X}_{m,n}$ space-time lattice are $\mathbf{X}_{1,0} = \mathbf{K}_{group}$ and $\mathbf{X}_{0,-1} = \mathbf{K}_{phase}$ below with scale factor s_{gp}.

$$\mathbf{K}_{group} = \begin{pmatrix} \omega_{group} \\ k_{group} \end{pmatrix} = \begin{pmatrix} \dfrac{\omega_a - \omega_b}{2} \\ \dfrac{k_a - k_b}{2} \end{pmatrix} = \frac{\mathbf{K}_a - \mathbf{K}_b}{2} \ (0.5f) \qquad \mathbf{K}_{phase} = \begin{pmatrix} \omega_{phase} \\ k_{phase} \end{pmatrix} = \begin{pmatrix} \dfrac{\omega_a + \omega_b}{2} \\ \dfrac{k_a + k_b}{2} \end{pmatrix} = \frac{\mathbf{K}_a + \mathbf{K}_b}{2} \ (0.5g)$$

These relate to source vectors $\mathbf{K}_a$ and $\mathbf{K}_b$ of frequency-wavevector (ω_a, k_a) and (ω_b, k_b) of waves e^{ia} and e^{ib}.

$$\mathbf{K}_a = \begin{pmatrix} \omega_a \\ k_a \end{pmatrix} = \mathbf{K}_{group} + \mathbf{K}_{phase} \qquad (0.5h) \qquad\qquad \mathbf{K}_b = \begin{pmatrix} \omega_b \\ k_b \end{pmatrix} = \mathbf{K}_{group} - \mathbf{K}_{phase} \qquad (0.5i)$$

labels: $e^{ia} = e^{i(k_a x - \omega_a t)}$ $\qquad\qquad\qquad\qquad\qquad$ labels: $e^{ib} = e^{i(k_b x - \omega_b t)}$

Trick-2 Per-space-time coordinate lattices:"The keyboard of the gods"

The concept of frequency is innate to life. It begins with piscean, amphibian, avian, or mammalian mating calls that preceded the music that humans now so enjoy. It is wonderful to make a note, say mid-**A**, by just pressing a keyboard button and not have to actually wiggle something at 440Hz. That is the idea of the *per-space-time coordinates* $(\omega_{m,n}, k_{m,n})$ that **K**-vectors (0.5f-i) occupy.

However, we are asking for a 2-dimensional "keyboard of the gods" that lets you choose the frequency ω *and* the wavevector k or wavelength $\lambda = 2\pi/k$ with a single (ω, k)-key in per-space-time. You can then pick frequency *and* wave velocity ω/k. Pretty tall order, but then that's what we have gods for!

The (ω, k)-per-space-time keyboard is like a control panel for wave motion in (x, t)-space-time and serves as an introduction to Fourier space. For example, let two "mythical" source waves shown in the lower right of Fig. 0.3 be labeled by the following primitive $\mathbf{K}_a$ and $\mathbf{K}_b$-vectors.

$$\mathbf{K}_4 = \begin{pmatrix} \omega_4 \\ k_4 \end{pmatrix} = \begin{pmatrix} 4 \\ 4 \end{pmatrix} \qquad (0.5h)_{example} \qquad\qquad \mathbf{K}_2 = \begin{pmatrix} \omega_2 \\ k_2 \end{pmatrix} = \begin{pmatrix} 1 \\ 2 \end{pmatrix} \qquad (0.5i)_{example}$$

labels: $e^{ia} = e^{i(4 \cdot x - 4 \cdot t)}$ $\qquad\qquad\qquad\qquad\qquad$ labels: $e^{ib} = e^{i(2 \cdot x - 1 \cdot t)}$

This gives the following group and phase vectors using (0.5f-g).

$$\mathbf{K}_{group} = \begin{pmatrix} \omega_{group} \\ k_{group} \end{pmatrix} = \begin{pmatrix} (4-1)/2 = 1.5 \\ (4-2)/2 = 1.0 \end{pmatrix} = \frac{\mathbf{K}_4 - \mathbf{K}_2}{2} \qquad \mathbf{K}_{phase} = \begin{pmatrix} \omega_{phase} \\ k_{phase} \end{pmatrix} = \begin{pmatrix} (4+1)/2 = 2.5 \\ (4+2)/2 = 3.0 \end{pmatrix} = \frac{\mathbf{K}_4 + \mathbf{K}_2}{2} \ (0.5g)$$

$$(0.5f)_{example} \qquad\qquad\qquad\qquad\qquad\qquad\qquad (0.5g)_{example}$$

(a) Spacetime (x,t)

(b) Per-spacetime (ω,k)

Wave phase zero-paths

Wave phase vectors

Time t

Wave group vectors

Wavevector k

$K_{group} = (K_4 - K_2)/2$

$K_{phase} = (2.5, 3.0)$

K_4

$K_{phase} = (K_4 + K_2)/2$

K_2

Wave group node-paths

$K_{group} = (1.5, 1.0)$

$K_{group} = (1.5, 1.0)$

Space x

Frequency ω

CW lattice

PW lattice

K_{phase}

K_{group}

K_4

K_2

K_2

$K_2 = (ω_2, k_2)$
$= (1, 2)$

source 2

source 4

$K_4 = (ω_4, k_4)$
$= (4, 4)$
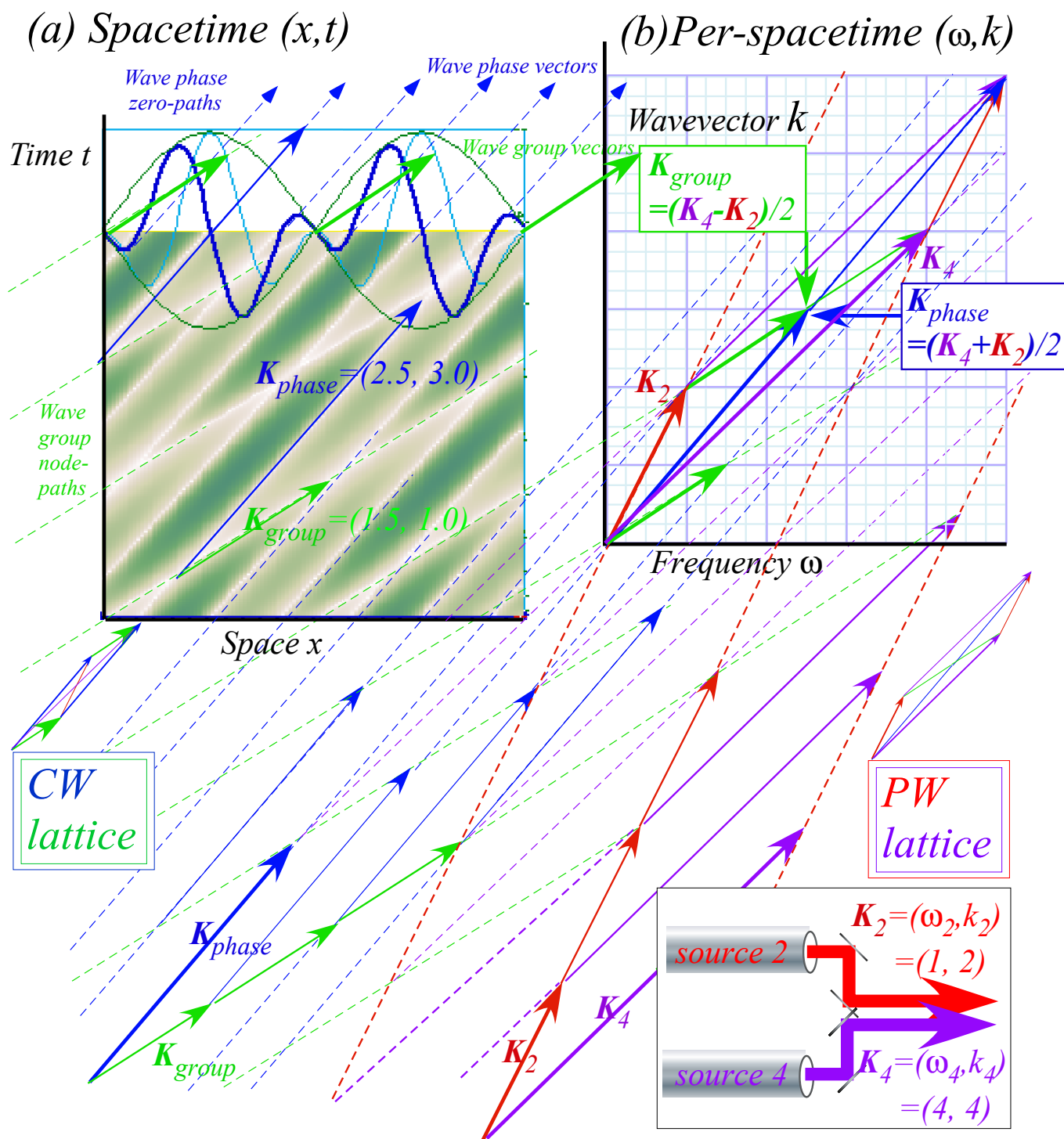
Fig. 0.3 "Mythical" sources and their wave coordinate lattices in (a) Spacetime and (b) Per-spacetime.
CW lattices of phase-zero and group-node paths intermesh with PW lattices of pulse, packet, or "particle" paths.

A simulation in Fig. 0.3a of the wave sum shows a grid of white lines traced by wave zeros accented at the top by blue arrows for six phase zeros and three green arrows at the zeros or nodes of the two group envelopes. All move to the right at speeds $V_{phase} = 2.5/3.0 = 0.83$ and $V_{group} = 1.5/1.0$, respectively, along the vectors $K_{phase} = (2.5, 3.0)$ and $K_{group} = (1.5, 1.0)$ that frame zero-line parallelogram cells in Fig. 0.3a.

Space-time (Fig. 0.3a) and per-space-time (Fig. 0.3b) match by scale factor $s_{gp} =\pi/4=0.785$ so $\mathbf{K}_{phase}$ and $\mathbf{K}_{group}$ define space-time wave-zero paths. Note that origin is shifted by $-\pi/4$ so the grid spacing is $\pi/2$. Scale s_{gp} is inversely proportional to zero-line parallelogram cell area $|\mathbf{K}_{phase} \times \mathbf{K}_{group}|$.

$$s_{gp}=\frac{\pi}{2\left|\mathbf{K}_{group}\times\mathbf{K}_{phase}\right|}=\frac{\pi}{2\left|\omega_{group}k_{phase}-\omega_{phase}k_{group}\right|}=\frac{\pi}{2\left|1.5\cdot3.0-2.5\cdot1.0\right|}=\frac{\pi}{4} \qquad (0.6a)$$

Fig. 0.4a-b relates wave length $\lambda=2\pi/k$ and period $\tau=2\pi/\omega$ to per-space-time $k=2\pi/\lambda$ and $\omega=2\pi/\tau$.

$(\lambda_{phase}=2\pi/3.0=2.09, \tau_{phase}=2\pi/2.5=2.51$)   (0.6b)   ($\lambda_{group}=2\pi/1.0=6.28$, $\tau_{group}=2\pi/1.5=4.18$) (0.6c)

Fig. 0.4c-d relates space-time (λ_4,τ_4) or (λ_2,τ_2) of input sources to reciprocal values (k_4,ω_4) or (k_2,ω_2).

$(\lambda_4=2\pi/4=1.57,$ $\tau_4=2\pi/4=1.57$)   (0.6d)   ($\lambda_2=2\pi/2=3.14$, $\tau_2=2\pi/1=6.28$)   (0.6e)

The scale factor s_{42} for the source *(4±2)*-wave sum is half the s_{gp} for their *(group·phase)*-products.

$$s_{42}=\frac{\pi}{2\left|\mathbf{K}_4\times\mathbf{K}_2\right|}=\frac{\pi}{2\left|\omega_4 k_2-\omega_2 k_4\right|}=\frac{\pi}{2\left|4\cdot2-1\cdot4\right|}=\frac{\pi}{8} \qquad (06.f)$$

The primitive source cell area $|\mathbf{K}_4 \times \mathbf{K}_2|$ is twice that of the cell area $|\mathbf{K}_{group} \times \mathbf{K}_{phase}|$ for product waves. This reflects a profound distinction between behavior of waves that are the result of interference effects and that of the primitive wave components before they get together.

Newton's corpuscles vs. wave interference: PW vs CW

One may take a classical view of K_2 and K_4 paths in Fig. 0.3 or Fig. 0.4c-d as tracks of pulse waves (PW) or wave packets (WP) that are more like particles than waves. Newton took a hard-line view of nature and ascribed reality to "corpuscles" but viewed waves as "illusory." He misunderstood optical interference phenomena and complained that it showed particles or "corpuscles" having "fits."

Newtons corpuscular views are parodied here by imagining that frequency $\upsilon_2=\omega_2/2\pi$ (or $\upsilon_4=\omega_4/2\pi$) is the rate at which source-2 (or 4) emits "corpuscles" of velocity $c_2=\omega_2/k_2$ (or $c_4=\omega_4/k_4$). It will be shown that PW peaks are a full wavelength $\lambda_2=2\pi/k_2$ (or $\lambda_4=2\pi/k_4$) apart while continuous wave (CW) crests and troughs have half-wavelength $\lambda_2/2=\pi/k_2$ (or $\lambda_4/2=\pi/k_4$) spacing as indicated at the bottom of Fig. 0.4. One can imagine PW "corpuscle paths" on alternating K_2 (or K_4) lines in Fig. 0.4c-d separated by a full wavelength λ_2 (or λ_4) in Fig. 0.4c-d.

The K_2 and K_4 paths are *diagonals* of the $\mathbf{K}_{group}(\mathbf{K}_{phase})$ wave-zero lattice in time *vs* space *(t,x)* in Fig. 0.4b that is identical, except for scale, with the per-space-time wavevector *vs* frequency space *(k,ω)* in Fig. 0.4a. As seen in Fig. 0.3a and Fig. 0.4a-b, the $\mathbf{K}_{group}$(or $\mathbf{K}_{phase}$) wave-zero paths are separated by half wavelengths $\lambda_{group}/2=\pi/1.0=3.14$ (or $\lambda_{phase}/2=\pi/3.0=1.05$). Unlike PW or "corpuscle" paths, the CW zero-paths are phase interference effects of wave "zig-zag" that appear at phase *0* and π-modulo *2π*.

In order that space-time *(x,t)*-plots can be superimposed on frequency-wavevector *(ω,k)*-plots, it is necessary to switch axes for one of them. The space-time *t(x)*-plots in Fig. 0.3a follow the *Minkowski convention* for a vertical time ordinate *(t-axis)* and horizontal space abscissa *(x-axis)*. That's opposite to Newtonian calculus texts that plot *x(t)*. However, the frequency-wavevector *k(ω)*-plots in Fig. 0.3a switch

axes with standard ω(k) convention so that *t(x)* slope due to space-time velocity *x/t* or *Δx/Δt (meter/second)*
in Fig. 0.4b equals per-time-per-space wave velocity ω*/k (per-second/per-meter)* in Fig. 0.4a.
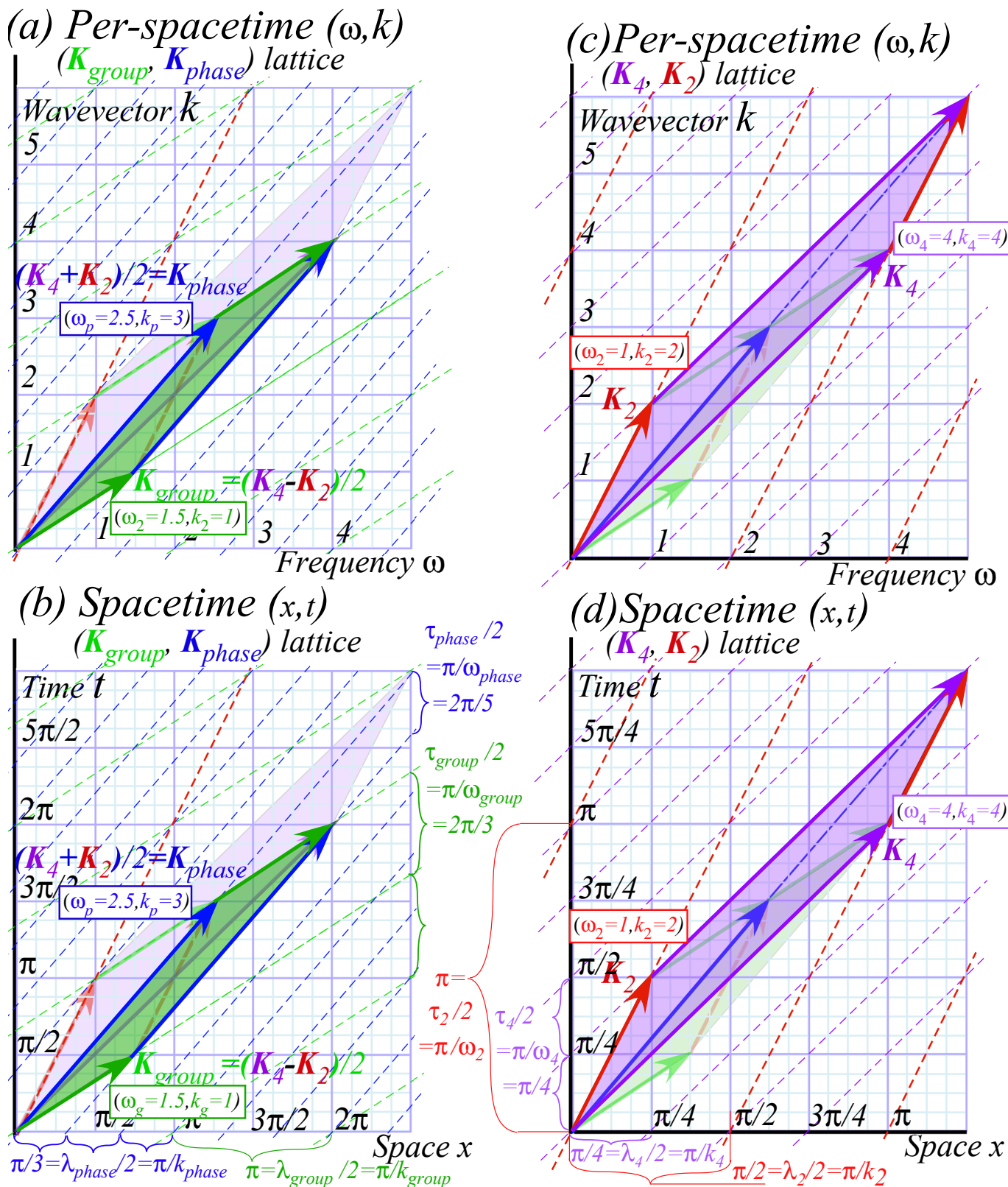
*Fig. 0.4 Comparing phase-group Continuous Wave (CW) lattice motion described in (a) Per-Spacetime and (b) Spacetime with
the corresponding primitive Pulse Wave (PW) lattice motion described in (a) Per-Spacetime and (b) Spacetime.*

This development shows wave-particle, wave-pulse, and CW-PW duality in the cells of each CW-PW wave lattice. Each (K_2 , K_4)-cell of a PW lattice has a CW vector $2P=2K_{phase}$ or $2G=2K_{group}$ on each diagonal, and each (P,G)-cell of the CW lattice has a PW vector K_2 or K_4 on each diagonal. This is due to sum and difference relations (0.5f-i) between (P,G)=(K_{phase}, K_{group}) and (K_2, K_4).

Superimposing *t(x)*-plots onto *k(ω)*-plots also requires that the latter be rescaled by the scale factor s_{gp} derived in (0.5e), but rescaling fails if cell-area determinant factor *D* is zero.

$$D = \omega_p k_g - \omega_g k_p = \left| \mathbf{K}_{phase} \times \mathbf{K}_{group} \right| \tag{0.7}$$

Co-propagating light beams $K_2 = (\omega_2, k_2)=(2c,2)$ and $K_4 = (\omega_4, k_4)=(4c,4)$ in Fig. 0.5b have *D=0* since all K-vectors including $\mathbf{K}_{phase}=(\omega_p, k_p)=(3c,3)$ and $\mathbf{K}_{group}= (\omega_g, k_g)=(c,1)$ lie on one *c*-baseline of speed *c* that has unit slope *(ω/ck=1)* if we rescale *(ω,k)*-plots to *(ω,ck)* and *(x,t)*-plots to *(x,ct)*.

In summary, *co-propagating* light waves absolutely fail to make coordinate grids! However, *counter-propagating* (right-left) light waves are another "matter" altogether. In Ch. 2 *counter-propagating* (right-left) light wave vectors ($\mathbf{R}$,$\mathbf{L}$)= (K_2,-K_4) are used to make CW bases (P= K_{phase}, G= K_{group}) with a non-zero value for area *D* =|$\mathbf{G}$x$\mathbf{P}$ |. Opposing PW base vectors are sum and difference ($\mathbf{R}$,$\mathbf{L}$)=(P +G, P-G) of CW bases so a PW cell area |$\mathbf{R}$x$\mathbf{L}$| is twice that of CW cell |$\mathbf{G}$x$\mathbf{P}$ |.

$$|\mathbf{R}x\mathbf{L}|= |(\mathbf{P}+\mathbf{G}) \text{ x } (\mathbf{P}-\mathbf{G})|=2|\mathbf{G}x\mathbf{P} | \tag{0.8}$$

Wave cell areas due to colliding CW are key geometric invariants for relativity and quantum mechanics as will be shown.

(a) Spacetime (x,ct)   (b) Per-spacetime (ω,ck)

Wave zero-paths all the same speed c

Time ct

Space x

K_{group}
$=(K_4-K_2)/2$

K_4

K_2

K_{phase}
$=(K_4+K_2)/2$

Wavevector ck

Frequency ω

source 2

Replaced by:

source 4

Infrared laser

$K_2 = (\omega_2, k_2)$
$= (2c, 2)$

Krypton laser

$K_4 = (\omega_4, k_4)$
$= (4c, 4)$
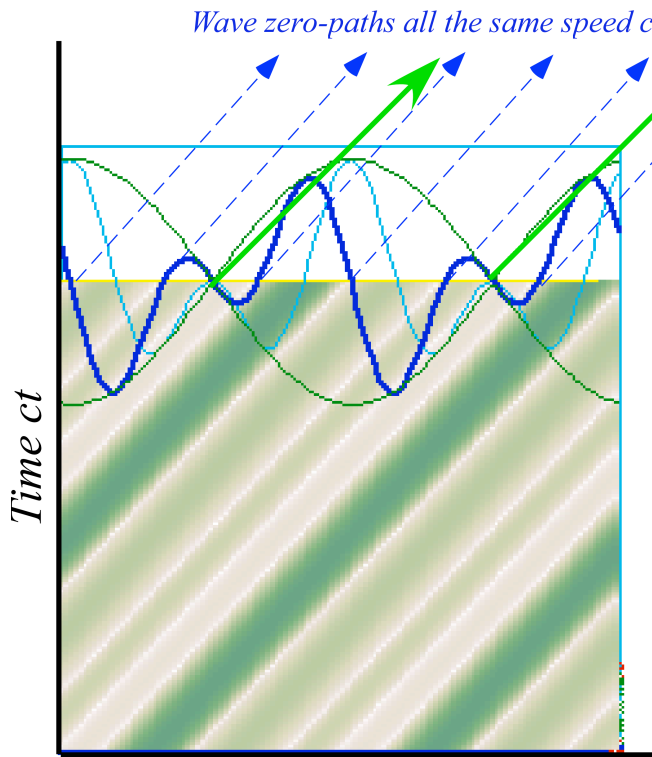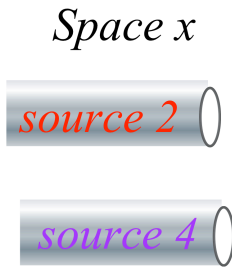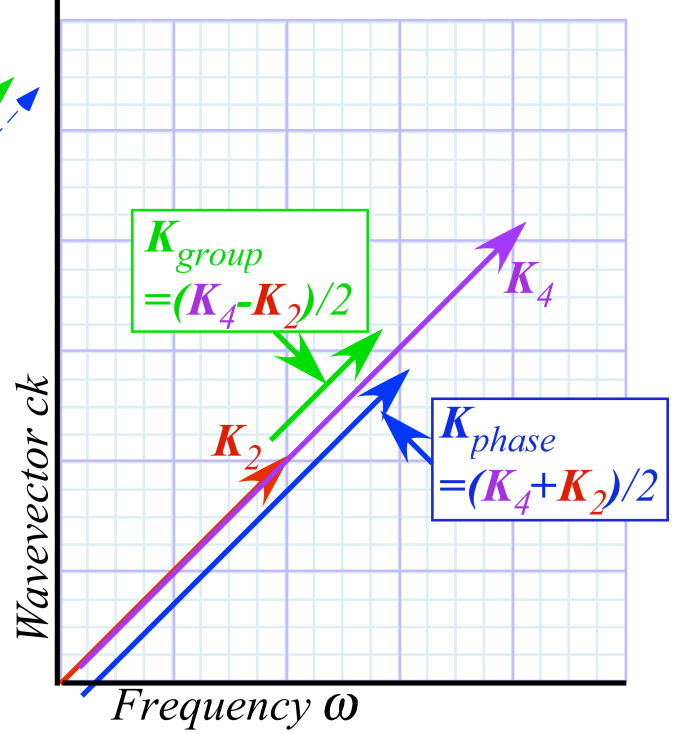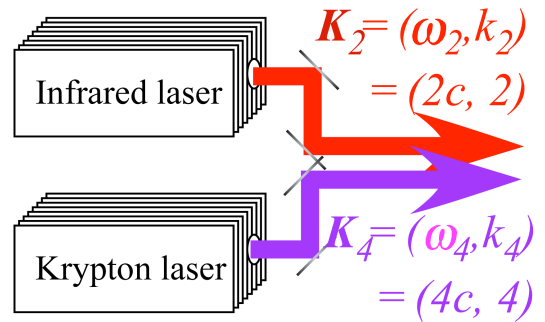
Fig. 0.5 Co-propagating laser beams produce a collapsed wave lattice since all parts have same speed c.

-- The Purest Light and a Resonance Hero – Ken Evenson (1932-2002) --

When travelers punch up their GPS coordinates they owe a debt of gratitude to an under sung hero who, alongside his colleagues and students, often toiled 18 hour days deep inside a laser laboratory lit only by the purest light in the universe.

Ken was an "Indiana Jones" of modern physics. While he may never have been called "Montana Ken," such a name would describe a real life hero from Bozeman, Montana, whose extraordinary accomplishments in many ways surpass the fictional characters in cinematic thrillers like *Raiders of the Lost Arc*.

Indeed, there were some exciting real life moments shared by his wife Vera, one together with Ken in a canoe literally inches from the hundred-foot drop-off of Brazil's largest waterfall. But, such outdoor exploits, of which Ken had many, pale in the light of an in-the-lab brilliance and courage that profoundly enriched the world.

Ken is one of few researchers and perhaps the only physicist to be twice listed in the *Guinness Book of Records*. The listings are not for jungle exploits but for his lab's highest frequency measurement and for a speed of light determination that made *c* many times more precise due to his lab's pioneering work with John Hall in laser resonance and metrology[†].

The meter-kilogram-second (mks) system of units underwent a redefinition largely because of these efforts. Thereafter, the speed of light *c* was set to *299,792,458ms^{-1}*. The meter was defined in terms of *c*, instead of the other way around since his time precision had so far trumped that for distance. Without such resonance precision, the Global Positioning System (GPS), the first large-scale wave space-time coordinate system, would not be possible.

Ken's courage and persistence at the Time and Frequency Division of the Boulder Laboratories in the National Bureau of Standards (now the National Institute of Standards and Technology or NIST) are legendary as are his railings against boneheaded administrators who seemed bent on thwarting his best efforts. Undaunted, Ken's lab painstakingly exploited the resonance properties of metal-insulator diodes, and succeeded in literally counting the waves of near-infrared radiation and eventually visible light itself.

Those who knew Ken miss him terribly. But, his indelible legacy resonates today as ultra-precise atomic and molecular wave and pulse quantum optics continue to advance and provide heretofore unimaginable capability. Our quality of life depends on their metrology through the Quality and Finesse of the resonant oscillators that are the heartbeats of our technology.

Before being taken by Lou Gehrig's disease, Ken began ultra-precise laser spectroscopy of unusual molecules such as HO_2, the radical cousin of the more common H_2O. Like Ken, such radical molecules affect us as much or more than better known ones. But also like Ken, they toil in obscurity, illuminated only by the purest light in the universe.

In 2005 the Nobel Prize in physics was awarded to Glauber, Hall, and Hensch[††] for laser optics and metrology.

† K. M. Evenson, J.S. Wells, F.R. Peterson, B.L. Danielson, G.W. Day, R.L. Barger and J.L. Hall, Phys. Rev. Letters 29, 1346(1972).

†† *The Nobel Prize in Physics, 2005*. http://nobelprize.org/
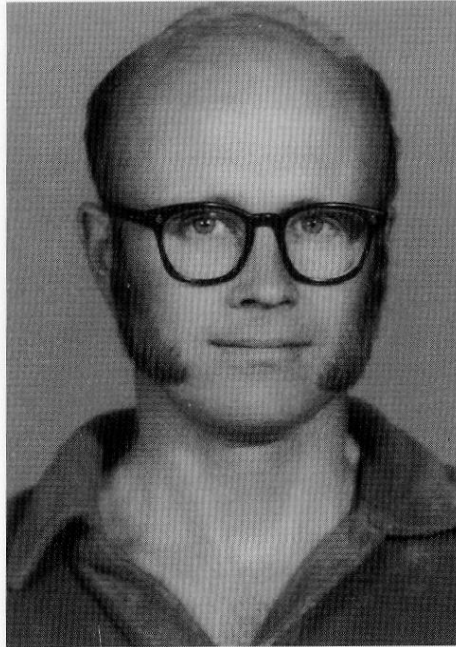
PAULINIA, BRASIL 1976

THE *SPEED OF LIGHT IS*
299,792,458 *METERS PER SECOND!*

Kenneth M. Evenson – 1932-2002

Chapter 1 Continuous Wave (CW) vs. Pulse Wave (PW) functions

The standard units of time t and space x are *seconds* and *meters*. Pure waves are labeled by inverse units that count waves *per-time* or *frequency* ν, which is *per-second* or *Hertz (1Hz=1 s⁻¹)* and waves *per-meter* that is called *wavenumber* κ whose old units were *Kaiser (1 K=1 cm⁻¹=100 m⁻¹)*. Inverting back gives the *period* $\tau=1/\nu$ or *time for one wave* and *wavelength* $\lambda=1/\kappa$ or the *space occupied by one wave*.

Physicists like angular or radian quantities of *radian-per-second* or *angular frequency* $\omega=2\pi\nu$ and *radian-per-meter* or *wavevector* $k=2\pi\kappa$ in plane *continuous wave (CW)* functions ψ.

$$\langle k,\omega|x,t\rangle = \psi_{k,\omega}(x,t) = e^{i(kx-\omega t)} = \cos(kx-\omega t) + i\sin(kx-\omega t). \qquad (1.1a)$$

Sine or cosine are circular functions of wave *phase (kx-ω t)* given in radians and defined here.

$$\tau = \frac{2\pi}{\omega} = \frac{1}{\nu} \qquad (1.1b) \qquad\qquad \lambda = \frac{2\pi}{k} = \frac{1}{\kappa} \qquad (1.1c)$$

They relate time τ and space λ parameters to *per*-time ω or ν and *per*-space k or κ wave parameters.

Phase velocity for 1-CW

Spacetime plots of the real field $\mathrm{Re}\,\psi_{k\omega}(x,t)$ for one CW laser light are shown in Fig. 1.1. The left-to-right moving wave $e^{i(kx-\omega t)}$ in Fig. 1.1(a) has a positive wavevector k while k is negative for right-to-left moving wave $e^{i(-|k|x-\omega t)}$ in Fig. 1.1(b). Light and dark lines mark time paths of crests, zeros, and troughs of $\mathrm{Re}\,\psi_{k\omega}(x,t)$. A zero-phase line (where kx-ωt is zero) or crest line has slope $c=V_{phase}$.

$$kx - \omega t = 0 \,, \quad \text{or:} \quad \frac{x}{t} = V_{phase} = \frac{\omega}{k} = \nu\lambda \qquad (1.1d)$$

Each white line in Fig. 1.1 has a phase is an odd multiple *(N=1,3,…)* of $\pi/2$ and marks a $\lambda/2$-interval.

$$kx - \omega t = \pm N\frac{\pi}{2} \,, \quad \text{or:} \quad x = V_{phase}t \pm N\frac{\pi}{2k} = V_{phase}t \pm N\frac{\lambda}{4}$$

Slope or *phase velocity V_{phase}* of all lightwave phase line is a *universal constant c=299,792,548m/s*. (Note tribute to Ken Evenson's *c*-measurement in Unit 4.) Velocity is a ratio of space to time *(x/t)* or a ratio of per-time to per-space *(ν/κ)* or *(ω/k)*, or a product of per-time and space *(νλ)=1/(τκ)*.

The standard wave quantities of (1.1) are labeled for a long wavelength example (infrared light) in the lower part of Fig. 1.1. Note that the $\mathrm{Im}\,\psi_{k,\omega}(x,t)$ wave precedes the $\mathrm{Re}\,\psi_{k\omega}(x,t)$ wave. A simple mnemonic is helpful, *"Imagination precedes reality by one quarter."* and applies to combined waves, too.

Axioms for light: 2-CW vs. 2-PW

        Beginning relativity courses paraphrase Einstein's light speed axiom as in Fig. 1.2a, *"Speed of a lightning flash is c according to passengers of any train,"* or simply, *"Pulse wave (PW) speed c is invariant."* For critically thinking students, that is a show-stopper. It boggles the mind that something of finite speed cannot *ever* be caught up to, indeed, cannot even *begin* to be caught.[i]
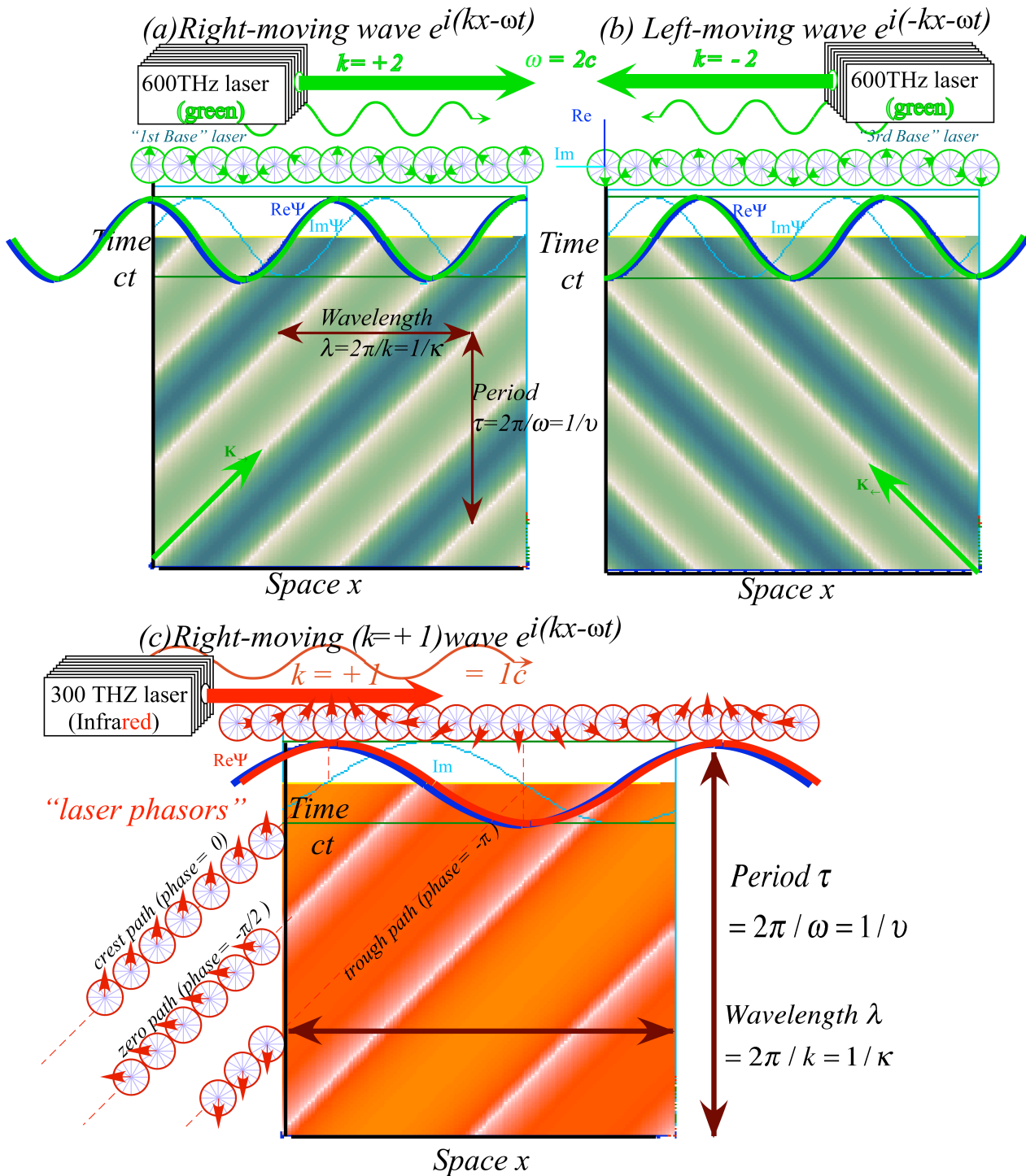
Fig. 1.1 Phasor and spacetime plots of moving CW laser waves. (a,c) Left-to-right. (b) Right-to-left.

Occam's razor can dissect the *c*-axiom into a less mind-boggling form. As Evenson viewed a frequency chain of multiple "colors" of continuous wave (CW) laser beams, he assumed that, "All *colors* have speed *c*." Had Einstein imagined trains viewing a *600THz* (green) laser as in Fig. 1.2b, his *c*-axiom might be, "CW speed is *c* according to passengers of any train *while frequency and wavelength vary by a Doppler effect that depends on velocity of the train*," or more simply, "*All colors go c.*"

A CW spectral component of a PW has a color variation with observer speed that a "white" PW does not. A colored wave (CW) will blue-shift if you approach its source or a red-shift if you run away from it. Doppler's theory of acoustical wave frequency shift existed 200 years before radar, masers, and lasers showed the ultra-precise 1st-order Doppler sensitivity of a coherent optical CW.

Also an optical Doppler shift depends on *one* relative velocity of source and observer while acoustical Doppler depends on *three* absolute (or three relative) velocities involving source, observer, and a "wind." This single-velocity simplicity of *en vacuo* optical Doppler shifts is crucial for relativity.

Consider a *600THz* green wave from a *600THz* source. One may ask, "Is it distinguishable from another *600THz* green wave sent by a *599THz* source approaching or a *601THz* source departing at just the right speed? Or, could *600THz* light, seen as we approach a fixed *599THz* source, ever differ in speed from *600THz* light seen as we depart a fixed *601THz* source? In short, "How many kinds of *600THz* light exist?"

Evenson's axiom follows if one answers, "There is only one kind of each frequency (color) and only one speed independent of source or observer velocity." An undesirable alternative is to have many different kinds of each color, corresponding to many ways to make each color by tuning source up (or down) while moving out (or in). (In fact, one color illuminating a gas, liquid, or solid may involve two or many varieties of mode dispersion with wave speeds ranging above or below *c*.) Evenson's axiom demands that light in a vacuum be one speed for all frequency. In short, light is *dispersion-free*.

If so, a PW must move rigidly at the speed *c* shared by its component CW colors. In this way one derives Einstein's PW law as a *theorem* arising from Evenson's CW *axiom*. Occam wins here!

Astronomical view of CW axiom

It also relates to appearance of distant nebulae and the night sky. If any colors were even a fraction of a percent slower than other frequencies, they would show up thousands or millions of years later with less evolved images than neighboring colors. We might then enjoy a sky full of blurry colorful streaks but would lose the clarity of Hubble astronomical images of colliding galaxies billions of light years away.

Spectroscopic view of CW axiom

Astronomy is just one dependent of Evenson's CW axiom. Spectroscopy is another. Laser atomic spectra are listed by frequency υ (s^{-1}) or period $\tau=1/\upsilon$ (s) while early tables list atomic lines from gratings by wavenumber κ (m^{-1}) or wavelength $\lambda=1/\kappa$ (m). The equivalence of time and space listings is a tacit assumption in Evenson's axiom. The axiom may be stated by the following summary of (1.1a-d).

$$c = \upsilon \cdot \lambda \ = \lambda/\tau \ = \upsilon/\kappa \ = 1/(\kappa \cdot \tau) = c = 299{,}792{,}548 m/s \qquad (1.1)_{summary}$$

(a) Einstein Pulse Wave (PW) Axiom: *PW speed seen by all observers is c*

Pulse wave (PW) train

PW peaks precisely locate places where wave is.
CW zeros precisely locate places where wave is not.

Continuous wave (CW) train
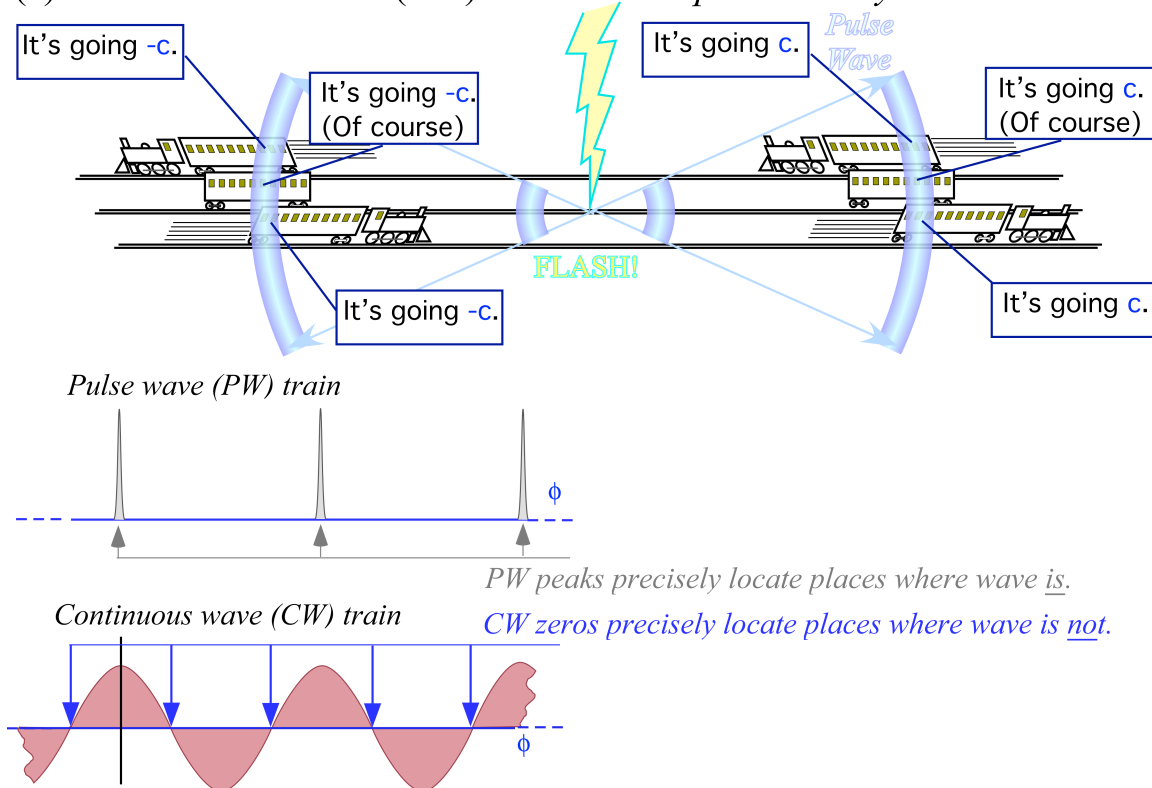
(b) Evenson Continuous Wave (CW) axiom: *CW speed for all colors is c*
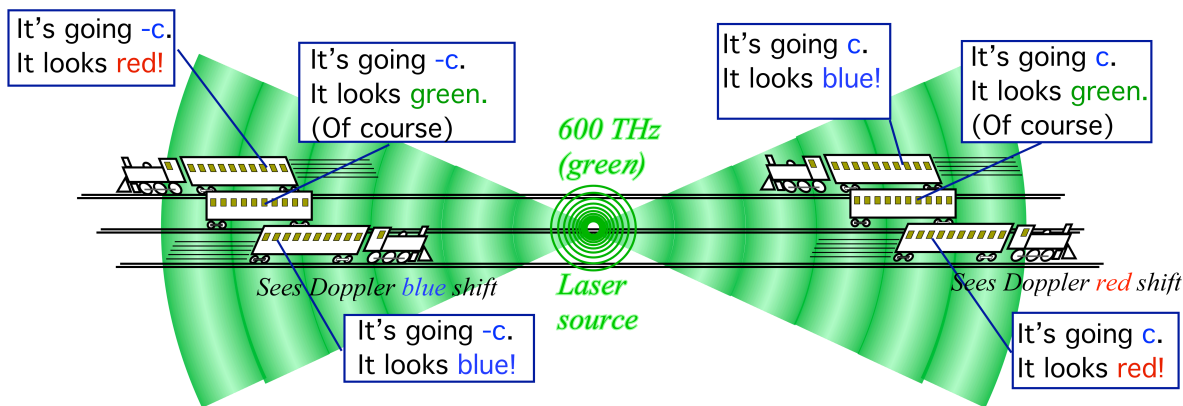
Fig. 1.2 Comparison of wave archetypes and axioms. *(a) Pulse Wave (PW) peaks locate where a wave is. Their speed is c for all observers. (b) Continuous Wave (CW) zeros locate where it is not. Their speed is c for all colors (or observers.)*

An atomic resonance is *temporal* and demands a precise *frequency*. Sub-nanometer atomic radii are thousands of times smaller than micron-sized wavelengths of optical transitions. Optical wavelength is not a key variable in atomic dipole approximations that ignore spatial dependence of light.

However, optical grating diffraction demands precise *spatial* fit of micron-sized wave*length* to micron grating slits. Optical frequency is not a key variable for time independent Bragg or Fraunhofer laws. Spatial geometry of a spectrometer grating, cavity, or lattice directly measures wavelength λ, and then frequency υ is determined indirectly from λ by axiom (1.1). That is valid if the light speed $c = \upsilon \cdot \lambda$ is invariant throughout the spectrum (and throughout the universe.)

A spectroscopist expects an atomic laser cavity resonating at a certain atomic spectral line in one rest frame to do so in *all* rest frames. Each λ or υ value is a *proper quantity* to be stamped on the device and officially tabulated for its atoms. Passersby may see output υ Doppler red shifted to $r\upsilon$ or blue shifted to $b\upsilon$. Nevertheless, all can agree that the device and its atoms are actually lit up and working!

Moreover, Evenson's CW axiom demands that υ and λ must Doppler shift *inversely* one to the other so that the product $\upsilon \cdot \lambda$ is always a constant *c=299,792,458 m·s⁻¹*. The same applies to τ and κ for which *$\kappa \cdot \tau$=1/c*. Also, there is an inverse relation that exists between Doppler blue and red shifts seen before and after passing a source. This is our second CW axiom. It involves time reversal symmetry.

Time reversal axiom

Atoms behave like tiny radio transmitters, or just as well, like receivers. Unlike macroscopic radios, atoms are time-reversible in detail since they have no resistors or similarly irreversible parts. Suppose an atom *A* broadcasting frequency υ_A resonates an approaching atom *B* tuned to receive a blue shifted frequency $\upsilon_B = b\upsilon_A$. If time runs backwards all velocity values change sign. Atom *B* becomes a *transmitter* of its tuned frequency $\upsilon_B = b\upsilon_A$ that is *departing* from atom *A* who is a *receiver* tuned to its frequency $\upsilon_A = (1/b)\upsilon_B$. Atom *A* sees υ_A *red*-shifted from *B*'s frequency υ_B by an *inverse* factor *r=1/b*.

$$b=1/r \qquad\qquad (1.2)$$

Phase invariance axioms viewed in a classical way

Optical CW axioms may be based on deeper phase invariance principles. Elementary CW function $\Psi=A \exp i(k\cdot x-\omega\cdot t)$ or its real part $Re\,\Psi=A \cos(k\cdot x-\omega\cdot t)$ has a phase angle $\Phi=(k\cdot x-\omega\cdot t)$ that is regarded as an invariant or proper quantity. Our rationale is that each space-time point of the wave has a phase clock or *phasor* $(Re\,\Psi, Im\,\Psi)$ turning at *angular* frequency $\omega=2\pi\cdot\upsilon$. Each phasor reading Φ could be stamped or

"officially" tabulated. All observers should agree on Φ even if Doppler shifts change frequency $\omega = 2\pi \cdot \upsilon$

and *wavevector* $k = 2\pi\kappa$ to new values (ω', k') or if space x and time t also transform to x', t'.

$$k \cdot x - \omega \cdot t = \Phi = k' \cdot x' - \omega' \cdot t' \qquad\qquad (1.3)$$

(Lorentz-Einstein transformations for both space-time x,t to x',t' and inverse space-time (ω,k) to (ω',k') are

derived in Ch. 2 using CW axioms (1.1) and (1.2) with a few algebraic or ruler-and-compass steps.)

Historically, invariance (1.3) relates to classical Legendre contact transforms of Lagrangian L to

energy E or Hamiltonian H. Differential Ldt is Poincare's *action invariant dS* or phase $d\Phi$ with an $\hbar$ factor.

$$L = p \cdot \dot{x} - H \qquad (1.4a) \qquad\qquad\qquad \hbar d\Phi = dS = Ldt = p \cdot dx - Hdt \qquad (1.4b)$$

Connecting (1.3) to (1.4b) requires quantum scaling relations $p=\hbar k$ of DeBroglie and $E=\hbar\omega$ of Planck.

Ch. 3 shows how such relations arise from CW axioms (1.1-2). Exact relativistic quantum and classical

mechanical relations are found in a few algebraic[ii] or ruler-and-compass steps. Elegant wave-geometric[iii]

interpretations of momentum, mass, energy, and Poincare's invariant are exposed in Ch. 4 and Ch. 5.[iv]

We surmised that Einstein might have liked geometric derivations since a compass first caught his

theoretical attention at an age of five.[v] Perhaps, it might also appeal to Poincare who also discovered

relativity around the time of Einstein's 1905 *annus mirabilis*. Poincare phase invariance (1.3) underlies

both CW lightspeed axiom (1.1) and time reversal axiom (1.2). Consider the $\Phi=0$ point.

$$k \cdot x - \omega \cdot t = 0 \qquad\qquad (1.5a)$$

Solving gives phase velocity x/t *(meters-per-second)* equal by (1.1) to υ/κ *(per second)-per-(per meter)*.

$$\frac{x}{t} = \frac{\omega}{k} = \frac{\upsilon}{\kappa} = c \qquad\qquad (1.5b)$$

Doppler shift $(\omega \rightarrow b\omega$ and $k \rightarrow bk)$ leaves phase velocity invariant. Phase $\Phi=(k\cdot x-\omega\cdot t)$ itself is invariant to

time reversal $((\omega \rightarrow -\omega)$ and $(t \rightarrow -t))$ and that supports (1.2), the inverse-Doppler relation $b=1/r$.

We find relativistic and quantum derivations based on classical mechanical laws to be clumsy at

best and wrong-way-to at worst. Simple wave interference with axioms (1.1-2) can unite relativity and

quantum theory. At the wave-phasor or "gauge" level, Nature may be seen as a big wave trick!

Comparing pulsed and continuous wave trains

It is instructive to contrast two opposite wave archetypes, the *Pulse Wave* (PW) train sketched in

Fig. 1.2a and the *Continuous Wave* (CW) train sketched in Fig. 1.2b. A CW is the more elementary

theoretical entity, indeed the *most* elementary entity in classical optics since it has just one value of

angular frequency $\omega=2\pi\cdot\upsilon$, one value of wavevector $k=2\pi\kappa$, and one amplitude A.

$$^{CW}\Psi_{k,\omega}(x,t) = Ae^{i(kx-\omega t)} = \langle k,\omega | x,t \rangle \tag{1.6}$$

The real part is the cosine wave $A\cos(kx - \omega t)$ shown in Fig. 1.2(b). Acronym CW fits <u>c</u>osine <u>w</u>ave, as

well. If frequency υ is in the visible *400-750*THz range, then CW could also stand for <u>c</u>olored <u>w</u>ave.

In contrast, the PW is a *less* elementary wave function and contains N harmonic terms of CW

functions where bandwidth N is as large as possible. Fig. 1.3 shows an example with $N=12$.

$$^{PW}\Psi_{N(k,\omega)}(x,t) = A(1 + e^{i(kx-\omega t)} + e^{i2(kx-\omega t)} + e^{i3(kx-\omega t)}\cdots + e^{iN(kx-\omega t)}) \tag{1.7}$$

An infinite-N PW is a train of Dirac $\delta(x-a)$-functions each separated by fundamental wavelength $\lambda=2\pi/k$.

The δ-spikes march in lockstep at light speed $c=\omega/k$ because of Evenson's CW axiom (1.1).

$$^{PW}\Psi_{N(k,\omega)}(x,t) \xrightarrow[N\to\infty]{} A \sum_{n=-\infty}^{\infty} \delta(x - ct - n\lambda)$$

Delta functions have infinite frequency bandwidth and are thus impractical. Realistic PW trains apply

cutoff or tapering amplitudes a_n to the harmonic so as to restrict frequency to a finite bandwidth Δ.

$$^{PW}\Psi_\Delta(x,t) = \sum_{n=0}^{\infty} a_n e^{in(kx-\omega t)} = \sum_{n=-\infty}^{\infty} G(x - ct - n\lambda) \quad \text{where: } a_n \ll 1 \text{ for } n > \Delta \tag{1.8}$$

One choice is the Gaussian taper $a_n = e^{-(n/\Delta)^2}$ that gives Gaussian PW functions $G(\theta) = e^{-(\theta\cdot\Delta)^2}$.

PW functions (1.8) involve an unlimited number of amplitude parameters a_n in addition to

fundamental frequency ω, while a CW function has a single amplitude parameter A. Thus, theory based

on CW properties is closer to an Occam ideal for axiomatic simplicity than one based on PW.

CW squares vs. PW diamonds in space-time plots

However, with regard to counter-propagating or colliding beams the PW *appear* in Fig. 1.4a to

have simpler properties than CW in Fig. 1.4b. PW have a simple classical Boolean OFF (0) over most of

space-time with an occasional ON (1) at a sharp pulse. On the other hand CW range gradually between +1

and −1 over most of space-time, but have sharp zeros (0) in between crest and trough. (A PW is *designed*

to make precise peaks that show where it *is*. A CW *naturally* has precise zeros that show where it is *not*.)

Interference between two colliding CW makes a square (**P**, **G**)-zero-grid that is subtler and sharper than the left-right moving (**L**,**R**)-peak-diamond grid made by two colliding PW. One should understand how this wave interference works to make these two archetypical types of wave space-time geometry.

Interference of colliding PW in Fig. 1.4a or Fig. 1.5b is *wysiwye (What you see is what you expect.)*. The pattern of interference for the sum of colliding CW in Fig. 1.4b and Fig. 1.5a is subtler. PW paths in space-time *(x,ct)* resemble baseline *diamonds* in Fig. 1.5b like paths in the American baseball sport. Meanwhile, CW zeros form Cartesian space-time *squares* in Fig. 1.5a with horizontal *x*-axial fixed time-lines *(ct=…1,2…)* and vertical temporal *ct*-axial lines of fixed location *(x=…1,2…)*.

PW peak diamonds seem simple but hide intricate networks of zeros near each peak. CW squares make truly simple and precise lattices of standing wave zeros of given by (1.9), which is just a factored sum of two equal-but-opposite colliding CW. Note that the *group envelope* factor $\left(\cos(kx)\right)$ is zero on lines

(kx/π+1/2=…0,1,2…) parallel to the *ct*-axis. The *phase* factor $\left(e^{-i\omega t}\right)$ has a zero real part on lines of

simultaneous time (ct/π+1/2=…0,1,2…) parallel to the *x*-axis. (At lattice corners, *both* factors are zero.)

$$^{CW}\Psi_{k,\omega} + {}^{CW}\Psi_{-k,\omega} = A\left(e^{i(kx-\omega t)} + e^{i(-kx-\omega t)}\right) = 2Ae^{-i\omega t}\left(\cos(kx)\right) \qquad (1.9)$$

CW wave-zeros vs. PW pulse paths

Phase and group wave *zeros* of 2-CW interference define a space-time wave-zero (**P**,**G**)-coordinate grid for light waves in Fig. 1.5 and more general waves in Fig. 1.6. Vector **P** points along a *phase zero path* and vector **G** points along a *group zero path*. They complement PW pulse peak or peak-path (**L**,**R**)-grid based on vector **L** that points along a *left moving peak path* and a vector **R** that points along a *right moving peak path*. The half-sum-and-difference relation of (**P**,**G**) to (**L**,**R**) is as follows.

$$\mathbf{P} = \tfrac{1}{2}(\mathbf{L} + \mathbf{R}) \qquad (1.10a)$$

$$\mathbf{G} = \tfrac{1}{2}(\mathbf{L} - \mathbf{R}) \qquad (1.10b)$$

The peak-path vectors {**L**,**R**) are then given by sum-and-difference of wave zero vectors {**P**,**G**).

$$\mathbf{L} = (\mathbf{P} + \mathbf{G}) \qquad (1.10c)$$

$$\mathbf{R} = (\mathbf{P} - \mathbf{G}) \qquad (1.10d)$$

Sum-and-differences are due to phase sum-and-differences. (Recall discussion of (4.8.21) in Unit 4.)

(a)Pulse Wave (PW)
   and
(b) CW components

Magnitude |Ψ|
Real part ReΨ
Imag. part ImΨ
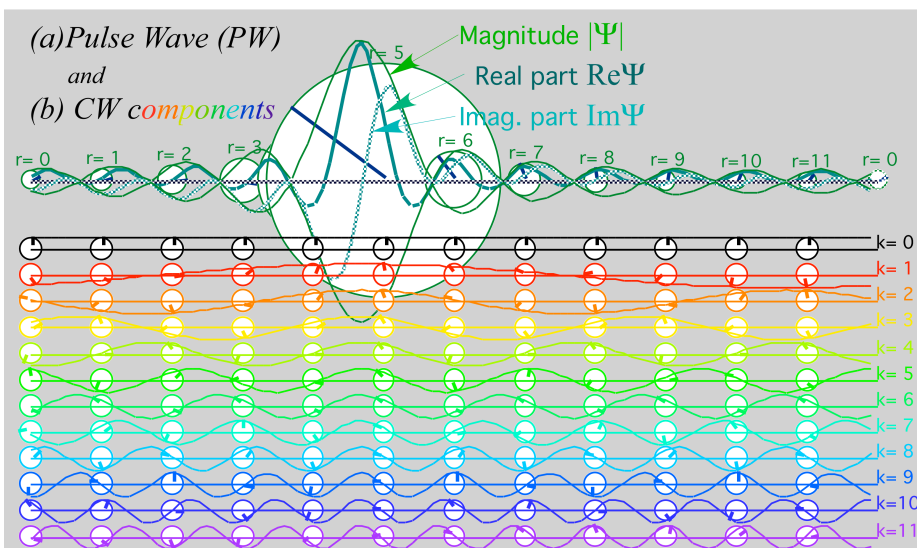
Fig. 1.3.
Pulse Wave (PW)
as a sum of
12 Fourier CW's

(a) PW parts: real ReΨ,
imaginary ImΨ and
magnitude |Ψ| waves.
.
(b) CW phasor clocks
  plot real ReΨ (↑)
       vs.
imaginary ImΨ (←)

(a)Pulse Wave (PW) Addition

↑↓*Standing pulses*

Fig. 1.4
Wave Addition

Time ct   *Time ct*

Space x   *Space x*

← *Left moving pulses*   PLUS   →*Right moving pulses*   EQUALS

(Zeros are diffuse)
Sharp peaks trace *diamond* grid

Sharp zeros trace
square grid
(Peaks are diffuse)
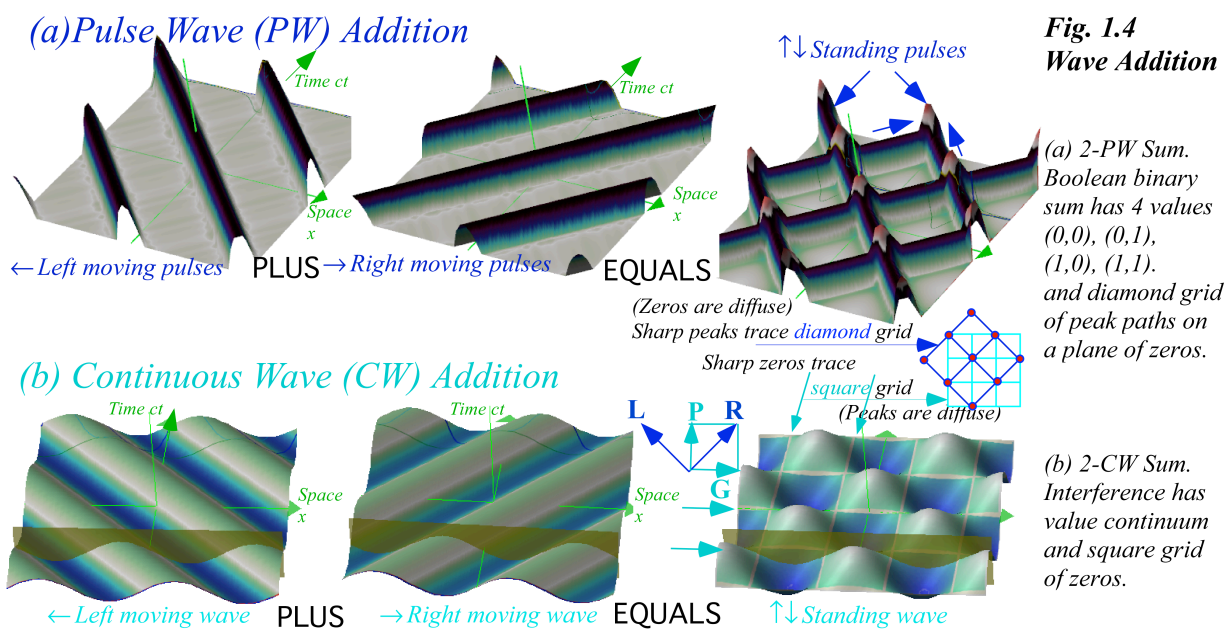
(a) 2-PW Sum.
Boolean binary
sum has 4 values
(0,0), (0,1),
(1,0), (1,1).
and diamond grid
of peak paths on
a plane of zeros.

(b) Continuous Wave (CW) Addition

Time ct   *Time ct*

Space x   *Space x*

L P R
G

← *Left moving wave*   PLUS   →*Right moving wave*   EQUALS   ↑↓*Standing wave*

(b) 2-CW Sum.
Interference has
value continuum
and square grid
of zeros.

Comparing wave-like vs particle-like behavior

Relations (1.10) highlight *wave-particle duality*. First, Newton saw light as particle-like. Then Young and Maxwell showed its wave-like nature. Finally, Planck, Einstein, and Compton found particle-like behavior of "photon" quanta. The label "photon" is reserved for quantum field eigenstates having decidedly more complicated behavior than is shown in semi-classical wave plots in Fig. 1.6 or colliding light waves in Fig. 1.5. Still the diamond left-and-right moving PW (**L**,**R**)-peak paths in Fig. 1.5b might be thought of as paths of fictitious particles or "photon bunches" that are well localized in space-time as they move at ±c in either direction. (Suppose a PW laser "spits" pulses (*patooey! patooey!…*) at *600Thz*.)

Optical pulse peaks do move like particles in between the points where "collisions" occur. (There we have very complicated wave interference.) But, these "particles" seem to pass through each other (or else recoil elastically). Newton described optical interference behavior as crazed "light having fits."

Square 2-CW (**P**,**G**) zero-paths in Fig. 1.5a are due to counter-propagating *600Thz* CW waves interfering wherever they exist in space-time. The wave between the zeros is delocalized in space-time compared to the PW peaks but the square white zero-lines are extremely sharp as are vectors **L**=*(ck,* ω*)* and **R**=*(-ck,* ω*)* that determine motion of left and right CW component laser beams while vectors **P**=*(0,*ω*)* and **G**=*(*ω*,0)* determine the real wave-zero lattice of their 2-CW interfering sum.

It is important to note that these vectors, appropriately scaled, describe both time-*vs*-space *(x,t)*-plots and Fourier inverse *per-time-space* or *reciprocal space-time* plots of frequency-*vs*-wavevector *(*ω*,k)*. A general example of this is derived and shown in a following Fig. 1.6 where the two kinds of plots may be superimposed. We will see that a *(*ω*,ck)* ⇄ *(ck,*ω*)* switch or else an *(x,ct)* ⇄ *(ct,x)* switch to the Newtonian format is needed in order to make a CW lattice and reciprocal PW lattice coincide and that entails a (**P**,**G**) ⇄ (**P**,**G**) switch. This is indicated in Fig. 1.5a to the right of the square space-time lattice.

PW (**L**,**R**)-peak paths are "particle-like" and stand out in space-time for *N*-CW wave trains. Then interference "fits" between pulses die off (to make Newton comfortable again.) But, CW (**P**,**G**)-zero paths, in contrast, are "wave-like" with very sharp lines in space-time for maximally interfering *2*-CW beats.
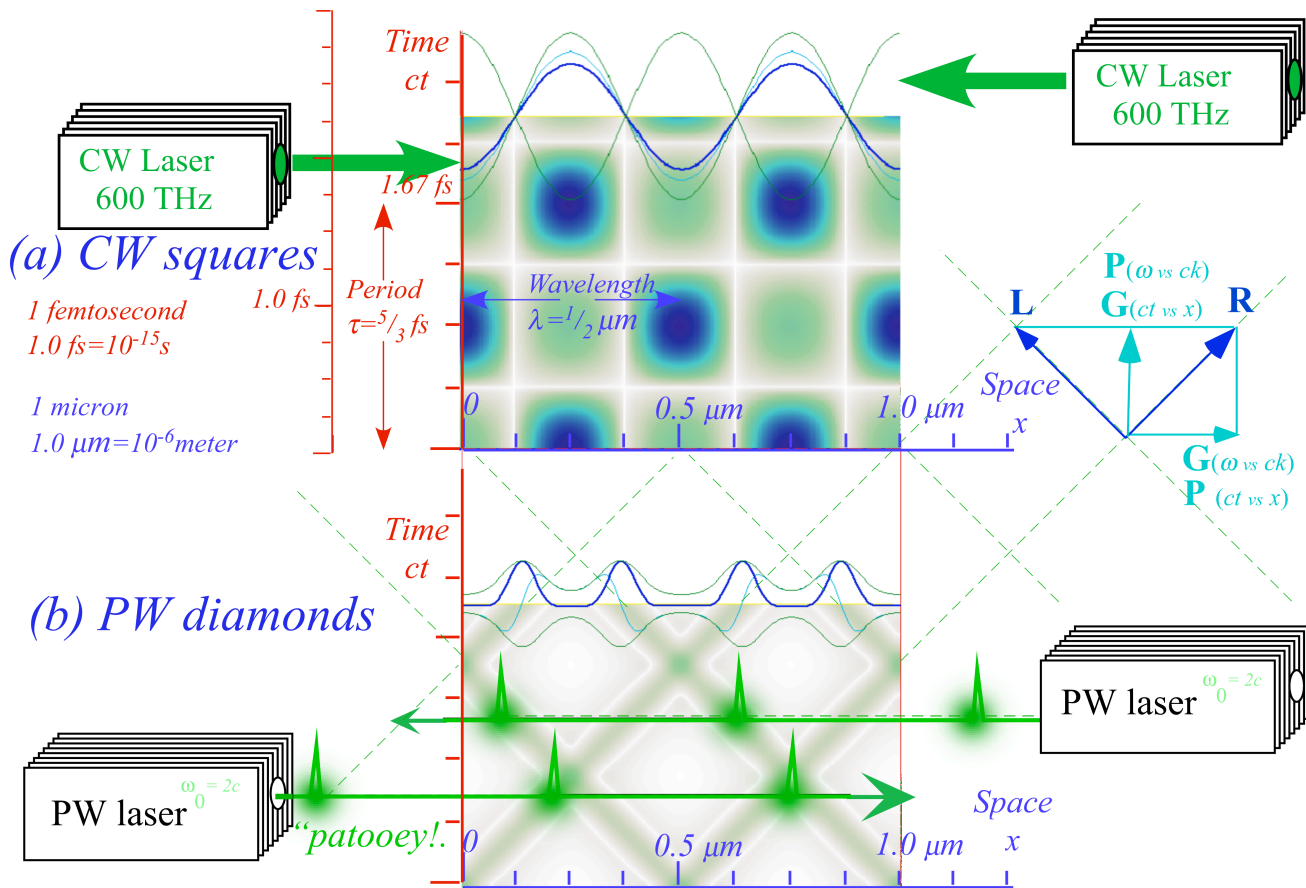
Fig. 1.5 Space-time grids (a) 2-CW standing-wave-zero squares. (b) 2-PW diamond pulse peak paths.

Chapter 2 When Light Waves Collide: Relativity of waves in spacetime

Let us represent counter-propagating frequency-ω laser beams by a baseball diamond in Fig. 2.1a spanned by CW vectors for waves moving left-to-right (**R** on 1st base) and right-to-left (**L** on 3rd base).

$$\mathbf{R}=\mathbf{K}_1=(ck_1,\omega_1)=\omega(1,1) \quad (2.1a) \qquad\qquad \mathbf{L}=\mathbf{K}_3=(ck_3,\omega_3)=\omega(-1,1) \qquad (2.1b)$$

Fig. 2.1 uses conventional (ck,ω)-plots for per-space-time and (x,ct)-plots for space-time. Both beams have frequency $\upsilon=\omega/2\pi=600THz$(green), the unit scale for ω and ck axes. For the **L**-beam, ck equals -ω.

Phase vector $\mathbf{P}=\mathbf{K}_{phase}$ and group vector $\mathbf{G}=\mathbf{K}_{group}$ are also plotted in (ω,ck)-space in Fig. 2.1b.

$$\mathbf{K}_{phase}=\frac{\mathbf{K}_1+\mathbf{K}_3}{2}=\frac{1}{2}\begin{pmatrix}ck_1+ck_3\\\omega_1+\omega_3\end{pmatrix} \qquad\qquad \mathbf{K}_{group}=\frac{\mathbf{K}_1-\mathbf{K}_3}{2}=\frac{1}{2}\begin{pmatrix}ck_1-ck_3\\\omega_1-\omega_3\end{pmatrix}$$
$$=\mathbf{P}=\begin{pmatrix}ck_p\\\omega_p\end{pmatrix}=\frac{\omega}{2}\begin{pmatrix}1-1\\1+1\end{pmatrix}=\omega\begin{pmatrix}0\\1\end{pmatrix} \quad (2.2a) \qquad =\mathbf{G}=\begin{pmatrix}ck_g\\\omega_g\end{pmatrix}=\frac{\omega}{2}\begin{pmatrix}1+1\\1-1\end{pmatrix}=\omega\begin{pmatrix}1\\0\end{pmatrix} \quad (2.2b)$$

Phase and group velocities of counter-propagating light waves may vary from c. These surely do!

$$\frac{V_{phase}}{c}=\frac{\omega_1+\omega_3}{ck_1+ck_3}=\frac{2}{0}=\infty \qquad (2.3a) \qquad\qquad \frac{V_{group}}{c}=\frac{\omega_1-\omega_3}{ck_1-ck_3}=\frac{0}{2c}=0 \qquad (2.3b)$$

The extreme speeds account for the square (Cartesian) wave-zero (WZ) coordinates plotted in Fig. 2.1c. As noted for Fig. 1.5, the group zeros or wave nodes are stationary and parallel to the time ct-axes, while the real-zeros of the phase wave are parallel to the space x-axes. The latter instantly appear and disappear periodically with infinite speed (2.3a) while standing wave nodes have zero speed (2.3b).

Fig. 2.1d shows 2-way pulse wave (2-PW) trains for comparison with the 2-CW WZ grid in Fig. 2.1c. As noted for Fig. 1.3, a PW function is an *N*-CW combination that suppresses its amplitude through *destructive* interference between pulse peaks that owe their enhancement to *constructive* interference.

Colliding PW's show no mutual interference in destroyed regions. Generally one PW is alone on its diamond path going +c parallel to 1st baseline $\mathbf{R}=\mathbf{K}_1$ or going –c parallel to 3rd baseline $\mathbf{L}=\mathbf{K}_3$.

$$\frac{V_1}{c}=\frac{\omega_1}{ck_1}=\frac{1}{1}=1 \qquad (2.4a) \qquad\qquad \frac{V_3}{c}=\frac{\omega_3}{ck_3}=\frac{1}{-1}=-1 \quad (2.4b)$$

But wherever two PW peaks collide, each of the CW pairs will be seen trying to form a square coordinate grid that 2-CW zeros would make by themselves. This begins to explain the tiny square "bases" seen at the corners of the space-time "baseball diamonds" in Fig. 2.1d simulation.

CW-Doppler derivation of relativity

Evenson's CW razor-cut of Einstein's PW axiom improves relativity development. However, quantifying Einstein's popular (and still common) derivation is difficult as is a step-by-step count for the CW derivation that follows. Let us just say that *several* steps are reduced to *fewer* and *clearer* steps. Most important is the wave-natural insight that is gained and the wave mechanics that follows.
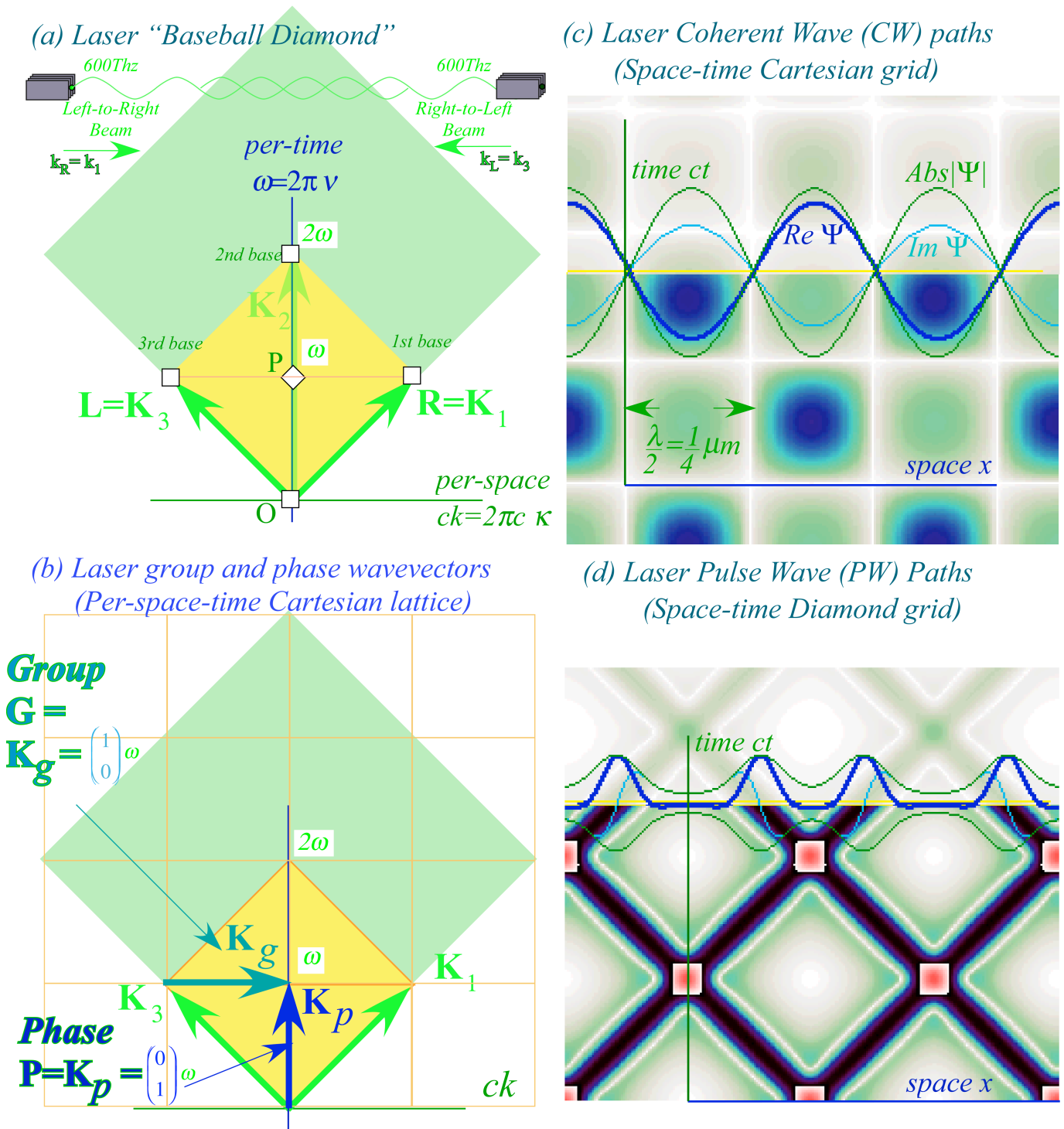
Fig. 2.1. Laser lab view of 600Thz CW and PW light waves in per-space-time (a-b) and space-time (c-d).

In fact, we could claim that a CW derivation takes *zero* steps. It is already done by a 2-CW wave pattern in Fig. 2.2c that automatically produces an Einstein-Lorentz-Minkowski[vi] grid of space-time coordinates. Still we need logical steps drawn in Fig. 2.2a-b that redo the Cartesian grid in Fig. 2.1 just by Doppler shifting each baseline one octave according to *c*-axiom (1.1) (*"Stay on baselines!"*) and *t*-reversal axiom (1.2) (*"If 1st base increases by one octave, 3rd base decreases by the same."*)

So Fig. 2.2 is just Fig. 2.1 seen by atoms going right-to-left fast enough to double *both* frequency $\upsilon=\omega/2\pi$ *and* wavevector ck of the vector **R** on 1st base (while halving vector **L** on 3rd base to obey (1.2).)

$$\mathbf{R}=\mathbf{K}_1=(\,ck'_1,\omega'_1)=\omega(2,2) \quad (2.5a) \qquad\qquad \mathbf{L}=\mathbf{K}_3=(\,ck'_3,\omega'_3)=\omega(-1/2,\,1/2) \quad (2.5b)$$

The atom sees head-on **R**-beam blue-shift to frequency $\upsilon_1'=2\upsilon=\omega_1'/2\pi=$*1200THz*(*UV*) by doubling green $\upsilon_1=\omega/2\pi=\upsilon_3=$*600THz*. It also sees the tail-on **L**-beam red-shift by half to $\upsilon_3'=\upsilon/2=\omega_3'/2\pi=$*300THz*(*IR*).

The phase vector $\mathbf{K}_{phase}$ and group vector $\mathbf{K}_{group}$ are plotted in *(ck',ω')*-space in Fig. 2.2b.

$$\mathbf{K}_{phase}=\frac{\mathbf{K}_1+\mathbf{K}_3}{2}=\frac{1}{2}\begin{pmatrix}ck'_1+ck'_3\\ \omega'_1+\omega'_3\end{pmatrix} \qquad\qquad \mathbf{K}_{group}=\frac{\mathbf{K}_1-\mathbf{K}_3}{2}=\frac{1}{2}\begin{pmatrix}ck'_1-ck'_3\\ \omega'_1-\omega'_3\end{pmatrix}$$

$$=\mathbf{P}'=\begin{pmatrix}ck'_p\\ \omega'_p\end{pmatrix}=\frac{\omega}{2}\begin{pmatrix}2-1/2\\ 2+1/2\end{pmatrix}=\omega\begin{pmatrix}3/4\\ 5/4\end{pmatrix} \quad(2.6a) \qquad =\mathbf{G}'=\begin{pmatrix}ck'_g\\ \omega'_g\end{pmatrix}=\frac{\omega}{2}\begin{pmatrix}2+1/2\\ 2-1/2\end{pmatrix}=\omega\begin{pmatrix}5/4\\ 3/4\end{pmatrix} \quad(2.6b)$$

Phase velocity is the inverse of group velocity in units of *c*, and V'_{group} is *minus the atoms' velocity!*

$$\frac{V'_{phase}}{c}=\frac{\omega'_1+\omega'_3}{ck'_1+ck'_3}=\frac{2+1/2}{2-1/2}=\frac{5}{3} \qquad (2.7a) \qquad\qquad \frac{V'_{group}}{c}=\frac{\omega'_1-\omega'_3}{ck'_1-ck'_3}=\frac{2-1/2}{2+1/2}=\frac{3}{5} \qquad (2.7b)$$

Velocity $u=V'_{group}=3c/5$ is the atoms' view for a lab speed of *zero* had by laser standing nodes. It is the speed of the lasers' group nodes (and its supporting lab bench!) relative to the atoms. Phase velocity $V'_{phase}=5c/3$ is the atoms' view for a lab speed of *infinity* had by lasers' real wave zeros. The *x*-zero lines are simultaneous in the laser lab but not so in the atom-frame. *x*-lines tip *toward ct*-lines in Fig. 2.2c.

Eqs. (2.5-7) use a Doppler blue-shift factor *b=2*. If each "*2*" is replaced by "*b*" then Eq. (2.7b) yields a relation for the laser velocity $u=V'_{group}$ relative to atoms in terms of their blue-shift *b*.

$$\frac{V'_{group}}{c}=\frac{u}{c}=\frac{b-1/b}{b+1/b}=\frac{b^2-1}{b^2+1} \tag{2.8a}$$

Inverting this gives the standard relativistic Doppler *b vs. u/c* relations.

$$b^2=\left(1+u/c\right)/\left(1-u/c\right) \quad \text{or:} \quad b=\sqrt{\left(1+u/c\right)/\left(1-u/c\right)}=\left(1+u/c\right)/\sqrt{1-u^2/c^2} \tag{2.8b}$$

First things first

    It is remarkable that most treatments of relativity first derive *second* order effects, time dilation and length contraction. Doppler and asimultaneity shifts are *first* order in *u* but treated second. Setting *2=b* in (2.6) using (2.8) gives vectors $\mathbf{G}' = \mathbf{K}_g = \binom{d}{a}$ and $\mathbf{P}' = \mathbf{K}_p = \binom{a}{d}$ with *dilation factor* $d = 1/\sqrt{1 - u^2/c^2}$ and

asimultaneity factor $a = u \cdot d/c$. (So *a* and *d* may be derived first here, too, but in a wavelike way.)

$$\mathbf{K}_{phase} = \frac{\omega}{2}\begin{pmatrix} b - 1/b \\ b + 1/b \end{pmatrix} = \omega \begin{pmatrix} (u/c)/\sqrt{1 - u^2/c^2} \\ 1/\sqrt{1 - u^2/c^2} \end{pmatrix} (2.9a) \qquad \mathbf{K}_{group} = \frac{\omega}{2}\begin{pmatrix} b + 1/b \\ b - 1/b \end{pmatrix} = \omega \begin{pmatrix} 1/\sqrt{1 - u^2/c^2} \\ (u/c)/\sqrt{1 - u^2/c^2} \end{pmatrix} (2.9b)$$

K-vector components *d* and *a* (in ω units) are Lorentz-Einstein (LE) matrix coefficients relating atom-values *(ck′,ω′)* or *x′,t′* to lab-values *(ck,ω)* or *x,t* based on lab unit vectors $\hat{\mathbf{G}} = \binom{1}{0}$ and $\hat{\mathbf{P}} = \binom{0}{1}$ in (2.2).

    The new K-vectors define the new coordinate grid of white-line wave-zero paths in space-time of Fig. 2.2c and, perhaps more importantly, the new *(ck′,ω′)* coordinates in per-space time of Fig. 2.2b.

    Einstein's PW axiom *"PW speed c is invariant,"* might give the impression that pulses themselves are invariant, but finite-Δ pulses in Fig. 2.2d clearly deform. Pulse speed is invariant but each CW square in Fig. 2.3a deforms into a Minkowski-like rhombus in Fig. 2.3b simply due to Doppler detuning beats.

Lorentz-Einstein transformations

The Lorentz[vii]-Einstein[viii] per-spacetime and spacetime transformations follow from **K**-vectors (2.9).

$$\begin{pmatrix} \omega' \\ ck' \end{pmatrix} = \begin{pmatrix} \dfrac{1}{\sqrt{1 - u^2/c^2}} & \dfrac{u/c}{\sqrt{1 - u^2/c^2}} \\ \dfrac{u/c}{\sqrt{1 - u^2/c^2}} & \dfrac{1}{\sqrt{1 - u^2/c^2}} \end{pmatrix} \begin{pmatrix} \omega \\ ck \end{pmatrix} (2.10a) \qquad \begin{pmatrix} x' \\ ct' \end{pmatrix} = \begin{pmatrix} \dfrac{1}{\sqrt{1 - u^2/c^2}} & \dfrac{u/c}{\sqrt{1 - u^2/c^2}} \\ \dfrac{u/c}{\sqrt{1 - u^2/c^2}} & \dfrac{1}{\sqrt{1 - u^2/c^2}} \end{pmatrix} \begin{pmatrix} x \\ ct \end{pmatrix} (2.10b)$$

Wave **K**-vectors are bases for space-time *and* per-space-time. One symmetric LE matrix, invariant to axis-switch *(ω,ck) ⇌ (ck,ω)*, applies to both. Conventional ω–ordinate *vs. ck*-abscissa per-space-time and *ct*-ordinate *vs. x*-abscissa space-time plots are used in Fig. 2.2 where $\widehat{\omega} = \mathbf{P} = \mathbf{K}_{phase}$ and $\widehat{ck} = \mathbf{G} = \mathbf{K}_{group}$ vectors serve as *x*-space and *ct*-time bases, respectively, and then also serve as ω–and-*ck*-bases.

    The left and right pulse wave (PW) vectors **L** and **R** in per-space-time Fig. 2.2a also define left and right PW paths in space-time Fig. 2.2d. This holds in either convention because **L** and **R** lie on 45° reflection planes that are eigenvectors of an axis-switch *(ω,ck) ⇌ (ck,ω)* with eigenvalues *+1* and *–1* while half-sum-and-difference vectors $\mathbf{P} = (\mathbf{L} + \mathbf{R})/2$ and $\mathbf{G} = (\mathbf{L} - \mathbf{R})/2$ simply switch $(\mathbf{P} \rightleftarrows \mathbf{G})$.

(a) Boosted Laser "Baseball Diamond"
(Per-space-time rectangle)

1200Thz

Left-to-Right
Beam

k'_R

per-time
$\omega' = 2\pi \nu$

300Thz

Right-to-Left
Beam

k'_L

2ω

R'
=K'$_1$

K_2

L=K$_3$

R=K$_1$

L'=K'$_3$

per-space
$ck' = 2\pi c\, \kappa'$

(c) (u=3c/5)-Boosted CW paths
(Space-time Minkowski grid)

time
ct'

time
ct

space x

space x'

(b) Boosted group and phase wavevectors
(Per-space-time Minkowski lattice)

Group

$$\mathbf{G'} = \begin{pmatrix} ck'_g \\ \omega'_g \end{pmatrix} = \begin{pmatrix} \frac{5}{4} \\ \frac{3}{4} \end{pmatrix} \omega$$

2ω

K'$_1$

K'$_3$

ck'

Phase

$$\mathbf{P'} = \begin{pmatrix} ck'_p \\ \omega'_p \end{pmatrix} = \begin{pmatrix} \frac{3}{4} \\ \frac{5}{4} \end{pmatrix} \omega$$

(d) Boosted PW Paths
(Rectangular grid)

time
ct

space
x

Fig. 2.2 Atom view of 600Thz CW and PW light waves in per-spacetime (a-b) and space-time (c-d) boosted to u=3c/5.

Geometry of Lorentz-Einstein contraction-dilation

　　　　Fig. 2.3 compares wave path space-time coordinate lines for the laser lab in top figure (a) and for the atom going right-to-left at speed *u=3c/5* in bottom figure (b).

　　　　The fast wave-phase zeros define the space-*x* axis and gridlines in either view where they go at a speed of *5c/3* in the atom view and at infinite speed ∞ in the lab view.

　　　　The slow wave-group zeros define the time-*ct* axis and gridlines in either view where they go at a speed of *3c/5* in the atom view and at zero speed 0 in the lab view.

　　　　The spatial separation of the slow wave-group zeros in Fig. 2.2c is *4/5* of the original *1/4μm* shown separating the stationary wave zeros in Fig. 2.1c or Fig. 1.5a. That is the Lorentz contraction factor

$$1/d = \sqrt{1 - u^2/c^2} \ . \tag{2.11}$$

　　　　The inverse time dilation factor *d=5/4* is the vertical height of the new "pitcher's mound" *P* in Fig. 2.2a that was originally of unit height in Fig. 2.1a. In space-time diamond of Fig. 1.5b the pitcher's mound is *5/6 fs* from origin or "home plate" and that dilates by factor *d=5/4* to *25/24 fs* in Fig. 2.2c.

　　　　So, objects seen by moving observers tend to appear shortened (Lorentz contraction) and have lengthend time periods (Einstein time dialation). These effects seem quite mysterious. Standard treatments of relativity begin (and often end) with these *2nd order* effects and their algebraic formulas that one memorizes for GRE testing. (See blue formulas in Fig. 2.4.) However, it is far less mysterious *1st order Doppler* effects that underlie relativity of the zig-zag waves of Fig. 2.2 and Fig. 2.3. Fig. 2.4 shows how the *2nd order* effects arise from wave-zero coordinate intersections with time and space axes. More detailed geometry of relativistic geometry is given in later discussion and figures. (See ahead to Figures 3.3, 3.4, 5.1, 5.4, and 5.5.) The invariant hyperbolas that determine space-time scaling in Fig. 2.4 are among the most important topics in the following chapter.
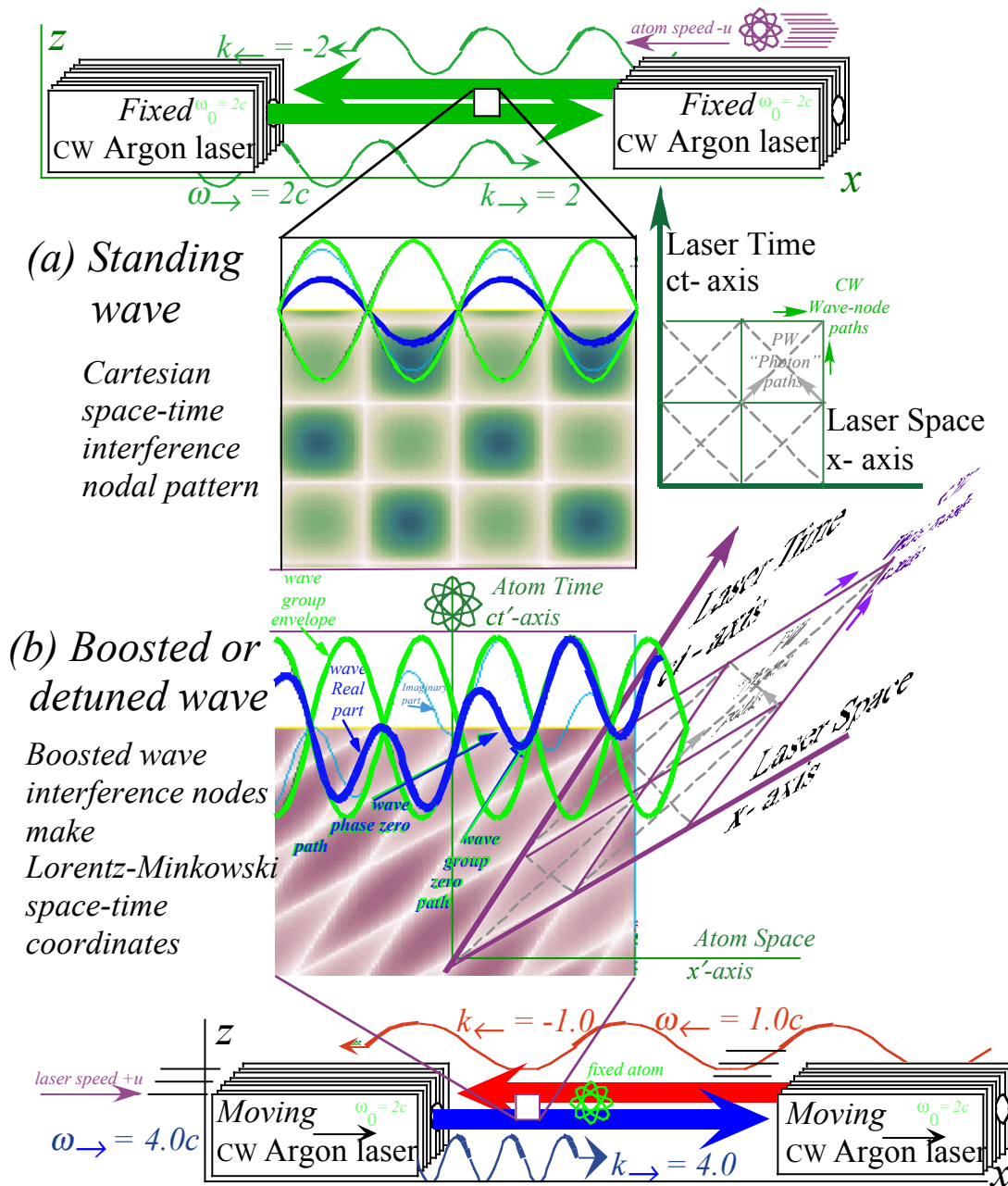
Fig. 2.3 *Lasers make Cartesian (x,ct)-wave frame for themselves and Minkowski (x′,ct′)-frame for atom.*

So, must relativity always be taught by imagining monstrous frames, mirrors, and smoke to trace bouncing "photon bunches" timed by cuckoo clocks synchronized by Swiss gnomes? Not! Perhaps, that 100-year old way serves as a humorous historical aside but current GPS systems and ultra high precision pioneered by Evenson, Hall, and coworkers begs our attention and critical thought. Now as his students are achieving better than 18-figure time and frequency measurements, it is time for theoretical pedagogy to sharpen Occam's razor accordingly. And, if there is history to review, it is first of Galileo and Euclid.

Time Dilation
$$\Delta t'/t' = 1/\sqrt{1-v^2/c^2}$$

Atom Time
ct′ - axis

Laser Time
ct - axis

invariant hyperbolas

$\Delta t'/t'$
$= 5/4$

1.0

1.0

Laser Space
x - axis

Length Contraction
$$\Delta L'/L' = \sqrt{1-v^2/c^2}$$

$\Delta L'/L' = 4/5$

Atom Space
x′ - axis

1.0
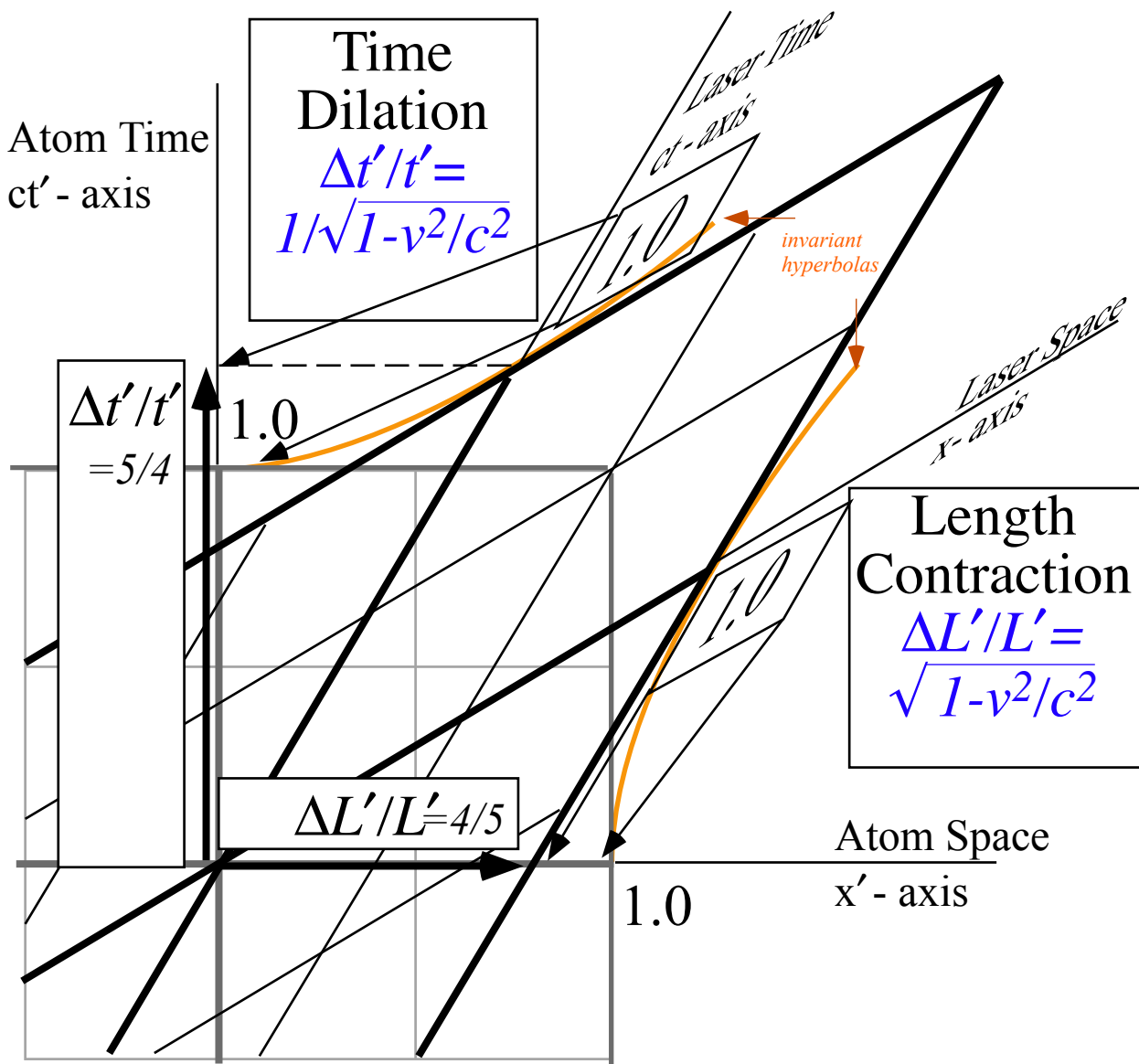
Fig. 2.4 Space-time grid intersections mark Lorentz contraction and Einstein time dilation.

Appendix 2.A New/Old Approaches to Relativistic Space-time Coordinates

        This is a new/old approach to special relativity that we used before discovering the more powerful wave-based approach. It is a PW (pulse wave) approach that takes a constant light speed as Gospel and derives space-time relativity. In this sense it is like the standard smoke-and-mirror-bouncing-photon approach copied for over 100 years from Einstein's famous railroad epic entitled *Meaning of Relativity*. His old trains are replaced here by spaceships and the smokey mirrored beams by spherical PW wavefronts in the vacuum of space-time.

Views from the lighthouses

        Space-time coordinate transformation is described thru a fictional spaceship going half the speed of light past two lighthouses. In Fig. 2.A.1 the ship is just passing a Main Lighthouse as it blinks in response to a signal from its North lighthouse companion located at one light second above it in the figure. It's about *186,000 miles* or *EXACTLY 299,792,458 meters according to NIST's Ken Evenson et. al.* (Recall tribute to Ken at the end of introductory Ch. 0 for Unit 2.)
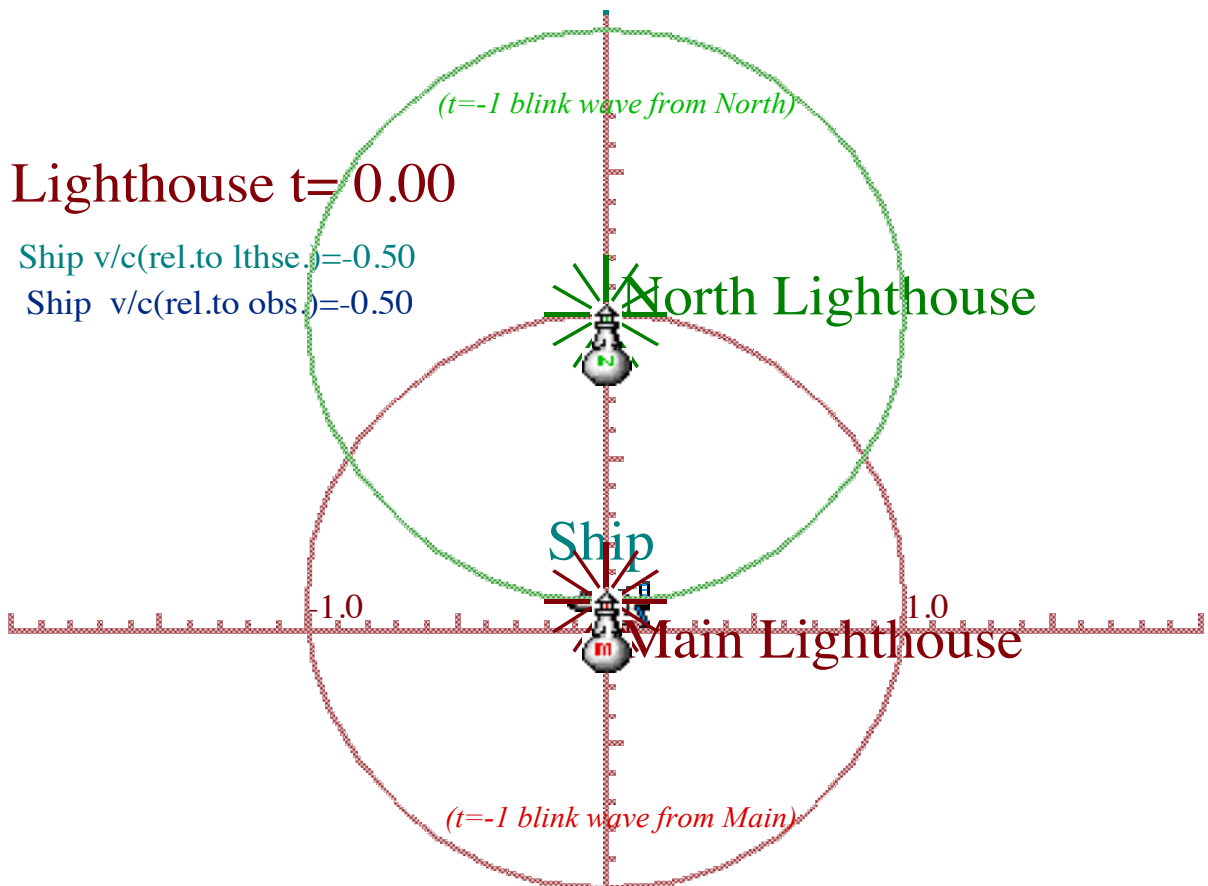
Fig. 2.A.1 Ship passing Main Lighthouse as it blinks at t=0.

        This arrangement is a simplified model for a *1Hz* laser resonator. The two lighthouses use each other to maintain a strict one-second time period between blinks. And, strict it must be to do relativistic timing. (Even stricter than *NIST* is the universal agency *BIGANN* or Bureau of Intergalactic Aids to Navigation at Night.) The simulations shown here are done using *RelativIt*. See website: www.uark.edu/ua/pirelli/php/lighthouse_scenarios.php   Some of the *RelativIt* animations are available there.

Lighthouse t= 1.00

Ship v/c(rel.to lthse.)=-0.50

North Lighthouse

Ship

-1.0

1.0
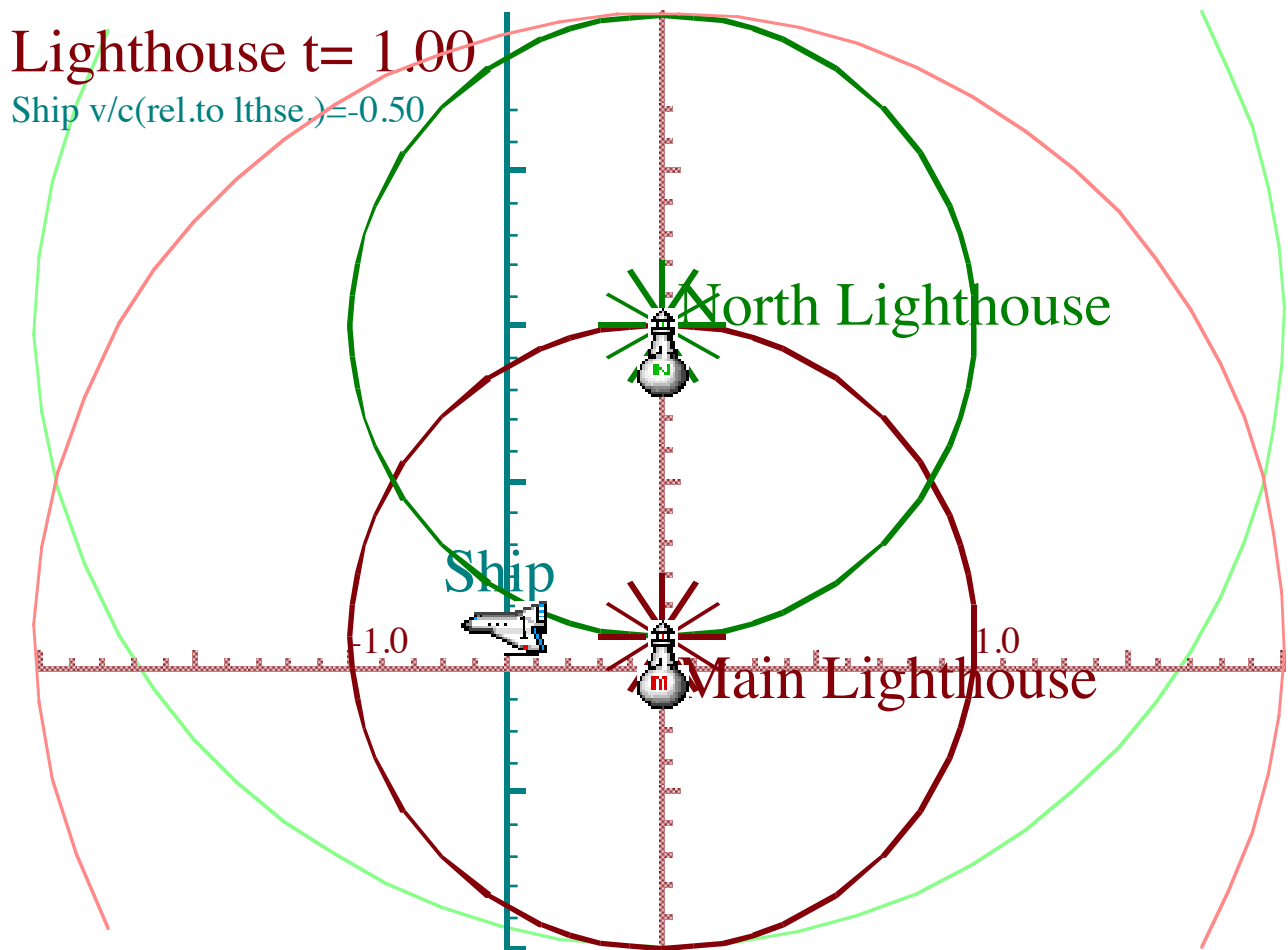
Main Lighthouse

Fig. 2.A.2 Main and North Lighthouses blink each other at precisely *t=1.*

At precisely *t=1 sec.* the two lighthouses blink again because that is how long it takes their respective *t=0* blink waves to reach each other. This is shown in Fig. 2.A.2. The ship, meanwhile, has only traveled half this far since its speed is *c/2*. Its velocity is *-c/2*, that is, negative, since it is going right to left.

Next, at precisely *t=2 sec.* the two lighthouses blink again. Also, the first (*t=1*) blink catches up to the ship and hits it, that is, the ship sees the first blink. This is shown in Fig. 2.A.3. Much of the discussion will center on two happenings or events labeled *Happening-1* and *Happening-2*. ("Event" is accepted physics terminology. "Happening" is oh-so-60's.)

The coordinates of *Happening-1* are, according to the Lighthouses, $(x_1=-1, ct_1=2)$ while for *Happening-2* they are, according to the Lighthouses, $(x_2=0, ct_2=2)$. Next, we will see how the ship views all this, that is what are ship coordinates (x'_1, ct'_1) and (x'_2, ct'_2) for the events. From that we deduce the essential transformation matrix for all events in special relativity. The ship has a very different transcription of these events as shown in the following figures beginning with Fig. 2.A.4.

Lighthouse t= 2.00

0 th blink wave
(From North)

Ship v/c(rel.to lthse.)=-0.50

1st blink wave
(From North)

North Lighthouse

Happening 1
(1st blink wave
from Main hits ship)

Happening 2
(2nd blink happens
at Main Lighthouse)

1.0

0

Ship

Main Lighthouse

1st blink wave
(From Main)

0 th blink wave
(From Main)
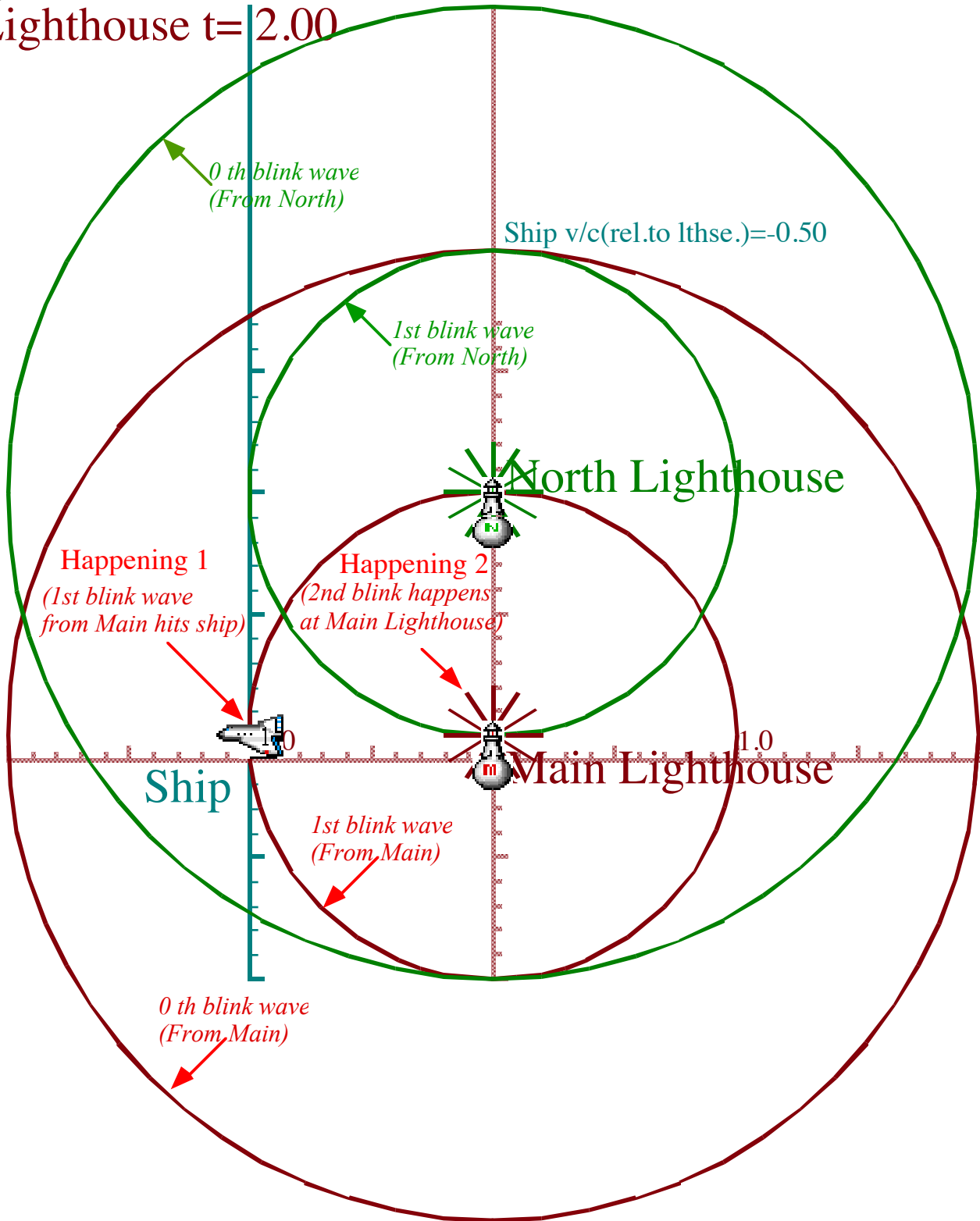
Fig. 2.A.3 Happening 1 (1st blink hits ship) and 2 (2nd blink at Main) both happen at t=2.

Ship v/c(rel.to lthse.)=-0.50

Ship time t' = 0.00

North Lighthouse

1.0   Ship   1.0
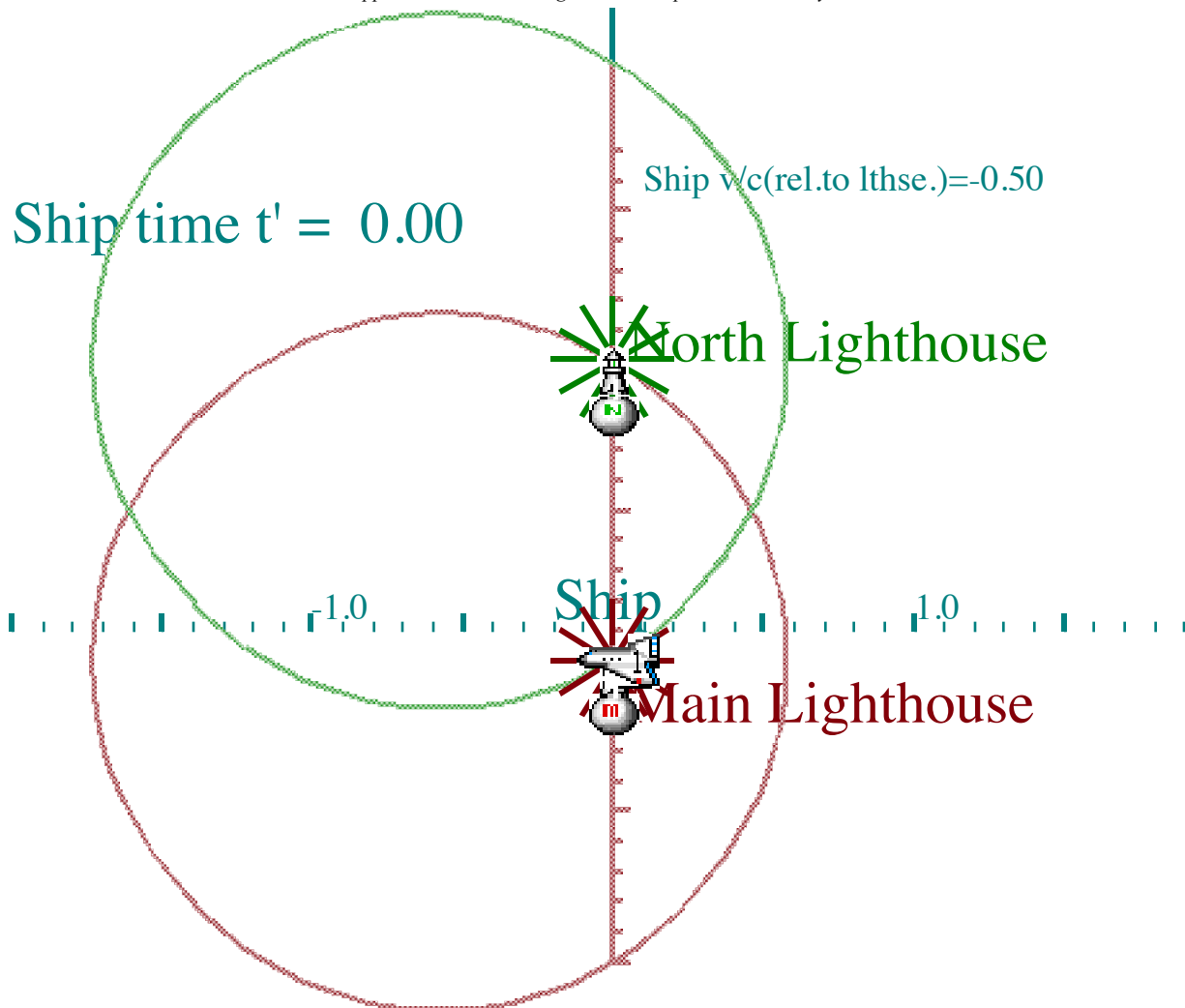
Main Lighthouse

Fig. 2.A.4 Beginning (t′ =0) snapshot for ship's view.

Views from the Ship

Now in Fig. 2.A.4, the ship is stationary and that means that the lighthouses are going in the opposite direction with a positive velocity of $v=+c/2$. Fig. 2.A.4 looks the same as Fig. 2.A.1 except the previous ($t=-1$) blink wave appears to have been "left behind" by the speeding lighthouses. Therein lies a secret of relativity. Snapshots of light pulses always appear to be *circles expanding around the points where they were emitted*. This is true no matter how fast you are going, or, more importantly, no matter how fast the emitter. You cannot speed up or slow down light by jerking your laser back and forth!

So Fig. 2.A.4 and several subsequent figures show previous blink waves expanding around points where the lighthouses were when that light was emitted and all expansions take place at a uniform speed of c. It's the law! And, it's one we can live with. Consequences of this law are quite remarkable. We explore consequences shortly including the fact that the ship sees the North blink-wave tipped by a so-called *stellar aberration angle* $\phi=60°$ relative to a vertical North-to-South wave ray track seen by the Main Lighthouse.

Ship time t' = 0.50

North Lighthouse

-1.0   Ship   1.0
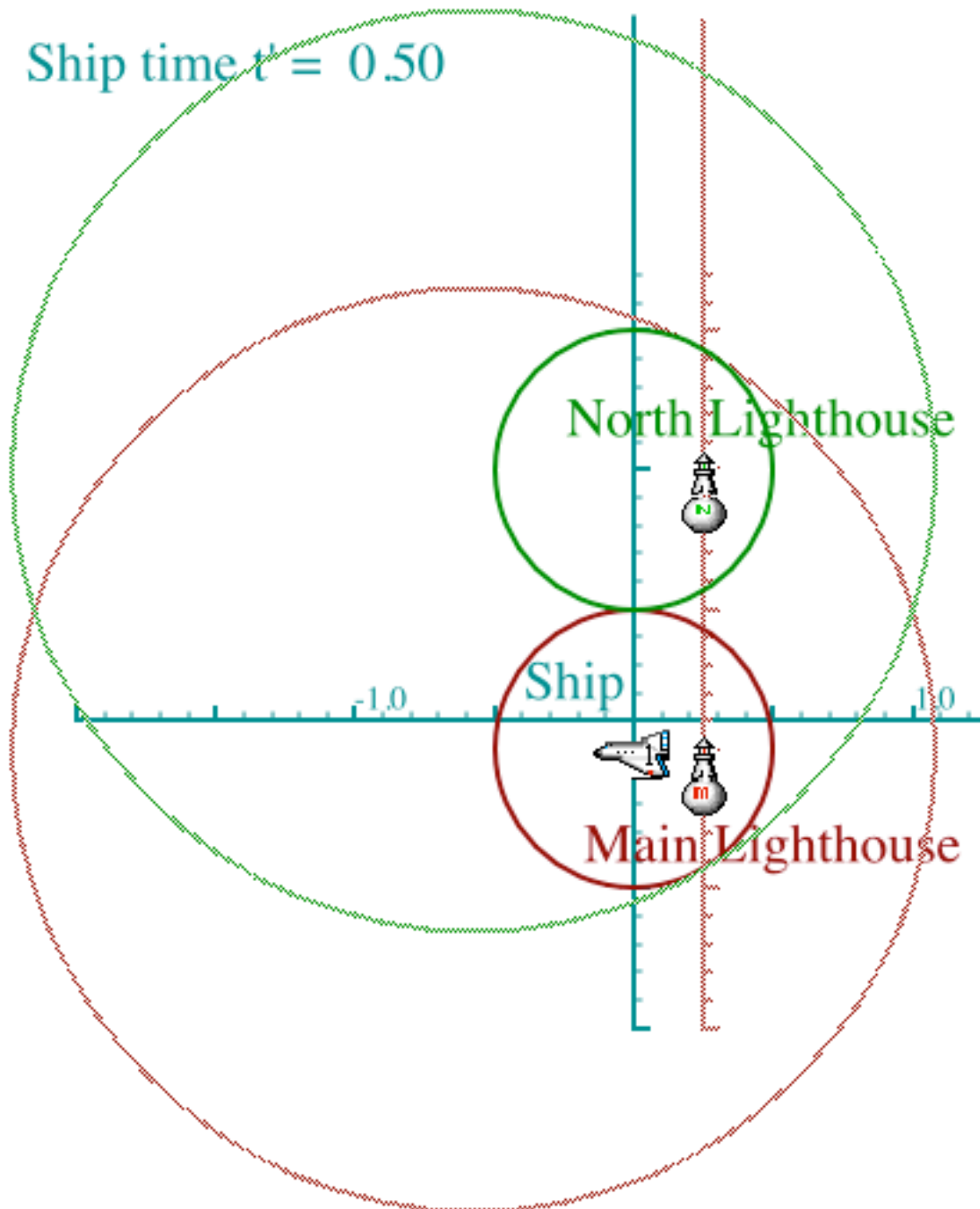
Main Lighthouse

Fig. 2.A.5 Early (t'=0.5) snapshot from ship's view.

   The *(t' =0.5)* view by ship shows the *(t' =0)* blink waves expanded to exactly half the distance between their emission points. Also, the lighthouses have moved half this distance, that is, a quarter of a light-second, and so Main will not be anywhere near the ship at *(t' =1.0)* when the *(t' =0)* blink wave from the North comes down to trigger Main to do its first or *(t=1)* blink. In fact it's *(t' =1.15)* before the blink at *(t' =0)* from the North finally catches the speeding Main Light to make it blink as shown in the next Fig. 2.A.6.

North Lighthouse

Ship time t' = 1.15

Ship v/c(rel.to lthse.)=-0.50

Ship

-1.0

Ship

1.0

Ship v/c(rel.to obs.)= 0.00
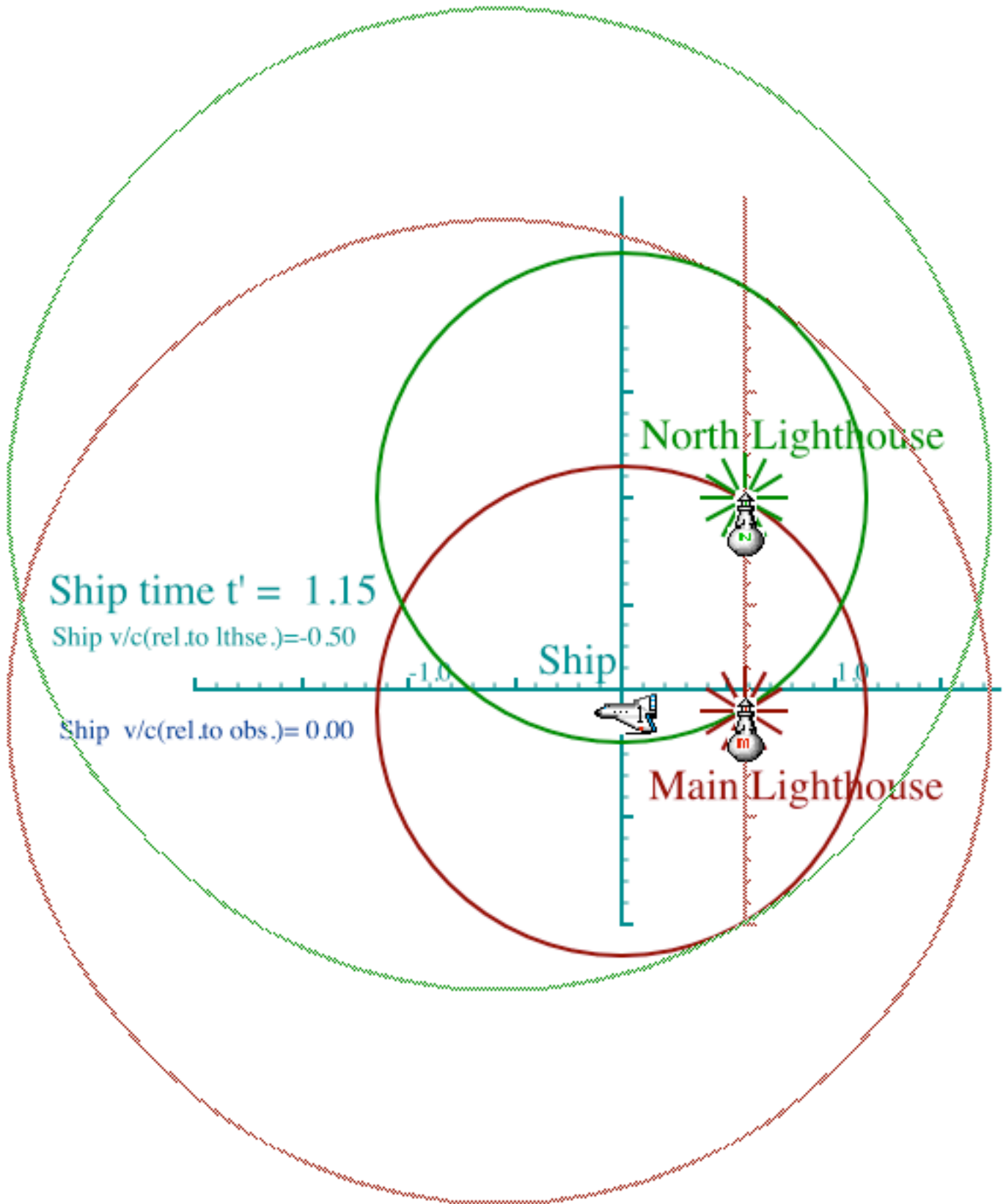
Main Lighthouse

Fig. 2.A.6 Later (t′ =1.15) snapshot from ship's view finally registers the first lighthouse blinks.

Ship time t' = 1.75

0 th blink wave
(From North)

Ship v/c(rel.to lthse.)=-0.50
Ship v/c(rel.to obs.)= 0.00

1st blink wave
(From North)

North Lighthouse

Happening 1
(1st blink wave
from Main hits ship)

-1.0

1.0

Ship

1st blink wave
(From Main)

Main Lighthouse

0 th blink wave
(From Main)
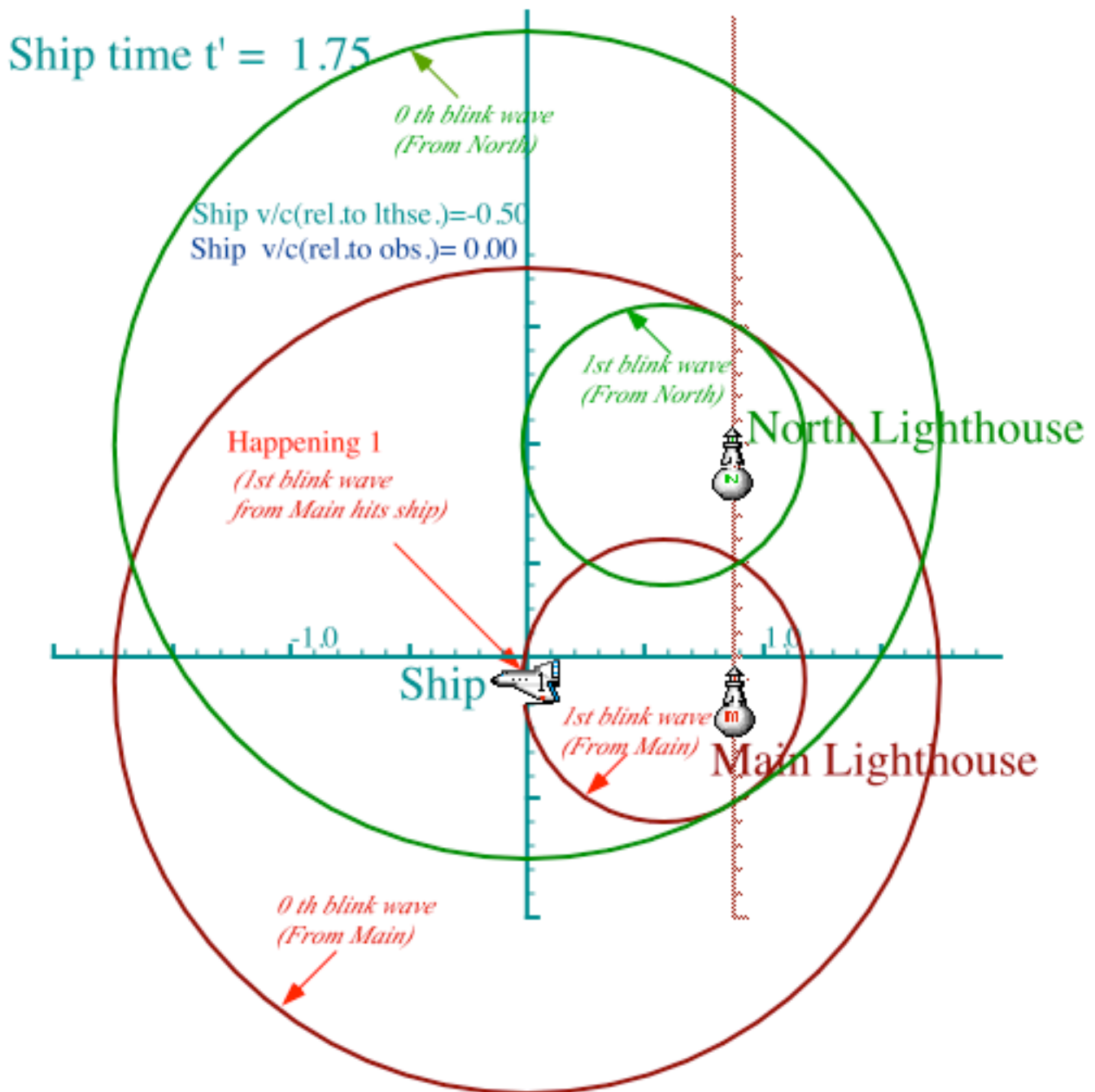
Fig. 2.A.7 Later (t′ =1.75) snapshot from ship's first registers Happening-1.

This shows *Einstein time dilation*. The ship perceives that the lighthouse is running about *15%* late at this speed of *v=c/2*. The next Figs. 2.A.7 and 2.A.8 show something even more surprising to a Newtonian worldview, the *relativity of simultaneity* where, unlike Fig. 2.A.3, *Happening-1* is not simultaneous with *Happening-2*. *Happening-1* (ship hit by 1st blink) happens early at *(t′ =1.75)* and before *Happening-2* (2nd blink) that occurs at *(t′ =2.30)*. (Recall Main cannot blink until a blink from the North hits it so *Happening-2* doesn't happen until *(t′ =2.30)*, or twice the time *(t′ =1.15)* for the first blink as shown in Fig. 2.A.8.)

Ship time t' = 2.30
Ship v/c(rel.to lthse.)=-0.50
Ship v/c(rel.to obs.)= 0.00

North Lighthouse

Happening 2
*(2nd blink happens
at Main Lighthouse)*

-1.0

Ship

1.0

Main Lighthouse
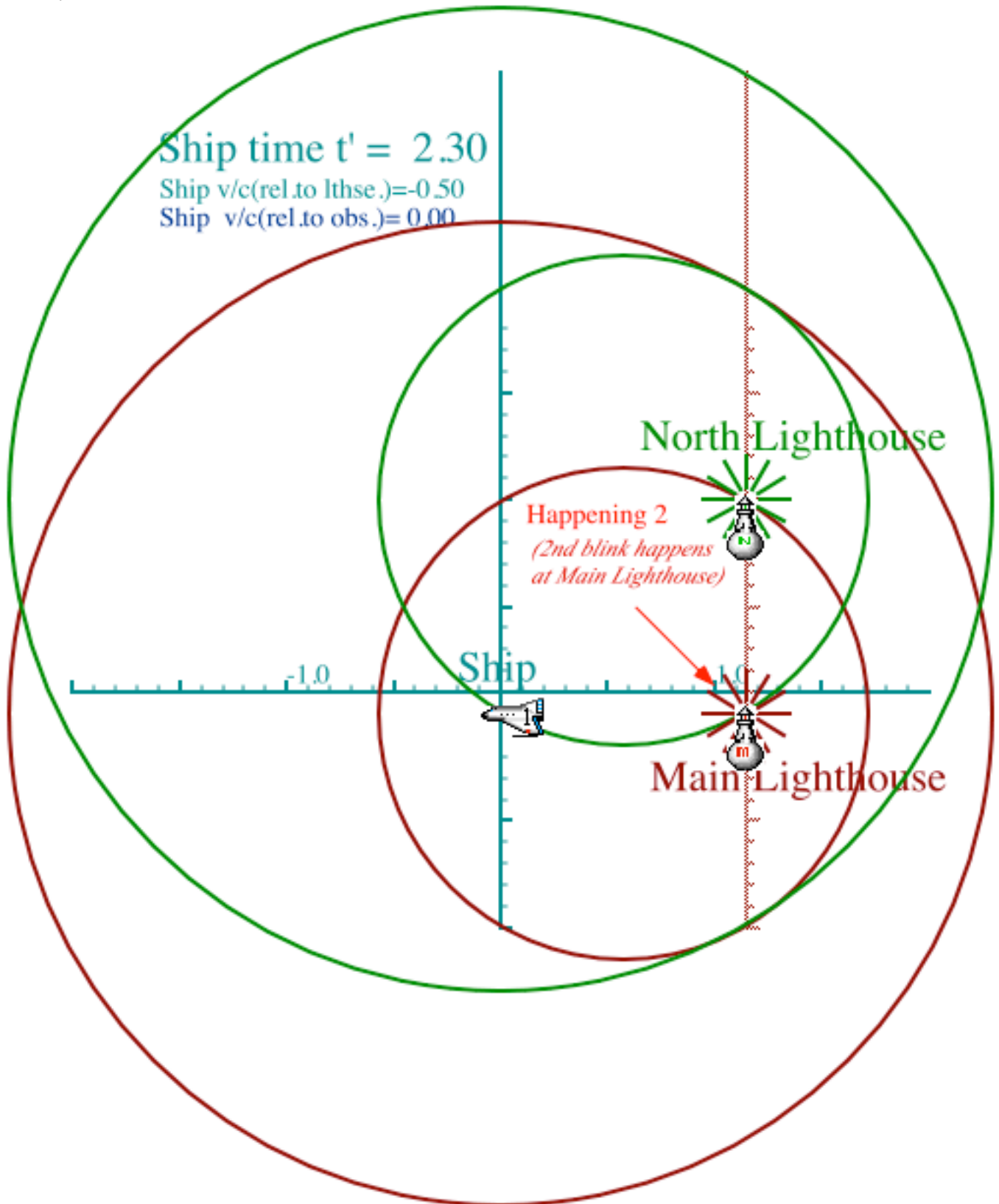
Fig. 2.A.8 Much later (t′ =2.30) snapshot from ship's finally registers Happening-2 .

Einstein time dilation

The time Δ observed between unit-time blinks by a moving ship is called the *Einstein dilation factor* Δ. Its derivation follows from a simple right triangle whose altitude is *c* or one light second as shown in Fig. 2.A.9. The triangle base *v*Δ is the distance traveled by the lighthouse before the North blink wave finally hits it after traveling a distance *c*Δ along the hypotenuse as seen by ship as given here.

$$c^2\Delta^2 = c^2 + v^2\Delta^2 \quad \text{or:} \quad \Delta^2\left(c^2 - v^2\right) = c^2 \quad \text{or:} \quad \Delta = \frac{1}{\sqrt{1 - \dfrac{v^2}{c^2}}} \qquad (2.A.1)$$

Note that the ship or any co-moving ship sees the *c*Δ hypotenuse ray tipped in the direction of travel by the *Stellar aberration angle* ϕ whose sine is sin ϕ = *v/c*. This is *ϕ=60°* for *v/c=1/2* in Fig. 2.A.9 or Fig. 2.A.4.
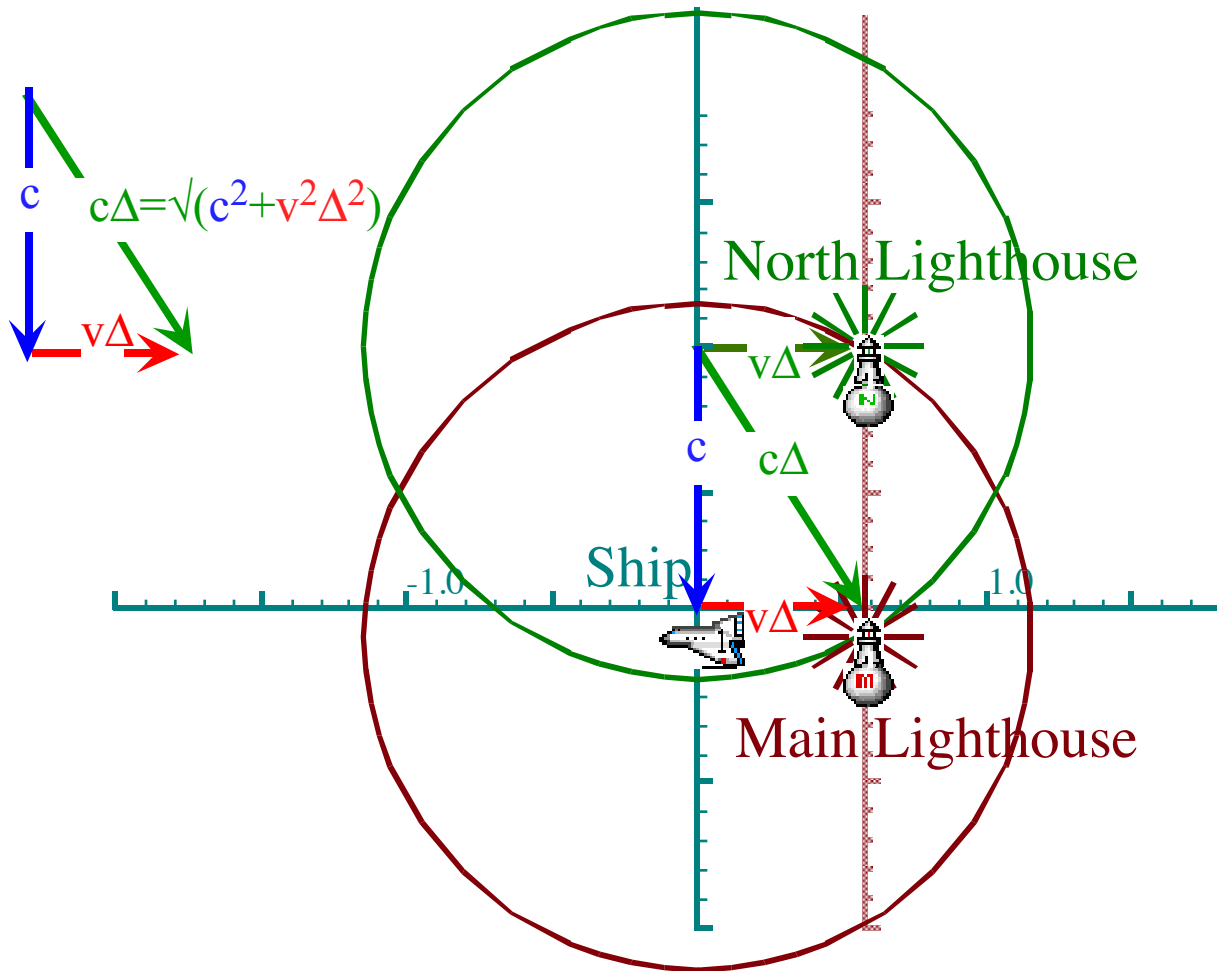
Fig. 2.A.9 Derivation of Einstein time dilation factor Δ or time between blinks .

For the above the lighthouse velocity relative to the ship is *v=c/2*. (2.A.1) gives a time dilation factor of *Δ=1/√0.75 = 1.1547* very close to the *15%* "lateness" in the Fig. 2.A.6 simulation. This lateness grows rapidly and without limit as *v* approaches *c*. For *v=4c/5*, (2.A.1) gives *Δ=5/3 = 1.67* that is a *67%* lateness or *dilation*.

From this we construct an event table to summarize discrepancies or disagreements between space and time coordinates used by the lighthouses and those used by the ship. This is shown below.

Comparing Ship and Lighthouse views: Happening tables

Happening 0: Ship passes Main Lighthouse.	Happening 1: Ship gets hit by first blink from Main Lighthouse.	Happening 2: Main Lighthouse blinks second time.
(Lighthouse space) $x = 0$	$x = -1.00\,c$	$x = 0$
(Lighthouse time) $t = 0$	$t = 2.00$	$t = 2.00$
(Ship space) $x' = 0$	$x' = 0$	$x' = c\,\Delta$
(Ship time) $t' = 0$	$t' = 1.75$	$t' = 2\Delta = 2.30$

One of the most important things to remember about the space coordinate x is that each observer frame *carries its own origin (x=0) with it wherever it goes*. If a 'Happening' happens to the Lighthouse then it happens at $x=0$, but if it happens to the ship then it happens at $x' =0$ no matter what the time is. Remembering this saves lots of confusion! Note also: the table above is for a <u>positive</u> lighthouse velocity: $v=c/2$ relative to the ship. You must always give velocity *as one thing relative to another*. Absolute velocity seems *meaningless* here.

We need a table like the one above for the case of a general velocity v of the lighthouse relative to the ship. (Note that if we base ourselves in the frame in which the ship is stationary then the lighthouse moves with a positive velocity $v=c/2$.) The zero entries stay the same for any value of v. The times for the second blink are $t=2\Delta$ and $t' = 2\Delta$ by definition. Ship's reading for the position of the second blink has to be velocity times travel time or v times 2Δ. ($x' = 2v\Delta$). This becomes $x' = c\Delta$ for $v=c/2$ as entered above.

The coordinates of *Happening 1* (1st blink hits ship) are found. To hit the ship in the lighthouse frame the 1st blink travels a negative distance $-c$ times $(t-1)$ since it doesn't start from $x=0$ until $t=1$. It hits the ship that has gone that distance starting at $t=0$ from the lighthouse. That distance is $-v$ times t.

$$x = -c\,(t-1) = -v\,t\,, \quad \text{or} \quad t = c/(c-v). \qquad (2.A.2)$$

The resulting x and t are entered in the first row under 'Happening 1' in the table below. At this time the ship is located at $x=-vt=-vc/(c-v)$ and that is entered in the table, too.

The lighthouse time for *Happening 1* is based on Fig. 2.A.7. This shows that the 1st blink travels the base of a right triangle that is $v\Delta$ long. It starts at time $t' =\Delta$ and goes at rate c for $(t'-\Delta)$ seconds or

$$v\Delta = c(t'-\Delta). \qquad (2.A.3)$$

Solving for t' gives the last entry $t' = (v+c)\Delta/c=(1+v/c)/\Delta$ in the *Happening 1*-column of the table.

$$(2.A.4)$$

Happening 0: Ship passes Main Lighthouse.	Happening 1: Ship gets hit by first blink from Main Lighthouse.	Happening 2: Main Lighthouse blinks second time.
(Lighthouse space) $x = 0$	$x = -vc/(c-v)$	$x = 0$
(Lighthouse time) $t = 0$	$t = c/(c-v)$	$t = 2.00$
(Ship space) $x' = 0$	$x' = 0$	$x' = 2v\Delta$
(Ship time) $t' = 0$	$t' = (v+c)\Delta/c=(1+v/c)/\Delta$	$t' = 2\Delta$

The last entry $t' = (v+c)\Delta/c=(1+v/c)/\Delta$ in the *Happening 1*-column is the time interval or *period* between hits recorded by the ship as it goes off into the night; the period in this case is *longer* than the BIGANN required blink period of 1 second. On the other hand, before the ship passed the lighthouse it was getting hit in the nose by a fast blink-blink-blink with a *shorter* period than 1 second. The formula for this period found by reversing light velocity c to $-c$ is $t' = (v-c)\Delta/(-c)=(1-v/c)/\Delta$.

Doppler shifts

One failing of standard approaches to relativity involves treatment of *1st order* effects such as Doppler shifts as *2nd* class citizens. The CW approach in Ch. 2 does first things first, but here Doppler is an afterthought.

Fig. 2.A.10 shows that the ship gets hit by blinks a lot more frequently before the lighthouse passes at $t=0$ than after it passes because blink waves are more densely packed in front of the lighthouse than behind it. This frequency down-shift is analogous to what you hear as a car goes by: "..EEEEEEEeooooow..", and is called a *Doppler Shift*. According to blink counters on the ship, the lighthouse period of $\tau_0 = 1$ second LHT (or blink rate of $\nu_0 = 1$ Hz) is increased in period by a factor equal to the ship time $t' = (v+c)\Delta/c=(1+v/c)/\Delta$ for Happening-1, that is, the time the ship sees between blink hits after $t'=0$. The inverse of this is a frequency ν' that is perceived to suffer a *down-shift* or a *red-shift* from the Lighthouse assigned frequency $\nu_0=1/\tau_0$.

$$\begin{array}{ll} \textcolor{red}{\textit{Ship Time}} \\ \textcolor{red}{\textit{between hits}} = t' = \tau_0(v+c)\Delta/c = \tau_0\dfrac{1+\dfrac{v}{c}}{\sqrt{1-\dfrac{v^2}{c^2}}} = \tau_0\sqrt{\dfrac{1+\dfrac{v}{c}}{1-\dfrac{v}{c}}} \;, & \textcolor{red}{\textit{Outbound}} \\ \textcolor{red}{\textit{(outbound)}} & \textcolor{red}{\textit{Observed}} = \nu' = 1/\tau' = \nu_0\sqrt{\dfrac{1-\dfrac{v}{c}}{1+\dfrac{v}{c}}} \quad (2.A.5a) \\ & \textcolor{red}{\textit{Frequency}} \end{array}$$

An inbound ship sees an *Inverse Doppler* or *blue-shift* an *up-shift* or *increase* in frequency to ν'.

$$\begin{array}{ll} \textcolor{blue}{\textit{Ship Time}} \\ \textcolor{blue}{\textit{between hits}} = t' = \tau_0(c-v)\Delta/c = \tau_0\dfrac{1-\dfrac{v}{c}}{\sqrt{1-\dfrac{v^2}{c^2}}} = \tau_0\sqrt{\dfrac{1-\dfrac{v}{c}}{1+\dfrac{v}{c}}} \;, & \textcolor{blue}{\textit{Outbound}} \\ \textcolor{blue}{\textit{(inbound)}} & \textcolor{blue}{\textit{Observed}} = \nu' = 1/\tau' = \nu_0\sqrt{\dfrac{1+\dfrac{v}{c}}{1-\dfrac{v}{c}}} \quad (2.A.5b) \\ & \textcolor{blue}{\textit{Frequency}} \end{array}$$

Again, the difference between "inbound" and "outbound" cases is a matter of sign difference $\pm c$ of velocity of the light perceived by the ship. The two shifts are inverses of each other as required by a time-reversal symmetry that underlies relativity and electromagnetism.

The difference is quite extreme as seen in Fig. 2.A.10(b) that shows the Doppler blink-wave pileup for a relative velocity of $u/c=4/5$. In astronomy and high energy physics the relative velocity has near-c values such as $u/c=0.999\,999\,999$. For these extremes the velocity parameter is replaced by the *rapidity parameter* ρ that is the logarithm $\rho=lnb$ of the Doppler blue-shift $b=e^\rho$. At low speeds rapidity is nearly equal to the velocity u in c units.

$$\rho \sim u/c \quad \text{(for } u<<c\text{)} \qquad (2.A.6)$$

(a) Ship view for *u/c=1/2*

time dilation Δ=2/√3

Ship v/c(rel.to 1thse.)=-0.50

Ship v/c(rel.to obs.)= 0.00

Lthse v/c(rel.to obs.)=0.50

North Lighthouse

Red-shift
factor 1/b=1/√3

Blue-shift
factor b=√3

Ship

-1.0

Lorentz contraction Δ=√3/2

Main Lighthouse

(b) Ship view for *u/c=4/5*

time dilation Δ=5/3

Ship v/c(rel.to 1thse.)=-0.80

Ship v/c(rel.to obs.)= 0.00

Lthse v/c(rel.to obs.)= 0.80

North Lighthouse

Red-shift
factor 1/b=1/3

Blue-shift
factor b=3

Ship

-1.0

Lorentz contraction Δ=3/5

Main Lighthouse

Fig. 4.A.10 Comparison of time dilation, Doppler shifts, and Lorentz contraction. (a) u/c=1/2. (b) u/c=4/5.

Appendix 2.B Lorentz Transformations and Minkowski Space

The disagreeable surveyors

The disagreements seen in Table (2.A.4) are analogous to the ones seen in coordinate rotation. Given a rotated grid such as shown in Fig. 2.B.1 one may relate the "disagreements" between a standard US surveyor and a "tipsy" one that headed straight for the saloon. They only agree on the point *(0,0)* of origin.
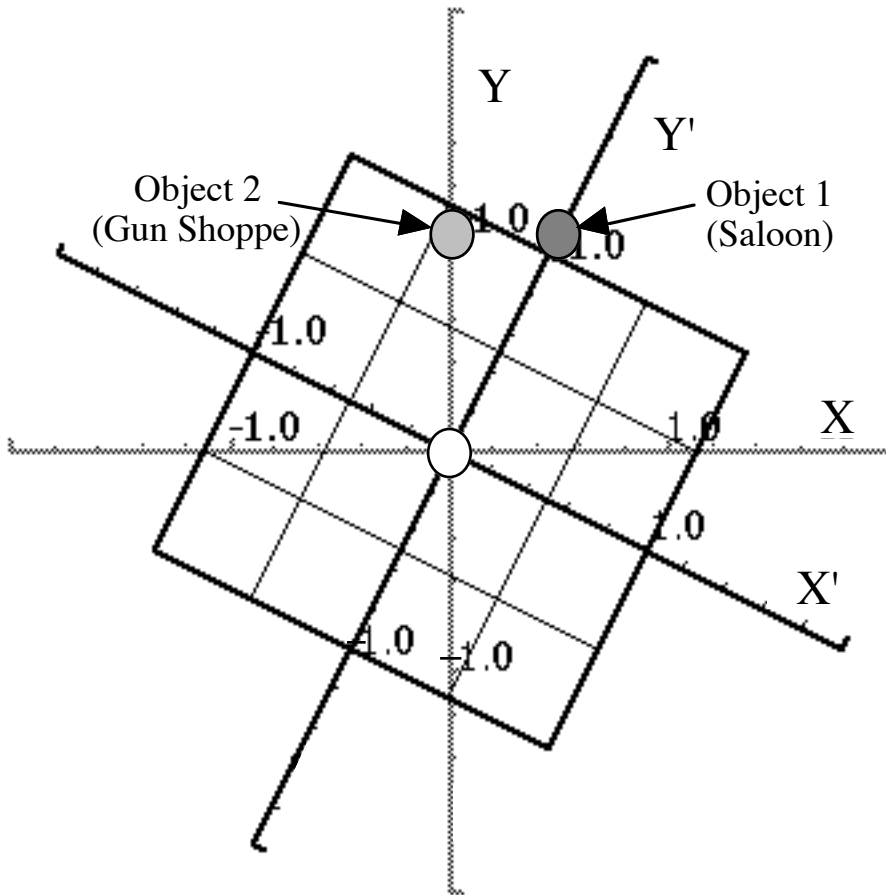
Fig. 2.B.1 Town map according to a "tipsy" surveyor.

Object 0: Town Square.		Object 1: Saloon.		Object 2: Gun Shoppe.	
(US surveyor)	$x = 0$		$x = 0.5$		$x = 0$
	$y = 0$		$y = 1.0$		$y = 1.0$
(2nd surveyor)	$x' = 0$		$x' = 0$		$x' = -0.45$
	$y' = 0$		$y' = 1.1$		$y' = 0.89$

Before the US surveyor heads for the gun shoppe (so he can shoot the "non-standard" surveyor) one needs to defuse a potential argument and write a simple coordinate transformation such as derived in Fig. 2.B.2.

$$x = x' \cos \theta + y' \sin \theta$$
$$y = -x' \sin \theta + y' \cos \theta$$

$$\cos \theta = \frac{1}{\sqrt{1 + \dfrac{b^2}{c^2}}}$$

$$\sin \theta = \frac{b/c}{\sqrt{1 + \dfrac{b^2}{c^2}}}$$
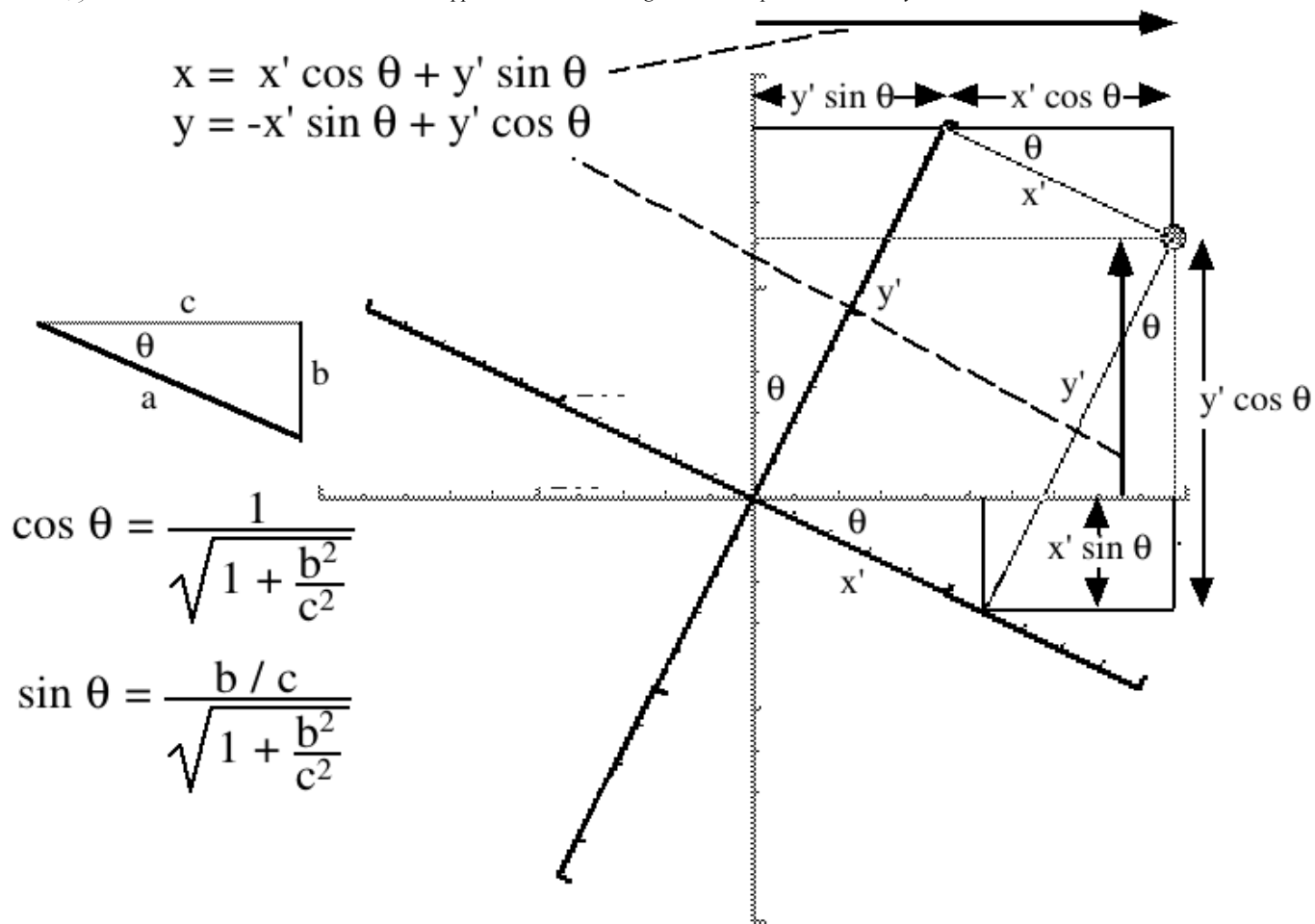
Fig. 2.B.2 Diagram and formulas for reconciliation of the two surveyor's data.

In the notation given above the transformation has a form that is very much like the one we will derive for spacetime. Note that the inverse transform is had by setting angle θ to -θ or slope *(b/c)* to *-(b/c)*.

$$x' = x\cos\theta - y\sin\theta = \frac{x}{\sqrt{1+\frac{b^2}{c^2}}} + \frac{-(b/c)y}{\sqrt{1+\frac{b^2}{c^2}}} \qquad\qquad x = x'\cos\theta + y'\sin\theta = \frac{x'}{\sqrt{1+\frac{b^2}{c^2}}} + \frac{(b/c)y'}{\sqrt{1+\frac{b^2}{c^2}}}$$

$$y' = x\sin\theta + y\cos\theta = \frac{(b/c)x}{\sqrt{1+\frac{b^2}{c^2}}} + \frac{y}{\sqrt{1+\frac{b^2}{c^2}}} \qquad\qquad y = -x'\sin\theta + y'\cos\theta = \frac{-(b/c)x'}{\sqrt{1+\frac{b^2}{c^2}}} + \frac{y'}{\sqrt{1+\frac{b^2}{c^2}}}$$

$$(2.B.1)$$

Remember that a coordinate diagram like Fig. 2.B.2 is a crummy and confusing way to derive this. See Chapter 1 for the better derivations starting from base vectors.

Now we will suppose that the spacetime relations are also a linear transformation.

$$x' = A\,x + B\,ct \qquad\qquad\qquad (2.B.2a)$$
$$ct' = C\,x + D\,ct \qquad\qquad\qquad (2.B.2a)$$

We solve for the unknown linear coefficients *A, B, C,* and *D* using the following table from App. 2.A.

Happening 0: Ship passes Main Lighthouse.	Happening 1: Ship gets hit by first blink from Main Lighthouse.	Happening 2: Main Lighthouse blinks second time.
(Lighthouse space) $x = 0$	$x = -vc/(c-v)$	$x = 0$
(Lighthouse time) $t = 0$	$t = c/(c-v)$	$t = 2.00$
(Ship space) $x' = 0$	$x' = 0$	$x' = 2v\Delta$
(Ship time) $t' = 0$	$t' = (v+c)\Delta/c$	$t' = 2\Delta$

$$(2.A.4)_{repeated}$$

To do this we stick in the values of *(x',ct')* and *(x,ct)* from the Happening Table. For Happening 1 we have

$$A\,x + B\,ct = x' , \qquad \text{or} \qquad A(-vc/(c-v)) + Bc(c/(c-v)) = 0 \;, or\; A = Bc/v \qquad (2.B.3a)$$
$$C\,x + D\,ct = ct' , \qquad \text{or} \qquad C(-vc/(c-v)) + Dc(c/(c-v)) = c\Delta(v+c)/c \;, \qquad (2.B.3b)$$

and for Happening 2 we have

$$A\,x + B\,ct = x' , \qquad \text{or} \qquad A(0) + Bc(2) = 2v\Delta \;, \qquad (2.B.4a)$$
$$C\,x + D\,ct = ct' , \qquad \text{or} \qquad C(0) + Dc(2) = 2c\Delta \;. \qquad (2.B.4b)$$

The last two equations immediately give $B=v\Delta/c$ and $D =\Delta$ where you should recall from (2.A.1) that the quantity $\Delta=1/\sqrt{(1-v^2/c^2)}$ is the blink time interval according to the ship. Put these values of B and D back into (2.B.3a-b) to derive $A = \Delta$ and $C= v\Delta/c$. This gives a general formula for converting lighthouse coordinates *(x,ct)* into ship coordinates *(x',ct')* or *vice-versa*. It is the *Lorentz Transformation* for speed v and *rapidity* ρ.

$$x' = \frac{x}{\sqrt{1-\frac{v^2}{c^2}}} + \frac{\frac{v}{c}ct}{\sqrt{1-\frac{v^2}{c^2}}} = x\cosh\rho + y\sinh\rho \qquad\qquad x = \frac{x'}{\sqrt{1-\frac{v^2}{c^2}}} - \frac{\frac{v}{c}ct'}{\sqrt{1-\frac{v^2}{c^2}}} = x'\cosh\rho - ct'\sinh\rho$$

$$(2.B.5a) \qquad\qquad\qquad\qquad\qquad\qquad (2.B.5b)$$

$$ct' = \frac{\frac{v}{c}x}{\sqrt{1-\frac{v^2}{c^2}}} + \frac{ct}{\sqrt{1-\frac{v^2}{c^2}}} = x\sinh\rho + y\cosh\rho \qquad\qquad ct = \frac{-\frac{v}{c}x'}{\sqrt{1-\frac{v^2}{c^2}}} + \frac{ct'}{\sqrt{1-\frac{v^2}{c^2}}} = -x'\sinh\rho + ct'\cosh\rho$$

To go 'backwards' like (2.B.5b) you only have to switch the sign of velocity v. The use of hyperbolic functions of rapidity $\rho=lnb$ will be explained shortly. For now note that $\cosh^2\rho - \sinh^2\rho = 1$ is satisfied by the A, B, C, and D, that is, $A^2-B^2 = 1$ and $D^2-C^2 = 1$ for all relative speeds $v =c\,\tanh\rho$.

In order to visualize and understand relativity it helps a great deal to plot these transformation equations as coordinate grids. The results are called *Minkowski coordinates* after a Polish mathematicians who happened also to be one of Einstein's math teachers. (It is interesting to note that Einstein himself resisted using these graphs, indeed his papers have precious few figures of any kind.) As seen in Fig. 2.B. 3 the Minkowski grids are actually quite striking but not quite as easy to grasp as those of a real rotation.
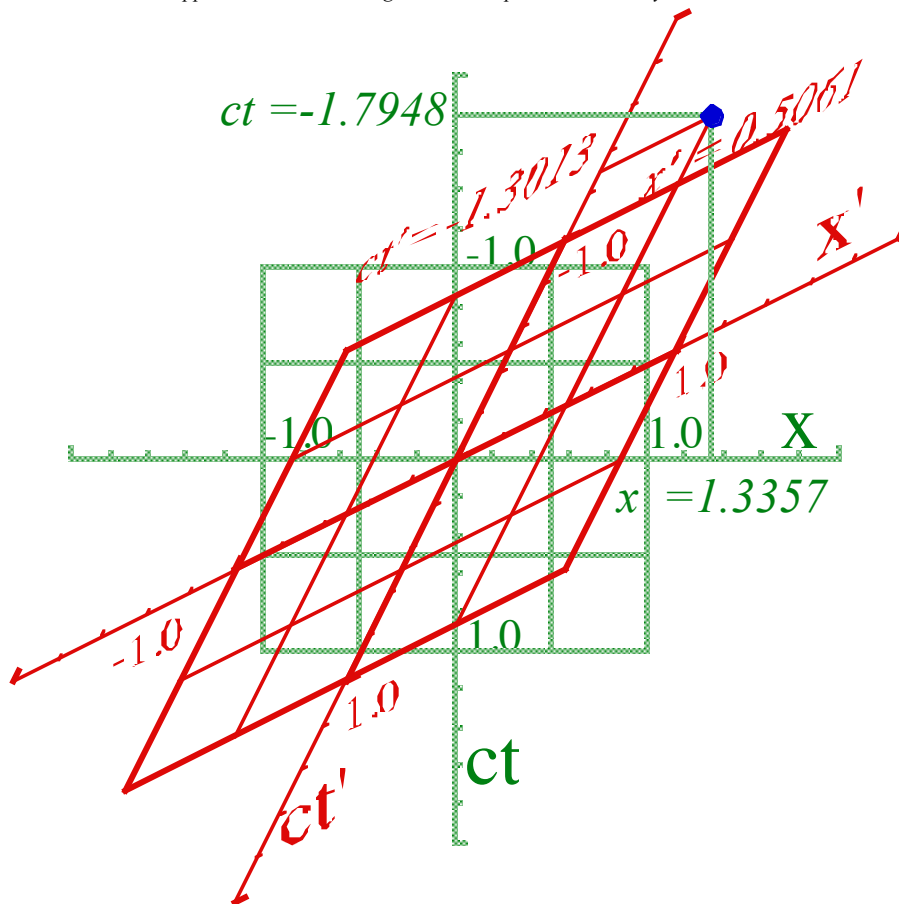
Fig. 2.B.3 Minkowski coordinates (x', ct') for ship going v=-c/2 relative to Lighthouse (x, ct) .

Note that the positive time or <u>future</u>, is <u>down</u> in these graphs. This is the classic *Newtonian convention* in which one plots an *x*-ordinate versus a *t*-abscissa. Note that the *(x′, ct′)* graph gets squeezed relative to the stationary *(x, ct)* graph. The resulting slope of the *ct′* axis is equal to the velocity in *c*-units, that is *v/c*. In this case that slope is *v/c =-1/2*.

This Newtonian slope-to-velocity relation happens because the *ct′* axis is the track of the origin *(x′=0)* of the ship, that is, its *space-time trajectory* or *world line*. As we will see, this slope *v/c* is equal to the hyperbolic tangent *tanh* ρ. However, ρ is called *rapidity* and is not an angle, but an area as will be shown.

A geometric interpretation of Lorentz transformations uses *invariants* of the transformations, functions whose numerical values are unchanged by it so the two protagonists agree on them. In Fig. 2.B. 4 we compare the circular invariants of the rotated surveyors with hyperbolic ones of the ship and lighthouse.

The surveyors agree on the distance from town center or origin, that is, the <u>sum</u> of squares of coordinates *(x²+y² = x′²+y′²)*. The ship and light houses agree on <u>difference</u> of squares of coordinates *(x²-ct² = x′²-ct′²)* that is, the speed of light *c*. Expanding circles of blink waves trace out cones in space-time as in Fig. 2.B.5. Their *(x,ct)* cross-section are hyperbolic conic sections called *light-cone* sections.

(a) Rotation Transformation and Invariants

$x = 1.65$

$y = -0.85$

$x^2 + y^2 = 3.43$

$x' = 1.00$

$y' = -1.56$

$x'^2 + y'^2 = 3.43$
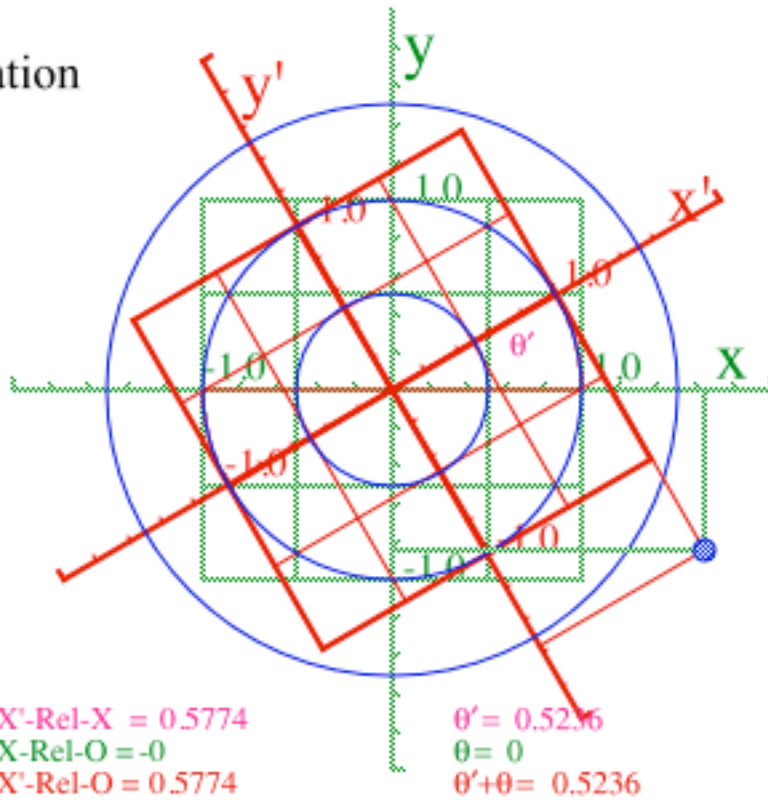
SlopeX'-Rel-X = 0.5774
SlopeX-Rel-O = -0
SlopeX'-Rel-O = 0.5774

$\theta' = 0.5236$
$\theta = 0$
$\theta' + \theta = 0.5236$

(b) Lorentz Transformation and Invariants

$x = 1.5453$

$ct = 0.9819$

$x^2 - (ct)^2 = 1.42$

$x' = 2.3512$

$ct' = 2.0260$

$x'^2 - (ct')^2 = 1.42$
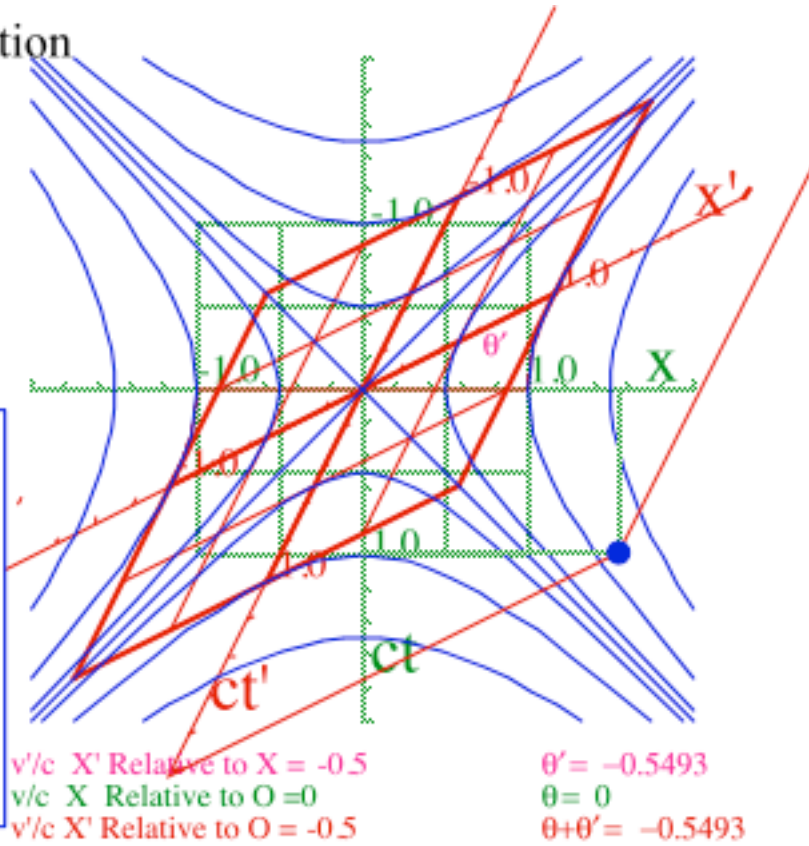
v'/c X' Relative to X = -0.5
v/c X Relative to O = 0
v'/c X' Relative to O = -0.5

$\theta' = -0.5493$
$\theta = 0$
$\theta + \theta' = -0.5493$

Fig. 2.B.4 Comparison of invariants (a) Rotation invariants are circles. (b) Lorentz invariants are hyperbolas.

Fig. 2.B.5 below is a plot of the North Lighthouse blink waves in *{x, y, ct}* coordinates. Blinks emitted at *t= -1/2, t=0*, and *t=+1/2* seconds trace three concentric *light cones* around the track or *world line* of the North Lighthouse. All observers will see the same cones. They are invariant to one's space-time viewpoint.
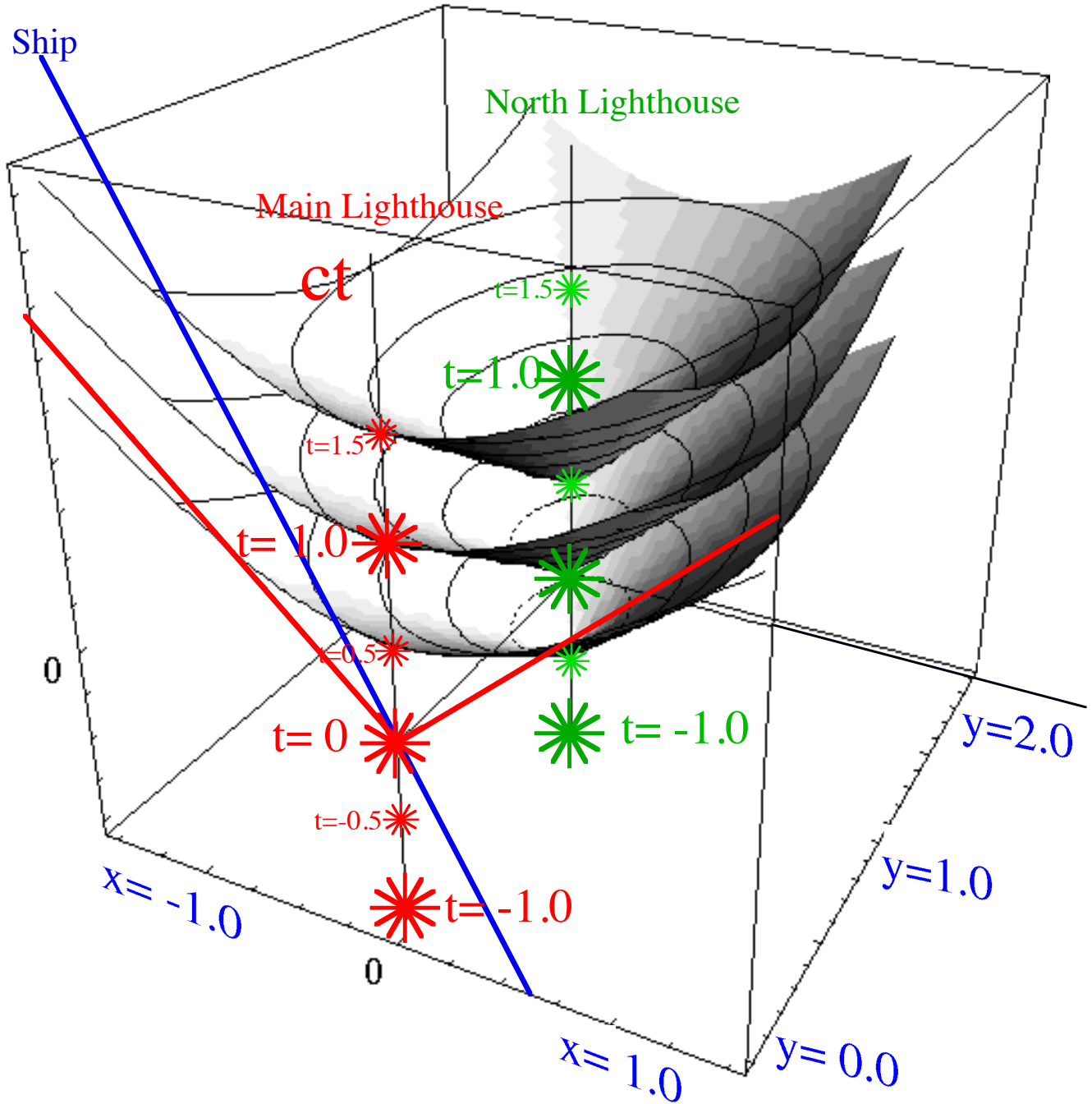
Fig. 2.B.5 Space-Space-Time plot of world lines for Lighthouses. North Lighthouse blink waves trace light cones.

Hyperbolic trigonometry

We are used to circular invariants and circular functions like sine and cosine that go with Cartesian rotation and elementary geometry and trigonometry. Relativistic Lorentz rotations have the transformation equations (2.B.5) in terms of <u>hyperbolic</u> functions sinhρ and coshρ. Invert these relations to get the 'angle' θ=ρ in terms of velocity where *rapidity* ρ is the logarithm of Doppler blue-shift factor in (2.A.5b).

$$\cosh\rho + \sinh\rho = e^{\rho} = \frac{1+\dfrac{v}{c}}{\sqrt{1-\dfrac{v^2}{c^2}}} = \sqrt{\frac{1+\dfrac{v}{c}}{1-\dfrac{v}{c}}}, \qquad \text{or:} \qquad \rho = \ln\sqrt{\frac{1+\dfrac{v}{c}}{1-\dfrac{v}{c}}} \qquad (2.B.6)$$

It turns out that the quantity θ=ρ is not an angle at all but an <u>area</u>. It is the gray area in Fig. 2.B.6 enclosed by the unit hyperbolic invariant $x^2 - (ct)^2 = 1$ and the two *x* and *x′* axes. To calculate this area we form a triangle of base $x=\cosh\theta$ and altitude $y=\sinh\theta$ which contains the area as shown below.

$y/x=\tanh\theta = v/c$

$y=\sinh\theta$
$x=\cosh\theta$
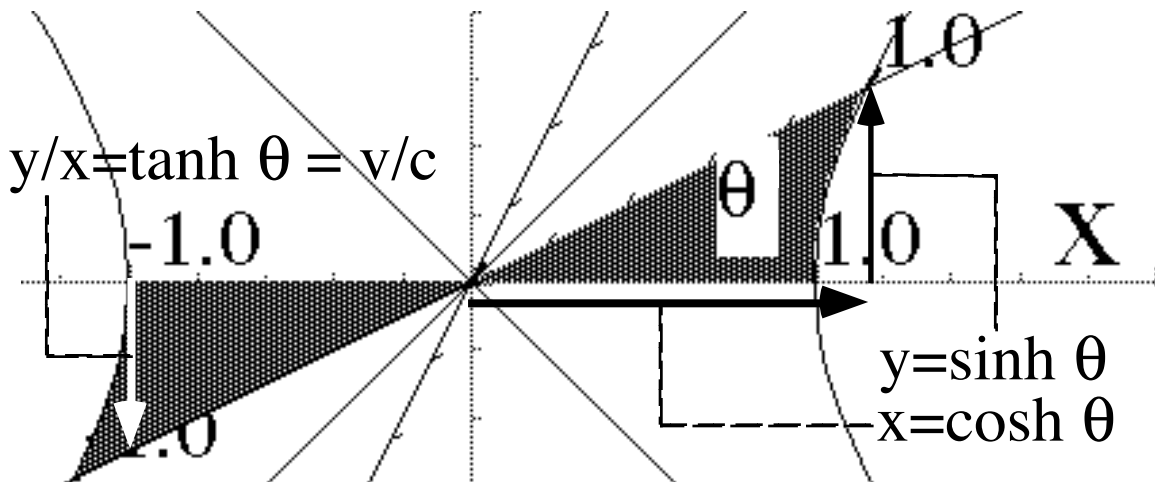
Fig. 2.B.6 Hyperbolic angle-area θ=ρ for unit hyperbola x²-(ct)²=1=cosh²θ - sinh²θ.

Note that the length of the tangent line between axes is the hyperbolic tangent *tanh θ =sinh θ/cosh θ*.

The desired area is found by subtracting the area under the hyperbola from that of the triangle. This will give us one-half of the gray area shown in the figure. Then *d(coshθ) = sinhθ dθ* is used.

$$\frac{Area}{2} = \frac{1}{2}base \cdot altitude - \text{area under curve} = \frac{1}{2}xy - \int y\,dx$$

$$\frac{Area}{2} = \frac{1}{2}\sinh\theta\cosh\theta - \int\sinh\theta\,d(\cosh\theta) \qquad (2.B.7)$$

$$\sinh^2\theta = \left(\frac{e^{\theta}-e^{-\theta}}{2}\right)^2 = \frac{1}{4}\left(e^{2\theta}+e^{-2\theta}-2\right) = \frac{\cosh 2\theta - 1}{2} \qquad (2.B.8)$$

$$\sinh\theta\cosh\theta = \left(\frac{e^{\theta}-e^{-\theta}}{2}\right)\left(\frac{e^{\theta}+e^{-\theta}}{2}\right) = \frac{1}{4}\left(e^{2\theta}-e^{-2\theta}\right) = \frac{1}{2}\sinh 2\theta \qquad (2.B.9)$$

This gives the gray area between hyperbolas subtended by radii.

$$\frac{Area}{2} = \frac{1}{2}\sinh\theta\cosh\theta - \int\sinh^2\theta\, d\theta = \frac{1}{4}\sinh 2\theta - \int\frac{\cosh 2\theta - 1}{2}\, d\theta$$

Using $\int\cosh a\theta\, d\theta = \frac{1}{a}\sinh a\theta$ we derive that the total gray area in Fig. 2.B.6 is equal to $\theta=\rho$.

$$Area = \theta = \rho \tag{2.B.10}$$

Note that the relativistic slope or velocity parameter $\beta=v/c$ is the hyperbolic tangent of this area.

$$\beta = \frac{v}{c} = \frac{\sinh\rho}{\cosh\rho} = \tanh\rho \tag{2.B.11}$$

Adding relativistic velocities and angles

Suppose, as before, that the ship has a velocity relative to the lighthouse that is half that of light, that is $v'=c/2$. Now suppose there is an observer that sees the lighthouse going at a velocity of $c/2$. What will that observer see for the velocity of the ship? Simply added the two velocities gives *0.5c + 0.5c = c*.

However, it does not work that way. As with the space-space tipping transformations *we need to add angles not slopes*. Consider the plot shown in Fig. 2.B.6 below. The figure shows angle-areas being added to give the correct total area of $\theta + \theta' = $ *0.5493 + 0.5493 = 1.0986*. The $\theta=\rho$ are obtained from the hyperbolic tangent relation (2.B.11). $\theta = tanh^{-1}(v/c) = tanh^{-1}(0.5) = 0.5493$. The hyperbolic tangent of the sum is correct: *tanh(1.0986) = 0.8*. The observer sees the ship going at *0.8c* or *4/5* of lightspeed.

A quick way to do relativistic velocity addition is to use the angle addition identity for the hyperbolic tangent. It is similar to the identity for the circular tangent.

$$\tanh(x + y) = \frac{\tanh x + \tanh y}{1 + \tanh x \tanh y} \tag{2.B.12}$$

Since the relative velocity ratio u/c is the hyperbolic tangent of the relative angle θ_u the identity gives:

$$\frac{u'}{c} = \tanh(\theta_u + \theta_v) = \frac{\tanh\theta_u + \tanh\theta_v}{1 + \tanh\theta_u \tanh\theta_v} = \frac{\dfrac{u}{c} + \dfrac{v}{c}}{1 + \dfrac{u}{c}\dfrac{v}{c}} \tag{2.B.13}$$

This is the standard *relativistic velocity addition formula*.

$$u' = \frac{u + v}{1 + \dfrac{uv}{c^2}} \tag{2.B.14}$$

This is the same result as our previous calculation which added *u=c/2* and *v=c/2* to get *0.8c*.

$$u' = \frac{\dfrac{c}{2} + \dfrac{c}{2}}{1 + \dfrac{1}{4}} = \frac{c}{\dfrac{5}{4}} = \frac{4c}{5} \tag{2.B.14}_{example}$$

The *rapidity addition formula* and its related *Doppler multiplication formula* are simpler to use.

$$\rho(u') = \rho(u) + \rho(v) \quad \text{(2.B.15a)} \qquad e^{\rho(u')} = b(u') = b(u)\cdot b(v) = e^{\rho(u)+\rho(v)} \quad \text{(2.B.15b)}$$

Relativity and quantum theory are fundamentally geometric or multiplicative scaling processes.

v'/c X' Relative to X = 0.5 $\theta' = 0.5493$
v/c X Relative to O = 0.5 $\theta = 0.5493$
v'/c X' Relative to O = 0.8 $\theta + \theta' = 1.0986$
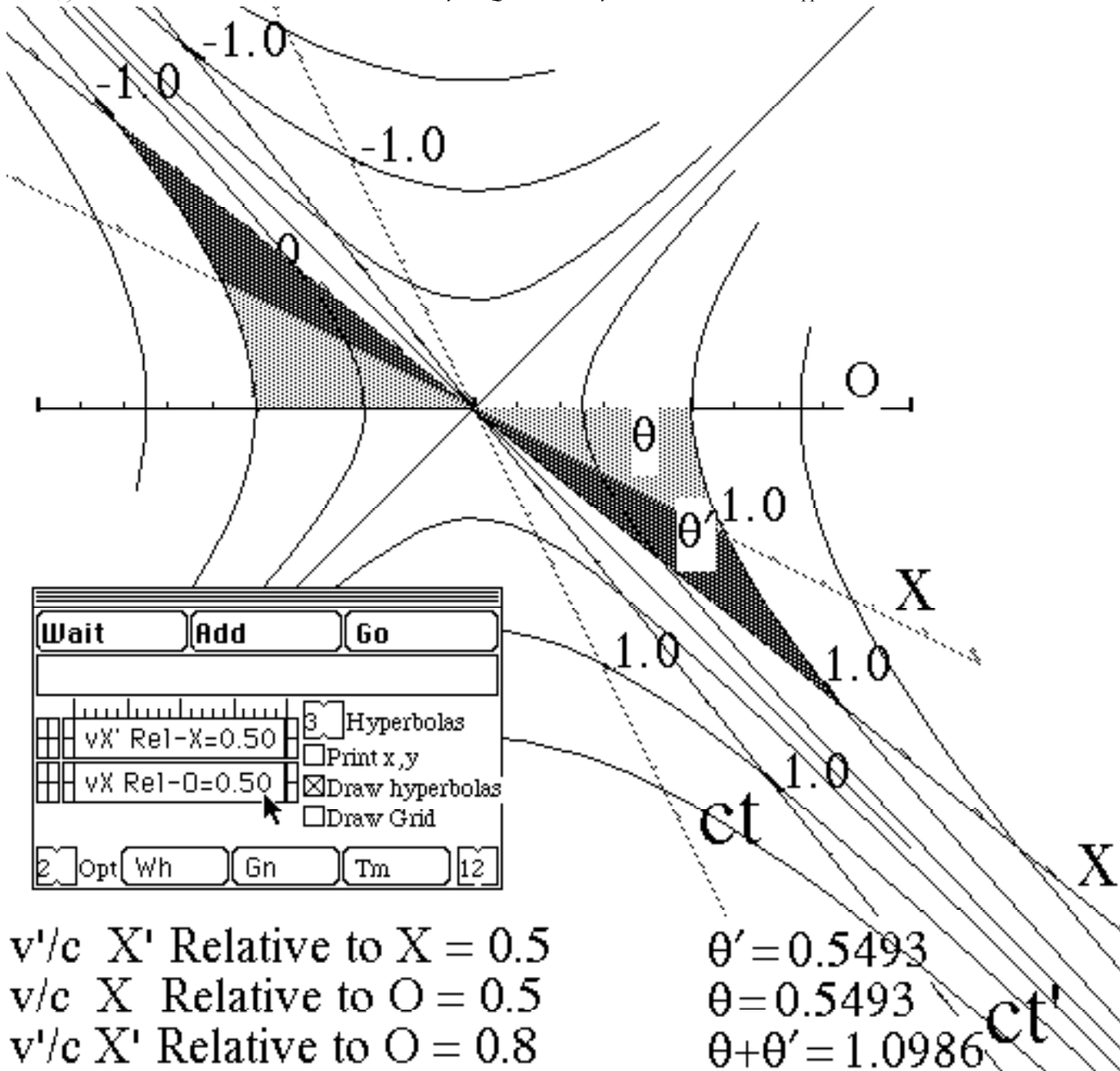
Fig. 2.B.7 Coordinate axis X' tipped by $\theta' = 0.549$ *relative to X-axis which in turn is tipped by* $\theta = 0.549$ *relative to O-axis.*

As you add more and more hyperbolic angle area you approach the speed of light. But there is an infinite amount of angle-area under the hyperbola. No matter how much more speed you add you will never get any closer to the speed *c* of light. It is like a horizon. You can approach it but never cross it.

Minkowski graphs of relativistic effects

Spacetime graphs such as Fig. 2.B.8 show Doppler effects and more. The blink wave paths are the ±45° lines intersecting at blink times of *t*= ...-1.0, 0.0, 1.0, 2.0,...sec. In the upper portion of Fig. 2.B.8 the blink waves from the main lighthouse are seen crossing the ship path, that is the *ct'*-axis or *x'=0*, every half second or so before the ship passes the lighthouse at *t=0=t'*. To be precise, the crossing time is √0.5/ √1.5=0.577 sec. according to Doppler blue-shift formula (2.A.5). But, after passage it's not until *t' = 1.73*

that the ship encounters another blink hit. This is the red-shift crossing time of $t' = \sqrt{1.5}/\sqrt{0.5} = \sqrt{3} = 1.732$ *sec.* The lighthouse claims the first hit (Happening 1) occurs at $t=2$ according its clocks, the same time as its second blink (*Happening 2*). This lighthouse moment of $t=2$ has a p<u>ast</u> ($t<2$ indicated by gray area) and a <u>future</u> ($t>2$ is the white area below the $t=2$ line.) The $t=2$ line is the space-time location of the lighthouse x-axis or "now-line" at this moment. The ship and lighthouse icons are a little misleading. A 3-dimensional object cannot be really drawn on one spatial dimension. Also, note that the North lighthouse lies above (or below, depending on convention) the page containing the Main lighthouse in Fig. 2.B.8. This was sketched in Fig. 2.B.5.
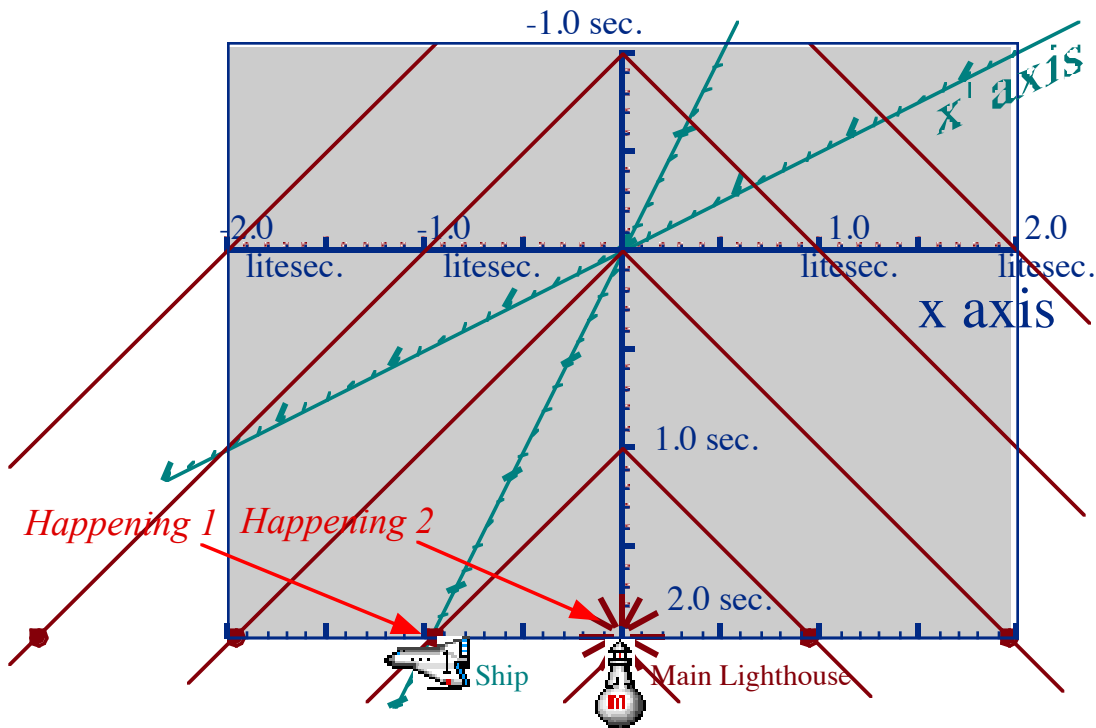
Fig. 2.B.8 Spacetime graph of ship passing lighthouse. (Lighthouse moment t=2 indicated.)

The ship draws its moments differently as seen in Fig. 2.B.9. Here the moment of *Happening 1* is indicated by the ship x'-axis at the moment $t' = 1.732$ *sec.* This ship moment of $t' = \sqrt{3}$ has a p<u>ast</u> ($t' < \sqrt{3}$ indicated by gray area) and a <u>future</u> ($t' > \sqrt{3}$ is the white area below the $t' = \sqrt{3}$ line.) Note that the ship's past overlaps with the lighthouse future in the leftward direction to which it is traveling, while behind the ship, the lighthouse has regions of its past that correspond to the ship's future. Very strange!

These graphs show why the ship does not regard *Happening 1* and *Happening* 2 to be simultaneous in the way that the lighthouse does. As far as the ship is concerned, points behind it belong to a lighthouse past, and so a 2nd blink (*Happening 2*) will come later, in fact not until $t' = 2.3$ *sec.*
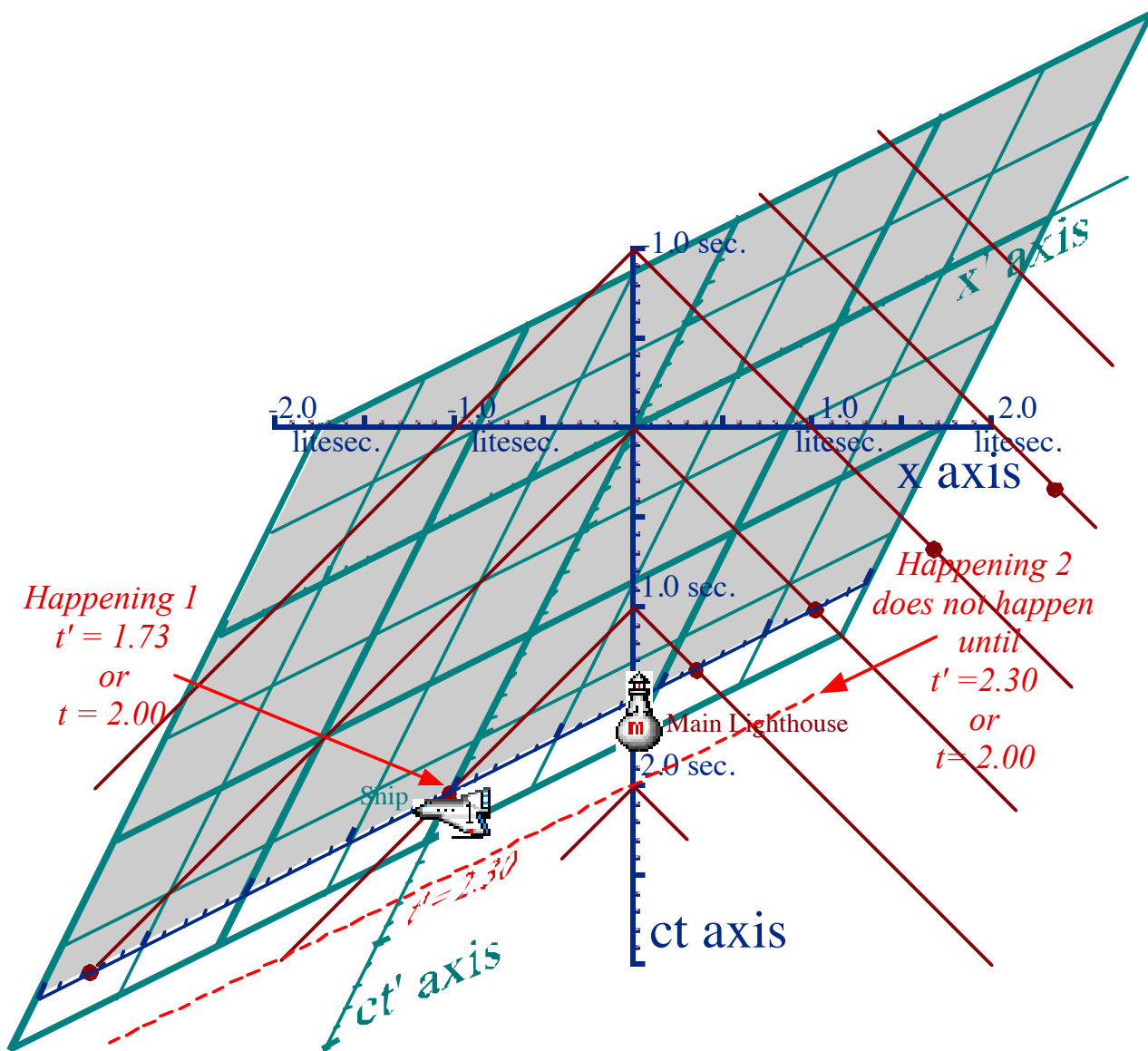
Fig. 2.B.9 Spacetime graph of ship passing lighthouse. (Ship moment t'=1.73 indicated.)

A ship or any observer moving with positive velocity relative to the lighthouse (that is, left to right) will record an opposite time order for *Happening 1* and 2. For such a reference frame, *Happening 2* will come <u>before</u> *Happening 1* since its *x*-axis will tip down to the right in Fig. 2.B.9. This event reversal could present a serious philosophical conundrum if, for example, *Happening 1* caused *Happening 2*. Generally, we prefer causes to precede effects, and this is known as the *causality principle*. Violations of causality are regarded with the same suspicion reserved for violation of energy conservation or the 2nd Law of Thermodynamics. Such violations are tolerated in microscopic quantum fluctuations but not in macroscopic classical averages.

For Happening 1 to actually <u>cause</u> Happening 2, it must send some kind of message, particle, or "force" at a speed greater than light. If a "cause" or particle goes from 1 to 2 it must cut across the light cone!

After Fig. 2.B.7 we noted that hyperbolic asymptotes or light cones were like horizons that one could approach indefinitely but should not expect to cross. This light barrier is considerably more serious than the so-called "sound-barrier." It cannot be broken by ordinary matter by simply having the "right-stuff." Anything that crosses the barrier however briefly pays a great price; it will be seen by many observers to be located at three or more places at one time! Doing this involves (possibly painful) annihilations and recreations as shown below.

Consider a case where Happening 1 comes just a little earlier than Happening 2 as shown in Fig. 2.B.10 so that faster-than-light travel is required to connect or "cause" the second Happening. Then the Ship's view of this is pretty strange as seen in Fig. 2.B.11 where *Happening 2* occurs <u>before</u> *Happening 1*. Any "cause" connecting the two has to go "backwards-in-time." The lighthouse sees the causative particle shown in Fig. 2.B.10 ride down to *Happening 1* then leap faster-than-light to *Happening-2* but the ship finds it at three places during the time between *Happening 2* and *Happening 1* in Fig. 2.B.11. It is as though a particle-anti-particle pair is created at Happening 2 and the anti-particle is annihilated at Happening 1!
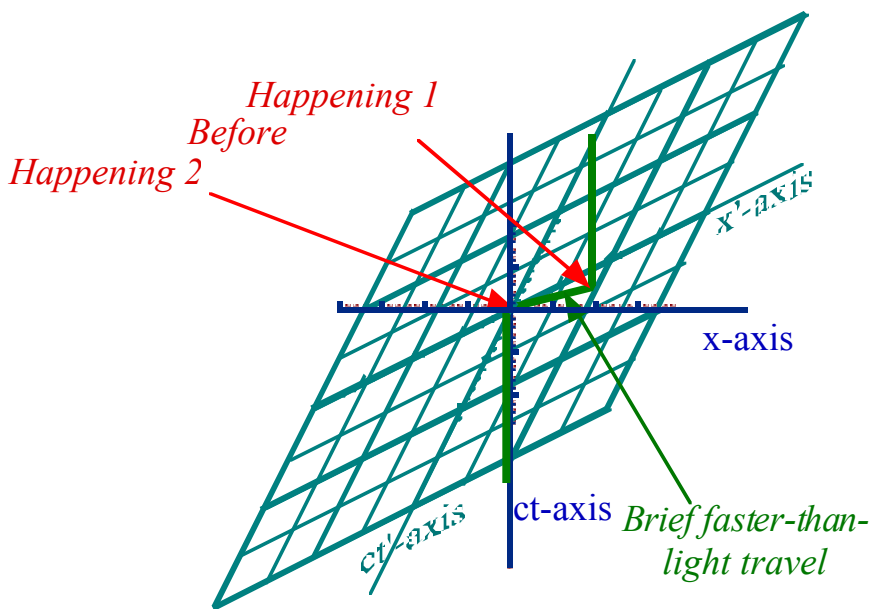
Fig. 2.B.10 Lighthouse plot of Happenings
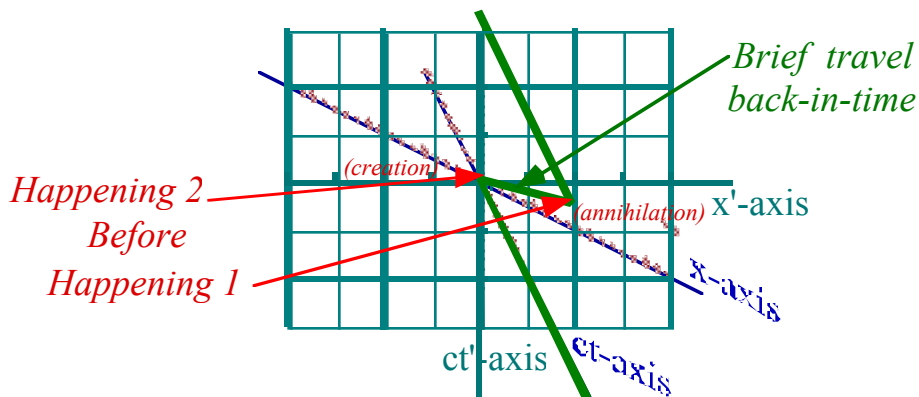
Fig. 2.B.11 Ship plot of two Happenings

Appendix 2.C Measures of velocity: Relativistic speedometers

Physical and geometric indicators of relative velocity mentioned in Sec. 2.A include Doppler shift *b*, slope *u/c* in space-time, rapidity ρ, and stellar aberration angle ϕ. Some of these are indicated in Fig. 2.C.1. The angle ρ°=tan⁻¹(*u/c*) of slope *u/c* that we will call "rho-oh" is totally non-standard, however, the hyperbolic quantity ρ=tanh⁻¹(*u/c*) known as *rapidity* is quite important as is the stellar aberration angle ϕ=sin⁻¹(*u/c*).

$$\rho=\tanh^{-1}(u/c) \quad (2.C.1) \qquad \rho°=\tan^{-1}(u/c) \quad (2.C.2) \qquad \phi=\sin^{-1}(u/c) \quad (2.C.3)$$

These might be called, respectively, the Minkowski angle ρ, the Einstein angle ρ°, and the Epstein angle ϕ, the latter named after the inventor of the *cosmic speedometer*, Lewis Carroll Epstein, author of a uniquely interesting approach to relativity entitled *Relativity Revisited* (Insight Press, San Francisco 1978). The Epstein angle is the angle one must tip a moving telescope to catch vertically falling starlight in the star-fixed inertial frame. Known as the stellar aberration angle long before Epstein came along, it is one of the first-order effects of velocity in the theory of special relativity. For Newtonian speeds (*u<<c*) these angles nearly equal and tiny.

$$\rho \sim \rho° \sim \phi \sim u/c \ \text{ for } (u<<c) \qquad\qquad (2.C.4)$$

Their behavior at higher speeds is quite different as shown in Fig. 2.C.1(a) where the 2nd order effects such as Einstein time dilation (Fig. 2.C.1(b)) and Lorentz contraction (Fig. 2.C.1(c)) become significant. As shown in Fig. 2.C.1 (a) the Epstein angle ϕ is found by dropping a vertical perpendicular from the (*u/c*)-point on the line defining the Einstein angle ρ° or Minkowski world line of *rapidity* ρ on the unit horizon tangent to the unit circle. The lower line has an angle ϕ that is greater than ρ° and is that of a starlight path.

Extending that starlight path back to the unit horizon begins the construction of the quantity coshρ that is the *Einstein dilation factor* coshρ in Fig. 2.C.1 (b) found where a vertical from the horizon intersection of the star-path ϕ-line hits the original ρ°-line. A lower horizon where the vertical perpendicular from the (*u/c*)-point hits the unit circle is the inverse *Lorentz contraction factor* sechρ shown in Fig. 2.C.1(c).

Each of these is a 2nd order effect, that is, they first vary as the square of rapidity or velocity.

$$\cosh\rho = 1+\frac{\rho^2}{2}+... \quad (2.C.5a) \qquad \text{sech}\,\rho = \frac{1}{\cosh\rho}=1-\frac{\rho^2}{2}+... \quad (2.C.5b)$$

The functions sinhρ and tanhρ are linear at first and are thus called 1st order variant.

$$\sinh\rho = \rho+... \quad (2.C.6a) \qquad\qquad \frac{u}{c}=\tanh\rho=\rho+... \quad (2.C.6b)$$

The 1st order functions of primary importance are the Doppler shift exponentials.

Blue shift: $e^\rho = 1+\rho+...$ (2.C.7a)   *Red shift:* $e^{-\rho}=1-\rho+...$ (2.C.7b)

The Doppler values are constructed in Fig. 2.C.1(d) along with the Minkowski grids and the hyperbolic invariant curves. This construction is based upon the geometry of both the circle and the hyperbola together. This all-important geometry is discussed using a following Fig. 2.C.2 and Fig. 2.C.3.

(a) Velocity parameters

Minkowski angle: $\rho = tanh^{-1}(u/c)$
(Rapidity or hyper-area)

Einstein angle: $\rho° = tan^{-1}(u/c)$
(Space-time path slope)

Epstein angle: $\phi = sin^{-1}(u/c)$
(Stellar aberration slope)

$\rho°$

ϕ

Lightcone angle=$\pi/4$

1

1

(b) Einstein time dilation

$cosh\ \rho$

$sinh\ \rho$

$cosh\ \rho$

$(u/c)cosh\ \rho = sinh\ \rho$

(u/c)

1

1

$\sqrt{1 - \dfrac{u^2}{c^2}}$

1

$cosh\ \rho$

(c) Lorentz length contraction

$cosh\ \rho$

(u/c)

1

$sech\ \rho$

$\sqrt{1 - \dfrac{u^2}{c^2}}$

$sech\ \rho$ 1 $cosh\ \rho$

(d) Minkowski *grids*, Doppler *shifts*, and *hyper-invariants*

$e^{+\rho}/2$ $e^{+\rho}/2$

$e^{+\rho}$

$cosh\ \rho$

$(u/c)cosh\ \rho = sinh\ \rho$ e^{ρ}

$cosh\ \rho$

(u/c)

1

$sech\ \rho$

$cosh\ \rho$

Euclid-mean circle

e^{ρ}

$e^{+\rho}/2$

$e^{+\rho}$

e^{ρ}

$e^{-\rho}/2$

$sech\ \rho$ 1 $cosh\ \rho$

Fig. 2.C.1 Geometry of relativistic parameters and functions of velocity.

Relations between circular and hyperbolic functions

The geometry and trigonometry of circular functions sinϕ, cosϕ, and tanϕ, as well as their inverse functions cscϕ, secϕ, and cotϕ, is well known in the form displayed in Fig. 2.C.2(a). The source of the word "tangent" is the tangent line segment leaning at angle ϕ in Fig. 2.C.2(a). The word "sine" is perhaps derived from "slope-incline" that is the altitude rise fraction of distance traveled on the inclined road (hypotenuse). The cosine is the distance traveled horizontally. The secant is a cut through the circle from the tangent intersection point outside and is the inverse of the cosine.

Less widely known is the geometry and trigonometry of hyperbolic functions sinhρ, coshρ, and tanhρ, as well as their inverse functions cschρ, sechρ, and cothρ shown in a similar form displayed in Fig. 2.C.2(b). They also measure altitudes, tangents and base segments but with respect to the unit hyperbola.

The combination of these functions is the heart of modern relativity and quantum physics. Particularly important is the dependency between the stellar aberration angle ϕ and the hyperbolic "angle" ρ. In the figure the value ϕ =0.8934 (or *51.19°*) is chosen. This means rapidity is ρ =0.8934 (or *u/c=* tanhρ =*0.7792*) as follows.

$$\sin\phi = \tanh\rho = 0.7792 \qquad (2.C.8a) \qquad\qquad \tan\phi = \sinh\rho = 1.2433 \qquad (2.C.8b)$$

$$\cos\phi = \text{sech}\rho = 0.6267 \qquad (2.C.9b) \qquad\qquad \sec\phi = \cosh\rho = 1.5955 \qquad (2.C.9b)$$

$$\csc\phi = \coth\rho = 1.2833 \qquad (2.C.10a) \qquad\qquad \cot\phi = \text{csch}\rho = 0.8043 \qquad (2.C.10b)$$

Note that cscϕ = cothρ =*1.2833* and tanϕ = sinhρ =*1.2433* are close but not equal, so near-coincidences might appear in the figures to give misleading results.

Both angle ϕ and "angle" ρ should be viewed as *area* ϕ and the hyperbolic *area* ρ as is done in the figure. The circular area is bounded by π but the hyperbolic area is unbounded and infinite in extent. For each segment on the unit-circle there is a corresponding equal-length segment on the unit-hyperbola. The circular tangent tanϕ is the same as the hyperbolic altitude sinhρ and the hyperbolic tangent tanhρ (relativistic velocity) is the altitude sinϕ of the circle at the aberration angle ϕ.

It is also interesting that the tangent line to the hyperbola is determined by base and altitude segments sechρ and cschρ on the main axes and by the intersection of ϕ–tipped segment tanϕ=sinhρ and vertical segment tanhρ=sinϕ.

It is quite a bizarre set of relations that exist between the circle and its "country-cousin" the hyperbola, and it has a lot to teach us about relativistic and quantum physics. The next figure fills in some of the geometric details that are relevant for the physics.

(a) Circlular Functions
(plane geometry)

Circlular arc area
ø =0.8934=angle
sin ø =0.7792
cos ø =0.6267
tan ø =1.2433
csc ø =1.2833
sec ø =1.5955
cot ø =0.8043

y

1.0 cotø

cscø

sinø   1   sinø   tanø

ø

cosø   secø   1.0   x

ø

x(space)

coshρ

coshρ   sinhρ

1.0   cschρ

coshρ

Hyperbolic arc area
ρ =1.0434=rapidity
sinh ρ =1.2433
cosh ρ =1.5955
tanh ρ =0.7792
csch ρ =0.8043
sech ρ =0.6267
coth ρ =1.2833

cothρ

tanhρ

1

tanhρ

sinhρ

1.0

ct (time)

sechρ

coshρ

ρ

e⁻ᵖ

e⁻ᵖ

cschρ

e⁺ᵖ

(b) Hyperbolic Functions
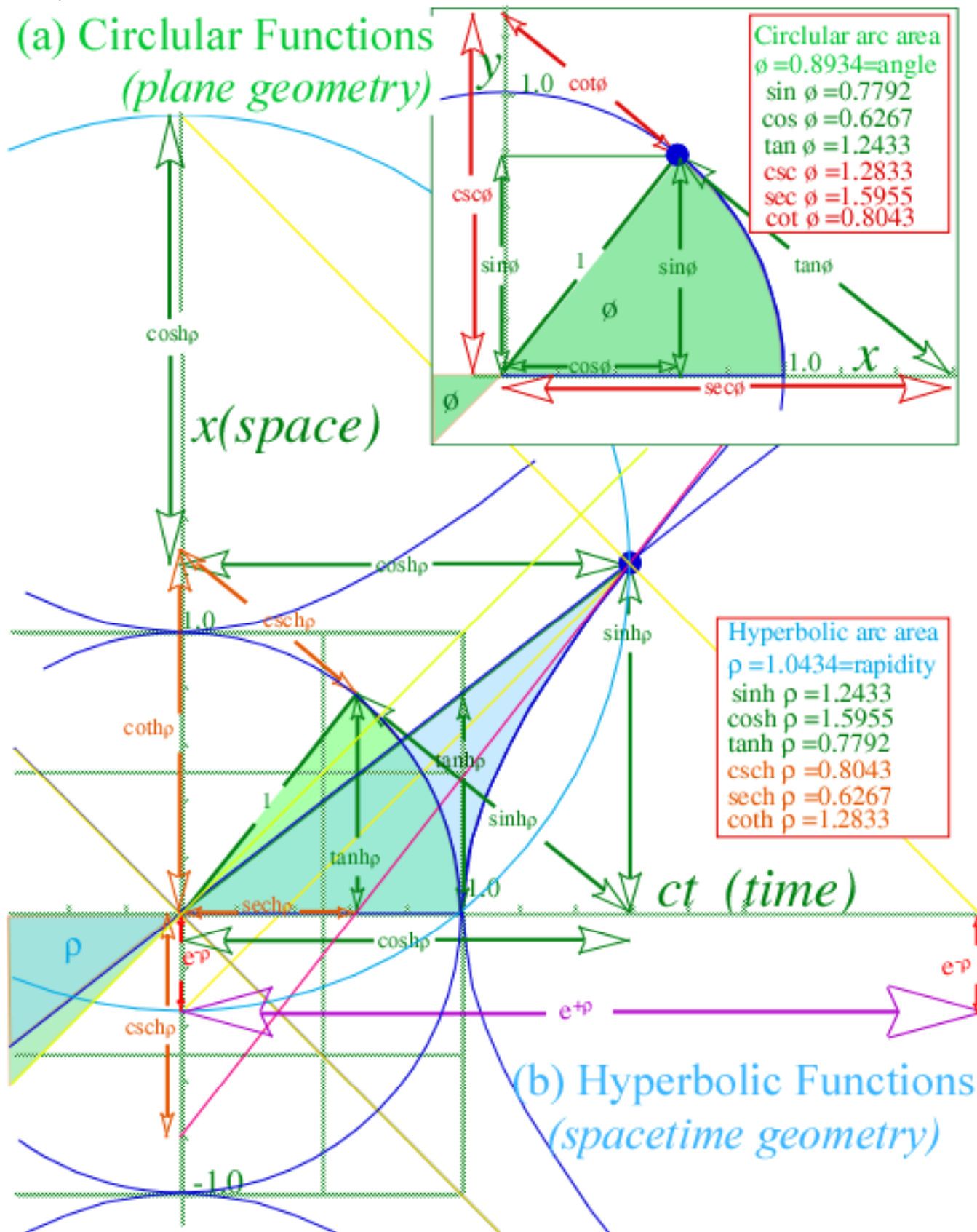### *(spacetime geometry)*

-1.0

Fig. 2.C.2 Trigonometry (a) Circular functions of aberration angle ϕ (b) Hyperbolic functions of rapidity ρ.

Geometry of circular and hyperbolic functions

The geometry and trigonometry of trigonometric ratios is further developed in Fig. 2.C.3 to show the rationale of the line segments in Fig. 2.C.1. It also shows the fundamental exponential functions $e^{-\rho}$ and $e^{+\rho}$ that are the Doppler blue and red shift ratios and whose half-sum and half-differences give the hyperbolic cosine $\cosh\rho$ and the hyperbolic sine $\sinh\rho$ ratios. Fig. 2.C.1 shows the half-sum and half-difference s.

$$\cosh\rho = \frac{e^{+\rho} + e^{-\rho}}{2} \qquad\qquad \sinh\rho = \frac{e^{+\rho} - e^{-\rho}}{2}$$

Fig. 2.C.3 is quite a collection of ratios, indeed, it might be called a ratio-riot! However, it contains some fundamental and simple but powerful results and it is worth the time it takes to understand it.

The intersection of segment $\tan\phi=\sinh\rho$, the segment $\sin\phi = \tanh\rho$, and the actual tangent line to the hyperbola is joined also by a horizontal line at vertical distance $\cot\phi = \operatorname{csch}\rho = 0.8043$ below the highest point at $\csc\phi = \coth\rho = 1.2833$ on the vertical (space) axis. (This high point on the vertical x-axis is not to be confused with the 2nd highest point at $\tan\phi = \sinh\rho = 1.2433$.)

The actual tangent line to the hyperbola also goes through the intersection of the *hyperbolic-cosine-circle* of radius $r=\cosh\rho=\sec\phi=1.5955$ around point ($x=\sinh\rho=\tan\phi=1.2433, ct=0$) and the *hyperbolic-sine-circle* of radius $r=\sinh\rho=\tan\phi=1.2433$ around point ($x=0, ct=\cosh\rho=\sec\phi=1.5955$). The actual tangent line slope is the inverse $\coth\rho=1.2833=\csc\phi$ to the slope $\tanh\rho=0.7792=\sin\phi$ of the hyperbolic radius vector that makes contact with the tangent at the point ($x=\sinh\rho=\tan\phi=1.2433, ct=\cosh\rho=\sec\phi=1.5955$).

To see the correspondence with the constructions in Fig. 2.C.1(c) it is necessary to view Fig. 2.C.3 (b) at right angles so the ct-axis (or frequency axis) points vertically as it would in Fig. 2.C.1(c). The *hyperbolic-cosine-circle* is the circle that takes the geometric mean of the Doppler ratios $e^{-\rho}$ and $e^{+\rho}$ to arrive at the unit invariant value $ct=1$ (or $\varpi=1$) on the time axis (or frequency axis).

(a) Circlular Functions
(plane geometry)

Circlular arc area
ø =0.8934=angle
sin ø =0.7792
cos ø =0.6267
tan ø =1.2433
csc ø =1.2833
sec ø =1.5955
cot ø =0.8043

1.0 cotø

cscø

sinø   1   sinø   tanø

ø

cosø   secø

ø

x(space)

cosh

(b) Hyperbolic Functions
(spacetime geometry)

Hyperbolic arc area
=1.0434=rapidity
sinh   =1.2433
cosh   =1.5955
tanh   =0.7792
csch   =0.8043
sech   =0.6267
coth   =1.2833

csch

coth

tanh

1

sinh

sinh

tanh

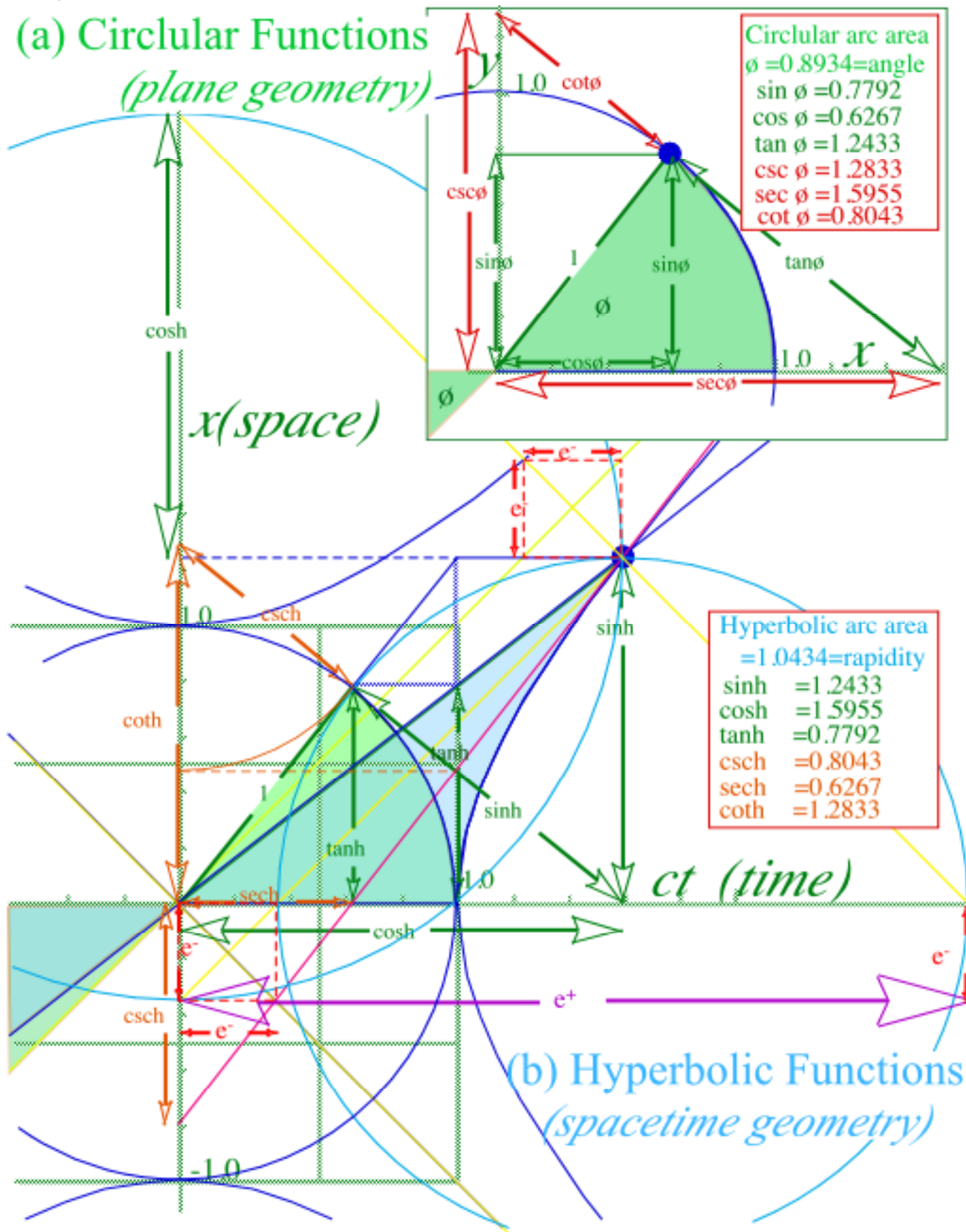1.0

sech

cosh

ct (time)

e⁻

csch

e⁻

e⁺

e⁻

-1.0

Fig. 2.C.3 Relativistic ratio geometry connecting (a)Circular ɸ-functions and (b)Hyperbolic ρ-functions.

Chapter 3. Invariance and Relative Phase: Galileo's revenge

Einstein relativity shows Galilean relativity, based on simple velocity sums and differences, to be a 400 year-old approximation that fails utterly at high speeds. Einstein also dethrones *infinite* velocity that is the one invariant velocity shared by Galilean observers regardless of their (finite) velocity. In its place reigns a finite velocity limit *c=299,792,458ms⁻¹* that is now the Einstein-Maxwell-Evenson invariant speed.

So it is remarkable that frequency sums and differences (1.10) simplify relativity by using Galilean-like rules for *angular* velocities $\omega_A = \dot{\phi}_A$ of light phases ϕ_A . Frequency sums or differences

$\omega_A \pm \omega_B$ from interference terms like $\psi_A\psi_B{}^* = ABe^{-i(\omega_A - \omega_B)t}$ between wave pairs $\psi_A = Ae^{-i\omega_A t}$ and

$\psi_B = Be^{-i\omega_B t}$ are *relative* frequencies (beat notes, overtones, etc.) subject only to simple addition and

subtraction rules that are like Galileo's rules for linear velocity. Simple angular phase principles deeply underlie modern physics, and so far there appears to be no *c*-like speed limit for an angular velocity ω.

Phase principles have electromagnetic origins. Writing oscillatory wave functions using real and imaginary parts is used to study AC phenomena or harmonic oscillators in Unit 4. Real part *q* of oscillator amplitude $q+ip= Ae^{-i\omega t}$ is its *position q=A*cosω*t*. Imaginary part *p=A*sinω*t* is oscillator *velocity v =-A*ωsinω*t* in units of angular frequency ω. Positive ω gives a clockwise rotation like that of classical phase space or analog clocks, so a minus sign in a conventional $Ae^{-i\omega t}$ phasor serves to remind us that wave frequency ω *defines* our clocks and wavevector *k=ω/c defines* our meter sticks. (Recall Fig. 1.10.5 and Fig. 4.2.1.)

A plane wave of wavevector *k* in Fig. 3.1 is drawn as a phasor array, one $A =|A|e^{ikx}$ for each location *x*. A plane wave advances in time according to $|A|e^{i(kx-\omega t)}$ at phase velocity *V=ω/k*. Similar convention and notation are used for light waves and for quantum matter waves, but only light waves have physical units, vector potential **A** and electric **E**-field, defining their real and imaginary parts. While classical laser wave phase is observable, only *relative* phase of a quantum wave ψ appears to be so.

The concept of relative phase (and frequency) arises in classical or quantum interference where a sum of two waves $\psi_A = Ae^{i\phi_A}$ and $\psi_B = Be^{i\phi_B t}$ may be represented at each position *x* by a vector sum of a phasor-A with a phasor-B as in Fig. 3.1a. (Fig. 3.1 has a sum of 12 phasors, one for each each *x*-point.) The result is a clockwise race around a track between the faster one, say A-phase $\phi_A = k_A x - \omega_A t$ of angular speed -ω$_A$, and the slower B-phase $\phi_B = k_B x - \omega_B t$ of angular speed -ω$_B$ as sketched in Fig. 3.1b.

Galilean relativity of phase angular velocity holds if the phase wave is governed by linear equations of motion such as Maxwell's equations. Very precise measurements of *en vacuo* light have verified this so far and Einstein relativity is a consequence. You might say this is Galieo's revenge!

(a) *Sum of Wave Phasor Array*
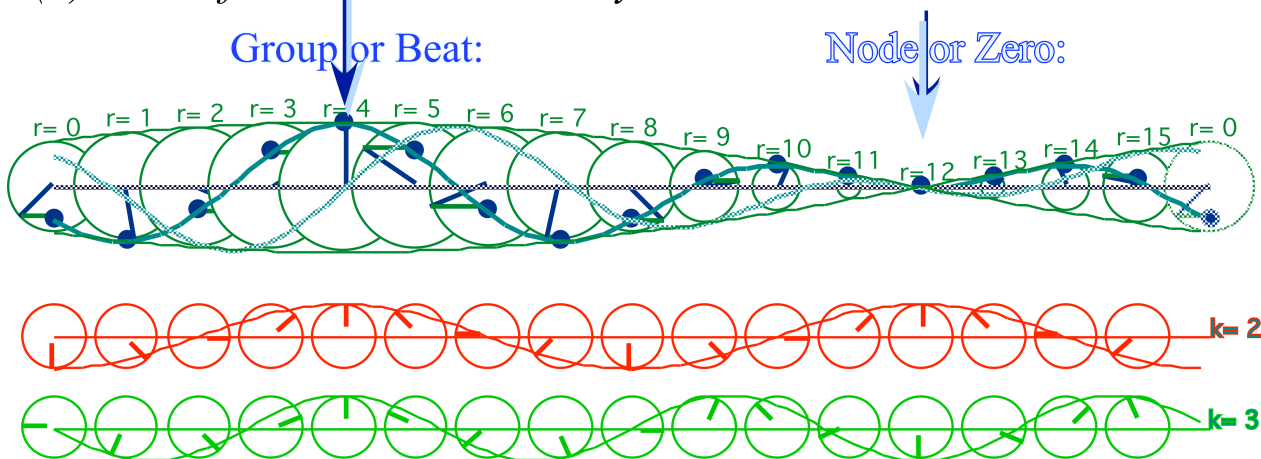
(b) *Typical Phasor Sum:*
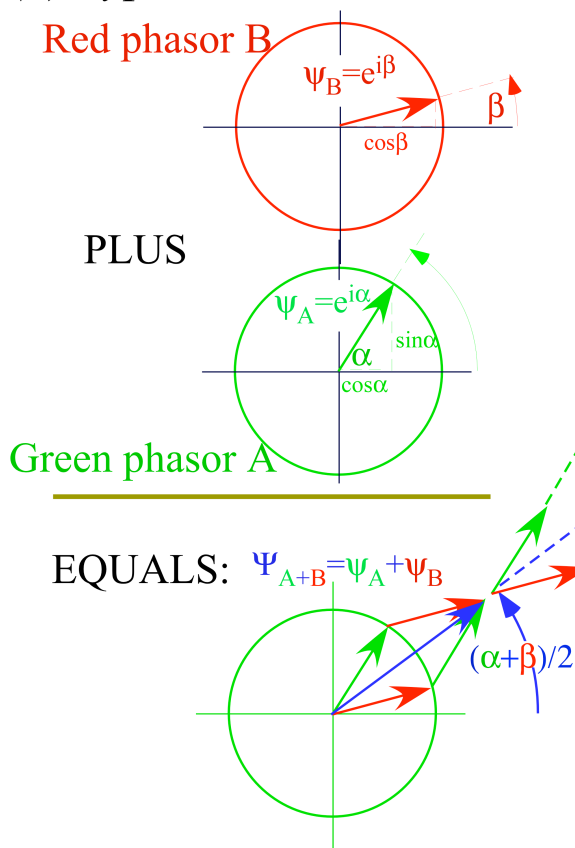
(c) *Phasor-relative views*
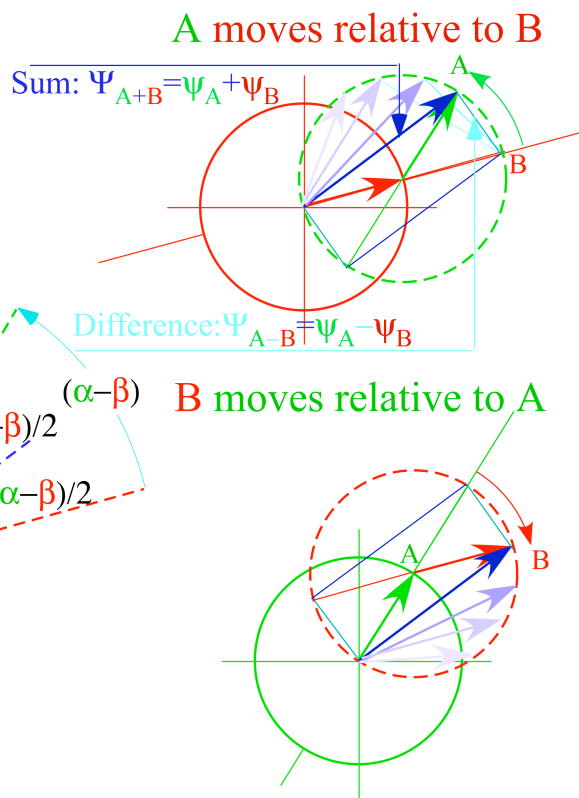
Fig. 3.1 Wave phasor addition. (a) Each phasor in a wave array is a sum (b) of two component phasors.
(c) In phasor-relative views either A or else B is fixed. An evolving sum-and-difference rectangle is inscribed in the (dashed) circle of the phasor moving relative to the fixed one.

Geometry of relative phase

When A passes B the sum is a maximum or *beat* that then subsides to a minimum or *node* when A is on the opposite side of the track from B. If amplitude magnitudes |A| and |B| are equal as they are in Fig. 3.1, then the wave node is a wave *zero* that defines one of the group **G**-lines in WZ coordinates of Fig. 1.4 through Fig. 2.2. The *relative* angular velocity $\Delta = \omega_A - \omega_B$ (beat angular frequency) is the angular rate at which A passes B. A-B passings occur δ times *(per sec.)* where δ is Δ divided by track length 2π.

$$\delta_{beat} = \Delta / 2\pi = \upsilon_A - \upsilon_B \tag{3.1}$$

If one could ride in an angular Galilean frame of phasor-B, then A would be seen passing at angular speed Δ with frequency δ. Suppose instead, one could ride at their *average* angular speed $\bar{\Omega}$.

$$\bar{\Omega} = \tfrac{1}{2}(\omega_A + \omega_B) \tag{3.2}$$

Then Galilean arithmetic (which lasers given no reason to doubt in these matters) implies that phasor A or B would each appear with a relative speed of plus-or-minus *half* their relative velocity.

$$\pm\tfrac{1}{2}\Delta = \pm\tfrac{1}{2}(\omega_A - \omega_B) \tag{3.3}$$

A point of view relative to phasor B is shown by the first of Fig. 3.1c. A dashed circle represents moving phasor A with ψ_A on one diagonal of an inscribed rectangle whose sides are the resultant sum $\psi_A + \psi_B$ and difference $\psi_A - \psi_B$. The other diagonal ψ_B appears fixed. A companion figure has ψ_A appear fixed instead. Resultants in either figure begin and end on a dashed circle traced by the phasor that is moving relative to the other. A rectangle-in-circle is a key Euclidian element of wave physics and is a key feature of a later figure (Fig. 3.3) that shows the essence of wave interference geometry.

The half-sum and half-difference angles in Fig. 3.1b and frequencies (3.2) and (3.3) appear in the interference formulas (1.10) that lead to relativistic Lorentz-Einstein coordinate relations (2.10) and their WZ grid plots of Minkowski coordinates in Fig. 2.2c. One key is the *arithimetic mean* $(\alpha + \beta)/2$ of phases that gives the *geometric mean* $(\psi_A \psi_B)^{1/2} = A e^{i(\alpha+\beta)/2}$ of wave phasor amplitudes. The other key is the *difference mean* $(\alpha - \beta)/2$ and that is the phase angle of a *cross mean* $(\psi_A \psi_B{}^*)^{1/2} = A e^{i(\alpha-\beta)/2}$.

Euclidian means and rectangle-in-circle constructions underlie relativistic wave geometry as is shown below. This geometry also leads to the geometry of contact transformations in classical mechanics that exposes relations between classical and quantum mechanics in Ch. 5.

Geometry of Doppler factors

Any number N of transmitter-receivers ("observers" or "atoms" previously introduced) may each be assigned a positive number b_{11}, b_{21}, b_{31}, …that is its Doppler shift of a standard frequency ω_1 broadcast by atom-1 and then received as frequency $\omega_{m1}= b_{m1}\omega_1$ by an atom-m. By definition a transmitter's own shift is unity. ($1= b_{11}$) Also, coefficient b_{m1} is independent of frequency since such *geometric* relations work as well on 1THz or 1Hz waves as both waves march in lockstep to the receiver by Evenson's CW axiom (1.1). The production times of a single wavelength of the 1Hz-wave and 10^{12} wavelengths of the 1THz wave must be the same *(1sec.)*, and so must be reception time for the two waves since they arrive in lock step, even if τ is shortened geometrically by $1/ b_{m1}$. Doppler is a *geometric* and *multiplicative* effect.

red shifted departing receivers *fixed receiver* *blue shifted oncoming receivers* *green reference source*

	300THz	400THz	600THz	900THz	1200THz	
300THz	300/300 $b_{11}=1$	300/400 $b_{12}=0.75$	300/600 $b_{13}=0.5$	300/900 $b_{14}=0.333$	300/1200 $b_{15}=0.25$	*10 Doppler red-shift ratios:* $r = \upsilon_{lo}/\upsilon_{hi}$
400THz	400/300 $b_{21}=1.333$	400/400 $b_{22}=1$	400/600 $b_{23}=0.667$	400/900 $b_{24}=0.449$	400/1200 $b_{25}=0.333$	
600THz	600/300 $b_{31}=2$	600/400 $b_{32}=1.5$	600/600 $b_{33}=1$	600/900 $b_{34}=0.667$	600/1200 $b_{35}=0.5$	
900THz	900/300 $b_{41}=3$	900/400 $b_{42}=2.25$	900/600 $b_{43}=1.5$	900/900 $b_{44}=1$	900/1200 $b_{45}=0.75$	
1200THz	1200/300 $b_{51}=4$	1200/400 $b_{52}=3$	1200/600 $b_{53}=2$	1200/900 $b_{54}=1.333$	1200/1200 $b_{55}=1$	

5 Doppler "no-shifts"

10 Doppler blue-shift ratios: $b = \upsilon_{hi}/\upsilon_{lo}$

Fig. 3.2 Doppler shift b-matrix for a linear array of variously moving receiver-sources.

If atoms travel at constant speeds on a straight superhighway, then b_{m1} in (2.8a) tells what is the relative velocity u_{m1} of the mth atomic receiver relative to the number-1 transmitter.

$$u_{m1}/c = (b_{m1}^{\;2} - 1)/(b_{m1}^{\;2} + 1) \tag{3.4}$$

The velocity u_{m1} is positive if the mth atom goes toward transmitter-1 and sees a blue ($b_{m1}>1$) shift, but if it moves away u_{m1} is negative so it sees a red ($b_{m1}<1$) shift. Transmitter-1 has no velocity relative to itself. ($u_{11}=0$) Infinite blue (or red) shift $b_{m1}=\infty$ (or $b_{m1}=0$) gives $u_{m1}=c$ (or $u_{m1}=-c$) and this defines the range of

parameters. The b_{m1} are constant until atom-*m* passes atom-*1* so relative velocity flips sign ($u_{1m} \rightarrow -u_{1m}$).

Doppler shift then inverts ($b_{1m} \rightarrow 1/b_{1m}$) as is consistent with axiom (1.2).

Suppose now $b_{12}, b_{22}, b_{32}, \dots$ are Doppler shifts of frequency ω_2 transmitted by the *second* atom and received by the mth atom as frequency $\omega_{m2} = b_{m2} \omega_2$. (Any atom (say the nth) may transmit, too.)

$$\omega_{mn} = b_{mn} \omega_n \tag{3.5a}$$

Recipients don't notice if atom-*n* just passes on whatever frequency ω_{nm} came from atom-*m*. If frequency ω_n in (3.5a) is $\omega_{n1} = b_{n1} \omega_1$ that atom-*n* got from atom-*1* then atom-*m* will not distinguish a direct ω_{m1} from a perfect frequency copy $b_{mn} b_{n1} \omega_1$ made by atom-*n* from atom-*1* and then passed on to atom-*m*.

$$\omega_{m1} = b_{m1} \omega_1 = b_{mn} b_{n1} \omega_1 \tag{3.5b}$$

A multiplication rule results for Doppler factors and applies to light from atom-*1* or any atom-*p*.

$$\omega_{mp}/\omega_p = b_{mp} = b_{mn} b_{np} \tag{3.5c}$$

An inverse relation results from atom-*p* comparing its own light to that copied by atom-*n*.

$$1 = b_{pp} = b_{pn} b_{np} \quad \text{or:} \quad b_{pn} = 1/b_{np} \tag{3.5d}$$

(Amplitude amplification is discussed later in Ch. 6 and has similar rules.)

Notice that copying or passing light means just that and does not include reflection or changing $+k$ to $-k$ or any other direction. This presents a problem for a receiver not in its transmitter's $(+k)$-beam and certainly for atom-*p* receiving its own beam. The relations (3.5) depend only on relative velocities and not positions (apart from the problem that a receiver might be on the wrong side of a transmitter).

An obvious solution is to let the receiver overtake its transmitter or failing that delegate a slave transmitter or receiver on its right side. Fig. 3.2 shows *N=5* receivers of a $\omega_3 = 600THz$ source whose various speeds produce a matrix of *N(N-1)=20* Doppler shifted frequencies ω_{mn} and factors b_{mn}.

Doppler rapidity and Euclid means business
     Composition rules (3.5c) suggest defining Doppler factors $b = e^\rho$ in terms of *rapidity* $\rho = \ln b$.

$$b_{mp} = b_{mn} b_{np} \quad \text{implies:} \quad \rho_{mp} = \rho_{mn} + \rho_{np} \qquad \text{where:} \quad b_{ab} = e^{\rho_{ab}} \tag{3.6}$$

Rapidity parameters ρ_{mn} mimic Galilean addition rules as do phase angles ϕ of wavefunctionss $e^{i\phi}$. Both ρ and ϕ are the parameters that underlie relativity and quantum theory. In fact, by (3.4) rapidity ρ_{mn} approaches the relative velocity parameter u_{mn}/c between atom-*m* and atom-*n* for speeds much less than *c*. Rapidity is also convenient for astronomically large Doppler ratios b_{ab} since then the numerical value of $\rho_{ab} = \ln b_{ab}$ is much less than b_{ab} while u_{mn}/c approaches 1 in a way that is numerically inconvenient.

At intermediate relativistic speeds the geometric aspects of Doppler factors provide a simple and revealing picture of the nature of wave-based mechanics. Pairs of counter moving continuous waves (CW) have mean values between a **K**-vector $\mathbf{R}=\mathbf{K}_1=(ck_1,\omega_1)$ going left-to-right and an $\mathbf{L}=\mathbf{K}_3=(ck_3,\omega_3)$ going right-to-left. A key quantity is the *geometric mean* ϖ of left and right frequencies.

$$\varpi = \sqrt{\omega_1\omega_3} \tag{3.7}$$

In Fig. 3.2a frequency $\omega_1=1$ or $\omega_3=4$ is a blue *(b=e^{+\rho}=2)* or red *(r=e^{-\rho}=1/2)* shift of mean $\varpi = \sqrt{1\cdot 4} = 2$.

$$\omega_1 = b\varpi = e^{\rho}\varpi \tag{3.8a} \qquad\qquad \omega_3 = r\varpi = e^{-\rho}\varpi \tag{3.8b}$$

In units of $2\pi\cdot 300THz$, frequency values $\omega_3=1$ and $\omega_1=4$ were used in Fig. 2.2. Their half-sum *5/2* is their *arithmetic mean*. That is the radius of the circle in Fig. 3.2b located a *half-difference (3/2)* from origin.

$$\frac{\omega_1+\omega_3}{2} = \varpi\frac{e^{+\rho}+e^{-\rho}}{2} = \varpi\cosh\rho = \varpi\frac{5}{2} \tag{3.9a} \qquad \frac{\omega_1-\omega_3}{2} = \varpi\frac{e^{+\rho}-e^{-\rho}}{2} = \varpi\sinh\rho = \varpi\frac{3}{2} \tag{3.9b}$$

By (2.8) the difference-to-sum ratio is the group or *mean frame* velocity-to-*c* ratio $u/c=3/5$ for *b=2*.

$$\frac{\omega_1-\omega_3}{\omega_1+\omega_3} = \frac{\sinh\rho}{\cosh\rho} = \tanh\rho = \frac{u}{c} \tag{3.9c} \qquad\qquad \frac{4-1}{4+1} = \frac{u}{c} = \frac{3}{5} \tag{3.9d}$$

The geometric mean ($\varpi = \sqrt{1\cdot 4} = 2$) in units of $2\pi\cdot 300THz$ is the initial *600THz* green laser lab frequency used in Fig. 2.1. Diamond grid sections from Fig. 2.2b are redrawn in Fig. 3.3b to connect with the geometry of the Euclidian rectangle-in-circle elements of interfering-phasor addition in Fig. 3.1c.

Various observers see single CW frequencies ω_1 or ω_3 shifted to $\omega'_1=e^{+\rho}\omega_1$ and $\omega'_3=e^{-\rho}\omega_3$, that is, to values between zero and infinity. But, because factor $e^{-\rho}$ cancels $e^{+\rho}$, all will agree on the 2-CW mean value $\varpi =[\omega_1\omega_3]^{1/2}=[\omega'_1\omega'_3]^{1/2}$. A 2-CW function has an *invariant* ϖ of its *rest frame* (Recall Fig. 2.2c) seen at velocity $u=c(\omega_1-\omega_3)/(\omega_1+\omega_3)$. A single CW has no rest frame or frequency since all observers see it going *c* as in Fig. 1.1. To make a home frame, a single CW must marry another one!

(a)

Geometric mean:

$[1 \cdot 4]^{1/2} = \quad = 2$

(ROOT-PRODUCT)

Difference mean:

$[4 - 1]/2 = 3/2$

(HALF-DIFFERENCE)

Arithmetic mean:

$[4 + 1]/2 = 5/2$

(HALF-SUM)

2

3/2

3/2

ck

-1   0   1   2   3   4

$\omega_3 = 1$

$\omega_1 = 4$

(b)

ω' relative velocity:
$u/c = \tanh\rho = 3/5$

u

c

$Br = Be^{-\rho}$

Geometric mean or Base:

$\overline{\omega} = B = 2$

3

4

2

blue shift

$Bb = Be^{+\rho} = 2B$

(HALF-SUM)

$B\cosh\rho = B(5/2)$

(HALF-DIFFERENCE)

red shift

$Br = Be^{-\rho} = B/2$

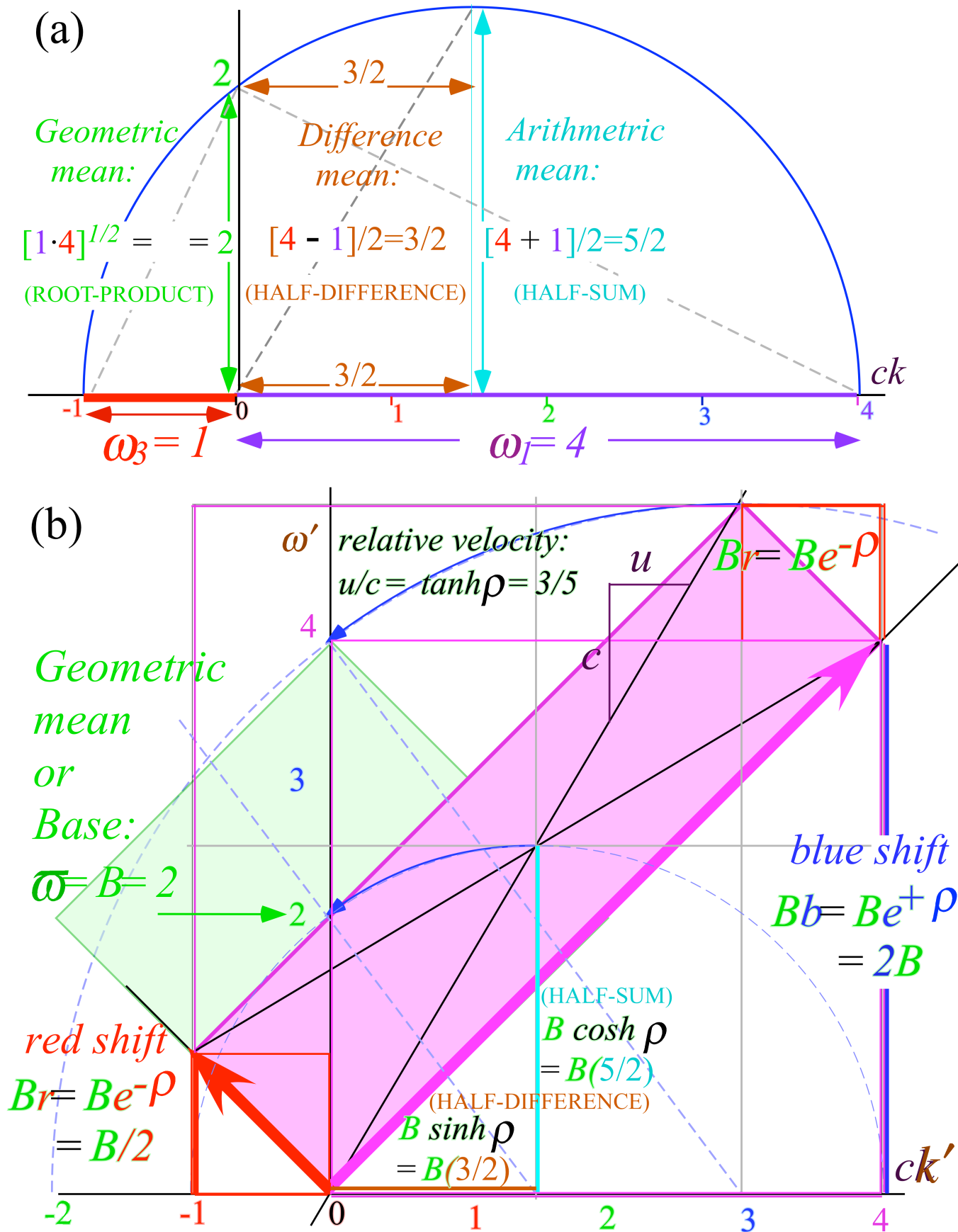$B\sinh\rho = B(3/2)$

ck'

-2   -1   0   1   2   3   4

Fig. 3.3a Euclidian mean geometry for counter-moving waves of frequency 1 and 4. (300THz units).

Fig. 3.3b Geometry for the CW wave coordinate axes in Fig. 2.2.

Invariance of proper time (age) and frequency (rate of aging)

Space, time, and frequency may seem to have an out-of-control fluidity in a wavy world of relativism, so it is all the more important to focus on relativistic invariants. Such quantities make ethereal light billions of times more precise than any rusty old meter bar or clanking cuckoo clock.

It is because of the time-reversal (1.2) and Evenson axiom (1.1) that product $\omega_1\omega_3=\varpi^2$ is invariant to inverse blue-and-red Doppler shifts $b=e^{+\rho}$ and $r=e^{-\rho}$. It means the blue-red shifted diamond in Fig. 3.3b or Fig. 2.2 has the same area **R′xL′** as the original green "home field" baseball diamond area **RxL** drawn below it and in Fig. 2.1. Constant products $\omega_1\omega_3=const.$ give families of hyperbolas.

$$|\mathbf{R}\mathbf{x}\mathbf{L}|=2|\mathbf{G}\mathbf{x}\mathbf{P}|=2|\mathbf{K}_{group}\mathbf{x}\mathbf{K}_{phase}|=2|\varpi^2\cosh^2\rho -\varpi^2\sinh^2\rho|=2\varpi^2$$

One hyperbola in Fig. 3.4a intersects bottom point $B=\varpi$ (*"pitchers' mound"*). The other hits *2B* (*2nd base*). Each horizontal **P** -hyperbola is defined by the phase vector $\mathbf{P}=\mathbf{K}_{phase}$ or some multiple of **P**.

$$\mathbf{K}_{phase} = \frac{\varpi}{2}\begin{pmatrix} e^{\rho} - e^{-\rho} \\ e^{\rho} + e^{-\rho} \end{pmatrix} = \varpi\begin{pmatrix} \sinh\rho \\ \cosh\rho \end{pmatrix} = \begin{pmatrix} ck_p \\ \omega_p \end{pmatrix} \quad \text{on P-hyperbola:} \quad \left(\omega_p\right)^2 - \left(ck_p\right)^2 = \varpi^2 \qquad (3.10a)$$

Each vertical **G** -hyperbola is defined by the wave group vector $\mathbf{G}=\mathbf{K}_{group}$ or some multiple of **G**.

$$\mathbf{K}_{group} = \frac{\varpi}{2}\begin{pmatrix} e^{\rho} + e^{-\rho} \\ e^{\rho} - e^{-\rho} \end{pmatrix} = \varpi\begin{pmatrix} \cosh\rho \\ \sinh\rho \end{pmatrix} = \begin{pmatrix} ck_g \\ \omega_g \end{pmatrix} \quad \text{on G-hyperbola:} \quad \left(ck_g\right)^2 - \left(\omega_g\right)^2 = \varpi^2 \quad (3.10b)$$

The **G**-vectors serve as tangents to **P**-hyperbolas and vice-versa. The tangent slope $\frac{d\omega}{dk}$ to any $\omega(k)$ curve is a well known definition of group velocity. Fig. 3.4b shows how $\frac{d\omega}{dk}$ of a P-hyperbola is equal to secant slope $\frac{\Delta\omega}{\Delta k}$ in Fig. 3.4a as defined in the $u=V_{group}$ equation (2.7b) based on CW axioms.

Phase velocity $\frac{\omega}{k}=V_{phase}$ and its **P**-vector is an axis-switch $(\omega,ck) \rightleftarrows (ck,\omega)$ of $\frac{\Delta\omega}{\Delta k}$ and its **G**-vector. In conventional c-units $V_{group}/c<1$ and $1<V_{phase}/c$ are inverses according to (2.7). ($V_{phase}\cdot V_{group}=c^2$)

Features on per-space-time (ck,ω) plots of Fig. 3.3-Fig. 3.4 reappear on space-time (x,ct) plots as noted in Fig. 2.1 and Fig. 2.2. A space-time invariant analogous to (3.10) is called *proper-time τ*.

$$\left(ct\right)^2 - \left(x\right)^2 = \left(c\tau\right)^2 = \left(ct'\right)^2 - \left(x'\right)^2 \qquad (3.11)$$

It conventional to locate oneself at *(0,ct)* or presume one's origin *x=0* is located on oneself. Then (3.11) reduces to time axis *ct=c\tau*. A colloquial definition of proper time is *age*, a digital readout of one's computer clock that all observers may note.

(a)

$c \, \Delta k$

P *hyperbolas*

ω'

$\varpi = 2B = 4$

c *line*

G *hyperbolas*

$\Delta\omega$

$\varpi = B = 2$

R

P

G

$B \cosh \rho$

$B \sinh \rho$

$B \, e^{-\rho}$

L

ck

-2   -1   0   1   2   3   4

(b)

$$\frac{\omega}{k} = \frac{c^2}{u}$$

Phase velocity

u

c

u

Group velocity

c

$$\frac{d\omega}{dk} = u = \frac{c^2 k}{\omega}$$

B=2

$$\omega = B \cosh \rho$$

$$k = \frac{B}{c} \sinh \rho$$

ck

Fig. 3.4 (a) Horizontal G-hyperbolas for proper frequency B=ϖ and 2B and vertical P-hyperbolas for proper wavevector k. (b) Tangents for G-curves are loci for P-curves, and vice-versa. Note: secant Δω/Δk and tangent dω/dk are always *exactly* equal.

By analogy, ϖ is *proper-frequency*, a *rate of aging* or a digital readout on each of the spectrometers in Fig. 3.2. Each reading is available to all observers.

$$(\omega)^2 - (ck)^2 = (\varpi)^2 = (\omega')^2 - (ck')^2 \qquad (3.12)$$

The same hyperbolas (3.12) mark tics on the laser lab *(ω,ck)*, the atom frame *(ω',ck')*, or any other frame.

The proper frequency of a wave is that frequency observed after one Doppler shifts the wave's kinks away, that is, the special frequency ϖ seen in the frame in which its wavevector is zero (*ck=0*) in (3.12). Hence a single CW has a proper frequency that is identically zero (ϖ =0) by Evenson's axiom (ω=ck), so single CW light cannot age. If we could go *c* to catch up to light's home frame then its phasor clocks would appear to stop. Someone moving along a line of phasor clocks in Fig. 1.1c would always see the same reading, but that would be an infinite Doppler shift that one can only approach.

To produce a nonzero proper frequency $\varpi \neq 0$ requires interference of at least two CW entities moving in different directions and this produces a standing wave frame like Fig. 2.1c moving at a speed less than *c* as shown in Fig. 2.2c. Matched CW-pairs of **L** and **R** baselines frame a "baseball diamond" for which the phase wavevector k_p in (2.2a) is zero. Then frame velocity $u=V_{group}$ in (2.3b) is zero, too.

Fig. 3.5 shows the plots of per-spacetime "baseball diamond" coordinates for comparison of lab and atom frame views. While Fig. 3.5a is a "blimp's-eye view" of the lab-frame diamond in Fig. 2.1, the atom frame view in Fig. 3.5b looks like the baseball field seen by a spectator sitting in the grandstands above the dugout. Nevertheless, identical hyperbolas are used to mark grids in either view.

Each point on the lower hyperbola is a bottom point *ω'=B=2 (600THZ)* for the frame whose relative velocity *u'* makes it a *ω'*-axis (*k'=0*)-point, and every (*k'=0*)-point on the upper hyperbola is its bottom point *ω'=2B=4 (1200THZ)*, and so on for hyperbolas of any given proper frequency value ϖ. The same applies to space-time plots for which time *ct'* takes the place of per-time *ω'* and space *x'* takes the place of per-space *ck'*. Then bottom points are called proper time or *τ*-values from (3.11).

For single CW light the proper time must be constant since a single CW cannot age. It is a convention to make the baselines or *light cone* intersect at the origin in both time and space. This sets the baseline proper time constant τ to zero. Then invariants (3.11) reduce to baseline equations *x=±ct* or *x'=±ct'* for all frames. The space-time light cone relations are in direct correspondence with the per-space-time light cone relations ω=±ck or ω'=±ck' for zero proper frequency in all frames and are concise restatements of the Evenson CW axiom (1.1).

(a) Laser lab view
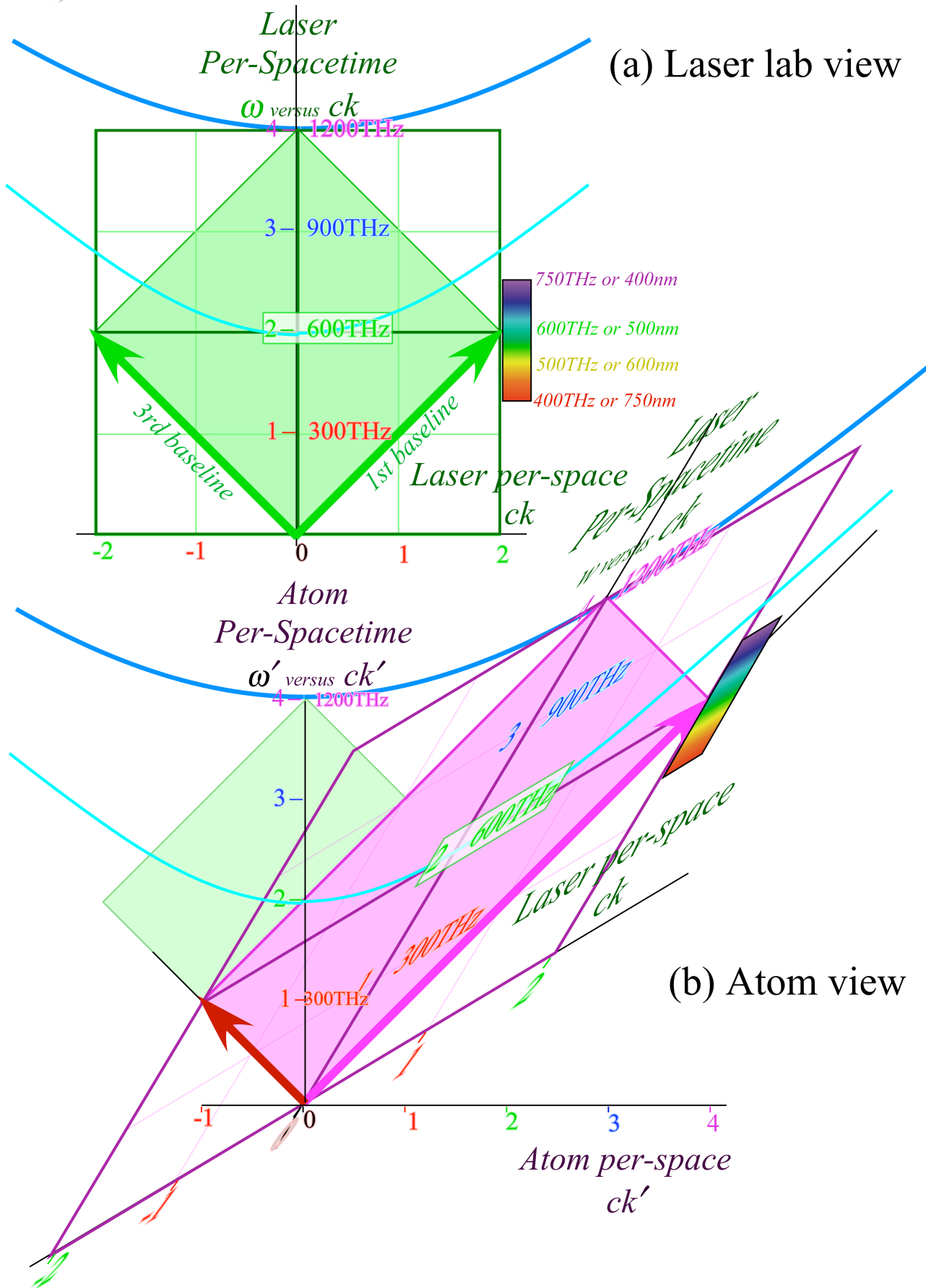
Laser
Per-Spacetime
ω *versus* ck

4 — 1200THz

3 — 900THz

750THz or 400nm

600THz or 500nm

500THz or 600nm

400THz or 750nm

2 — 600THz

3rd baseline

1st baseline

1 — 300THz

Laser per-space
ck

-2   -1   0   1   2

(b) Atom view

Atom
Per-Spacetime
ω' *versus* ck'

4 — 1200THz

Laser
Per-Spacetime
ω' versus ck
1200THz

3

3 — 900THz

900THz

2 — 600THz

600THz

2 —

Laser per-space
ck

1 — 300THz

300THz

1

1

2

-1   0   1   2   3   4

Atom per-space
ck'

Fig. 3.5 Dispersion hyperbolas for 2-CW interference (a) Laser lab view. (b)Atom frame view.

Chapter 4. Mechanics based on CW axioms

Each of the 2-CW structures or properties discussed so far are due to relative interference effects between pairs of 1-CW entities that, by themselves, lack key 2-CW properties such as a proper invariant frequency ϖ, a rest frame, or any speed below the mortally unattainable velocity of *c*. To acquire "mortal" properties requires an interference encounter or *pairing* of 1-CW with another.

Now we see how 2-CW interference endows other "mortal" properties such as classical *mass* and relativistic mechanics of energy-momentum that characterize a *quantum matter wave*. Such endowment lies in P-hyperbola phase relations (3.10a) that in turn are due to CW axioms (1.1) and (1.2).

$$\omega_p = B\cosh\rho \qquad ck_p = B\sinh\rho \qquad \frac{u}{c} = \tanh\rho$$
$$\approx B + \tfrac{1}{2}B\rho^2 \text{ (for } u \ll c) \text{ (4.1a)} \qquad \approx B\rho \text{ (for } u \ll c) \text{ (4.1b)} \qquad \approx \rho \text{ (for } u \ll c) \text{ (4.1c)}$$

Hyperbola in Fig. 3.4 has bottom $B=\varpi$ and **P**-vector components (ω_p, ck_p) with tangent slope u/c at **P**. At low group velocity $(u \ll c)$ the rapidity ρ approaches u/c. Then ω_p and k_p are simple functions of u.

$$\omega_p \approx B + \tfrac{1}{2}[B/c^2]u^2\cdots \qquad (4.2a) \qquad\qquad k_p \approx [B/c^2]u\cdots \qquad (4.2b)$$

The ω_p and k_p fit Newtonian-energy E and Galilean-momentum p. Is that a coincidence? Indeed, not!

$$E = const. + \tfrac{1}{2}Mu^2 \qquad (4.3a) \qquad\qquad p \approx Mu \qquad (4.3b)$$

Wave ω and k *results* (4.2), scaled by a *single* factor $s=Mc^2/B$, match classical E and p *definitions* (4.3).

$$E = s\omega_p \approx sB + \tfrac{1}{2}[sB/c^2]u^2\cdots \qquad (4.4a) \qquad\qquad p = sk_p \approx [sB/c^2]u\cdots \qquad (4.4b)$$

In Newton's mechanics, only energy *difference* ΔE counts, so he might ignore the term *E=const.* (4.3a). But, in (4.4a) that *const.=sB* is the proper phase *carrier-frequency* value $B=\varpi$ at hyperbola bottom B in Fig. 3.4b. That is scaled by $s=Mc^2/B$ to $sB=s\varpi$ in Fig. 4.1. It is *Einstein rest energy* and not ignorable!

$$const. = sB = Mc^2 = s\varpi \qquad (4.4c)$$

ϖ-mass-energy equivalence is a huge idea due to Einstein (1905) and Planck (1900). *k*-vector-momentum equivalence by DeBroglie came later (1921). CW results (4.1) give both directly and *exactly*.

$$E = s\omega_p = Mc^2\cosh\rho = \frac{Mc^2}{\sqrt{1 - u^2/c^2}} \quad (4.5a) \qquad\qquad p = sk_p = Mc\sinh\rho = \frac{Mu}{\sqrt{1 - u^2/c^2}} \qquad (4.5b)$$

Scale factor s in Planck[ix] $E=s\omega$ or DeBroglie[x] $p=sk$ laws is found experimentally. The lowest observed s-value is Planck angular constant $\hbar=1.05\cdot10^{-34}J\cdot s$. That is Planck's axiom $E=\hbar\omega_n=Nh\upsilon$ for $N=1$. Integer N is Planck's optical quantum number later called *photon-number*. At first, Planck regretted his

1900 axiom $E=Nh\upsilon$. It seems inconsistent with ω^2-dependence of classical oscillator energy $E=A^2\omega^2$. In

1905, Einstein resolved this. A key idea is *quantized amplitude* $A_N=\sqrt{(hN/\upsilon)}$. (Even amplitude is wavy!)
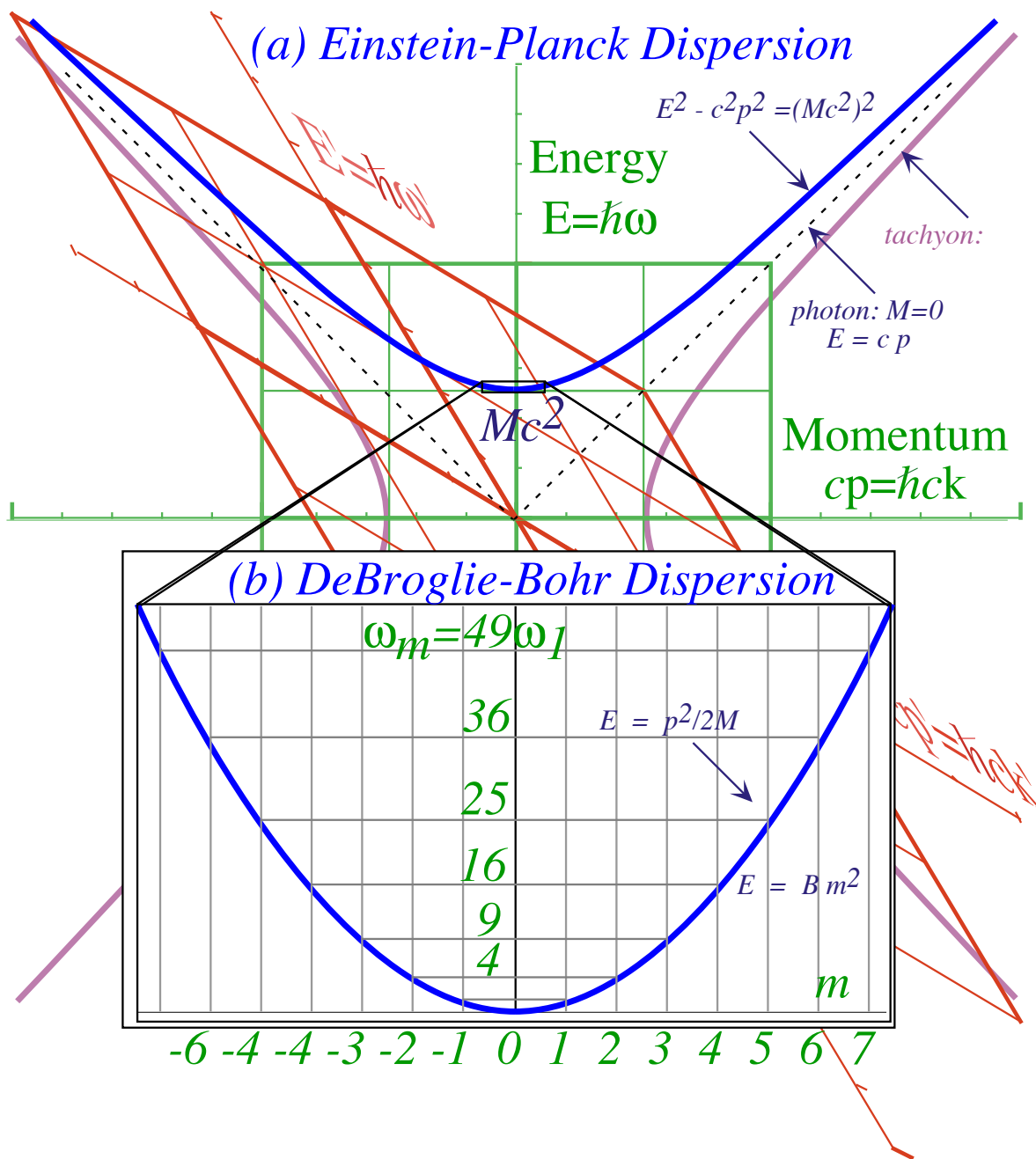

Fig. 4.1 Energy vs. momentum dispersion functions including mass M, photon, and tachyon.
   (a) Relativistic (Einstein-Planck-deBroglie) case: $(Mc^2)^2=E^2-(cp)^2 = 1$ or $\mu^2=\omega^2-(ck)^2 = 1/\hbar^2$.
   (b) Non-relativistic (Bohr-Schrodinger-deBroglie) case: $E=-(1/2M)p^2$ or $\omega = \hbar k^2/2M$

Quantized cavity modes and "fuzzy" hyperbolas
Cavity boundary conditions "*1st-quantize*" classical wave mode variables (ω_n, k_n) so as to have discrete

numbers $n=1,2,3,...$ of half-wave anti-nodes that fit in a cavity of length-ℓ as shown at the top of Fig. 4.2.

$$k_n=\pi/\lambda_n= n\cdot\pi/\ell \qquad (4.6a) \qquad\qquad \omega_n=c\,k_n = c\,n\cdot\pi/\ell \qquad (4.6b)$$

Planck's axiom "*2nd-quantizes*" each fundamental mode frequency ω_n to have discrete quantum numbers $N_n=0,1,2,3,...$ of photons. Each level $E_N(n)=\hbar N_n \omega_n$ labels a hyperbola in Fig. 4.2 whose number n of anti-nodes and N of photons is *invariant*. This lends *object-permanence* to cavity "light particles" or photons.

As discussed in Ch. 6, laser waves are *coherent state* combinations of N-photon states that have *semi-classical* properties that include well-defined wave phase. One "fuzzy" hyperbola of uncertain N and mass-energy replaces the ladders in Fig. 4.2. This is a kind of 2nd Occam-razor cut after the 1st cut of PW into CW. As discussed in Ch. 6, it resolves CW into coherent combinations of "*2nd-quantized*" photons.
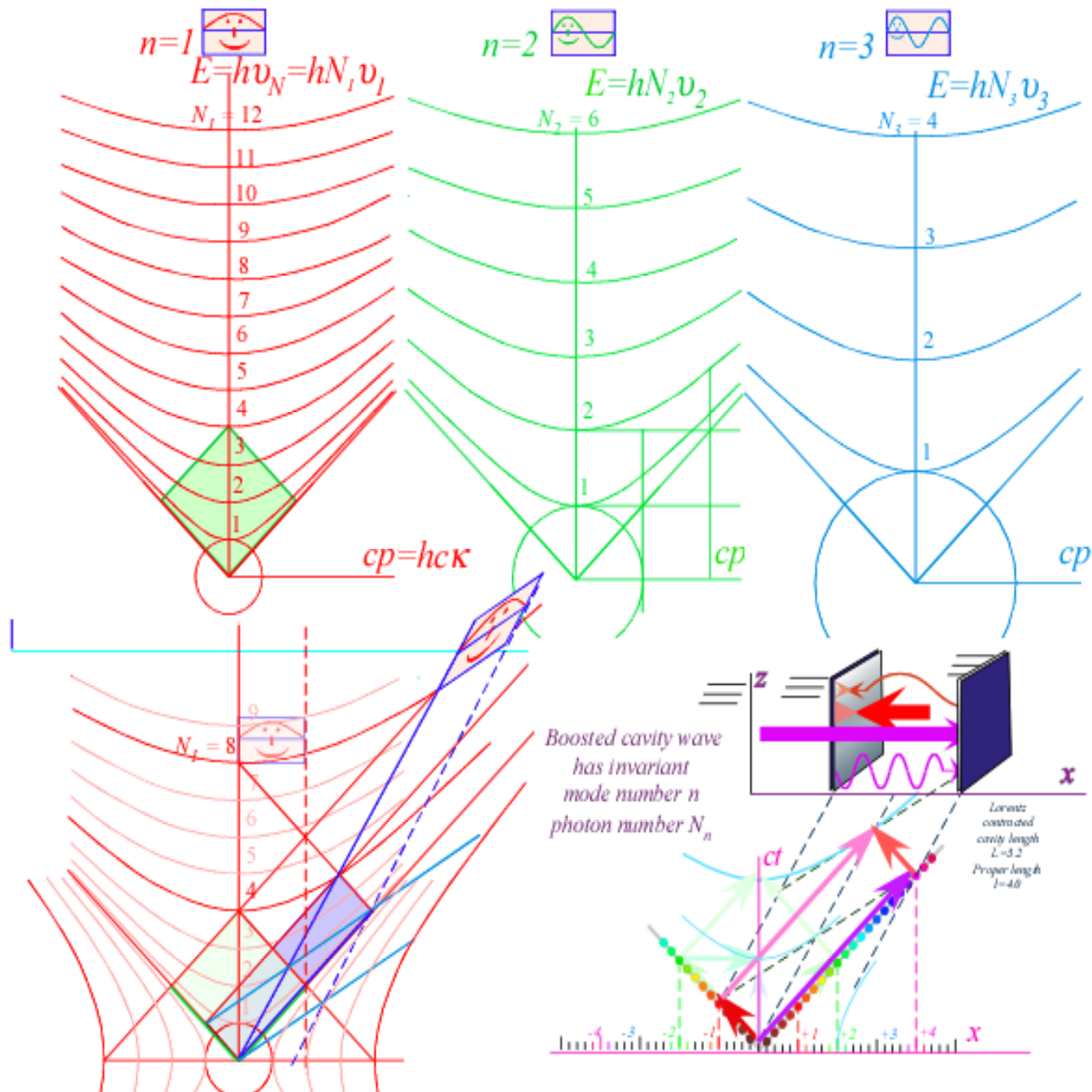
Fig. 4.2 Optical cavity energy hyperbolas for mode number n=1-3 and photon number N=0, 1, 2,....

Alternative definitions of wave mass

      If mass or rest energy is due to proper phase frequency ϖ, then a quantum matter wave has mass without invoking hidden Newtonian "stuff." With Occam logical economy, 2-CW light led to *exact* mass-energy-momentum *(ω,k)* relations (4.5) and not just low-speed classical ones (4.3). Now we see how 2-CW results expose some salient definitions of mass or matter that a classical theory might overlook.

      First, the Einstein-Planck wave frequency-energy-mass equivalence relation (4.4c) ascribes *rest mass M_{rest}* to a scaled proper carrier frequency $s\varpi /c^2$. The scale factor s is Planck's $s=\hbar N$ for N quanta.

$$M_{rest} = E / c^2 = \hbar N \varpi / c^2 \tag{4.7}$$

For rest electron mass $m_e = 9.1 \cdot 10^{-31}kg$ or $M_p = 1.67 \cdot 10^{-27}kg$ of a proton, the proper frequency times $N=2$ is called *zwitterbevegun* ("trembling motion") and is as mysterious as it is huge. (Electron rest frequency $\varpi_e = m_e c^2/\hbar = 7.76 \cdot 10^{+20}(rad)s^{-1}$ is the Dirac (e^+e^-)-pair production[xi] threshold as discussed in Ch. 8.)

      Second, we define *momentum-mass M_{mom}* by ratio p/u of momentum (4.5b) to velocity u. (Galileo's $p=M_{mom}u$) Now M_{mom} varies as $\cosh\rho \rightarrow e^\rho / 2$ at high rapidity ρ but approaches invariant M_{rest} as $\rho \rightarrow 0$.

$$\frac{p}{u} \equiv M_{mom} = \frac{M_{rest}c}{u}\sinh\rho = M_{rest}\cosh\rho \xrightarrow{u \rightarrow c} M_{rest}e^\rho / 2$$
$$= M_{rest} \bigg/ \sqrt{1-u^2/c^2} \xrightarrow{u \ll c} M_{rest} \tag{4.8}$$

Frame velocity u is wave group velocity and the Euclid mean construction of Fig. 3.3a shows u is the slope of the tangent to dispersion function $\omega(k)$. A derivative of energy (4.5a) verifies this once again.

$$V_{group} = \frac{d\omega}{dk} = \frac{dE}{dp} = \frac{c^2 p}{E} = u \tag{4.9}$$

      Third, we define *effective-mass M_{eff}* as ratio $\dot{p}/\dot{u} =F/a=dp/du$ of momentum-*change* to acceleration. (Newton's $F=M_{eff}a$) M_{eff} varies as $\cosh^3\rho \rightarrow e^{3\rho}/2$ at high rapidity ρ but also approaches M_{rest} as $\rho \rightarrow 0$.

$$\frac{F}{a} \equiv M_{eff} \equiv \frac{dp}{du} = \frac{\hbar dk}{dV_{group}} = \hbar \bigg/ \frac{d}{dk}\frac{d\omega}{dk} = \hbar \bigg/ \frac{d^2\omega}{dk^2}$$
$$= M_{rest} \bigg/ \left(1-u^2/c^2\right)^{3/2} \xrightarrow{u \ll c} M_{rest} \tag{4.10}$$

      Effective mass is $\hbar$ divided by the curvature of dispersion function $\omega(k)$, a general quantum wave mechanical result. Geometry of a dispersion hyperbola $\omega=B\cosh\rho$ is such that its bottom *(u=0)* radius of curvature *(RoC)* is the rest frequency $B=M_{rest}c^2/\hbar$, and this grows exponentially toward ∞ as velocity u approaches c. The 1-CW dispersion *($\omega=\pm ck$)* is flat so its *RoC* is infinite everywhere and so is photon

effective mass $M_{eff}(\gamma)=\infty$. This is consistent with the (*All colors go c*)-axiom (1.1). The other extreme is photon rest mass $M_{rest}(\gamma)=0$. Between these extremes, photon momentum-mass depends on CW color ω.

$$M_{rest}(\gamma)=0 \quad (4.11a) \qquad M_{mom}(\gamma)=p/c=\hbar k/c=\hbar\omega/c^2 \quad (4.11b) \qquad M_{eff}(\gamma)=\infty \quad (4.11c)$$

For Newton this would confirm light's "fits" to be crazy to the point of uncontrollable schizophrenia.

A 2-CW *600THz* cavity has zero total momentum *p*, but each photon adds a tiny mass M_γ to it.

$$M_\gamma=\hbar\omega/c^2=\omega\ (1.2\cdot 10^{-51})kg\cdot s= 4.5\cdot 10^{-36}kg \qquad\qquad (\textit{for: } \omega=2\pi\cdot 600THz)$$

In contrast, a 1-CW state has no rest mass, but 1-photon momentum (4.5b) is a non-zero value $p_\gamma=M_\gamma c$.

$$p_\gamma=\hbar k=\hbar\omega/c=\omega\ (4.5\cdot 10^{-43})kg\cdot m=1.7\cdot 10^{-27}kg\cdot m\cdot s^{-1} \qquad\qquad (\textit{for: } \omega=2\pi\cdot 600THz)$$

This $p=Mc$ resembles Galilean relation $p=Mu$ in (4.3b) and is perhaps another case of Galileo's revenge!

Absolute vs. relative phases: Method in madness

Probably Newton would find a CW theory to be quite mad. Claiming that heavy hard matter owes its properties to rapid hidden "carrier" phase oscillations would not elicit a Newtonian invitation to the Royal Society but rather to a lunatic asylum. Even though CW results (4.2) give Newtonian axioms (4.3) at low speeds, the result would seem to fail at high speeds where exact results (4.5) sag below Newton's. Also, having an enormous constant Mc^2 be part of energy would, in 1670, seem insanely meaningless.

But, in 1905[xii] Einstein relations appear with both Mc^2 and energy sag. Now Einstein's classical training left him leery of hidden quantum wave phases with dicey interpretations of intensity $\Psi^*\Psi$ as *probability*. Also, he may have asked why observable results depend on a square $\Psi^*\Psi=|\Psi|^2$ that kills that overall phase frequency, seemingly losing the one quantity that represents (or *is*) the total mass-energy.

Square $|\Psi|^2$ of a 2-CW $\Psi=e^{ia}+e^{ib}$ loses phase factor $e^{i(a+b)/2}$ leaving group functions $\cos^2(\frac{a-b}{2})$ of *differences* $\omega_1-\omega_3$ or k_1-k_3 of 1st or 3rd base frequencies or *k*-vectors. Group beat frequency $\Delta\omega=\omega_1-\omega_3$ is zero in the rest frame of Fig. 2.1c where it is a stationary wave. In Fig. 2.2c or any other frame, $|\Psi|^2$ is not stationary but is observed to have velocity $V_{group}\neq 0$. Fourier sums of $m=3$ or more terms $\Psi = a_1e^{i(k_1x-\omega_1 t)} + a_2e^{i(k_2x-\omega_2 t)} + a_3e^{i(k_3x-\omega_3 t)} + ...$ may have multiple beats in $\Psi*\Psi$ as in Fig. 2.2d.

$$P =|\Psi|^2= \Psi*\Psi = \sum a_i * a_j e^{i(\Delta k_{ij}x-\Delta\omega_{ij} t)} \qquad\qquad (4.12)$$

With $m(m-1)/2$ observable *difference* $\Delta\omega_{ij} = \omega_1 - \omega_j$ or *beat* notes, *P* cannot rest in any frame. Differences or derivatives are observable while absolute Ψ-frequency stays hidden *until two quantum objects interfere*. Then new beats arise from differences between the two absolute frequencies and others. A new absolute phase (not in $|\Psi|^2$) is the sum of all. But, we can only observe beats of relative frequency! That may be a quantum version of Einstein's popularized saw, "It's *all* relative." Phase velocity escapes with its Galilean arithmetic intact in Fig. 3.1, but here it finally surrenders its absolutes to relativism.

Total phase gives total energy *E* or momentum *p*, but *differential*s are what one feels due to work ΔE or impulse Δp. Invariant quantities like ϖ and M_{rest} depend on *total* phase but intensity (4.12) has only differentials Δk_{ij} or *relative* beats $\Delta\omega_{ij}$. Among frame-dependent relative quantities are group velocity *u* (4.9), M_{mom} (4.8), and M_{eff} (4.10), but rest mass M_{rest} (4.4c) is a frame-invariant absolute quantity. Also note

that M_{mom} and M_{eff} approach M_{rest} at zero velocity. Now $|\Psi|^2$ may register an ϖ beat with a DC *(static $\omega_0=0$)* wave, but lack of resonance confines *($\omega_0=0$)*-carrier waves to beat only locally.

Phase frequency ω_p in a quantum wave $e^{ip}\cos g = e^{-i(k_p x - \omega_p t)}\cos(k_g x - \omega_g t)$ is fast and silent like a carrier frequency of radio wave. Group frequency ω_g is like the audible signal, much slower and heard in resonant beats $\omega_a - \omega_b$ involving carrier and receiver. Atomic "carrier" frequencies $\omega_p = M_p c^2/\hbar$ due to rest mass are enormous as are those of atomic measuring devices that play the role of "receivers" in quantum experiments. Measurement involves resonant contact of an atom and devices that horse-trade beats at truly huge frequencies.

One way to avoid huge $Mc^2/\hbar$-related phase frequencies is to ignore them and approximate the relativistic equation $E=Mc^2\cosh\rho$ of (4.5a) by the Newtonian approximation (4.4a) that deletes the big rest-energy constant $sB=Mc^2$. The exact energy (4.5a) that obeys CW axioms (1.1) is rewritten in terms of momentum (4.5b) below to give a Bohr-Schrodinger (BS) approximation (4.14) with Mc^2 deleted.

$$E = \frac{Mc^2}{\sqrt{1-u^2/c^2}} = Mc^2\cosh\rho = Mc^2\sqrt{1+\sinh^2\rho} = \sqrt{\left(Mc^2\right)^2 + \left(cp\right)^2} \qquad (4.13)$$

$$E = \left[\left(Mc^2\right)^2 + \left(cp\right)^2\right]^{1/2} \approx Mc^2 + \frac{1}{2M}p^2 \xrightarrow[BS-approx]{} \frac{1}{2M}p^2 \qquad (4.14)$$

If only frequency difference affect observation based on $|\Psi|^2$ (4.12), the BS claim is that energy origin may be shifted from *($E=Mc^2$, $cp=0$)* to *($E=0$, $cp=0$)*. (*Frequency is relative!*) Hyperbola (4.13) in Fig. 4.1a, for u way less then c, approaches the BS parabola (4.14) in Fig. 4.1b. That is the only $E(p)$ Newton knew.

Group velocity $u=V_{group}=\frac{d\omega}{dk}$ of (4.9) is a relative or differential quantity so origin shifting does not affect it. However, phase velocity $\frac{\omega}{k}=V_{phase}$ is greatly reduced by deleting Mc^2 from $E=\hbar\omega$. It slows from $V_{phase}=c^2/u$ that is always faster than light to a sedate sub-luminal speed of $V_{group}/2$. Having V_{phase} go slower than V_{group} is an unusual situation but one that has achieved tacit approval for BS matter waves.[xiii] The example used in Fig. 1.6 of Ch. 1 is a 2-CW BS matter wave exhibiting this low V_{phase}.

Standard Schrodinger quantum mechanics, so named in spite of Schrodinger's protests[xiv], uses Newtonian kinetic energy (4.14) or (4.3) with potential φ (as the *const.*-term) to give a BS Hamiltonian.

$$H=p^2/2M + \varphi \quad \text{or:} \quad \hbar\omega = \hbar^2 k^2/2M + \langle\varphi\rangle_k \qquad (4.15)$$

The CW approach to relativity and quantum exposes some problems with such approximations.

First, a non-constant potential φ must have a vector potential **A** so that *(φ,c**A**)* transform like *(ω,c**k**)*

in (2.10a) or *(ct,**x**)* in (2.10b) or as *(E,c**p**)* with scaling laws **p**=ℏ**k** and *E*=ℏω. Transformation demands

equal powers for frequency (energy) and wavevector (momentum) such as the following.

$$(E\text{-}\varphi)^2 = (\mathbf{p}\text{-}c\mathbf{A})^2/2M + Mc^2 \qquad \text{or:} \qquad (\hbar\omega\text{-}\langle\varphi\rangle_k)^2 = (\hbar\mathbf{k}\text{-}c\mathbf{A})^2/2M + Mc^2 \qquad (4.16)$$

Also, varying potentials perturb the vacuum so single-CW's may no longer obey axioms (1.1-2).

Diracs's elegant solution obtains ±pairs of hyperbolas (4.13) or (4.16) from avoided-crossing

eigenvalues of *4x4* Hamiltonian matrix equations with negative frequency hyperbolas. The negative-ω

hyperbolas in Fig. 4.1 are (conveniently) hidden by the BS approximate dispersion parabola.

Dirac's ideas require three-dimensional wavevectors and momenta. But first, fundamental

Lagrangian-Hamiltonian geometric relations of quantum phase and frequency relate relativistic classical

and quantum mechanics in the following Ch. 5. These relations expose more of the logic of phase-based

Evenson axiom (1.1), Doppler *T*-symmetry axiom (1.2), and Euclid frequency means in Fig. 3.3.

Chapter 5. Classical vs. quantum mechanics

The CW-spectral view of relativity and quantum theory demonstrates that wave phase and in particular, optical phase, is an essential part of quantum theory. If so, classical derivation of quantum mechanics might seem about as viable as Aristotelian derivation of Newtonian mechanics.

However, the 19th century mechanics of Hamilton, Jacobi, and Poincare developed the concept of *action S* defined variously by area $\oint pdq$ in phase-space or a Lagrangian time integral $\int L\, dt$. The latter action definition begins with the Legendre transformation of Lagrangian L and Hamiltonian H functions.

$$L = p \cdot \dot{x} - H \qquad (5.1a)$$

L is an explicit function of x and velocity $u = \dot{x}$ while the H is explicit only in x and momentum p.

$$0 = \frac{\partial L}{\partial p} \quad (5.1b) \qquad p = \frac{\partial L}{\partial \dot{x}} \quad (5.1c) \qquad\qquad 0 = \frac{\partial H}{\partial \dot{x}} \quad (5.1d) \qquad \dot{x} = \frac{\partial H}{\partial p} \qquad (5.1e)$$

Multiplying by dt gives the differential *Poincare invariant dS* and its *action integral* $S = \int L\, dt$.

$$dS = L\, dt = p \cdot dx - H\, dt \qquad (5.2a) \qquad\qquad S = \int L\, dt = \int p \cdot dx - \int H\, dt \qquad (5.2b)$$

Planck-DeBroglie scaling laws $p=\hbar k$ and $E=\hbar\omega$ (4.5) identify action S as scaled quantum phase $\hbar\Phi$.

$$\hbar\, d\Phi = L\, dt = \hbar k \cdot dx - \hbar\omega\, dt \quad (5.3a) \qquad\qquad \Phi = \int k \cdot dx - \int \omega\, dt \qquad (5.3b)$$

If action dS or phase dΦ is integrable, then *Hamilton-Jacobi equations* or (k,ω) equivalents hold.

$$\frac{\partial S}{\partial x} = p \quad (5.4a) \qquad \frac{\partial S}{\partial t} = -H \quad (5.4b) \qquad\qquad \frac{\partial \Phi}{\partial x} = k \quad (5.4c) \qquad \frac{\partial \Phi}{\partial t} = -\omega \qquad (5.4d)$$

Phase-based relations (5.4c-d) define angular frequency ω and wave number k. The definition (3.8) of wave group velocity is a wave version of Hamilton's velocity equation (5.1e).

$$\dot{x} = \frac{\partial H}{\partial p} \quad \text{equivalent to: } u = V_{group} = \frac{\partial \omega}{\partial k}$$

The coordinate Hamilton derivative equation relates to wave diffraction by dispersion anisotropy.

$$\dot{p} = -\frac{\partial H}{\partial x} \quad \text{equivalent to: } \quad \dot{k} = -\frac{\partial \omega}{\partial x}$$

Classical HJ-action theory was intended to analyze families of trajectories (PW or particle paths), but Dirac and Feynman showed its relevance to matter-wave mechanics (CW phase paths) by proposing an approximate semi-clasical wavefunction based on the Lagrangian action as phase.

$$\Psi \approx e^{i\Phi} = e^{iS/\hbar} = e^{i\int L\, dt/\hbar} \qquad (5.5)$$

The approximation symbol ($\approx$) indicates that only phase but not amplitude is assumed to vary here. An x-derivative (5.4a) of semi-classical wave (5.5) has the **p**-operator form in standard BS quantum theory.

$$\frac{\partial}{\partial x}\Psi \approx \frac{i}{\hbar}\frac{\partial S}{\partial x}e^{iS/\hbar} = \frac{i}{\hbar}p\Psi \quad (5.6a) \qquad\qquad \frac{\hbar}{i}\frac{\partial}{\partial x}\Psi = p\Psi \qquad (5.6b)$$

The time derivative is similarly related to the Hamiltonian operator. The HJ-equation (5.4b) makes this appear to be a BS Hamiltonian time equation.

$$\frac{\partial}{\partial t}\Psi \approx \frac{i}{\hbar}\frac{\partial S}{\partial t}e^{iS/\hbar} = -\frac{i}{\hbar}H\Psi \qquad (5.7a) \qquad\qquad i\hbar\frac{\partial}{\partial t}\Psi = H\Psi \quad (5.7b)$$

However, these approximations like the BS approximations of (4.14) ignore relativity and lack economy of logic shed by light waves. The Poincare phase invariant of a matter-wave needs re-examination.

Contact transformation geometry of a relativistic Lagrangian

A matter-wave has a rest frame where $x'=0=k'$ and its phase $\Phi = kx-\omega t$ reduces to $-\mu\tau$, a product of its proper frequency $\mu=N\varpi$ (or $Mc^2/\hbar$) with proper time $t'=\tau$. Invariant differential $d\Phi$ is reduced, as well, using the Einstein-Planck rest-mass energy-frequency equivalence relation (4.4c) to rewrite it.

$$d\Phi = kdx-\omega dt=-\mu \; d\tau = -(Mc^2/\hbar) \; d\tau. \qquad (5.8)$$

τ-Invariance (2.21) or time dilation in (2.10b) gives proper $d\tau$ in terms of velocity $u=\frac{dx}{dt}$ and lab dt.

$$d\tau = dt \sqrt{(1-u^2/c^2)} = dt \; sech \; \rho \qquad (5.9)$$

Combining definitions for action $dS=Ldt$ (5.2) and phase $dS = \hbar d\Phi$ (5.3) gives the Lagrangian L.

$$L =-\hbar\mu\tau = -Mc^2\sqrt{(1-u^2/c^2)} = -Mc^2 sech \; \rho \qquad (5.10)$$

Fig. 5.1 plots this free-matter Lagranian L next to its Hamiltonian H using units for which $c=1=M$.
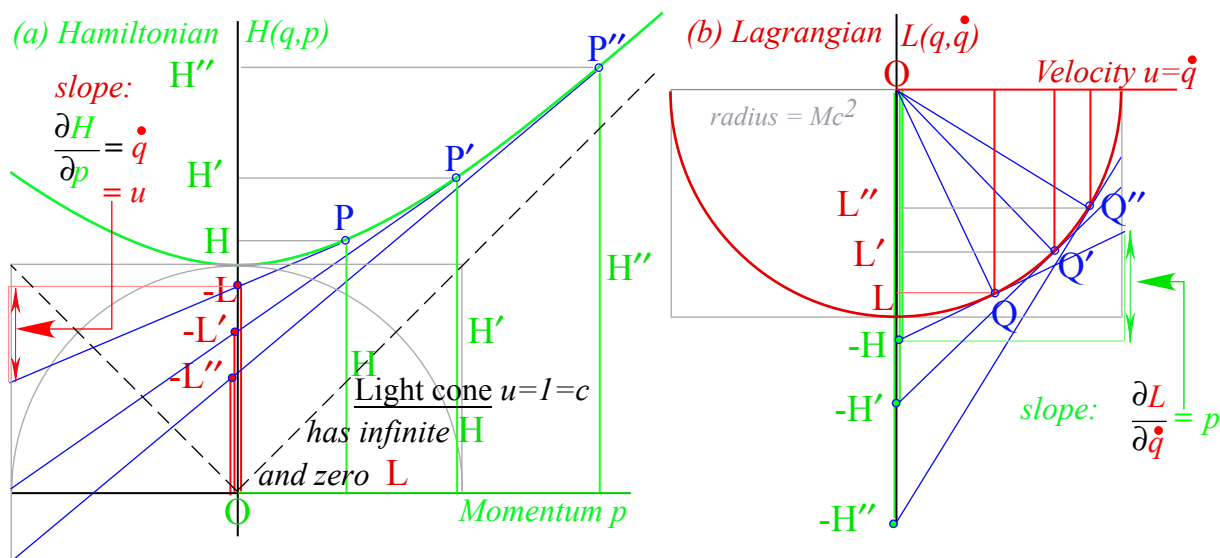

Fig. 5.1. Geometry of contact transformation between relativistic (a) Hamiltonian (b) Lagrangian

Relativistic matter Lagrangian (5.10) is a circle (Fig. 5.1b). L-values L, L', and L'' in Fig. 5.1 are contact Legendre transforms of H-values H, H', and H'' of Hamiltonian hyperbola in Fig. 5.1a. Abscissa p

and ordinate *H* of a point P in plot (a) gives negative intercept *-H* and slope *p* of tangent *HQ* contacting the transform point *Q* in plot (b) and *vice-versa*. (Contact geometry is really wave-action-energy mechanics.)

If $p = Mu$, Lagrange kinetic energy $L = \frac{1}{2}Mu^2$ is Hamilton $H = p^2/2M$. Then circle *L* and hyperbola *H both* approximate a Newtonian parabola at low speed *u<<c*. But, as *u→c* the *L*-circle rises above the parabola and the *H*-hyperbola sags below it and instead approaches contacting *c*-asymptote in Fig. 5.1.

Action integral *S=∫Ldt* is to be *minimized*. Feynman's interpretation of *S* minimization is depicted in Fig. 5.2. A mass flies so that its "clock" τ is *maximized*. (Proper frequency $\mu = Mc^2/\hbar$ is constant for fixed rest mass, and so minimizing –μτ means maximizing +τ.) An interference of Huygen wavelets favors stationary and extreme phase. This favors the fastest possible clock as is sketched in Fig. 5.3.

Feynman described families of classical paths or rays fanning out from each space-time point on a wavefront of constant phase Φ or action *S*. Then, according to an application of Huygen's principle to matter wave, new wavefronts are continuously built in Fig. 5.3 through interference from "the best" of all the wavelets emanating from a multitude of source points on each preceding wavefront. Thus classical momentum **p**=∇*S* by (5.4a) for the "best" ray ends up normal to each wavefront.

The "best" are so-called *stationary-phase* rays that are extremes in phase and thereby satisfy *Hamilton's Least-Action Principle* requiring that ∫*Ldt* is minimum for "true" classical trajectories. This in turn enforces Poincare' invariance by eliminating, by de-phasing, any "false" or non-classical paths because they do not have an invariant (and thereby stationary) phase. "Bad rays" cancel each other in a cacophonous mish-mash of mismatched phases. Each Huygen wavelet is tangent to the next wavefront being produced. That contact point is precisely on the ray or true classical trajectory path of minimum action and on the resulting "best" wavefront. Time evolution from any wavefront to another is thus a contact transformation between the two wavefronts described by the geometry of Huygens Principle.

Thus a Newtonian clockwork-world appears to be the perennial cosmic gambling-house winner in a kind of wave dynamical lottery on an underlying wave fabric. Einstein's God may not play dice, but some persistently wavelike entities seem to be gaming at enormous $Mc^2/\hbar$-rates down in the cellar!

It is ironic that Evenson and other metrologists have made the greatest advances of precision in human history, not with metal bars or ironclad classical mechanics, but by using the most ethereal and dicey stuff in the universe, light waves. This motivates a view of classical matter or particle mechanics that is more simply and elegantly done by its relation to light and its built-in relativity, resonance, and quantization that occurs when waves are subject to boundary conditions or otherwise confined. While Newton was complaining about "fits" of light, that crazy stuff was just trying to tell him something!

Derivation of quantum phenomena using a classical particle paradigm seems silly now. If particles are made by waves, optical or otherwise, rather than *vice versa* as Newton believed, the case is closed. Also, CW trumps PW as CW symmetry axioms (1.1-2) derive classical results (4.4) while giving exact relations (4.5) for relativity and quantum theory tossed into the bargain. Such Occam economy is found lacking on a PW path from Newton to Einstein and Planck.

Thus basic CW sum-and-difference phase relations seem to underlie the physics of Poincare contact geometry. This in turn is based on circular and hyperbolic geometry described next.
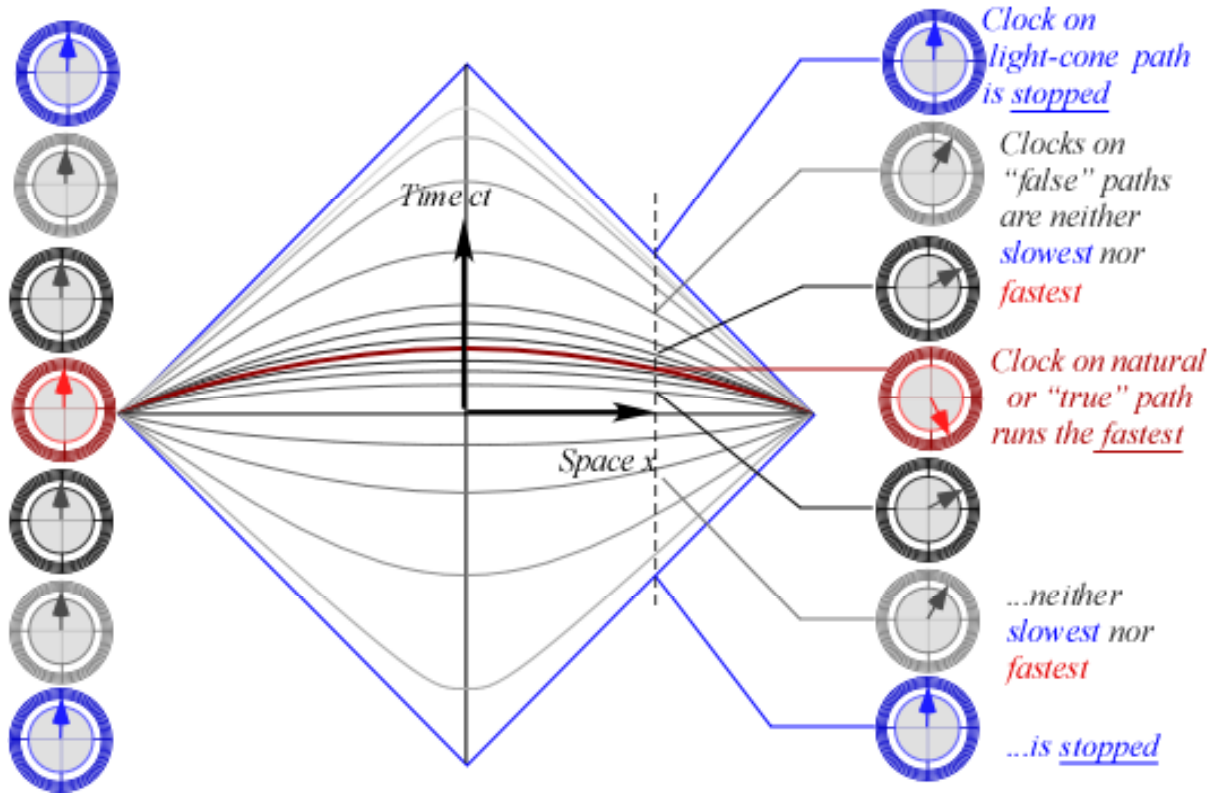
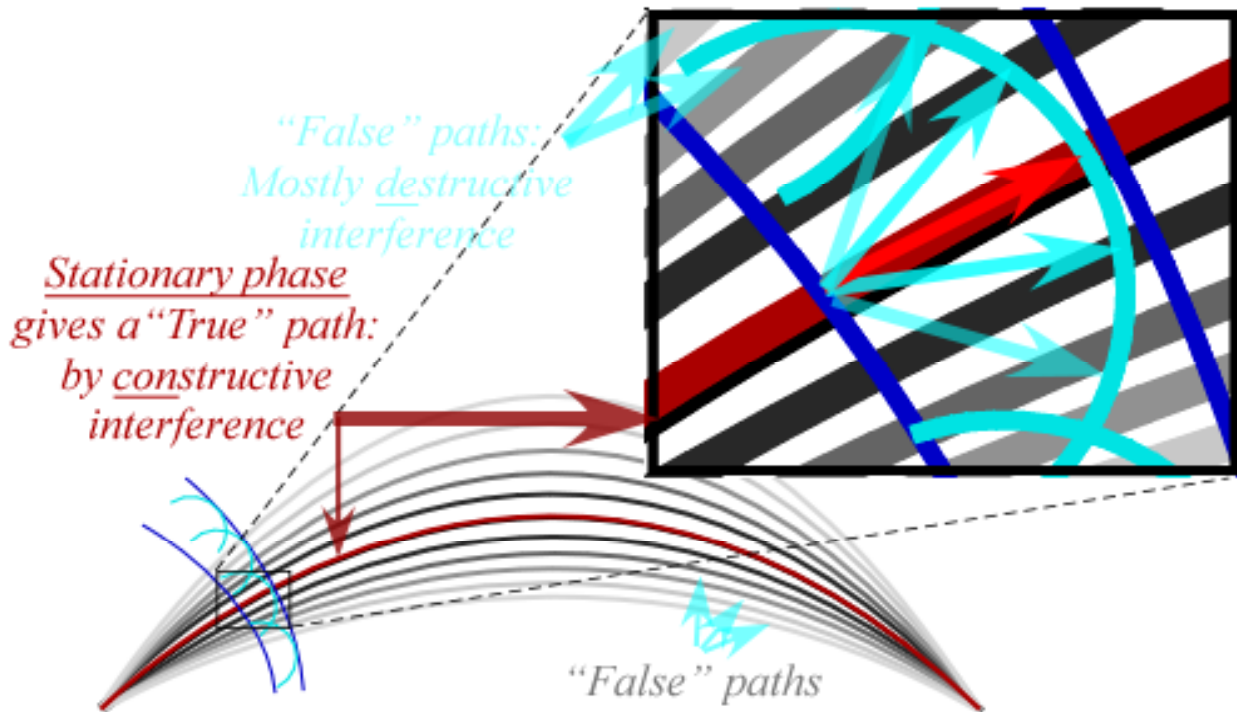*Fig. 5.2 "True" paths carry extreme phase and fastest clocks. Light-cone has only stopped clocks.*

Fig. 5.3 Quantum waves interfere constructively on "True" path but mostly cancel elsewhere.

Geometry of circular and hyperbolic functions

Geometry of half-sum and half-difference phase **P**=(**R**+**L**)*/2* and group **G**=(**R**-**L**)*/2* vectors is based on trigonometric exponential identities that are crown jewels of 18th century mathematics and have Euclidian geometric origins shown in Fig. 5.4. Phase angle-ϕ identities apply to Fig. 5.4a.

$$e^{+i\phi} = \cos\phi + i\sin\phi \qquad (5.11a) \qquad \cos\phi = (e^{+i\phi} + e^{-i\phi})/2 \qquad (5.11b)$$
$$e^{-i\phi} = \cos\phi - i\sin\phi \qquad\qquad i\sin\phi = (e^{+i\phi} - e^{-i\phi})/2$$

Circular function *tan*ϕ is named for a tangent to a unit circle shown in Fig. 5.4(a). Its inc*line* (s*ine*) elevation is *sin*ϕ. The complimentary tangent or cotangent *cot*ϕ completes the tangent distance between axes where ϕ is circle arc-length-ϕ or *subtended area*-ϕ. Hyperbolic functions use area ρ for "angle."

$$e^{+\rho} = \cosh\rho + \sinh\rho \qquad (5.12c) \qquad \cosh\rho = (e^{+\rho} + e^{-\rho})/2 \qquad (5.12d)$$
$$e^{-\rho} = \cosh\rho - \sinh\rho \qquad\qquad \sinh\rho = (e^{+\rho} - e^{-\rho})/2$$

Fig. 5.4b shows how hyperbolic functions relate to circular ones in Fig. 5.4a. The circular sine equals the hyperbolic tangent (*sin*ϕ =*tanh*ρ) and *vice versa* (*tan*ϕ =*sinh*ρ). Each circular function has a segment that matches one for a hyperbolic function, for example (*cos*ϕ =*sech*ρ) matches (*sec*ϕ =*cosh*ρ). These relations recap the CW view of the Legendre contact transformation in Fig. 5.1 that underlies classical and quantum theory that is in the algebra and geometry for every bit of light-and-matter in and around us!

In Fig. 5.4, circular area ϕ and hyperbolic area ρ have been chosen so that *tan*ϕ =*1.15*=*sinh*ρ and *sin*ϕ =*0.75*=*tanh*ρ, that is for *u=3c/4*. The tangent to the circle in Fig. 5.4a-b is like the one that contacts the Lagrangian circle in Fig. 5.1b to contact-transform it to the Hamiltonian hyperbola in Fig. 5.1a, and *vice versa* the hyperbolic tangent in Fig. 5.4b is like the one that transforms the Hamiltonian hyperbola in Fig. 5.1a to the Lagrangian circle in Fig. 5.1b.

The hyperbolic tangent *u/c=tanh*ρ of (2.19) corresponds to frame rapidity ρ and group velocity $u=V_{group}=\frac{d\omega}{dk}$ in (2.8), (4.9) and in Fig. 3.3a-b. The circular tangent angle ϕ or inclination *sin*ϕ belongs to Lagrangian velocity function (5.10) in Fig. 5.1b. (The horizontal axis of the latter in the vertical axis of Fig.11. This geometry is symmetric to axis-switching.) As u and ρ approach c and ∞, respectively, the circular angle ϕ approaches $\pi/2$.

This angle ϕ is the *stellar velocity aberration angle*, that is, the polar angle that vertical starlight is seen by a horizontally moving astronomer to tip into her direction of motion. Aberration angle ϕ, like rapidity ρ, is 1st-order in velocity u and both ρ and ϕ equal u/c at low speeds. (See the discussion of Fig. 5.6 near the end of this chapter. This deepens the development to include 4-vector space-time.)

Many of the twelve circular-hyperbolic trigonometric ratios in Fig. 5.1 belong to one or more physical or geometric effects shown before beginning with Euclid's rectangle-in-circle mean construction of Fig. 3.3. These are overlapped in a kind of global ratio riot Fig. 5.1. This riot is collected and labeled in Fig. 5.5b-d. This is the basis of the discussion below of the role of tangent-contact geometry in CW analysis of Poincare contact transformation and relativistic quantum waves.
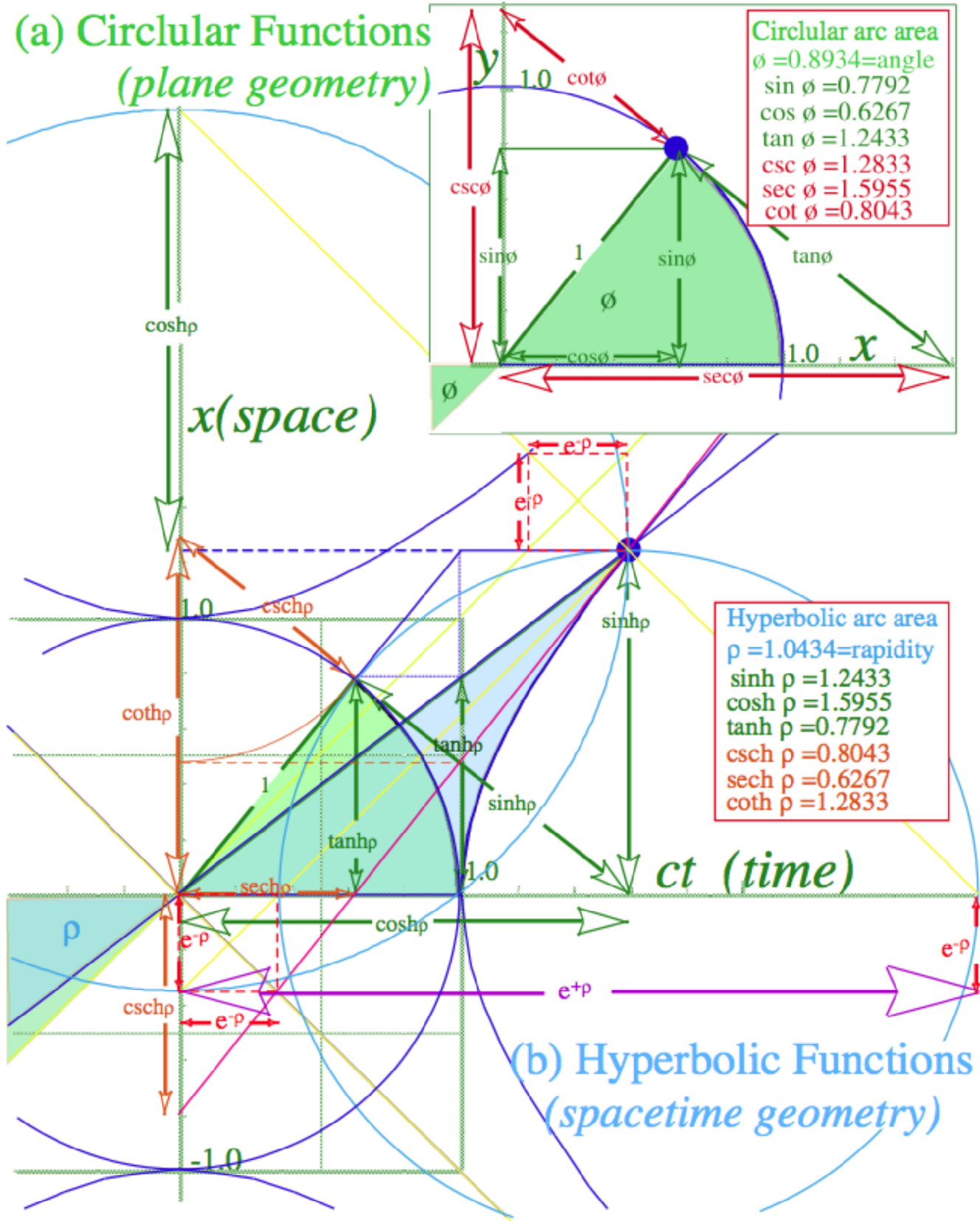
Fig. 5.4 Trigonometric geometry (a) Unit circular area ϕ=σ =0.8934 (b) Unit hyperbolic area ρ=1.0434.

Hyper-circular contacts

Beginning with the Euclidian mean diagram of Fig. 3.3, three mean frequencies arise from an interfering pair of left-moving "red" and right-moving "blue" beams of frequency ω_L and ω_R. First is a half-sum phase frequency $\omega_p=(\omega_R+\omega_L)/2$ (arithmetic mean) that defines the circle radius in Fig. 3.3. Second is a half-difference group beat frequency $\omega_g=(\omega_R-\omega_L)/2$ (difference mean) that is radial distance of circle center to origin. Third is a root-product proper frequency $\varpi =(\omega_R\cdot\omega_L)^{1/2}$ (geometric mean) that is the base radius or bottom of a $\omega(k)$ hyperbola of rest energy $B=\hbar\varpi =Mc^2$ above origin in Fig. 3.3.

Phase and group frequencies are defined as ratios or shifts of the geometric mean frequency ϖ, and this begins with the Doppler shift definition of the red $\omega_L=e^{-\rho}\varpi$ and blue $\omega_R=e^{+\rho}\varpi$ CW components. Ratio values $\omega_p=\varpi cosh\rho$ and $\omega_g=\varpi sinh\rho$ define each point on a ϖ-hyperbola dispersion curve in Fig. 5.5. Fig. 5.5 is based on circles with three different radii, one for each mean frequency. The base circle-*b* drawn centered at origin has radius $B=\hbar\varpi =Mc^2$ of the Lagrangian circle in Fig. 5.1b. A smaller circle-*g* has group radius $\hbar\omega_g=Bsinh\rho$. A larger circle-*p* has phase radius $\hbar\omega_p=Bcosh\rho$ of the Euclidean circle in Fig. 3.3 and is drawn with dashed lines in Fig. 5.5. (Base value *B* is scaled for energy here.) Circle-*p* of larger radius $\hbar\omega_p=Bcosh\rho$ is centered at $cp=\hbar\omega_g=Bsinh\rho$, a horizontal distance equal to the radius of the smaller circle-*g*, while the latter is centered at $E=\hbar\omega_p=Bcosh\rho$, a vertical distance equal to the radius of the larger circle-*p*. Tangents that contact circles or hyperbolas define many of the physical quantities labeled in the zoom-in view of Fig. 5.5b. Intersections and chords shared by two of the circles also provide the key quantities as seen in Fig. 5.5a.

So far the CW development has emphasized the Doppler ratio as a starting point beginning with Fig. 2.2 and culminating with the Euclidean means of Fig. 3.3. However, most developments of relativity start with velocity *u*, and that geometric approach is excerpted in a simplified construction of Fig. 5.5c where $u/c=45/53$ and Fig. 5.5d where $u/c=3/5$. (Fig. 5.5a-b and most other figures use $u/c=3/5$.) Once the velocity u/c line intersects the basic *b*-circle and its horizontal tangent of unit-energy ($B=1=Mc^2$), it only takes three more lines to derive Lagrangian $-L=Bsech\rho$, then momentum $cp=Bsinh\rho$, and finally the Hamiltonian $H=Bcosh\rho$. Then a compass is used to check accuracy with the phase *p*-circle by making sure it goes from *(cp,H)* to the *(0,B)*-point on top of the *b*-circle. The *p*-circle goes on to intersect the negative *cp*-axis at the Doppler red shift $rB=Be^{+\rho}$. Finally, the group *g*-circle in Fig. 5.5a-b has a chord intersection with the *p*-circle that is the hyperbolic contact tangent, and it grazes the ϕ-angle normal to the Lagrangian circle tangent in Fig. 5.5b. This helps to clarify geometry of *H-L* contact transformations of Fig. 5.1 for reciprocal space-time *(ω,ck)* and *(Φ,u/c)*. The constructions also apply to space-time.

If Fig. 5.5 is in space-time, the segment $-L=Bsech\rho$ is Lorentz contraction $\ell = B\sqrt{1-u^2/c^2}$. The $H=Bcosh\rho$ and $cp=Bsinh\rho$ segments are, respectively Einstien time dilation $d = B/\sqrt{1-u^2/c^2}$ and asimultaneity $a=ud/c$ coefficients. Node-to-node or peak-to-peak gaps contract by $\ell=4/5$ in Fig. 2.2d-e.

As speed reduces in Fig. 5.5c-d from $u/c=45/53$ to $u/c=3/5$ or to lower values, the Lagrangian velocity angle ϕ and Hamiltonian rapidity ρ approach the velocity ratio u/c. Galilean velocity addition rules resume. In the opposite ultra-relativistic regime, ϕ approaches $\pi/2$, ρ approaches ∞, and u/c nears unit slope or *45°* in Fig. 5.5c. But, Galilean-like rules (3.6) apply to rapidity ρ at all speeds (so far).

(a) *Geometry of relativistic transformation and wave based mechanics*

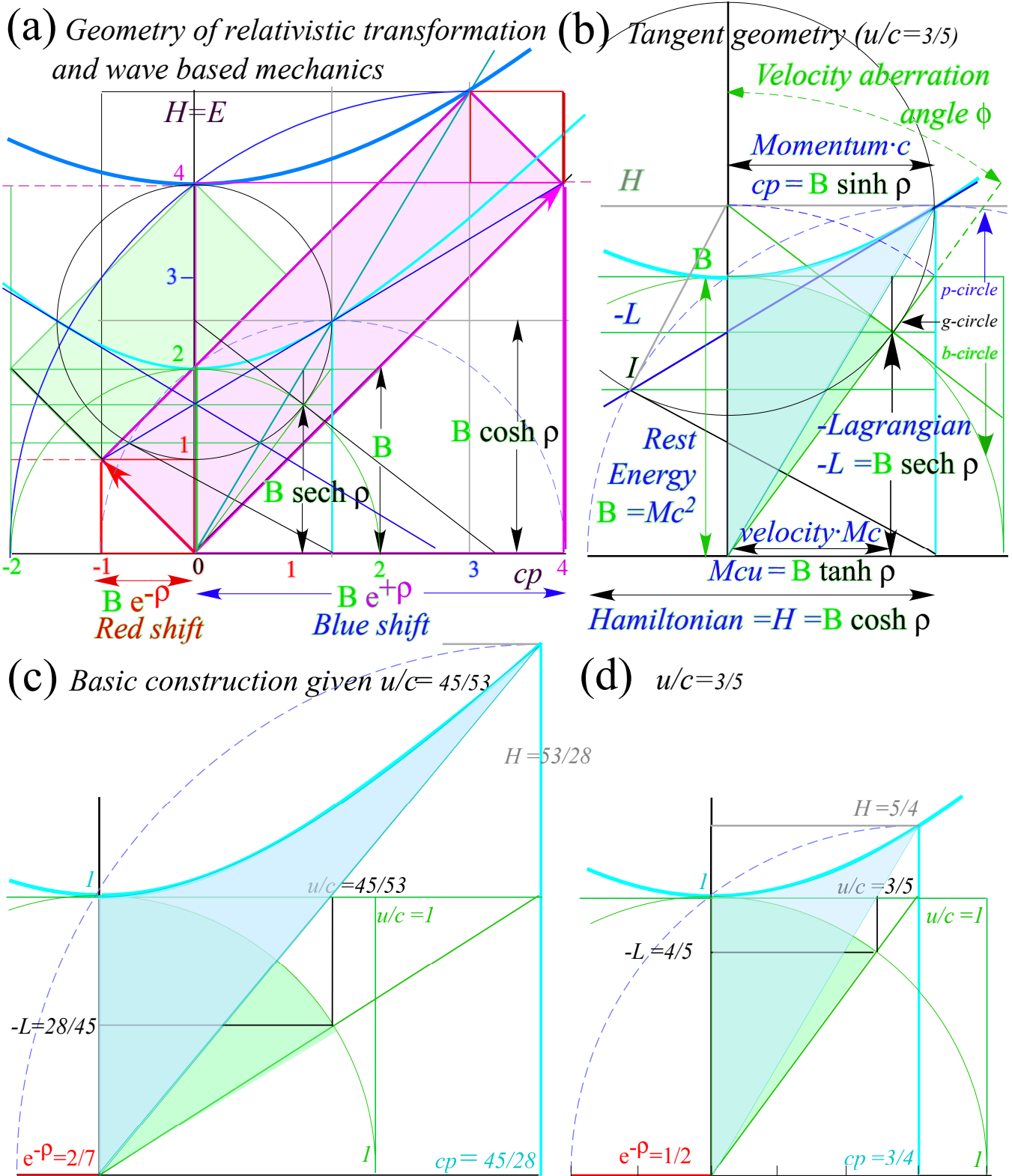# (b) *Tangent geometry (u/c=3/5)*

Fig. 5.5 Relativistic wave mechanics geometry. (a) Overview. (b-d) Details of contacting tangents.

Transverse vs. longitudinal Doppler: Stellar aberration

   A novel description of relativity by L. C. Epstein[xv] in *Relativity Visualized* introduces a "cosmic speedometer" consisting of a telescope tube tipped to catch falling light pulses from a distant overhead star. A stationary telescope points straight up the x-axis at the apparent position S of the star. (Fig. 5.6a) But, with velocity $\mathbf{u}=u_z\mathbf{e}_z$ across to the star beam x-axis, the telescope has to tip to catch the starlight, so the apparent position S' tips toward $\mathbf{u}$. (Fig. 5.6b).

The telescope tips by a *stellar aberration angle* $\sigma(\phi$ in (5.11a) or Fig. 5.4a.). The sine of angle σ is velocity ratio $\beta= u_z/c$ which is the hyper-tangent of relativistic rapidity υ_z (ρ in (5.12a) or Fig. 5.4b.)

$$\beta= u_z/c =sin\ \sigma = tanh\ \upsilon_z \tag{5.13}$$

   Proper time τ and frequency ϖ invariance (3.10) forces 4-vector components normal to velocity $\mathbf{u}$ of a boost to be unchanged. That is, a boost along z of (ct,z) to (ct',z') (or (ω,ck_z) to $(\omega',ck_{z'})$) must preserve both $(x,y)=(x',y')$ and $(ck_x,ck_y)=(ck_{x'},ck_{y'})$ just as a rotation in the xy-plane of (x,y) to (x',y') leaves unaffected the components $(ct,z)=(ct',z')$ and $(\omega,ck_z)=(\omega',ck_{z'})$ transverse to the rotation.
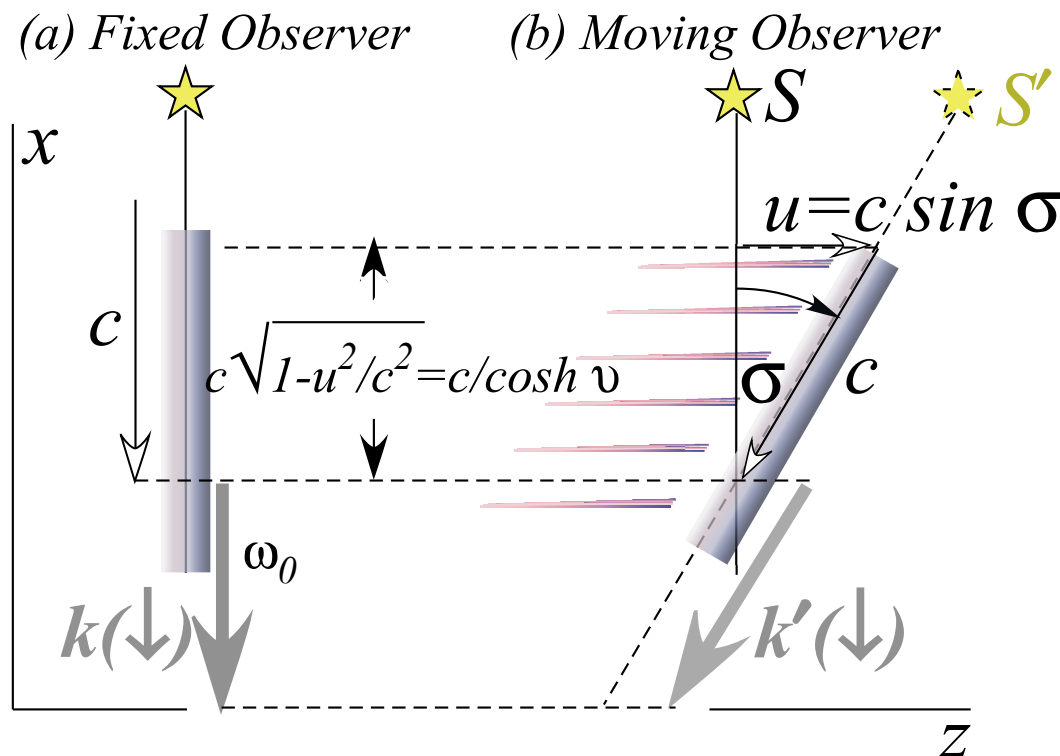

Fig. 5.6 Epstein's cosmic speedometer with aberration angle σ and transverse Doppler shift $cosh\upsilon_z$.

   Invariant (3.10) demands light-speed conservation as sketched in Fig. 5.6b. Starlight speed down the σ-tipped telescope is c, so the x-component of starlight velocity reduces from c to

$$c_{x'}=c\ cos\ \sigma=c\sqrt{(1- u_z^2/c^2)} = c/cosh\ \upsilon_z\ . \tag{5.14}$$

(a) Laser frame ω_0 (b) z-($\rightarrow$ Moving) ship
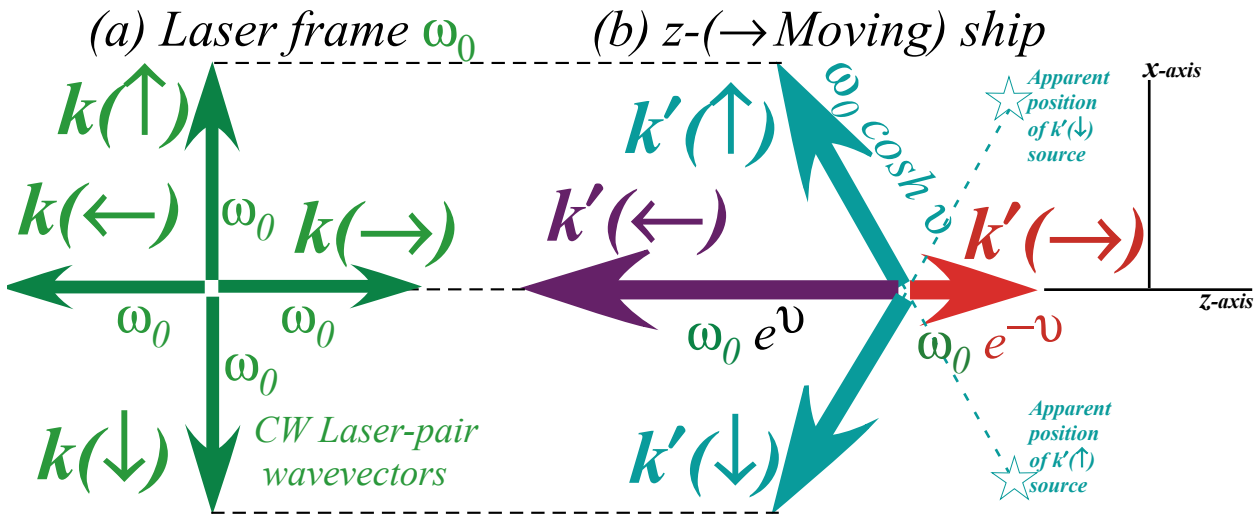

Fig. 5.7 CW version of cosmic speedometer showing transverse and longitudinal k-vectors.

Transformation (5.17a) below assures that x-or-y-components of $\mathbf{k}\downarrow$ are unchanged by u_z-boost.

$$(ck_x, ck_y) = (ck_{x'}, ck_{y'}) \tag{5.15}$$

So the length of $\mathbf{k}\downarrow$ increases by a factor $\cosh \upsilon$ as shown in Fig. 5.7 as does the frequency $\omega'\downarrow$.

$$c|k'\downarrow| = c|k\downarrow| \cosh\upsilon_z = \omega_0 \cosh \upsilon_z = \omega_0/\sqrt{(1-u^2/c^2)} \tag{5.16}$$

If the observer crosses a star ray at very large velocity, that is, lets u_z approach c, then the star angle σ approaches $90°$ and the frequency increases until the observer sees an X-ray or γ-ray star coming almost head on! The $\cosh\upsilon_z$ factor is a *transverse Doppler shift*. For large υ_z, it approaches e^{υ_z}, which is the ordinary *longitudinal Doppler shift* upon which the CW relativity derivations of Ch. 2 are based. Relations (5.13-16) are summarized in a 4-vector transformation: ω_0 has a *transverse Doppler shift* to $\omega_0\cosh\upsilon_z$, so $ck_z=0$ becomes $ck_{z'}= -\omega_0 \sinh\upsilon_z$, but the x-component is unchanged: $ck_{x'}= \omega_0 = ck_x$.

$$\begin{pmatrix} \omega'\downarrow \\ ck'_x\downarrow \\ ck'_y\downarrow \\ ck'_z\downarrow \end{pmatrix} = \begin{pmatrix} \cosh\upsilon_z & \cdot & \cdot & -\sinh\upsilon_z \\ \cdot & 1 & \cdot & \cdot \\ \cdot & \cdot & 1 & \cdot \\ -\sinh\upsilon_z & \cdot & \cdot & \cosh\upsilon_z \end{pmatrix} \begin{pmatrix} \omega\downarrow \\ ck_x\downarrow \\ ck_y\downarrow \\ ck_z\downarrow \end{pmatrix} = \begin{pmatrix} \cosh\upsilon_z & \cdot & \cdot & -\sinh\upsilon_z \\ \cdot & 1 & \cdot & \cdot \\ \cdot & \cdot & 1 & \cdot \\ -\sinh\upsilon_z & \cdot & \cdot & \cosh\upsilon_z \end{pmatrix} \begin{pmatrix} \omega_0 \\ -\omega_0 \\ 0 \\ 0 \end{pmatrix} = \omega_0 \begin{pmatrix} \cosh\upsilon_z \\ -1 \\ 0 \\ \sinh\upsilon_z \end{pmatrix}$$

$$\tag{5.17a}$$

If starlight had been $\mathbf{k}\leftarrow$ or $\mathbf{k}\rightarrow$ waves going along $\mathbf{u}$ and z-axis, the usual longitudinal Doppler blue shifts $e^{+\upsilon_z}$ or red shifts $e^{-\upsilon_z}$ would appear on both the k-vector and the frequency, as stated by the following.

$$\begin{pmatrix} \omega'_\rightarrow \\ ck'_{x\rightarrow} \\ ck'_{y\rightarrow} \\ ck'_{z\rightarrow} \end{pmatrix} = \begin{pmatrix} \cosh\upsilon_z & \cdot & \cdot & -\sinh\upsilon_z \\ \cdot & 1 & \cdot & \cdot \\ \cdot & \cdot & 1 & \cdot \\ -\sinh\upsilon_z & \cdot & \cdot & \cosh\upsilon_z \end{pmatrix} \begin{pmatrix} \omega_0 \\ 0 \\ 0 \\ \pm\omega_0 \end{pmatrix} = \omega_0 \begin{pmatrix} \cosh\upsilon_z \mp \sinh\upsilon_z \\ 0 \\ 0 \\ -\sinh\upsilon_z \pm \cosh\upsilon_z \end{pmatrix} = \omega_0 \begin{pmatrix} e^{\mp\upsilon_z} \\ 0 \\ 0 \\ \pm e^{\mp\upsilon_z} \end{pmatrix}$$

$$\tag{5.17b}$$

The Epstein speedometer tracks light pulses and particles in space and time. Instead of space-x and time-ct coordinates of a Minkowski graph, he plots space coordinate-x against *proper* time-$c\tau$. This view has all things, light γ and particle P included, moving at the speed of light as shown in Fig. 5.8. Light never ages, so its "speedometer" is tipped to the maximum along x-axis.
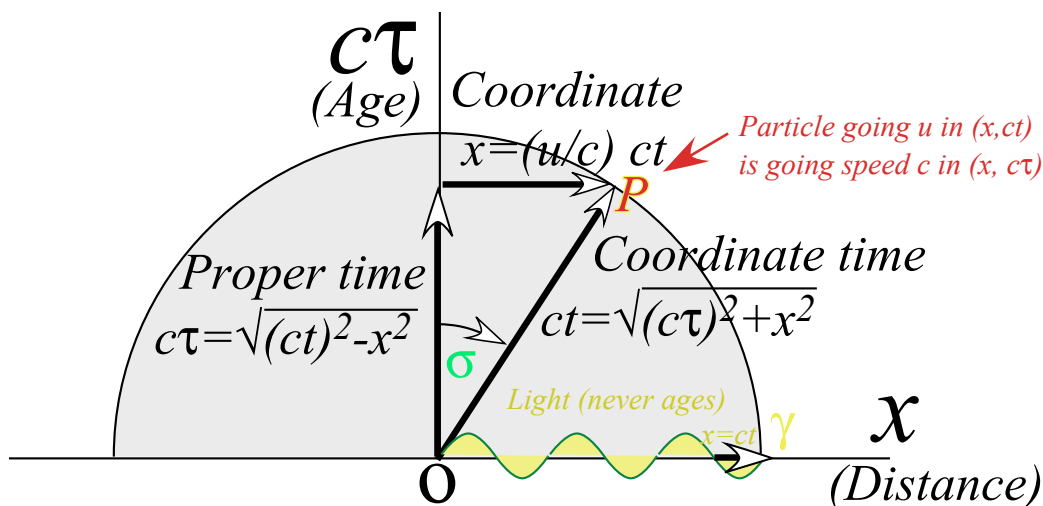
Fig. 5.8 Space-proper-time plot makes all objects move at speed c along their cosmic speedometer.

One cute feature of the Epstein space-proper-time view is its take of the Lorentz-Fitzgerald contraction of a proper length L to $L'=L\sqrt{1-u^2/c^2}$. (Recall discussion around (2.11).) As shown in Fig. 5.9 below, L' is simply the projection onto the *x*-axis of a length L tipped by σ.
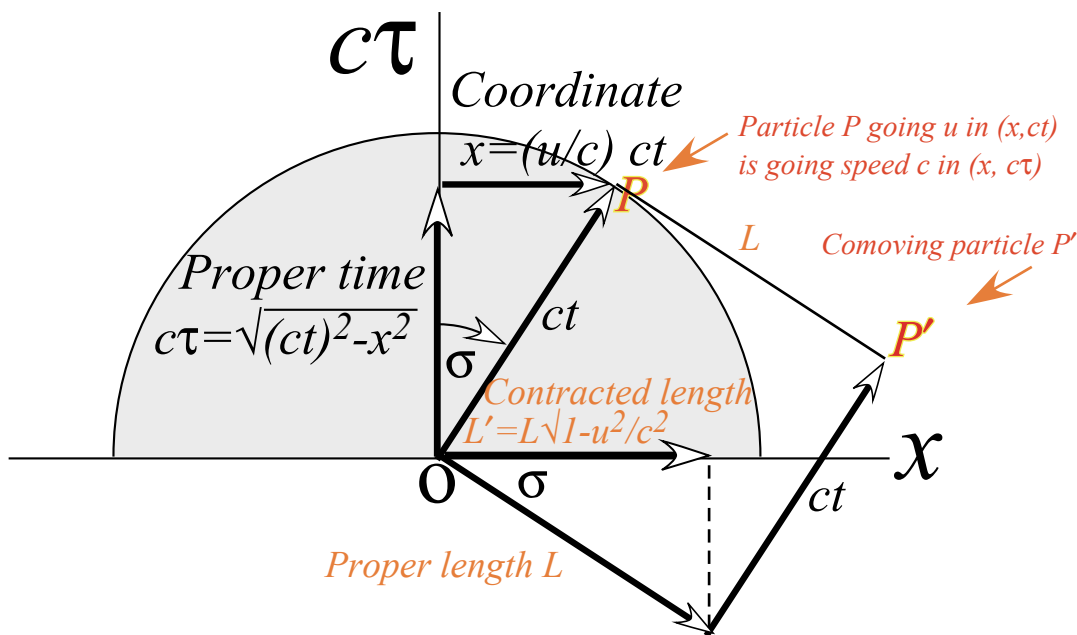

Fig. 5.9 Space-proper-time plot of Lorentz contraction as geometric projection of rotated line L.

The problem with the *(x,cτ)* view is that a space-time event is not plotted as a single point for all observers. Since the time parameter τ is an invariant, the *(x,cτ)* graph it is not a metric space.

Graphical wave 4-vector transformation

Geometric constructions combining Fig. 5.6 and Fig. 5.7 help to quantitatively visualize 4-wavevector transformations. One is shown in Fig. 5.10. The *c*-dial of the "speedometer" is first set to the

desired **u**-speed which determines angle σ. The top of the *c*-dial (which may also represent a transverse $c\mathbf{k}\uparrow$-vector in units of Lab frequency ω_0) is projected parallel to the velocity axis until it intersects the *c*-dial vertical axis. A transformed $c\mathbf{k}'\uparrow$-vector of length $\omega'\uparrow = \omega_0 \, cosh \, \upsilon$ results, similar to $c\mathbf{k}'\downarrow$ in (5.17a). Both $c\mathbf{k}'\uparrow$ and $c\mathbf{k}'\downarrow$ have a projection on the velocity axis of $\omega_0 sinh \, \upsilon$ while maintaining their transverse components ω_0 and $-\omega_0$, respectively, in order to stay on the light cone.

A dashed circle of radius *cosh* υ in Fig. 5.10 is drawn concentric to the *c*-dial and determines the longitudinal vectors $c\mathbf{k}'_\rightarrow$ and $c\mathbf{k}'_\leftarrow$ of Doppler shifted length and frequency $\omega_0 e^{-\upsilon}$ and $\omega_0 e^{\upsilon}$, respectively, as required by transformation (5.17b). This construction is part of Fig. 5.4 and Fig. 5.5.
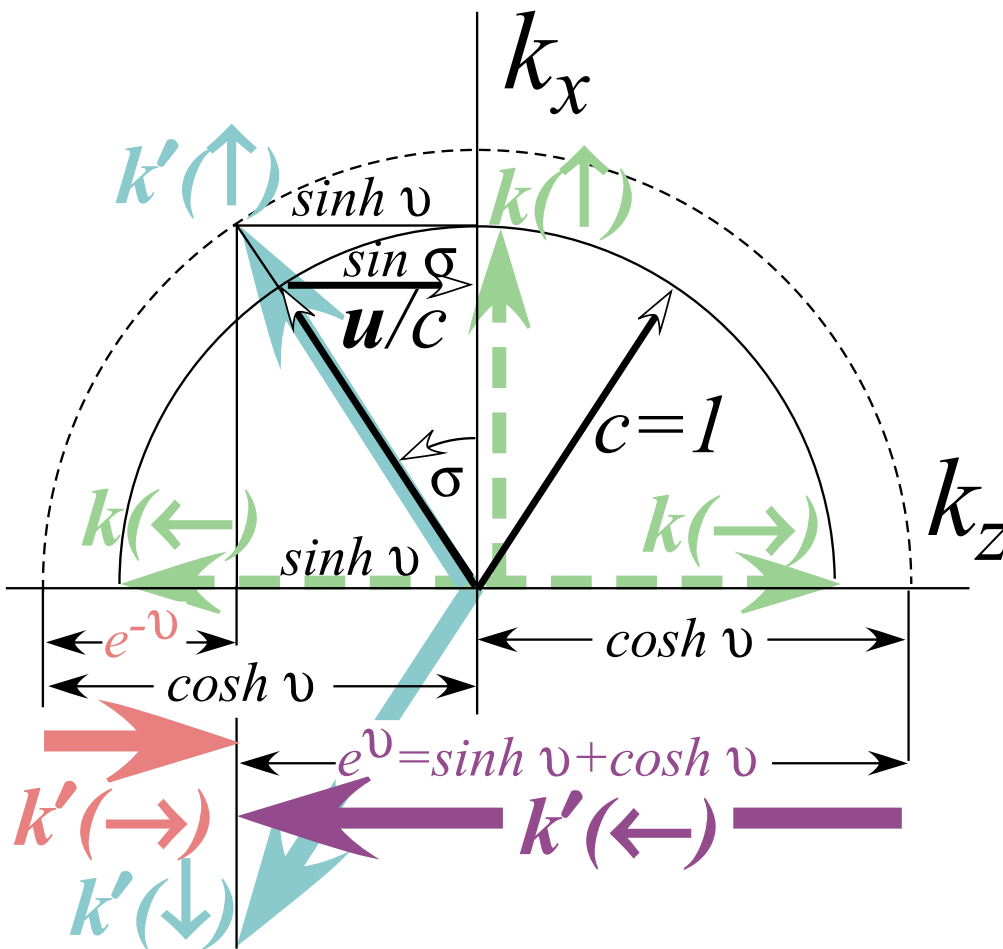

Fig. 5.10 CW cosmic speedometer. Geometry of Lorentz boost of counter-propagating waves.

Symmetry and conservation principles

In Newtonian theory the first law or axiom is momentum conservation. Physical axioms, by definition, have only experimental proof. Logical proof is impossible unless a theory like Newton's becomes sub-summed by a more general theory with finer axioms. Proof of an axiom then undermines it so it becomes a theorem or *result* of more basic axioms. (Or else an axiom might be *dis*proved or reduced to an approximate result subject to certain conditions.)

The logic of axioms yielding results or *theorems* in mathematical science probably goes back two thousand years to the time of Euclid's *Elements*. Also, axiomatic approaches to philosophy and natural

science show up in writings as early as that of Occam or even Aristotle, but it is not until the European Renaissance that experiments began to be precise enough to support mathematical models. By the European Enlightenment period, mathematical logic of physical science had become more effective and productive than any preceding philosophy due in no small part to increasingly precise evidence.

As stated by introduction, current time and frequency measurements have achieved almost unimaginable precision. In celebration of this, two continuous wave (CW) axioms (1.1-2) have been used to undermine Newtonian axioms for mass, energy, and momentum. They then became approximate results (4.4) and give rise to exact equivalents of Newtonian concepts in Einstein and Planck relativity and quantum theory in (4.5). It is a non-trivial example of undermining axioms by Occam razor-cutting.

The undermining of Newton's first axiom (momentum conservation) by the shaved CW axioms is a good example to expose the logic involved. CW logic leads to the DeBroglie scaling law (4.5b) that equates momentum **p** to wavevector **k** scaled in $\hbar$ units. A rough statement of how CW axioms undermine or "prove" **p**-conservation axioms is that **k**-conservation is required by wave coherence and so **p**=$\hbar$**k** must be conserved, as well. However, that oversimplifies a deeper nature of what is really *symmetry* logic.

A strength (and also, weakness) of CW axioms (1.1-2) is that they are *symmetry* principles due to the Lorentz-Poincare isotropy of space-time that invokes invariance to translation $\mathbf{T}(\delta, \tau)$ in the vacuum. Operator **T** has plane wave eigenfunctions $\psi_{k,\omega} = Ae^{i(kx-\omega t)}$ with roots-of-unity eigenvalues $e^{i(k\cdot\delta-\omega\cdot\tau)}$.

$$\mathbf{T}\left|\psi_{k,\omega}\right\rangle = e^{i(k\cdot\delta-\omega\cdot\tau)}\left|\psi_{k,\omega}\right\rangle \quad (5.18a) \qquad\qquad \left\langle\psi_{k,\omega}\right|\mathbf{T}^\dagger = \left\langle\psi_{k,\omega}\right|e^{-i(k\cdot\delta-\omega\cdot\tau)} \quad (5.18b)$$

This also applies to 2-part or "2-particle" states $\Psi_{K\Omega} = \psi_{k_1,\omega_1}\psi_{k_2,\omega_2}$ where exponents add (k,ω)-values of each constituent to $K=k_1+k_2$ and $\Omega=\omega_1+\omega_2$, and $\mathbf{T}(\delta,\tau)$-eigenvalues also have the form $e^{i(K\cdot\delta-\Omega\cdot\tau)}$ of (5.1). Matrix $\left\langle\Psi'_{K'\Omega'}\right|\mathbf{U}\left|\Psi_{K\Omega}\right\rangle$ of **T**-symmetric evolution **U** is zero unless $K' = k'_1 + k'_2 = K$ and $\Omega' = \omega'_1 + \omega'_2 = \Omega$.

$$\left\langle\Psi'_{K'\Omega'}\right|\mathbf{U}\left|\Psi_{K\Omega}\right\rangle = \left\langle\Psi'_{K'\Omega'}\right|\mathbf{T}^\dagger(\delta,\tau)\mathbf{U}\mathbf{T}(\delta,\tau)\left|\Psi_{K\Omega}\right\rangle \quad \text{(if } \mathbf{UT} = \mathbf{TU} \text{ for all } \delta \text{ and } \tau)$$
$$= e^{-i(K'\cdot\delta-\Omega'\cdot\tau)}e^{i(K\cdot\delta-\Omega\cdot\tau)}\left\langle\Psi'_{K'\Omega'}\right|\mathbf{U}\left|\Psi_{K\Omega}\right\rangle = 0 \quad \text{unless: } K' = K \text{ and: } \Omega' = \Omega$$

(5.19)

T-symmetry requires total energy $E = \hbar\Omega$ and total momentum $P = \hbar K$ be *conserved* for archetypical CW states, but laboratory CW have momentum uncertainty $\Delta\mathbf{k}=1/\Delta\mathbf{x}$ due to finite beam size $\Delta\mathbf{x}$ and energy uncertainty due to time limits. So, Newton's 1st law or axiom is verified but only as an ideal limit.

Symmetry is to physics what religion is to politics. Both are deep and grand in principle but roundly flaunted in practice. Both gain power quickly by overlooking details. In Ch.4 relativistic and quantum kinetic properties of a massive "thing" arise from those of an optical 2-CW function in one space dimension. This means that mass shares *symmetry* with 2-CW light, not that mass *is* 2-CW light. Massive "things" do not vanish if a laser turns off, but our tiny optical mass $\hbar N\omega/c^2$ is quickly gone!

Puzzling questions remain. Why do simple *wave* optics lead directly to general properties (4.5) of relativity and quantum mechanics of a massive *particle*? How does a cavity of counter-propagating green light *waves* act like it holds *particles* of mass $M=\hbar\omega/c^2$?

A short answer to one question is that particles are waves, too, and so forced by Lorentz symmetry to use available hyperbolic invariants $\omega^2 - (ck)^2 = (Mc^2/\hbar)^2$ for dispersion. To answer the second question entails further loss of classical innocence. In Ch. 6 Occam's razor is again applied to cut semi-classical

CW laser fields down to single field quanta $\hbar\varpi$ or *photons*. So the second short answer is that waves are particles, too, even for optical dispersion $(\omega^2 - (ck)^2 = 0)$.

By many accounts, quantum theory begins with Planck axiom $E=\hbar N\omega$. This is distinguished from the scaling law $E=s\omega$ derived in (4.5a) since its scale factor $s=\hbar N$ is not an obvious consequence of CW phase axioms (1.1-2) that lead to (4.5). CW logic involves additional axioms for Maxwell electromagnetic energy E and field amplitude quantization to render Planck's axiom. This is discussed shortly.

1st and 2nd Quantization: phase vs. amplitude

Waves resonate at discrete wave numbers $k_m = m\frac{2\pi}{L} = mk_1$ in a ring or cavity of length L. Then relations (4.5b) between k and momentum p force p-quantization $p_m = \hbar k_m = mp_1$ so momentum quantum numbers[xvi] *m=0, ±1, ±2,...* count waves on ring L as in Bohr electron orbitals or for cavity modes in (4.6a). Then Planck dispersion $E_m = \hbar\omega(k_m)$ (4.5a) gives electron energy levels $E_m = m^2 E_1$ for the BS approximation $E_1 = p_1^2 / 2M$ or for cavity fundamental frequency levels (4.6b). Wave-fitting in x-space is called *1st quantization*. Related fitting in wave amplitude space is called *2nd quantization*.

Heisenberg[xvii] showed quanta p_m or E_m arise from eigenvalues (literally "own-values") of matrix operators **p** or **H** whose eigenvectors ("own-vectors") $|p_m\rangle$ or $|E_m\rangle$ may be superimposed.

$$|\Psi\rangle = \psi_1 |E_1\rangle + \psi_2 |E_2\rangle + \psi_3 |E_3\rangle + \ldots \qquad (5.20)$$

(Dirac's bra-ket[xviii] notation came later.) Allowing things to be at (or in) m places (or states) allows mean values $\bar{E} = \langle\Psi|\mathbf{H}|\Psi\rangle$ to range continuously from lowest quantum levels E_1 to the highest E_m.

$$\bar{E} = \langle\Psi|\mathbf{H}|\Psi\rangle = |\psi_1|^2 E_1 + |\psi_2|^2 E_2 + |\psi_2|^2 E_2 + \ldots \qquad (5.21)$$

For classicists, the notion that each multiple-personality-k has a probability $|\psi_k|^2$ seems, if not crazy, then at least dicey in the sense of Einstein's skeptical quote, *"God does not play dice…"* [xix]

But, superposition is an idea borrowed from classical waves. Resulting interference makes them ultra-sensitive to relative position and velocity, a *first* order sensitivity that leads elegantly to relativity transformation (2.10) and kinematic relations (4.5) by geometry of optical phase kx-ωt of $\psi=Ae^{i(kx-\omega t)}$.

Amplitude "*A*" of wave (1.6) or (1.9) is set arbitrarily since only real wave zeros were needed. It is ignored in (5.5). Without Maxwell and Planck rules, CW amplitude or wave *quantity* is undefined and un-quantized while wave quality (frequency and phase) may be well defined and quantized. Amplitudes need a similar treatment that is begun in Ch. 6.

Chapter 6. Variation and quantization of optical amplitudes

What is deduced from wave phase alone? Wave *amplitude* has so far been skirted for Occam economy: *"Pluralitas non est ponenda sine neccesitate"* (Assume no plurality without necessity.) CW phase axioms (1.1-2) give Lorentz-Doppler and Planck-DeBroglie symmetry relations yet 2-CW amplitudes (1.10) are not defined beyond assuming their 1-CW amplitudes match. Standing wave grid reference frames in Fig. 2.1 and Fig. 2.2 are just points where amplitude is *zero*, that is, loci of real wave function *roots*.

Discussion of non-zero amplitude variation begins with counter-propagating 2-CW dynamics involving two 1-CW amplitudes $A_\rightarrow$ and $A_\leftarrow$ that we now allow to be *un*matched. ($A_\rightarrow \neq A_\leftarrow$)

$$A_\rightarrow e^{i(k_\rightarrow x - \omega_\rightarrow t)} + A_\leftarrow e^{i(k_\leftarrow x - \omega_\leftarrow t)} = e^{i(k_\Sigma x - \omega_\Sigma t)}[A_\rightarrow e^{i(k_\Delta x - \omega_\Delta t)} + A_\leftarrow e^{-i(k_\Delta x - \omega_\Delta t)}] \quad (6.1a)$$

Half-sum mean phase rates $(k_\Sigma, \omega_\Sigma)$ and half-difference means $(k_\Delta, \omega_\Delta)$ appear here as in (1.10).

$$k_\Sigma = (k_\rightarrow + k_\leftarrow)/2 \quad (6.1b) \qquad\qquad k_\Delta = (k_\rightarrow - k_\leftarrow)/2 \quad (6.1c)$$
$$\omega_\Sigma = (\omega_\rightarrow + \omega_\leftarrow)/2 \qquad\qquad\qquad \omega_\Delta = (\omega_\rightarrow - \omega_\leftarrow)/2$$

Also important is amplitude mean $A_\Sigma = (A_\rightarrow + A_\leftarrow)/2$ and half-difference $A_\Delta = (A_\rightarrow - A_\leftarrow)/2$. Wave motion depends on standing-wave-ratio *SWR* or the inverse standing-wave-quotient *SWQ*.

$$SWR = \frac{(A_\rightarrow - A_\leftarrow)}{(A_\rightarrow + A_\leftarrow)} \quad (6.2a) \qquad\qquad SWQ = \frac{(A_\rightarrow + A_\leftarrow)}{(A_\rightarrow - A_\leftarrow)} \quad (6.2a)$$

Recall mean frequency ratios for group velocity (2.3b) or its inverse that is phase velocity (2.3a).

$$V_{group} = \frac{\omega_\Delta}{k_\Delta} = c\frac{(\omega_\rightarrow - \omega_\leftarrow)}{(\omega_\rightarrow + \omega_\leftarrow)} \quad (6.3a) \qquad\qquad V_{phase} = \frac{\omega_\Sigma}{k_\Sigma} = c\frac{(\omega_\rightarrow + \omega_\leftarrow)}{(\omega_\rightarrow - \omega_\leftarrow)} \quad (6.3b)$$

A 2-state amplitude continuum is bounded by a pure right-moving 1-CW ($A_\rightarrow = 1, A_\leftarrow = 0$) of *SWR=1* and a pure left-moving 1-CW ($A_\rightarrow = 0, A_\leftarrow = 1$) of *SWR=-1*. A 2-CW standing-wave ($A_\rightarrow = \frac{1}{\sqrt{2}} = A_\leftarrow$) has *SWR=0*.

Wave paths for various *SWR* values are drawn in Fig. 6.1 for *600THz* 2-CW pairs and in Fig. 6.2 for Doppler shifted *300THz* and *1200THz* 2-CW pairs at the same *SWR* values. The *SWQ* is the ratio of the envelope peak (interference maximum) to the envelope valley (interference minimum), and *vice versa* for *SWR=1/SWQ*. Single frequency 2-CW paths of nonzero-*SWR* in Fig. 6.1 do a galloping motion. Each wave speeds up to peak speed *c/SWR=c·SWQ* as it first shrinks to squeeze through its envelope minima and then slows to resting speed *c·SWR* as it expands to its maximum amplitude. Only at zero-*SWR* do 2-CW zero-paths appear to travel at a constant group speed (6.3a) and phase speed (6.3b) as in Fig. 6.1c or 6.2c. (For 1-CW paths or unit *SWR=±1* there is just one speed ±c by axiom (1.1).)

The real and imaginary parts take turns. One gallops while the other rests and *vice versa* and this occurs twice each optical period. If frequency ratio (6.3) and amplitude ratio (6.2) have opposite signs as in Fig. 6.1c (±0 or ±∞) and in Fig. 6.2e (±3/5 or ±5/3), wave zero paths will follow a right angle staircase. 1-frequency staircase ($V_{group}=0=SWR$) in Fig. 6.1c is a Cartesian grid like Fig. 2.1c. 2-frequency waves ($V_{group}\neq0$) have Minkowski grids like Fig. 2.2c for *SWR=0* or quasi-Cartesian stair steps like Fig. 6.2e for $V_{group}=-cSWR$. To broadcast Cartesian grids to a *u*-frame one tunes both V_{group} and *cSWR* to *u*.
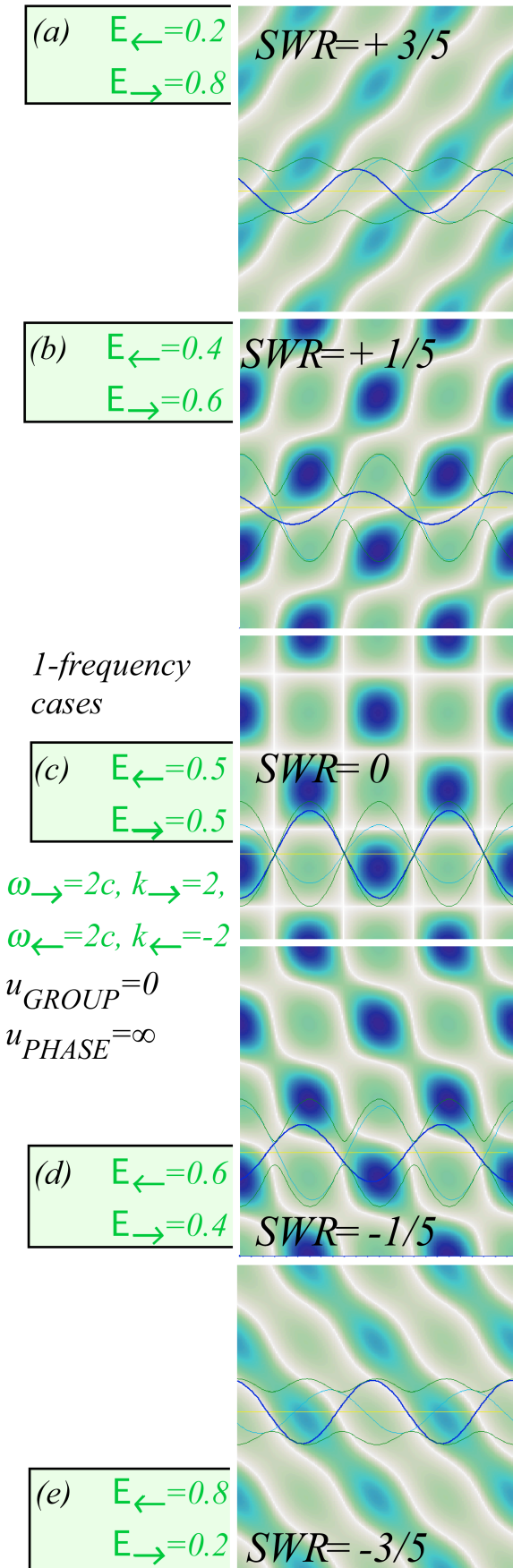
(a) E$_{\leftarrow}$=0.2   *SWR=+ 3/5*
E$_{\rightarrow}$=0.8

(a) E$_{\leftarrow}$=0.2   *SWR=+ 3/5*
E$_{\rightarrow}$=0.8

(b) E$_{\leftarrow}$=0.4   *SWR=+ 1/5*
E$_{\rightarrow}$=0.6

(b) E$_{\leftarrow}$=0.4   *SWR=+ 1/5*
E$_{\rightarrow}$=0.6

1-frequency cases

2-frequency cases

(c) E$_{\leftarrow}$=0.5   *SWR= 0*
E$_{\rightarrow}$=0.5

(c) E$_{\leftarrow}$=0.5   *SWR= 0*
E$_{\rightarrow}$=0.5

$\omega_{\rightarrow}$=2c, k$_{\rightarrow}$=2,
$\omega_{\leftarrow}$=2c, k$_{\leftarrow}$=-2

$\omega_{\rightarrow}$=4c, k$_{\rightarrow}$=4
$\omega_{\leftarrow}$=1c, k$_{\leftarrow}$=-1

u_{GROUP}=0
u_{PHASE}=∞

u_{GROUP}/c=3/5
u_{PHASE}/c=5/3

(d) E$_{\leftarrow}$=0.6
E$_{\rightarrow}$=0.4   *SWR= -1/5*

(d) E$_{\leftarrow}$=0.6
E$_{\rightarrow}$=0.4   *SWR= -1/5*

(e) E$_{\leftarrow}$=0.8
E$_{\rightarrow}$=0.2   *SWR= -3/5*

(e) E$_{\leftarrow}$=0.8
E$_{\rightarrow}$=0.2   *SWR= -3/5*

*Fig. 6.1 Monochromatic (1-frequency)
2-CW wave space-time patterns.*
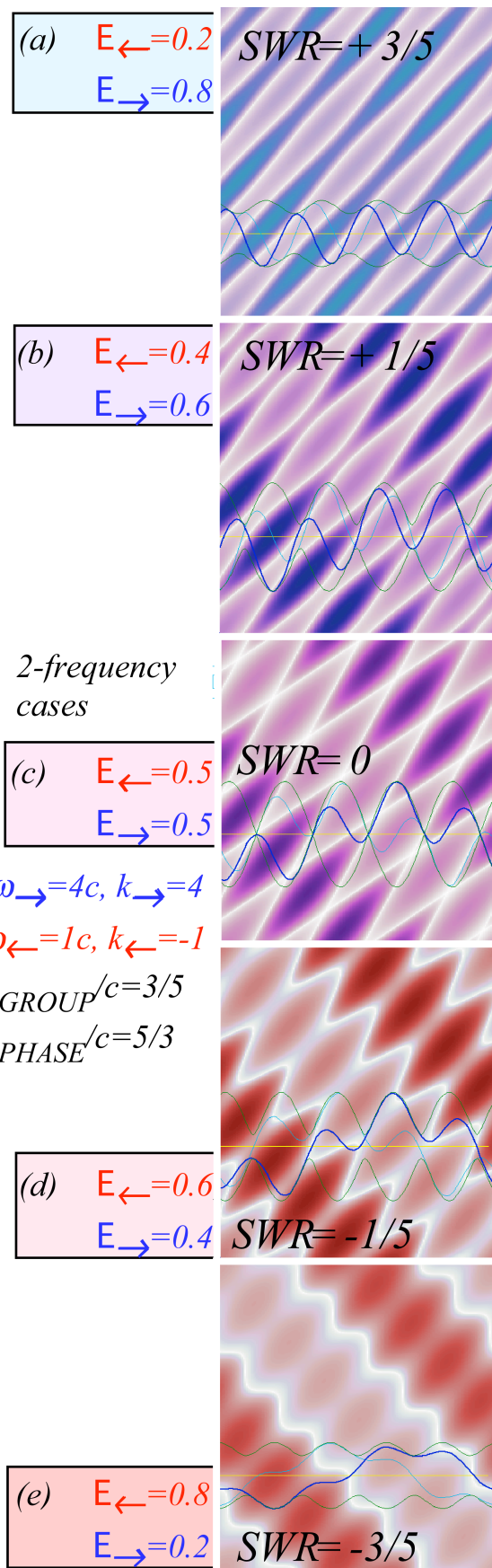
*Fig. 6.2 Dichromatic (2-frequency)
2-CW wave space-time patterns.*

   Galloping is a fundamental interference property that may be clarified by analogy with elliptic orbits of isotropic 2D-harmonic oscillators and in particular with elliptic polarization of optical wave amplitudes. Fig. 6.3 relates polarization states and wave states of Fig. 6.1 beginning with left (right)-circular polarization that is analogous to a left (right)-moving wave in Fig. 6.3g (Fig. 6.3a). As sketched in Fig. 6.3(b-e), galloping waves are general cases analogous to general states of elliptic polarization or general 2DHO orbits obeying a Keplerian geometry shown in Fig. 6.3h. Standing waves correspond to plane-polarization. Polarization in the x-plane of Fig. 6.3d corresponds to a standing cosine wave and y-plane polarization (not shown) would correspond to a standing sine wave.

   Isotropic oscillator orbits obey Kepler's law of constant orbital momentum. Orbit angular velocity slows down by a factor b/a at major axes or aphelions $\pm a$ and then speeds up by a factor a/b at minor axes or perihelions $\pm b$ just as a galloping wave, twice in each period, slows down to $SWR \cdot c$ and speeds up to $SWQ \cdot c$. The galloping or eccentric motion of the eccentric anomaly angle $\phi(t)$ in Fig. 6.3h is a projection of a uniformly rotating mean anomaly (phase angle $\omega \cdot t$) of the isotropic oscillator, and this gives a Keplarian relation of the two angles seen in the figure.

$$\tan\phi(t) = \frac{b}{a}\tan\omega \cdot t \tag{6.4a}$$

The eccentric anomaly time derivative of ϕ (angular velocity) gallops between $\omega \cdot b/a$ and $\omega \cdot a/b$.

$$\dot\phi = \frac{d\phi}{dt} = \omega \cdot \frac{b}{a}\frac{\sec^2\omega t}{\sec^2\phi} = \frac{\omega \cdot b/a}{\cos^2\omega t + (b/a)^2 \cdot \sin^2\omega t} = \begin{cases} \omega \cdot b/a & \text{for: } \omega t = 0,\ \pi,\ 2\pi... \\ \omega \cdot a/b & \omega t = \pi/2,\ 3\pi/2,... \end{cases} \tag{6.4b}$$

The product of angular moment r^2 and $\dot\phi$ is orbital momentum, a constant proportional to ellipse area.

$$r^2\frac{d\phi}{dt} = constant = (a^2\cos^2\omega t + b^2 \cdot \sin^2\omega t)\frac{d\phi}{dt} = \omega \cdot ab$$

Consider galloping wave zeros of a monochromatic wave (6.1a) having SWQ (6.2b).

$$0 = \operatorname{Re}\Psi(x,t) = \operatorname{Re}\left[A_\rightarrow e^{i(k_0 x - \omega_0 t)} + A_\leftarrow e^{i(-k_0 x - \omega_0 t)}\right] \quad \text{where: } \omega_\rightarrow = \omega_0 = \omega_\leftarrow = ck_0 = -ck_\leftarrow$$

$$0 = A_\rightarrow\left[\cos k_0 x\ \cos\omega_0 t + \sin k_0 x\ \sin\omega_0 t\right] + A_\leftarrow\left[\cos k_0 x\ \cos\omega_0 t - \sin k_0 x\ \sin\omega_0 t\right]$$

$$(A_\rightarrow + A_\leftarrow)\left[\cos k_0 x\ \cos\omega_0 t\right] = -(A_\rightarrow - A_\leftarrow)\left[\sin k_0 x\ \sin\omega_0 t\right]$$

Space $k_0 x$ varies with time $\omega_0 t$ in the same way that eccentric anomaly varies in (6.4a).

$$\tan k_0 x = -SWQ \cdot \cot\omega_0 t = SWQ \cdot \tan\omega_0\overline{t} \quad \text{where: } \omega_0\overline{t} = \omega_0 t - \pi/2 \tag{6.5a}$$

Speed of galloping wave zeros is the time derivative of root location x in units of light velocity c.

$$\frac{dx}{dt} = c \cdot SWQ\frac{\sec^2\omega_0\overline{t}}{\sec^2 k_0 x} = \frac{c \cdot SWQ}{\cos^2\omega_0\overline{t} + SWQ^2 \cdot \sin^2\omega_0\overline{t}} = \begin{cases} c \cdot SWQ & \text{for: } \overline{t} = 0,\ \pi,\ 2\pi... \\ c \cdot SWR & \overline{t} = \pi/2,\ 3\pi/2,... \end{cases} \tag{6.5b}$$

Single frequency 2-CW paths in Fig. 6.1 have a constant product of instantaneous wave velocity and wave amplitude analogous to the constant product of orbital velocity and radius. So vacuum optical amplitude and phase motion obey a funny version of Kepler and Galileo's rules. The extent to which 14th century geometric relations underlie basic wave physics has not been fully appreciated.
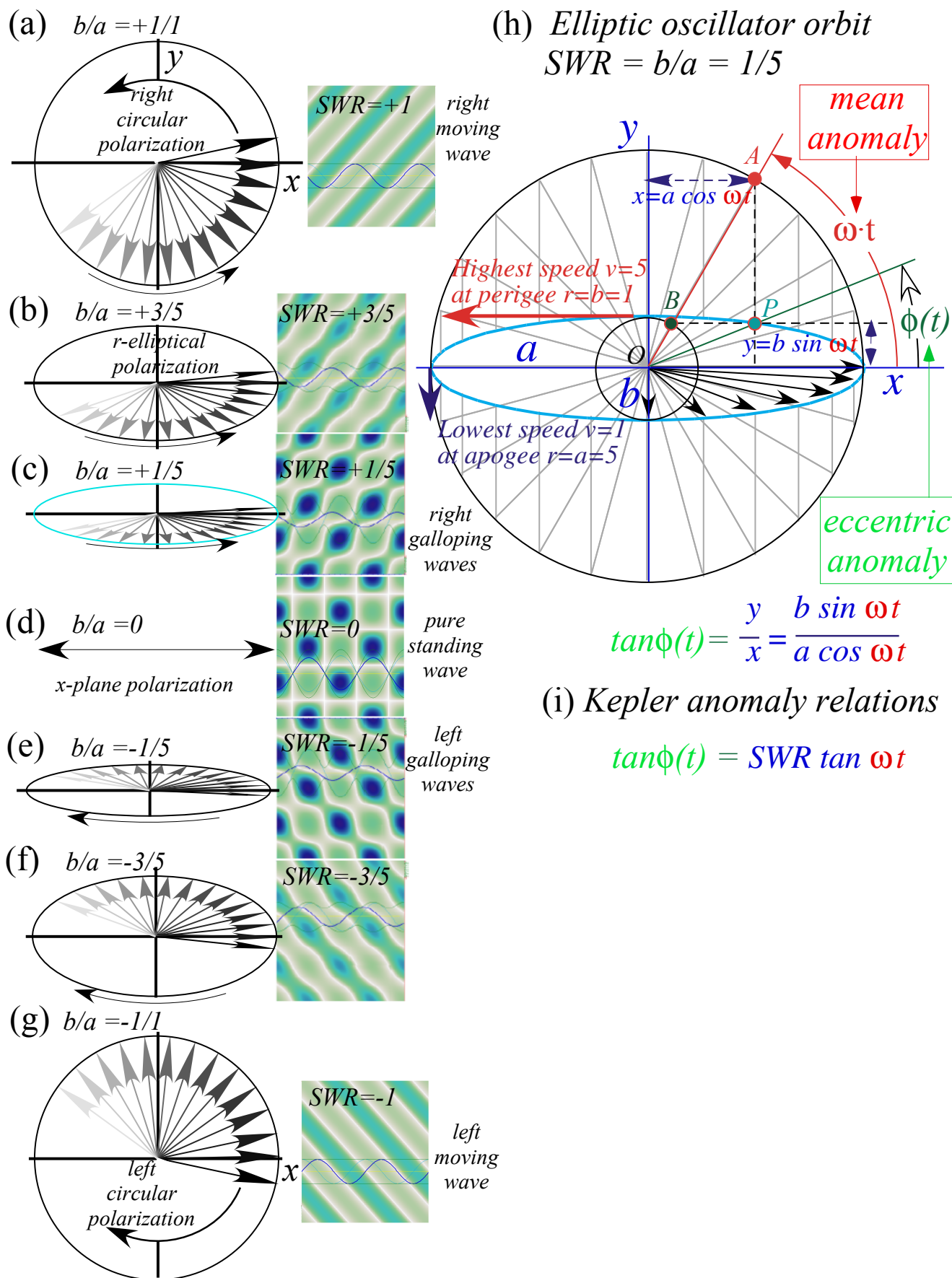
(a) *b/a =+1/1*

right circular polarization

SWR=+1   *right moving wave*

(b) *b/a =+3/5*

r-elliptical polarization

SWR=+3/5

(c) *b/a =+1/5*

SWR=+1/5   *right galloping waves*

(d) *b/a =0*

SWR=0   *pure standing wave*

x-plane polarization

(e) *b/a =-1/5*

SWR=-1/5   *left galloping waves*

(f) *b/a =-3/5*

SWR=-3/5

(g) *b/a =-1/1*

SWR=-1   *left moving wave*

left circular polarization

(h) *Elliptic oscillator orbit*
SWR = b/a = 1/5

mean anomaly

A

$x = a \cos \omega t$

ω·t

Highest speed v=5 at perigee r=b=1

B   *P*

$y = b \sin \omega t$

ϕ(t)

a

o

b

x

Lowest speed v=1 at apogee r=a=5

eccentric anomaly

$$\tan \phi(t) = \frac{y}{x} = \frac{b \sin \omega t}{a \cos \omega t}$$

(i) *Kepler anomaly relations*

$$\tan \phi(t) = SWR \tan \omega t$$

Fig. 6.3 (a-g) Elliptic polarization ellipses relate to galloping waves in Fig. 6.1. (h-i) Kepler anomalies.

Maxwell amplitudes and energy

Classical Maxwell field amplitudes $\mathbf{E} = -\dot{\mathbf{A}}$ and $\mathbf{B} = \nabla \times \mathbf{A}$ are derivatives of vector potential $\mathbf{A}$. Maxwell energy U per volume V or total energy $U \cdot V$ is a sum of amplitude squares $\mathbf{E} \cdot \mathbf{E}$ and $c^2 \mathbf{B} \cdot \mathbf{B}$.

$$\langle U \rangle \cdot V = \left\langle \frac{\varepsilon_0}{2} \mathbf{E} \cdot \mathbf{E} + \frac{1}{2\mu_0} \mathbf{B} \cdot \mathbf{B} \right\rangle \cdot V \qquad \mu_0 \varepsilon_0 = \frac{1}{c^2} \qquad (6.7)$$

Fourier analysis of $\mathbf{A}$ into amplitudes $\mathbf{a}_k$ and $\mathbf{a}_k^*$ leads to a harmonic oscillator sum over each plane CW mode frequency $\omega_k = \pm c \mid \mathbf{k}_m \mid$, $\mathbf{k}_m$-vector allowed by a large-cavity, and polarization $\alpha = x, y$ normal to $\mathbf{k}_m$.

$$\langle U \rangle \cdot V = 2\varepsilon_0 V \sum \omega_k^2 \mathbf{a}_k^* \mathbf{a}_k \qquad (6.8)$$

Harmonic oscillator frequency is independent of amplitude. This is consistent with CW phase axiom (1.1) and dispersion relations (3.5) derived from 2-CW superposition, but such a simple axiom seems unable to derive the Maxwell vector amplitude structure of 2-dimensional polarization normal to $\mathbf{k}_m$ of each wave mode or even to establish that its wave variables $\mathbf{A}$, $\mathbf{B}$, $\mathbf{E}$, or $\mathbf{k}_m$ are, in fact, 3D vectors.

The CW axiom (1.1) gives what is effectively a 2-dimensional harmonic oscillator (2DHO) with two complex amplitudes *(a$_L$, a$_R$)* for the two longitudinal propagation directions, but each comes with two transverse polarization amplitudes *(a$_x$, a$_y$)* that describe the second 2DHO in Maxwell light, namely polarization ellipsometry used in Fig. 6.3 as an analogy for propagation left-and-right along *z*.

Quantized optical fields

Mode amplitude $\mathbf{a}_k$ or $\mathbf{a}_k^*$ in classical electromagnetic energy $\sum \omega_k^2 \mathbf{a}_k^* \mathbf{a}_k$ are replaced by oscillator operators $\mathbf{a}_k$ or $\mathbf{a}_k^\dagger$ for a field Hamiltonian with explicit linear frequency dependence of Planck.

$$\mathbf{H} = \Sigma \hbar \omega_k (\mathbf{a}_k^\dagger \mathbf{a}_k) \Rightarrow \langle \mathbf{H} \rangle = \Sigma \hbar \omega_k N_k \qquad (6.9)$$

The **H**-eigenstates $|N_1 N_2 \cdots N_k \rangle$ for exactly quantized photon numbers $\langle \mathbf{a}_k^\dagger \mathbf{a}_k \rangle = N_k$ fix a definite energy value $\hbar \omega_k N_k$ for each mode-k_m but has quite *un*certain field phase. Average energy of one mode is

$$\langle U_k \rangle \cdot V = 2\varepsilon_0 V \langle \mathbf{E}_k \cdot \mathbf{E}_k \rangle = \hbar \omega_k N_k \qquad (6.10a)$$

where a 1-CW-1-photon E-field and vector potential A-amplitude is as follows.

$$\langle \| \mathbf{E}_k \| \rangle_{N_k = 1} = \sqrt{\frac{\hbar \omega_k}{2\varepsilon_0 V}} \quad (6.10b) \qquad\qquad \langle \| \mathbf{A}_k \| \rangle_{N_k = 1} = \sqrt{\frac{\hbar}{2\varepsilon_0 \omega_k V}} \qquad (6.10c)$$

Field quantization is called 2nd-quantization to distinguish 1st-quantization k_m *mode* numbers *m*, used for classical light, from "purely quantum" *photon* numbers $n = N_{k_m}$ for wave amplitude. This may be a prejudice that waves (particles) are usual (unusual) for light but unusual (usual) for matter.

Amplitudes involve relations (6.7) to (6.10) that are more complex than axioms (1.1-2) for wave phase. While Maxwell-Planck relations lack the simplicity of the latter, they do derive the linear dispersion (1.1) by Fourier transform of the Maxwell wave equations, and they show optical wave amplitude has an internal symmetry analogous to that of wave frequency. The following discussion of this analogy involves a Doppler shift of wave *amplitude* with invariance or covariance of photon number N_k

and standing wave ratio *(SWR)* (6.5). Also, one begins to see how Born quantum probability formulas $\langle n \rangle = \psi * \psi$ arise and are consistent with Dirac amplitude covariance.

Relativistic 1-CW covariance of Poynting flux

Maxwell-Planck energy density *U(Joule/m³)* in (6.10a) leads to a related Poynting flux **S***[Joule/(m²·s)]*.

$$\vec{\mathbf{S}} = \vec{\mathbf{E}} \times \vec{\mathbf{B}} = \left\langle U_k \right\rangle c\hat{\mathbf{k}} = 2\varepsilon_0 c \left\langle \mathbf{E}_k \bullet \mathbf{E}_k \right\rangle \hat{\mathbf{k}} = \hbar \omega_k \bar{n}_k \hat{\mathbf{k}} \quad \text{where: } n_k = cN_k / V\left[m^{-2}s^{-1}\right] \quad (6.11)$$

Flux **S** contains two frequency factors, the fundamental laser frequency ω_k and the photon count rate n_k per*[(m²·s)]*. Frequency ω_k is quantum *quality* of a laser beam and rate n_k is its quantum *quantity*. The product $\hbar\omega_k \cdot n_k$ is Poynting *flux*. Rate n_k and frequency ω_k both Doppler shift by an exponential $e^{\pm\rho}$ of rapidity ρ in (2.16). So do 1-CW fields $E_{\pm k}$ as may be shown by Lorentz transforming them directly.

$$E'_{+k} = e^{+\rho}E_{+k} \quad (6.12a) \qquad\qquad\qquad E'_{-k} = e^{-\rho}E_{-k} \qquad (6.12b)$$

Thus both electric field polarization **E**-amplitudes E_x an E_y of a 1-CW field undergo the same $e^{\pm\rho}$ Doppler shift that the frequency ω_k or wavevector k experience. Scaling **E** in (6.11) by 1-photon factor (6.10) gives probability wave ψ below whose square $\psi*\psi$ is a volume photon count *N/(m³)*.

$$\psi_k = \sqrt{\frac{2\varepsilon_0 V}{\hbar \omega_k}} E_k \Rightarrow \left\langle \ \psi_k * \psi_k \ \right\rangle = \left\langle N_k \right\rangle = \bar{N}_k = \bar{n}_k \frac{V}{c} \qquad (6.13a)$$

Or, *flux* probability wave ψ (italicized) is scaled so its square $\psi*\psi$ is expected flux photon count *n/(m²·s)*.

$$\psi_k = \sqrt{\frac{2\varepsilon_0 c}{\hbar \omega_k}} E_k \Rightarrow \left\langle \psi_k * \psi_k \right\rangle = \left\langle n_k \right\rangle = \bar{n}_k = \frac{c}{V} \bar{N}_k \qquad (6.13b)$$

Due to the $1/\sqrt{\omega_k}$ scaling of (6.13) the Doppler factor of $\psi_{\pm k}$ drops an $e^{\pm\rho/2}$ factor from E_k in (6.12).

$$L_z(\rho)|\psi\rangle = \begin{pmatrix} \psi'_{+k} \\ \psi'_{-k} \end{pmatrix} = \begin{pmatrix} e^{+\rho/2} & 0 \\ 0 & e^{-\rho/2} \end{pmatrix} \begin{pmatrix} \psi_{+k} \\ \psi_{-k} \end{pmatrix} = e^{\sigma_z \rho/2}|\psi\rangle \qquad (6.14)$$

This is a starting point for the spinor form of Lorentz transformation for Dirac amplitudes.

Relativistic 2-CW invariance of cavity quanta

Mean photon number $\bar{N}_k$ of a 2-CW cavity mode, unlike a 1-CW flux quantum n_k, is invariant to cavity speed. By analogy, 2-CW modes have variant group-phase velocity (V_{group}, V_{phase}), energy-momentum *(ħck,ħω)*, but invariant mean velocity $c = \sqrt{V_{group}V_{phase}}$ and frequency $\varpi = \sqrt{\omega_{+k}\omega_{-k}} = \sqrt{\omega^2 - c^2 k^2}$.

$$\frac{V_{group}}{c} = \frac{\omega_{+k} - \omega_{-k}}{\omega_{+k} + \omega_{-k}} \quad (6.15a) \qquad\qquad \frac{V_{phase}}{c} = \frac{\omega_{+k} + \omega_{-k}}{\omega_{+k} - \omega_{-k}} \quad (6.15b)$$

Linear dispersion $\omega_{\pm k} = \pm ck$ and (1.11) or (2.7) are used. Note the analogy to *SWR* relations (6.2).

$$SWR = \frac{E_{+k} - E_{-k}}{E_{+k} + E_{-k}} \qquad (6.15c) \qquad\qquad SWQ = \frac{E_{+k} + E_{-k}}{E_{+k} - E_{-k}} \qquad (6.15d)$$

Each ratio (6.15) is a wave velocity that Doppler-transforms like relativistic (non-Galilean) velocity.

$$SWR' = \frac{SWR + u/c}{1 + SWR \cdot u/c} \quad (6.16a) \qquad \frac{V'_m}{c} = \frac{V_m/c + u/c}{1 + (V_m/c) \cdot (u/c)} \quad (6.16b)$$

Velocity $u_{AB}/c = \tanh\rho_{AB}$ is a hyperbolic sum since rapidity is a simple sum $\rho_{AB} = \rho_A + \rho_B$ by (3.6).

$$\frac{u_{AB}}{c} = \tanh\rho_{AB} = \tanh(\rho_A + \rho_B) = \frac{\tanh\rho_A + \tanh\rho_B}{1 + \tanh\rho_A \tanh\rho_B} = \frac{u_A/c + u_B/c}{1 + u_A u_B/c^2} \qquad (6.17)$$

The energy and momentum flux values are found for counter-k 2-CW beam functions $\Psi_{\rightleftarrows}$.

$$\Psi_{k\rightleftarrows} = \psi_{\rightarrow} e^{i(k_{\rightarrow}x - \omega_{\rightarrow}t)} + \psi_{\leftarrow} e^{i(k_{\leftarrow}x - \omega_{\leftarrow}t)}$$

Lab 1-CW flux number expectation values $|\psi_k|^2 = \langle n_k \rangle$ give 2-CW flux expectations in lab.

$$\langle E \rangle = \langle \hbar\omega \rangle = \hbar\omega_{\rightarrow} \langle n_{\rightarrow} \rangle + \hbar\omega_{\leftarrow} \langle n_{\leftarrow} \rangle = \hbar\omega_{\rightarrow} |\psi_{\rightarrow}|^2 + \hbar\omega_{\leftarrow} |\psi_{\leftarrow}|^2$$

$$\langle cp \rangle = \langle \hbar ck \rangle = \hbar ck_{\rightarrow} \langle n_{\rightarrow} \rangle + \hbar ck_{\leftarrow} \langle n_{\leftarrow} \rangle = \hbar\omega_{\rightarrow} |\psi_{\rightarrow}|^2 - \hbar\omega_{\leftarrow} |\psi_{\leftarrow}|^2$$

The relation (6.13b) of quantum field ψ_k and classical Maxwell E_k-field expectation is used.

$$\langle E \rangle = \hbar\omega_{\rightarrow} |\psi_{\rightarrow}|^2 + \hbar\omega_{\leftarrow} |\psi_{\leftarrow}|^2 = 2\varepsilon_0 c \left(|E_{\rightarrow}|^2 + |E_{\leftarrow}|^2 \right) \qquad (6.18a)$$

$$\langle cp \rangle = \hbar\omega_{\rightarrow} |\psi_{\rightarrow}|^2 - \hbar\omega_{\leftarrow} |\psi_{\leftarrow}|^2 = 2\varepsilon_0 c \left(|E_{\rightarrow}|^2 - |E_{\leftarrow}|^2 \right) \qquad (6.18b)$$

Values $\langle cp \rangle$ and $\langle E \rangle$ lie on an invariant hyperbola of constant geometric means $\varpi\bar{N}$ or $|\bar{\mathbf{E}}|^2$.

$$\langle E \rangle^2 - \langle cp \rangle^2 = (2c\varepsilon_0)^2 \left[\left(|E_{\rightarrow}|^2 + |E_{\leftarrow}|^2 \right)^2 - \left(|E_{\rightarrow}|^2 - |E_{\leftarrow}|^2 \right)^2 \right] = (2c\varepsilon_0)^2 \left[4|E_{\rightarrow}|^2 |E_{\leftarrow}|^2 \right]$$

$$\langle E \rangle^2 - \langle cp \rangle^2 = 4 \left(2c\varepsilon_0 |E_{\rightarrow}|^2 \right) \left(2c\varepsilon_0 |E_{\leftarrow}|^2 \right) = 4 \left(\hbar\omega_{\rightarrow} \langle n_{\rightarrow} \rangle \right) \left(\hbar\omega_{\leftarrow} \langle n_{\leftarrow} \rangle \right) \qquad (6.19)$$

$$\sqrt{\langle E \rangle^2 - \langle cp \rangle^2} = 2c\varepsilon_0 |2\bar{\mathbf{E}}|^2 = (\hbar\varpi)(2\bar{n}) \qquad (6.20a)$$

The geometric mean frequency ϖ, mean quantum number $\bar{n}$, and mean field $|\bar{\mathbf{E}}|$ are defined.

$$\varpi = \sqrt{\omega_{\rightarrow}\omega_{\leftarrow}} \quad (6.20b) \qquad \bar{n} = \sqrt{n_{\rightarrow}n_{\leftarrow}} \quad (6.20c) \qquad |\bar{\mathbf{E}}| = \sqrt{E_{\rightarrow}E_{\leftarrow}} \quad (6.20d)$$
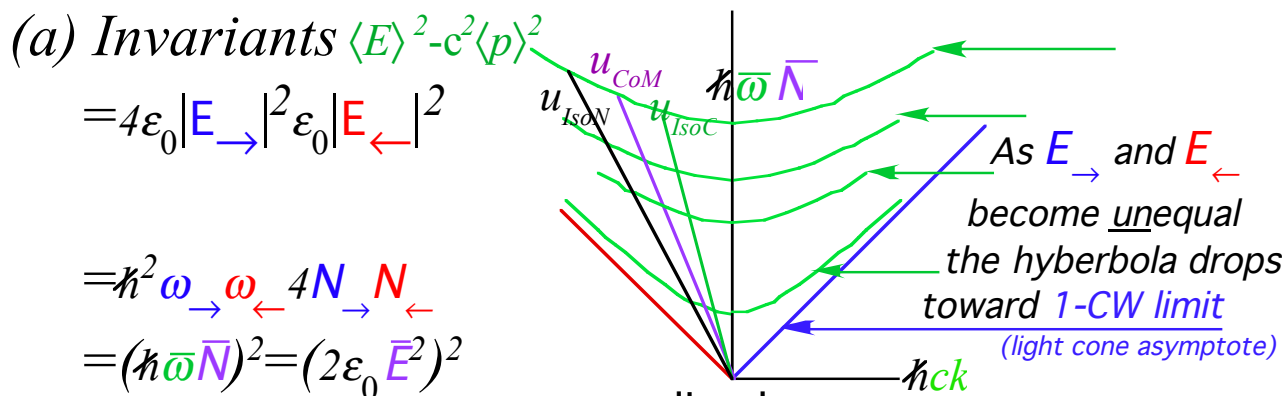
Doppler relations imply Lorentz invariance for the mean number $\bar{n}$ and for the mean frequency ϖ as well as their geometric mean $\sqrt{n\varpi}$ that is $2c\varepsilon_0$ times the mean field $|\bar{\mathbf{E}}|$ and applies to a general 2-CW beam function Ψ. A factor 2 on $|2\bar{\mathbf{E}}|$ or $2\bar{n}$ in (6.20a) is consistent with 1-photon 2-CW states having equal average number $n_{\rightarrow} = \bar{n} = n_{\leftarrow} = \frac{1}{2}$ and total 1-photon Planck energy expectation $E = \hbar\omega$.

Ideal cavities balance field $E_{\rightarrow} = \bar{\mathbf{E}} = E_{\leftarrow}$, frequency $\omega_{\rightarrow} = \varpi = \omega_{\leftarrow}$, and number. But, a general beam with $\omega_{\rightarrow} \neq \omega_{\leftarrow}$, $n_{\rightarrow} \neq n_{\leftarrow}$, and $E_{\rightarrow} \neq E_{\leftarrow}$ has a center-of-momentum CoM-frame of zero flux where

$E_{\to}^{CoM} = E_{\leftarrow}^{CoM}$ by (6.18b), an isochromatic *IsoC*-frame with $\omega_{\to}^{IsoC} = \omega_{\leftarrow}^{IsoC}$, and an *IsoN*-frame with

balanced photon count $N_{\to}^{IsoN} = N_{\leftarrow}^{IsoN}$. Frame speeds u^α may be distinct as sketched in Fig. 6.4.

$$\frac{u^{CoM}}{c} = \frac{E_{\to} - E_{\leftarrow}}{E_{\to} + E_{\leftarrow}} \text{ (6.21a)} \qquad \frac{u^{IsoC}}{c} = \frac{\omega_{\to} - \omega_{\leftarrow}}{\omega_{\to} + \omega_{\leftarrow}} = \frac{V^{Group}}{c} \text{ (6.21b)} \qquad \frac{u^{IsoN}}{c} = \frac{n_{\to} - n_{\leftarrow}}{n_{\to} + n_{\leftarrow}} \text{ (6.21c)}$$

Flux invariant $|\bar{\mathbf{E}}|$ is maximized by balanced amplitude $E_{\to} = E_{\leftarrow}$ but is zero if $E_{\to}$ or $E_{\leftarrow}$ is zero.

Thus optical rest mass (6.20a) decreases continuously as a 2-CW beam is unbalanced toward 1-CW.
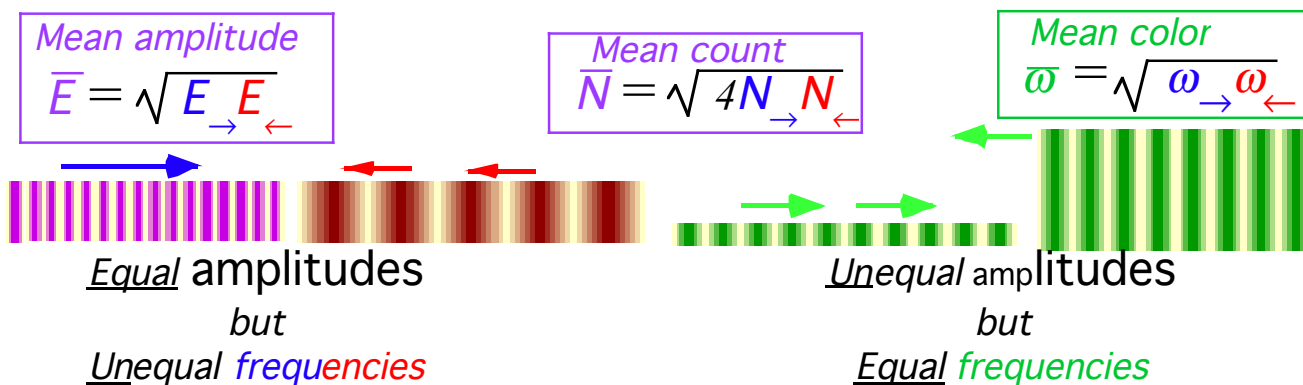
Fig. 6.4. Cavity 2-CW modes. (a) Invariant "mass" hyperbolas. (b) COM frame. (c) ISOC frame.

It is argued in Ch. 4 that mass is a coherent 2-CW interference effect that is not possible for a 1-CW beam. If we replace Planck energy relation $\varepsilon = Nh\upsilon$ by a Maslov form $\varepsilon = (N + \bar{\alpha})h\upsilon$ it has a tiny zero-point energy minimum $\bar{\alpha}h\upsilon$. Does a tiny mass $\bar{\alpha}h\upsilon / c^2$ exist for 1-CW and even 0-CW beams in all frames in spite of the incoherence of such zero-point fluctuations? Such a presence in (6.20) may be ruled out if the speed-of-light axiom (1.1) is exact. There may still be much to learn about zero-point effects in QED and cosmology but this seems to indicate that their directly observable effects do not exist.

N-Photon vs Coherent-α-states

Optical fields **A** or **E** have quantum expectation values of field operators based on mode amplitudes $\mathbf{a}_k$ or $\mathbf{a}_k^*$ in classical energy $\sum \omega_k^2 \mathbf{a}_k^* \mathbf{a}_k$. Each $\mathbf{a}_k$ or $\mathbf{a}_k^*$ is replaced by oscillator boson operator $\mathbf{a}_k$ or $\mathbf{a}_k^\dagger$ in a quantum field Hamiltonian $\mathbf{H} = \sum \hbar\omega_k (\mathbf{a}_k^\dagger \mathbf{a}_k + \bar{\alpha})$ whose eigenstates $|N_1 N_2 \cdots N_k\rangle$ have exact quantized photon numbers $\langle \mathbf{a}_k^\dagger \mathbf{a}_k \rangle = N_k$ for each mode-k_m.

Each mode phase quanta m and amplitude quanta N_m are invariant constants that define another hyperbola with Einstein-Planck proper frequency $\varpi_{N,m} = \hbar N_m \omega_m$ as sketched in Fig. 6.4a and Fig. 4.2. The problem is that absolute certainty of photon number N_m implies totally *un*certain field phase just as absolutely certain k_m of 1-CW symmetry implies totally *un*certain position in space and time.

Space-time position coordinates were defined by taking 1-CW combinations to make 2-CW coordinates of Fig. 2.1c or Fig. 2.2c. Ultimately an *n*-CW pulse-wave (PW) of Fig. 2.1d or Fig. 2.2d was localized with as low a space-time uncertainty $\Delta\tau$ as desired but it acquires per-space uncertainty or bandwidth $\Delta\upsilon$ according to Fourier-Heisenberg relation $\Delta\upsilon \cdot \Delta\tau > 1$.

So also must photon-number states be combined if amplitude and phase uncertainty are to be reduced to the point where wave space-time coordinates can emerge. Such combinations are known as coherent states or α-states of harmonic oscillation. Sharper wave zeros require fuzzier hyperbolas.

Fuzzy hyperbolas vs. fuzzy coordinates

Model micro-laser states are *coherent* states $|\alpha\rangle = \Sigma_N \psi_N |N\rangle$ made of single-mode eigenstates $|N\rangle = (\mathbf{a}_1^\dagger)^N |0\rangle$ with amplitudes $\psi_N = \alpha^N e^{-\alpha^2/2} / \sqrt{N!}$. Variable $\alpha = x + ip = |\alpha| e^{i\Phi}$ is average mode phase, and $(x = \mathrm{Re}\,\alpha, p = \mathrm{Im}\,\alpha)$, rescaled by a quantum field factor f, are field averages $(\langle A \rangle, \langle \dot{A} \rangle = -\langle E \rangle)$.

$$\langle \alpha | A | \alpha \rangle = \langle A \rangle = (\alpha + \alpha^*) f = (\alpha + \alpha^*) \sqrt{\frac{\hbar}{2\varepsilon_0 \omega V}} \qquad (6.22)$$

Amplitude factor f makes Planck's $\bar{E} = \hbar\omega\bar{N}$ equal Maxwell field energy $\bar{E} = \bar{U} \cdot V$.

$$\langle U \rangle V = 2\varepsilon_0 \omega^2 V \langle A^2 \rangle = \hbar\omega |\alpha|^2 = \hbar\omega\bar{N} \qquad (6.23)$$

A fundamental laser mode in a *0.25μm* cubic cavity (See **E**-wave sketched in a strip of Fig. 2.2c.) has green light with $\hbar\varpi = 4 \cdot 10^{-19} \, Joule$ or *2.5eV* per photon. The average photon number $\bar{N} = |\alpha|^2 = 10^{10}$ models a laser with mean energy $\bar{E} = \bar{U} \cdot V = \hbar\varpi\bar{N} = 4.0 \, nanoJ$ in a volume $V = (\frac{1}{4}\mu m)^3$. Photon number uncertainty $\Delta N = |\alpha| = 10^5$ varies inversely to phase uncertainty.

$$\Delta\Phi \cdot \Delta N = \pi \quad (6.24a) \qquad\qquad \Delta\Phi = \pi/\alpha \sim 3\cdot10^{-5} \quad (6.24b)$$

Amplitude expectation value $\langle N|A|N\rangle$ is zero for $|N\rangle$ states due to *in*coherence of phase, but number value $\langle N|\mathbf{a}_k^\dagger \mathbf{a}_k|N\rangle = N$ is exact as is proper frequency ϖN due to the phase factor $(e^{-i\varpi t})^N$ of $(\mathbf{a}_1^\dagger)^N$.

A volume V with $(N=10^{10})$-photons has energy $E = \hbar\omega N$ or mass-equivalent $M = E/c^2 = 10^{-25}\,kg$ on a hyperbola 10^{10} quanta above the $N=1$ hyperbola. A coherent-state $|\alpha=10^5\rangle$ has a mass $M = 10^{-25}\,kg$ with uncertainty $\Delta M = 10^{-30}\,kg$ so its *phase* uncertainty $3\cdot10^{-5}$ is low enough to make an *(x,ct)*- grid (Fig. 6.6a) but a low-α state (Fig. 6.6c) has too few photon counts-per-grid to plot sharply. Photon-number eigenstate $|N\rangle$ in Fig. 6.6d is a total wash even for high-N since $\Delta N = 0$ implies maximal phase uncertainty *($\Delta\Phi = \infty >> 2\pi$)*.
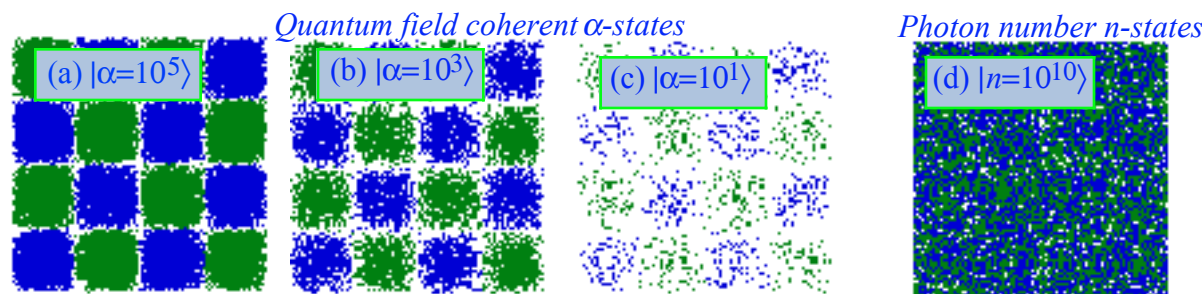
Fig. 6.6 Simulated spacetime photon counts for coherent (a-c) and photon-number states (d).

Deeper symmetry aspects of pair creation

Discussion of relativity and quantum theory of wave amplitude requires further details. This includes Dirac's extraordinary theory that 2-CW light of certain frequencies in a vacuum may create "real" matter that does not vanish when the light is turned off. For example, we know that two *0.51MeV* γ-ray photons of frequency $\omega_e = m_e c^2/\hbar$ may create an electron and positron "hole" that form positronium $e + \bar{e}$ pairs. Also, *0.94GeV* γ-rays with $\omega_p = m_p c^2/\hbar$ may create proton-anti-proton $p + \bar{p}$ pairs, and so on.

Dirac creation processes raise questions, "What "cavity" traps *0.51MeV* γ-pairs into stable $e + \bar{e}$ pairs?" The discussion so far has only begun to define 2-CW symmetry properties by phase rates in per-spacetime *(K,Ω)*-quantum variables. Conservation (5.2) of these kinetic *(K,Ω)*-values implies that $e + \bar{e}$ or $p + \bar{p}$ pairs have the same *(K,Ω)*-values as the 2-CW light that "creates" them.

However, space-time symmetry arguments by themselves seem unable to derive internal lepton or baryon structure that might show how light becomes "trapped." That question still lies beyond the scope of this discussion, and indeed, still largely beyond what is presently known. In fact, the current standard Weinberg-Salam model of high energy electroweak and strong quantum-chromo-dynamics (QCD) has abandoned the Dirac picture almost entirely. Pauli's apparent dislike for Dirac may have had an effect.

In its place have there has arisen a large and controversial area known as super-symmetric-string-theory or "superstrings" that has generated over 10,000 publications in about 40 years and promised a "theory of everything" that would include quantum gravity. However, as discussed in the introduction, this flurry of mathematical activity is yet to yield new experimental insight or provide a better way to develop existing areas of classical mechanics, relativity or quantum theory.

Appendix 6.A. Laser Wave 4-Vector Coordinate Frames

Chapter 4 introduced the idea of a two-dimensional space-time *(x,ct)* coordinate system generated by a pair of continuous wave (CW) lasers. (Fig. 2.1c) They generated Lorentz-Einstein-Minkowski coordinates shown in Fig. 2.2c and labeled in Fig. 2.3 or Fig. 2.4. Now we discuss 3-dimensional problems involving the full 4-dimensional space-time $x^\mu = (\mathbf{r}, ct)$ coordinate systems made by counter-propagating CW lasers generating waves of 4-dimensional wavevector-frequency $k^\mu = (c\mathbf{k}, \omega)$.

Counter propagating waves in space-time

The general 1D wavefunction (6.1) generalizes to the following $\Psi_{\{\mu\}}(\mathbf{r},t)$ made of waves with wavefront planes of constant phase sketched in Fig. 6A.0.

$$\Psi_{A_\rightarrow,\omega_\rightarrow,\mathbf{k}_\rightarrow;A_\leftarrow,\omega_\leftarrow,\mathbf{k}_\leftarrow}(\mathbf{r},t) = A_\rightarrow e^{i(\mathbf{k}_\rightarrow \bullet \mathbf{r} - \omega_\rightarrow t)} + A_\leftarrow e^{i(\mathbf{k}_\leftarrow \bullet \mathbf{r} - \omega_\leftarrow t)} \tag{6A.1}$$

Single-$\mathbf{k}$-vector waves $\Psi_\mathbf{k}(\mathbf{r},t)$ with zero *SWR* have simple phase properties and transformation rules.

$$\Psi_\mathbf{k}(\mathbf{r},t) = (e^{i(\mathbf{k}_\rightarrow \bullet \mathbf{r} - \omega_\rightarrow t)} + e^{i(\mathbf{k}_\leftarrow \bullet \mathbf{r} - \omega_\leftarrow t)})/2 \tag{6A.2}$$

An expo-cosine identity generalizing (4.3.1) defines 3-D phase and group-envelope waves.

$$\Psi(\mathbf{r},t) = \Psi_\mathbf{k}(\mathbf{r},t) = \frac{1}{2} e^{i(\mathbf{k}_\rightarrow \bullet \mathbf{r} - \omega_\rightarrow t)} + \frac{1}{2} e^{i(\mathbf{k}_\leftarrow \bullet \mathbf{r} - \omega_\leftarrow t)}$$

$$= e^{i\frac{(\mathbf{k}_\rightarrow + \mathbf{k}_\leftarrow)\bullet\mathbf{r} - (\omega_\rightarrow + \omega_\leftarrow)t}{2}} \cos \frac{(\mathbf{k}_\rightarrow - \mathbf{k}_\leftarrow)\bullet\mathbf{r} - (\omega_\rightarrow - \omega_\leftarrow)t}{2} \tag{6A.3a}$$

$$= e^{i(\bar{\mathbf{K}}\bullet\mathbf{r} - \bar\Omega t)} \cos(\bar{\mathbf{k}}\bullet\mathbf{r} - \bar\omega t) \quad \text{where:} \tag{6A.3b}$$

$$\bar{\mathbf{K}} = \frac{(\mathbf{k}_\rightarrow + \mathbf{k}_\leftarrow)}{2}, \qquad\qquad \bar{\mathbf{k}} = \frac{(\mathbf{k}_\rightarrow - \mathbf{k}_\leftarrow)}{2},$$
$$\bar\Omega = \frac{(\omega_\rightarrow + \omega_\leftarrow)}{2}, \qquad\qquad \bar\omega = \frac{(\omega_\rightarrow - \omega_\leftarrow)}{2}. \tag{6A.3c}$$

The *Lab Frame* has stationary phase planes normal to a beam axis-*z* between the two lasers of frequency ω_0 with opposing wavevectors. Phase-*0* plane spacing is laser proper wavelength $\lambda_0 = 2\pi c/\omega_0$.

$$\Psi_{\mathbf{k}_0}(\mathbf{r},t) = e^{-i(\omega_0 t)} \cos(\mathbf{k}_0 \bullet \mathbf{r}) \tag{6A.4a}$$

$$\text{where: } \bar{\mathbf{k}} = \mathbf{k}_\rightarrow = -\mathbf{k}_\leftarrow = \mathbf{k}_0 \text{, and } \bar\Omega = \omega_\rightarrow = \omega_\leftarrow = \omega_0 \tag{6A.4b}$$

The group planes of zero $\text{Re}\Psi$ are fixed normal to $\mathbf{k}_0$.

$$\mathbf{k}_0 \bullet \mathbf{r} = \pm\pi/2, \pm3\pi/2, ... \tag{6A.4c}$$

The phase zeros periodically go infinitely fast in the $\mathbf{k}_0$-direction at certain times.

$$...\omega_0 t = \pm\pi/2, \pm3\pi/2, ... \tag{6A.4d}$$

This is the same lab frame described before in Fig. 2.2. A frame boosted along the beam *z*-axis appeared in Fig. 2.3. There was no 3-dimensional boosting or rotation.

However, three dimensions presents a much more complicated range of possible symmetry transformations involving the six *Lorentz group* parameters for *x*, *y*, and *z* boosts and rotations or, including translations, nine parameters of the *Poincare' group*. Nevertheless, by appealing to continuous-wave optical thought experiments it is possible to simplify the derivation and visualization of this enormous symmetry of locally flat space-time for both classical and quantum theory. Of course real lab

experiments would be dicey at best. Squared-off laser waves would have difficulty achieving planarity over more than a few microns unless a great distance separated them as is imagined for CW star-pairs in Fig. 5.7 and Fig. 5.10.
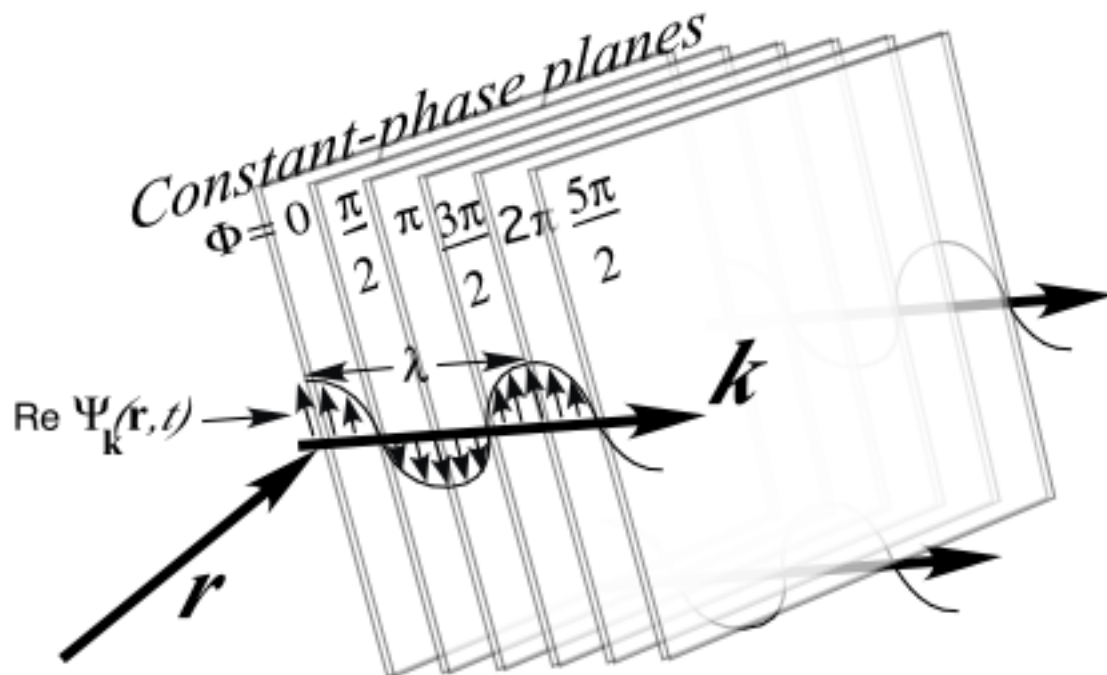

Fig. 6A.0 Sketch of a plane wavefunction $\Psi_k(\mathbf{r},t) = A\exp i(\mathbf{k}\cdot\mathbf{r} - \omega t)$ *with wavevector* $\mathbf{k}$.

CW positioning system

Here we imagine orthogonal pairs of CW lasers that form a positioning grid similar to what is used for coherent laser cooling. The wave dynamics associated with each pair automatically broadcasts a set of relativistic $\mathbf{k}$-vectors and coordinate planes for any observer. (Laser waves already "know" relativity!) In principle, an observer can ascertain orientation and velocity relative to the Lab grid, and by coordinate plane integration, translation position, as well. The key axiom is phase invariance (1.3) restated here.

$$\Phi = -\mu\tau = \mathbf{k}\cdot\mathbf{r} - \omega t = \mathbf{k}\cdot\mathbf{r} - (\omega/c)(ct) = \mathbf{k}'\cdot\mathbf{r}' - (\omega'/c)(ct'). \qquad (1.3)_{restated}$$

First is individual laser phase invariance. Pairs $(ct_0,\mathbf{r}_0)$ and $(\omega_0,c\mathbf{k}_0)$ are in Lab frame.

$$\Phi_{\rightarrow} = \mathbf{k}'_{\rightarrow}\cdot\mathbf{r}' - \omega'_{\rightarrow}t' = \mathbf{k}_{\rightarrow}\cdot\mathbf{r} - \omega_{\rightarrow}t = \;\mathbf{k}_0\cdot\mathbf{r}_0 - \omega_0 t_0 \qquad (6A.5a)$$

$$\Phi_{\leftarrow} = \mathbf{k}'_{\leftarrow}\cdot\mathbf{r}' - \omega'_{\leftarrow}t' = \mathbf{k}_{\leftarrow}\cdot\mathbf{r} - \omega_{\leftarrow}t = -\mathbf{k}_0\cdot\mathbf{r}_0 - \omega_0 t_0 \qquad (6A.5b)$$

Individual laser 4-vectors are, by definition, located on the light cone or null-invariant.

$$c^2\mathbf{k}'_{\rightarrow}\cdot\mathbf{k}'_{\rightarrow} - \omega'^2_{\rightarrow} = c^2\mathbf{k}_{\rightarrow}\cdot\mathbf{k}_{\rightarrow} - \omega^2_{\rightarrow} = \;c^2 k_0^2 - \omega_0^2 = 0 \qquad (6A.6a)$$

$$c^2\mathbf{k}'_{\leftarrow}\cdot\mathbf{k}'_{\leftarrow} - \omega'^2_{\leftarrow} = c^2\mathbf{k}_{\leftarrow}\cdot\mathbf{k}_{\leftarrow} - \omega^2_{\leftarrow} = \;c^2 k_0^2 - \omega_0^2 = 0 \qquad (6A.6b)$$

If any pair of 4-vectors $(\alpha,\mathbf{a})$ and $(\beta,\mathbf{b})$ are Lorentz covariant, then so is any linear combination of them.

$$(\gamma,\mathbf{c}) = A(\alpha,\mathbf{a}) + B(\beta,\mathbf{b}) = (A\alpha + B\beta, A\mathbf{a} + B\mathbf{b})$$

In other words, invariance of α^2-$\mathbf{a}\cdot\mathbf{a} = \alpha'^2$-$\mathbf{a}'\cdot\mathbf{a}'$ and β^2-$\mathbf{b}\cdot\mathbf{b} = \beta'^2$-$\mathbf{b}'\cdot\mathbf{b}'$ implies invariance for the combination γ^2-$\mathbf{c}\cdot\mathbf{c} = \gamma'^2$-$\mathbf{c}'\cdot\mathbf{c}'$, as well. So, phase invariance (1.3) applies to sum $\bar{\mathbf{K}} = (\mathbf{k}_{\rightarrow} + \mathbf{k}_{\leftarrow})/2$ and

difference $\bar{\mathbf{k}} = (\mathbf{k}_{\rightarrow} - \mathbf{k}_{\leftarrow})/2$ wavevectors attached to corresponding sum $\bar{\Omega} = (\omega_{\rightarrow} + \omega_{\leftarrow})/2$ and difference

$\bar{\omega} = (\omega_{\rightarrow} - \omega_{\leftarrow})/2$ frequencies. However, the new invariants have different values.

$$\bar{\mathbf{K}}' \bullet \mathbf{r}' - \bar{\Omega}'t' = \bar{\mathbf{K}} \bullet \mathbf{r} - \bar{\Omega}t = \; 0 - \omega_0 t_0 \tag{6A.7a}$$

$$\bar{\mathbf{k}}' \bullet \mathbf{r}' - \bar{\omega}'t' = \bar{\mathbf{k}} \bullet \mathbf{r} - \bar{\omega}t = \; \mathbf{k}_0 \bullet \mathbf{r}_0 - 0 \tag{6A.7b}$$

In fact, sum and difference vectors are not on the light cone like their laser components (6A.6).

$$\bar{\Omega}'^2 - c^2\bar{\mathbf{K}}' \bullet \bar{\mathbf{K}}' = \bar{\Omega}^2 - c^2\bar{\mathbf{K}} \bullet \bar{\mathbf{K}} = \; \omega_0^2 - 0 \qquad = c^2 k_0^2 \tag{6A.8a}$$

$$\bar{\omega}'^2 - c^2\bar{\mathbf{k}}' \bullet \bar{\mathbf{k}}' \; = \bar{\omega}^2 - c^2\bar{\mathbf{k}} \bullet \bar{\mathbf{k}} \; = \; 0 - c^2\mathbf{k}_0 \bullet \mathbf{k}_0 \; = -c^2 k_0^2 \tag{6A.8b}$$

The sum vector $(\bar{\Omega}, c\bar{\mathbf{K}})$ in (6A.8a) has a proper frequency $\mu = \omega_0 = ck_0$ and behaves like a massive particle. Because of this, uniform wave guide modes have the dispersion of a massive particle which is a *mass-shell M-hyperboloid* (6A.8a) first plotted in Fig. 3.4a. This will be used later.

The difference vector $(\bar{\omega}, c\bar{\mathbf{k}})$ has an imaginary proper frequency $\mu = ick_0$. Such an object is called a *Feinberg τ-Tachyon*, and is quite unlike ordinary matter. A real mass starts out at zero wavevector *(k=0)* with real (proper) frequency $\mu = \omega_0$, zero group velocity $d\omega/dk$, and infinite phase velocity ω/k. In contrast, tachyons start out at zero frequency *(ω=0)* with a real wavevector k_0, zero phase velocity *($\omega/k.$=0)* and infinite group velocity *($d\omega/dk$=∞)*. A tachyon dispersion curve is a vertical τ-hyperbola given by (6A.8b) and drawn below the photon asymptote in Fig. 4.1a. Such a τ-wave is also known as an "instanton" since it everywhere at the instant it has infinite group velocity. Our name for the τ-wave is less poetic: it is simply the group cosine envelope which is static in the Lab CPS frame. (It *defines* Lab-frame's coordinate planes.)

As the observer's rest frame changes velocity **u**, the sum vector $(\bar{\Omega}, c\bar{\mathbf{K}})$ follows an *M*-hyperbola (6A.8a) while difference vector $(\bar{\omega}, c\bar{\mathbf{k}})$ follows a tachyon hyperbola (6A.8b). Meanwhile, pairs of laser 4-wavevectors *(ω→,ck→)* or *(ω←,ck←)* (for light moving along the *x*-axis) and *(ω↑,ck↑)* and *(ω↓,ck↓)* (for light moving along the vertical *z*-axis) each follow null light-cone-invariants (6A.6). The details of how *(ω→,ck→)*, *(ω←,ck←)*, *(ω↑,ck↑)*, and *(ω↓,ck↓)* transform is sketched in Fig. 5.10.

Wavevector defined coordinate planes

Examples of the effects of *x*-boosts, *z*-boosts and combinations of them on Lab wavevector pairs are plotted in Fig. 6A.1 where the relative velocity is *3c/5*. Fig. 6A.1b is identical to the pair of wavevectors shown in the preceding Fig. 5.10, and Fig. 6A.1c is the same thing rotated by *90°*.

Also shown are the CPS coordinate grid planes as seen in the observer's frame at a particular instant of the observer's time. These are planes that are the group *phase=0 mod π* planes in the CPS frame and fixed to it so they are moving rigidly in any boosted observer's frame opposite to the boost. They are obtained from the wavevector differences such as *(**k**→ - **k**←)* by solving (6A.7b) as repeated below.

$$\bar{\mathbf{k}} \bullet \mathbf{r} - \bar{\omega}t = \; \mathbf{k}_0 \bullet \mathbf{r}_0 = 0, \pm\pi, \pm 2\pi, ... \tag{6A.9}$$

At the observer instant *t=0* one simply obtains a plane through origin and normal to *(**k**→ - **k**←)/2*.

This wave based solution is simpler than trying to use a Lorentz coordinate transformation to find

observer coordinates *(ct, x, y, z)* in terms of CPS coordinates (ct_0, x_0, y_0, z_0). The latter would be easy if one desired observer values of CPS planes at a fixed CPS time t_0, but it is quite inconvenient if, as is the case, we desire their location as the observer sees them at his instant *t*.

The effect of doing $u_x/c=3/5$ and $u_z/c=3/5$ boosts singly and in sequence of different orders is shown in Fig. 6A.1. A single boost induces an 80% Lorentz contraction *(1/cosh υ =0.8)* in the direction of the boost. Two Lorentz boosts induce a rotation in rotation group R(3) a subgroup of the Lorentz group. In the study of spin-orbit effects this rotation is called *Thomas precession*, a topic intended for later Units.
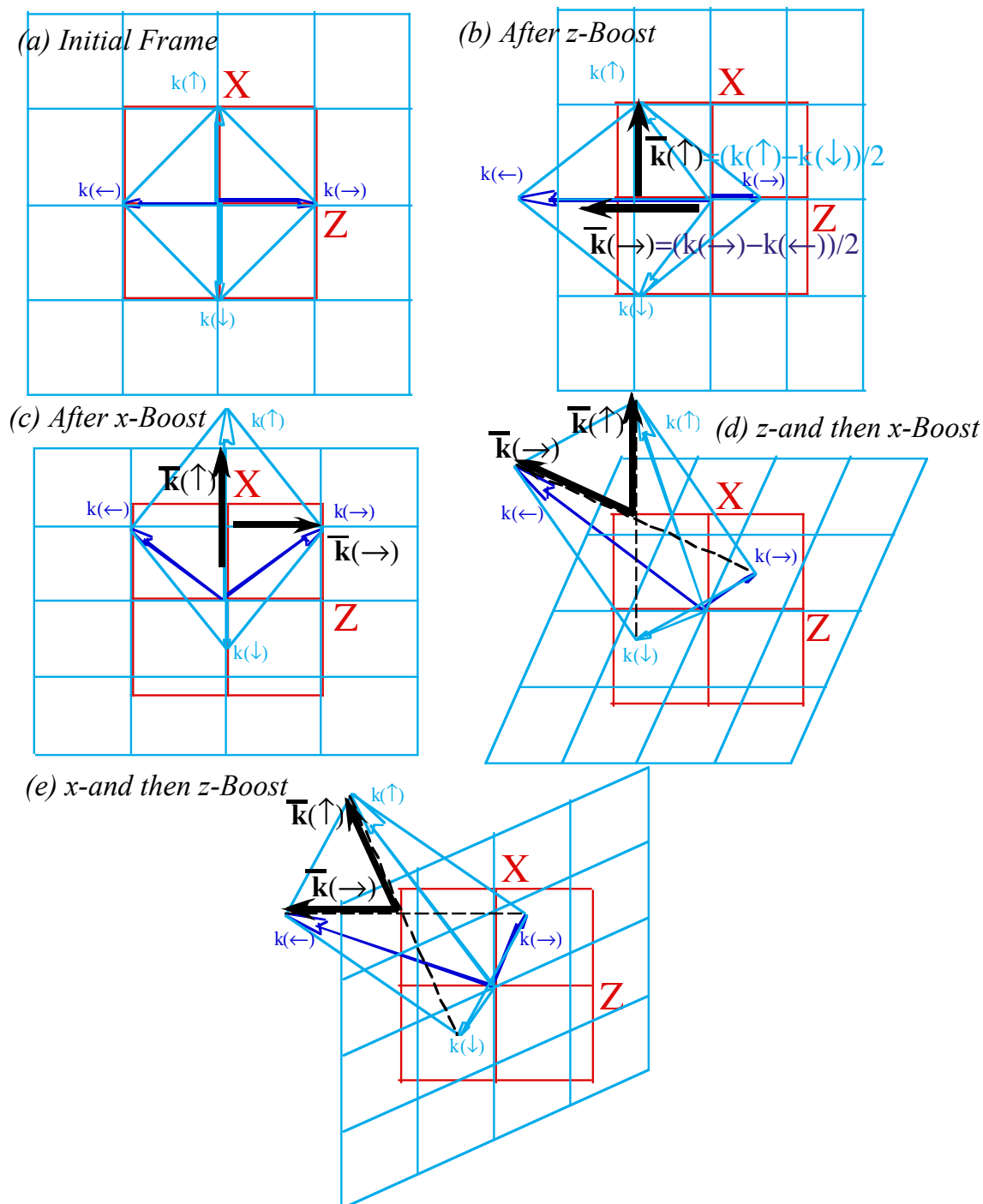
Fig. 6A.1 Examples of sequential relativistic transformations of a tetrad of light wavevectors.

Appendix 6.B. Wave Guide Dispersion and Cavity Eigenfrequencies

A wave guide confines 3-dimensional *(c**k**, ω)* light waves to propagate in one dimension. The result is a hyperbolic dispersion function of the form (3.12) in Fig. 3.4 or of quantum matter waves in Fig. 4.1.

$$\omega^2 = \mu^2 - (ck)^2 \qquad \text{(6B.1)}$$

Putting end plates on a guide further confines the wave to a cavity mode and restricts its frequency dispersion to discrete or "quantized" frequency eigenvalues ω_m. This is discussed below.

2-Dimensional wave mechanics: guided waves and dispersion

A two or three-dimensional wave will be seen to exceed the *c*-limit when it approaches an axis obliquely. It happens for plane waves. The phase velocities along coordinate axes are given by

$$v_x = \omega/k_x, \qquad\qquad v_y = \omega/k_y, \qquad\qquad v_z = \omega/k_z. \qquad \text{(6B.2)}$$

Each of the components (k_x, k_y, k_z) must be less than or equal to magnitude k. Thus, all the component phase velocities equal or exceed the phase velocity ω/k which is *c* for light! In fact, <u>water</u> waves can exceed *c* ; if a wave breaks parallel to shore the 'break-line" moves infinitely fast since k_x is zero.

This has application to the basic wave mechanics of a wave guide consisting of a 'Hall of Mirrors" along the *x*-axis shown in Fig. 6B.1. Let two parallel mirrors on either side of the *x*-axis be separated by a distance *y=W*. The South wall will be at *y=-W/2* and the North wall at *y=W/2*. (*z*-axis or "up" is into the page of Fig. 6B.1.) The Hall should have a floor and ceiling at *z=±H/2*, but its position doesn't matter as long as we consider only waves moving in the *xy*-plane direction. The effect of *H* is discussed later.
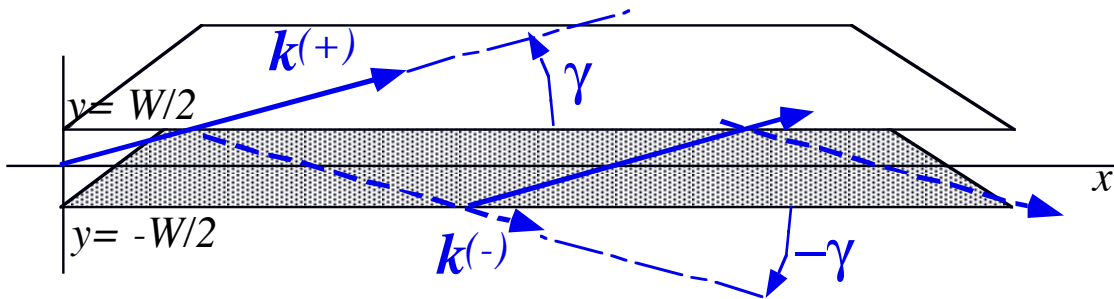

Fig. 6B.1 A "hall of mirrors" model for an optical wave guide of width W.

Now consider what would happen if you shine a laser or maser down this hall. (In quantum jargon, "we propagate a photon beam.") Let the beam be at an angle γ to the *x*-axis in the plane of the Fig. 6B.1. Two waves will result as shown in Fig. 6B.1. One you send in with its **k**-vector $\mathbf{k}^{(+)}$ pointing at angle +γ .

$$\mathbf{k}^{(+)} = (k^{(+)}{}_x, k^{(+)}{}_y, 0) = (k\cos\gamma, k\sin\gamma, 0)$$

Then its *y*-reflected mirror image will have its **k**-vector $\mathbf{k}^{(-)}$ pointing at angle -γ.

$$\mathbf{k}^{(-)} = (k^{(-)}{}_x, k^{(-)}{}_y, 0) = (k\cos\gamma, -k\sin\gamma, 0).$$

By adding the two waves with $\mathbf{k}^{(+)}$ and $\mathbf{k}^{(-)}$ you can make a wave function inside the Hall of Mirrors that vanishes at the mirror surface boundaries located at *y=±W/2*.

$$\begin{aligned}
\Psi(\mathbf{r},t) &= exp\ i(\ \mathbf{k}^{(+)}\cdot\mathbf{r}\ -\ \omega t) + exp\ i(\ \mathbf{k}^{(-)}\cdot\mathbf{r}\ -\ \omega t)\\
&= exp\ i(k\,x\cos\gamma\ +k\,y\sin\gamma - \omega t) + exp\ i(k\,x\cos\gamma\ -k\,y\sin\gamma - \omega t)\\
&= exp\ i(k\,x\cos\gamma\ -\ \omega t)\ [\ exp\ i(\,k\,y\sin\gamma\,) + exp\ i(\,-k\,y\sin\gamma\,)]\\
&= e^{\ i(k\,x\cos\gamma\ -\ \omega t)}\ [\ 2\cos(\,k\,y\sin\gamma\,)\ ] \qquad\qquad\qquad \text{(6B.3)}
\end{aligned}$$

The wave function must vanish at mirror surfaces *(y=±W/2)* so that E-wave Ψ does not enter them in what is called a *transverse electric* (TE) mode. TE boundary conditions relate to angle γ as follows.

$$0 = 2 \cos(k\,(W/2)\sin\gamma)\,, \quad or:\ k\,(W/2)\sin\gamma = \pi/2\,, \quad or:\ \sin\gamma = \pi/(k\,W) \tag{6B.4a}$$

The wavevector magnitude is related to angular frequency by the usual $k=\omega/c$. Stated another way we fix the *y*-component of the $\mathbf{k}^{(+)}$ or $\mathbf{k}^{(-)}$ vectors to just fit a half-wave in the width *W* of the Hall of Mirrors.

$$k^{(+)}{}_y = k\sin\gamma = \pi/W \tag{6B.4b}$$

These conditions lead to what is called a *dispersion function ω(kₓ)* or *ω vs. kₓ relation*.

$$\omega = kc = c(k_x^2 + k_y^2 + k_z^2)^{1/2} = c(k_x^2 + \pi^2/W^2)^{1/2} \tag{6B.5a}$$

$$\omega = \surd(c^2 k_x^2 + \omega_{cut}^2)\ \ \text{where:} \qquad \omega_{cut} = \pi c/W. \tag{6B.5b}$$

A minimum or *cut-off frequency* $\omega_{cut} = \pi c/W$ is defined. Solving for k_x gives

$$k_x = (\omega^2/c^2 - \pi^2/W^2)^{1/2}. \tag{6B.5c}$$

This is the equation for a hyperbola in *(ω,ckₓ)* space is plotted below in Fig. 6B.2 and Fig. 6B.8.

$$\omega^2 - c^2 k_x^2 = \pi^2 c^2/W^2 = \omega_{cut}^2 \tag{6B.5d}$$
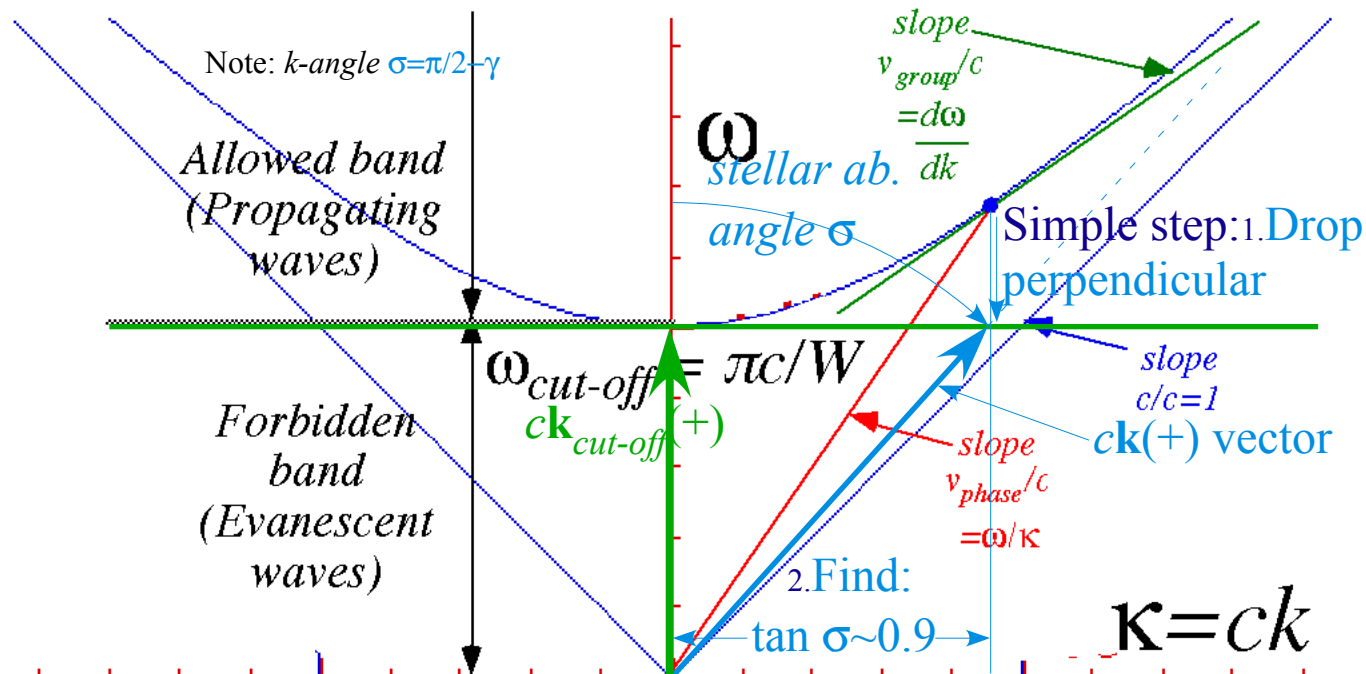

Fig. 6B.2 Dispersion function for a fundamental TE wave guide mode

The hyperbolic asymptotes are lines of slope equal to the speed of light *c*. (6B.5d) is a standard relativistic invariant function. All observers, no matter what their relative *x*-velocity, agree on how the light travels through space-time in a Hall of Mirrors. This holds only if the mirrors are 'ideal' in that their performance does not depend on their *x*-velocity. You can't tell if an 'ideal' mirror is sliding past you! But, real mirror atomic response varies with velocity. If photon frequency is blue shifted up to X-ray values, a real dispersion function loses relativistic invariance. Polarization waves of real material cannot be totally Lorentz invariant since its very presence breaks the symmetry of the vacuum.

The dispersion relation ω (k_x) is used to calculate the Hall wave velocities. From the dispersion relation ω (k_x) in (6B.6 a) we obtain the phase velocity from (4.4.7) and group velocity from (4.4.6b) for a mono-chromatic wave propagating down the Hall. (However, a group wave cannot be monochromatic!)

$$v_x \text{ (phase)} = \omega/k_x \qquad\qquad\qquad v_x \text{ (group)} = d\omega/dk_x = ck_x/\sqrt{(k_x{}^2 + \pi^2/W^2)}$$
$$= c\omega /(\omega^2 - \pi^2c^2/W^2)^{1/2} \quad \text{(6B.7 a)} \qquad = c(\omega^2 - \pi^2c^2/W^2)^{1/2}/\omega \qquad \text{(6B.7 b)}$$

Using (4.34b) we get the speeds in terms of angle γ and vacuum light speed *c*.

$$v_x \text{ (phase)} = c/\cos\gamma \qquad\qquad \text{(6B.7 c)} \qquad\qquad v_x \text{ (group)} = c\cos\gamma \qquad\qquad \text{(6B.7 d)}$$

As the wavelength is reduced (higher *k* and ω) v_x *(phase)* and v_x *(group)* approach *c* which is what light would do anyway if the Hall width *W* was huge. However, as wavelength grows (lower *k* and ω) the tipping angle γ grows from zero toward *90°* in order to match a half wave perfectly to the Hall width *W*. Then v_x *(phase)* approaches infinity while v_x *(group)* slows to a crawl as the frequency approaches a minimum *cut-off* value $\omega_{cut} = \pi c/W$. This is the *proper frequency* μ of a guided photon, the smallest red-shifted frequency a moving observer could see if k_x is Doppler shifted to zero. The next figures, done by the program *GuideIt* show how waves behave going down a hall at various frequencies.

Rays and wavefronts: Phase and group velocity

Fig. 6B.3 begins with light entering the Hall of Mirrors at γ=±*45°* to the *x*-axis. The rays of the *+45°* wave are being traced as they appear to reflect off the North wall into the *-45°* wave. Note that the wave amplitude (represented by wavy lines) is maximum in the center of the hallway *(y=0)* as required by the amplitude factor *[2 cos(k y sin γ)]* in (6B.3). The same factor makes the wave identically zero at the North and South walls *(y=± W/2)* according to (6B.4a), the TE boundary conditions.

The TE wave speed is v_x *(phase)* = *c*√2 according to (6B.7 c). But, the velocity v_x *(group)* =*c*/√2 is exactly half as fast. This is the velocity of the *rays*. Their progress down the *x*-axis of the hallway is slower than their actual speed *c* because they are ricocheting back and forth off the walls as seen in the figures below. This "off-the-wall" explanation of group velocity makes it clear why the group velocity is *c* times the cosine of the angle γ. It is the *x*-component of a tipped wave velocity vector. The rays are attached to *wave fronts* of constant phase. On the way up the wave front phase is *2nπ* (multiple of *2π)* indicated by a thin solid line. The phase changes by π when a ray bounces off a wall, so downward rays are attached to a wave front having a phase of *(2n-1)π,* indicated by a thin dotted line. Where solid *(2nπ)* fronts meet is a wave *crest.* Where dotted *(nπ)* fronts meet is a wave *trough.* A *node* is where fronts of opposite phase meet. This happens along walls that have a line of nodes according to TE boundary conditions.

A more detailed sketch of a wave mode similar to Fig. 6B.3 is shown in Fig. 6B.8. The E-field vectors are drawn as dot-circles (⊙) for up-out-of-plane +**E** cresting waves and cross-circles (⊗) for down-into-plane -**E** troughs. (Think of **E**-arrows with sharp points on (+) end and feathers on (-) end!) This shows how the **E**-field is indeed transverse the direction of motion and the waveguide floor and ceiling, but parallel and approaching zero close to the walls. It also shows that the phase wave appears to drag (-) charge at (⊙)-crests and (+) charge at (⊗)-troughs along ceiling and floor. Pretty spooky Hall!
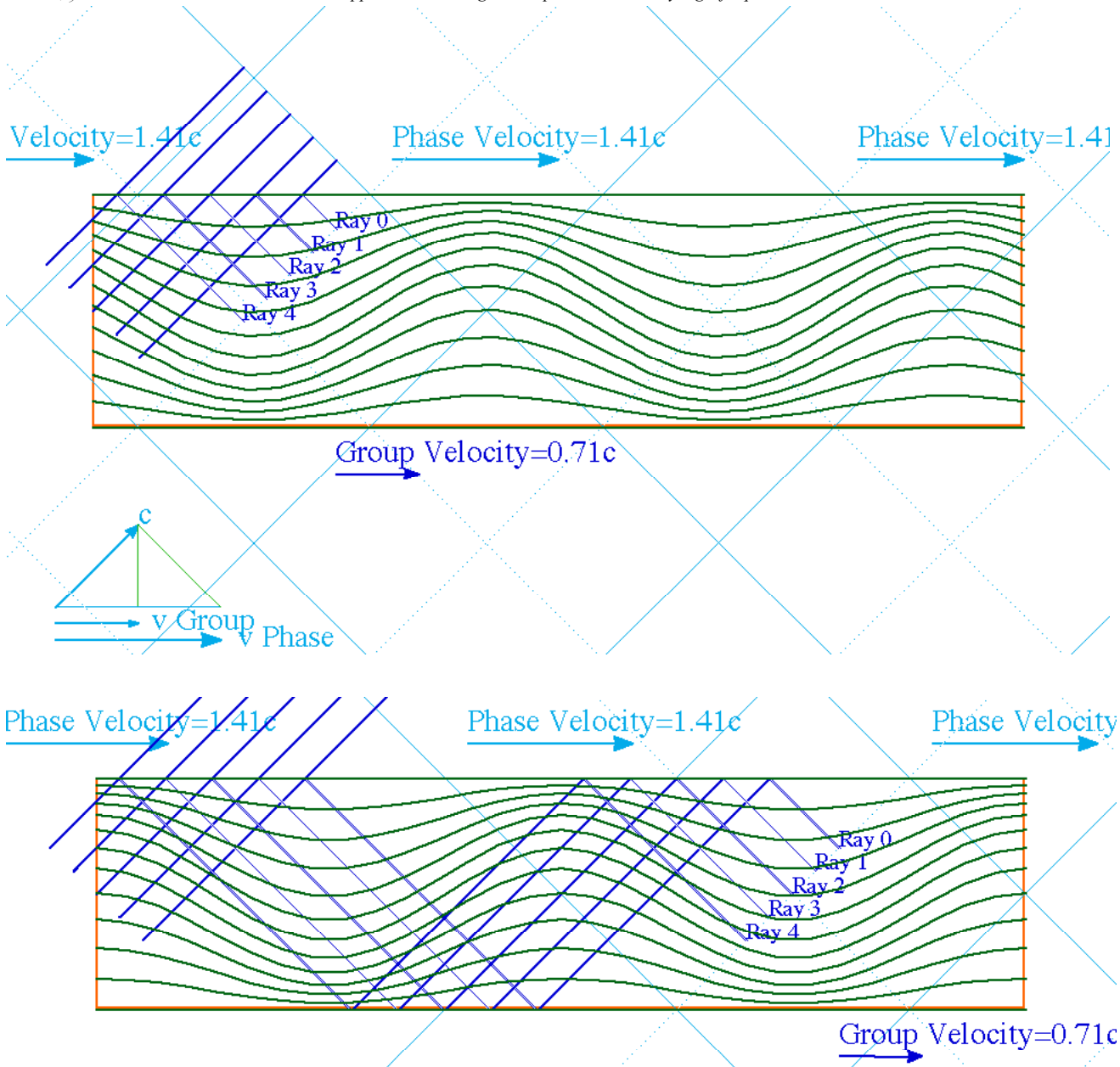
Velocity=1.41c   Phase Velocity=1.41c   Phase Velocity=1.41

Ray 0
Ray 1
Ray 2
Ray 3
Ray 4

Group Velocity=0.71c

c

v Group
v Phase

Phase Velocity=1.41c   Phase Velocity=1.41c   Phase Velocity

Ray 0
Ray 1
Ray 2
Ray 3
Ray 4

Group Velocity=0.71c

Fig. 6B.3 Right moving guide wave with $\gamma = 45°$, $V_{phase} = \sqrt{2}c$, $V_{group} = c/\sqrt{2}$.

The x-phase velocity v_x *(phase)* is speed of the *intersection* of wave fronts with walls (at nodes) or x-axis (at crests and troughs). In frame sequences below, note how much faster crests and troughs move than rays. The wave fronts go at velocity c along rays, that is, *perpendicular* to the fronts while rigid diamond-shaped wave patterns go at v_x *(phase)=1.41c* down the x-axis as shown in Fig. 6B.4.

Attached to the diamonds are nodal rectangles (actually *squares* in this example) whose borders lie along the top and bottom walls (as required by the y-boundary conditions (6B.4a)) and whose vertical sides lie half-way between the crests and troughs. Unlike the diamonds, the nodal squares are observable borders of the interference minima and maxima. The phase diamonds represent unobservable "artistic license."
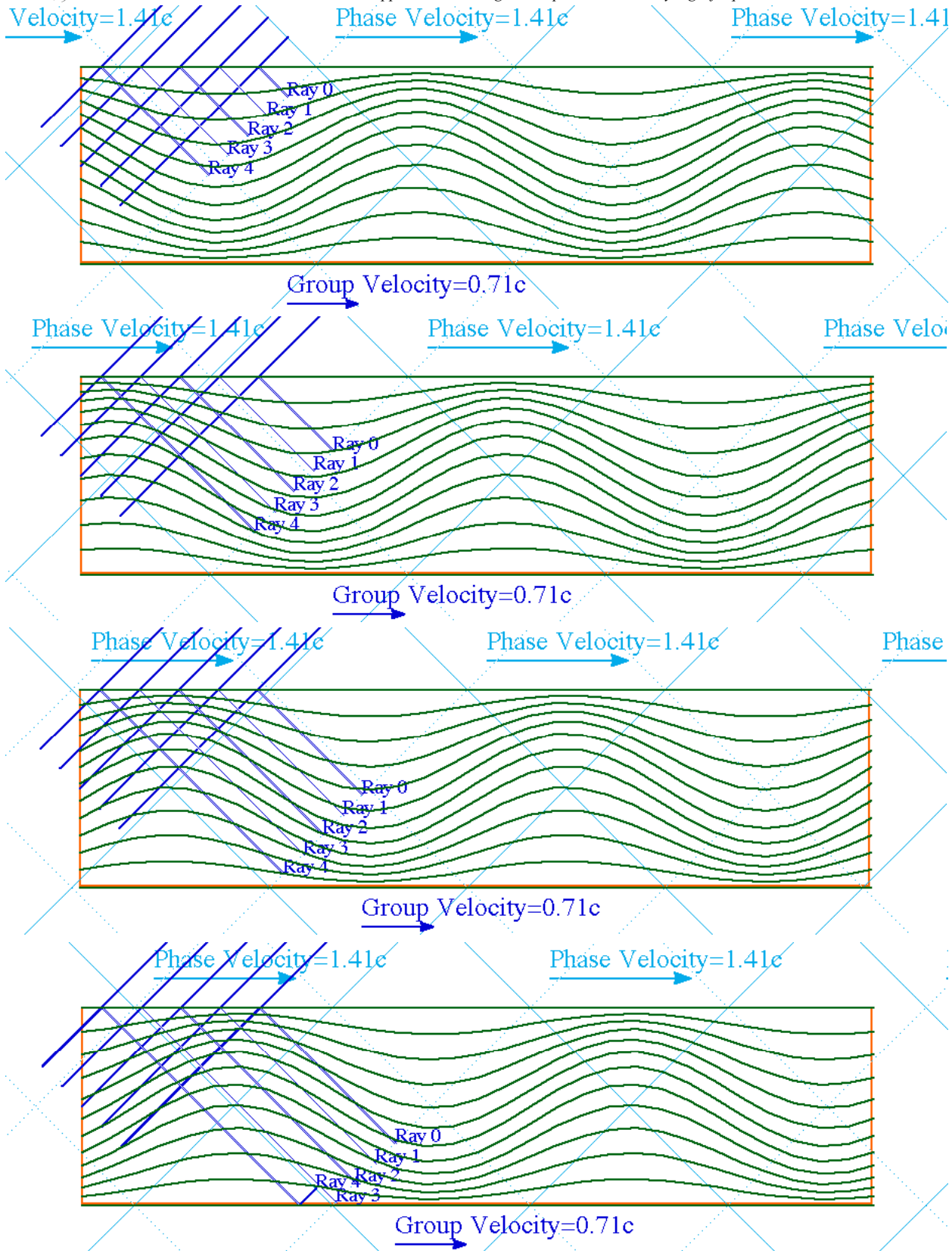
Fig. 6B.4 Right moving guide wave with γ = 45°. Rays are half as fast as wave crests.

Higher frequency means a lower γ with two velocities approaching c as shown in Fig. 6B.5a where γ=30°. As a Hall of mirrors gets much wider than the ~0.5 μm optical wavelength you can simply look down it with no detectable dispersion. In this limit V_{phase} and v_x *(group)* both converge on c.
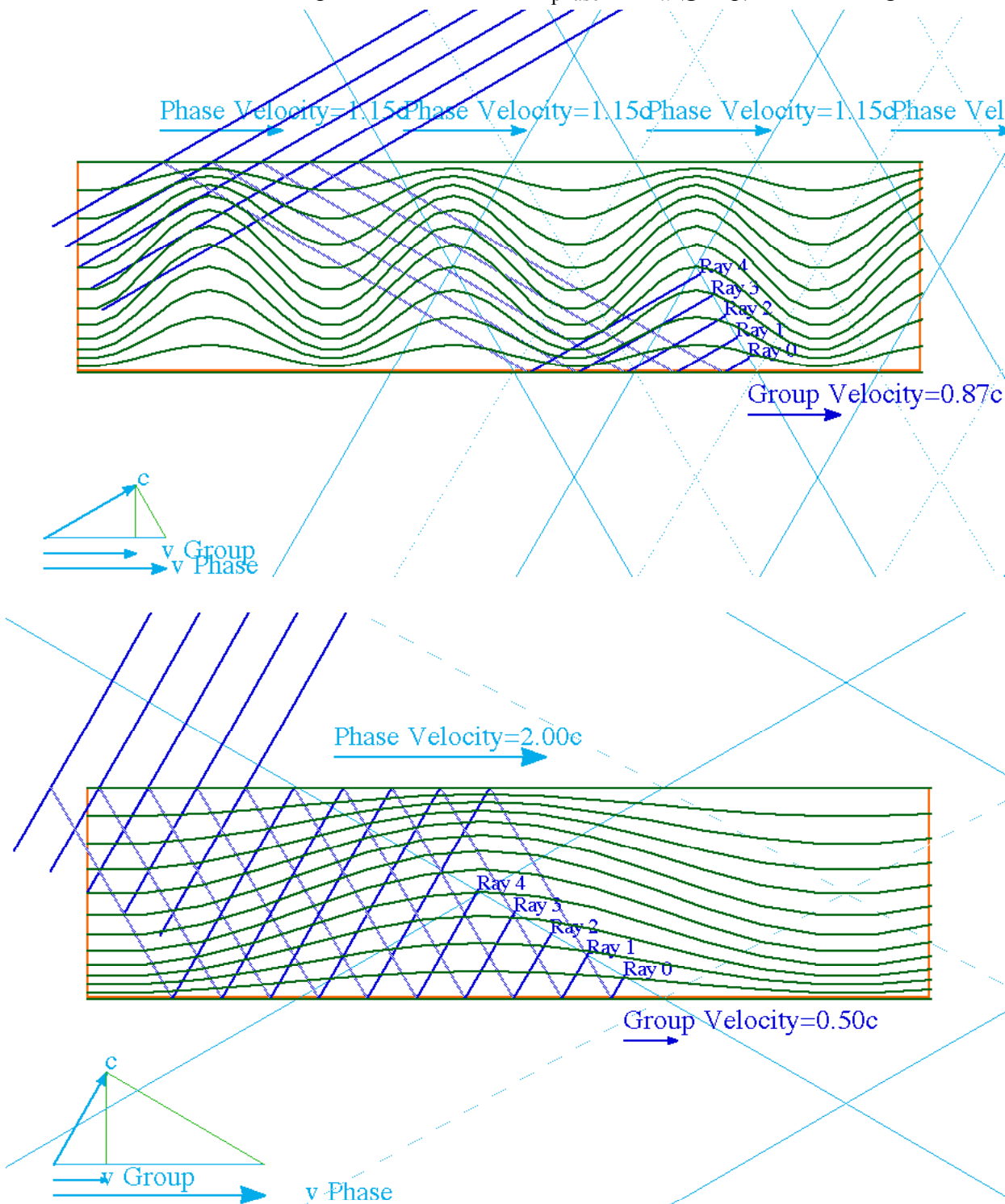

Fig. 6B.5 Guide waves. (a)Higher frequency case: γ = 30°, $v_{x\,(phase)}=c\sqrt{3}/2c$, $v_{x\,(group)}=c2/\sqrt{3}$.

(b)Lower frequency case: γ = 60°, $v_{x\,(phase)}= 2c$, $v_{x\,(group)}= c/2$.

Suppose the light frequency is reduced so the wavelength increases and the angle γ increases to *60°*. Then v_x *(phase)* grows to *2c* while the ray or group velocity reduces to v_x *(group)* = *c cos 60°=c/2*. That is one-half the speed of light and one-fourth v_x *(phase)* =2c as shown in Fig. 6B.5b.

   Group waves and "messages":(How do I send one?)

Group waves can carry "messages" as discussed in introductory Ch. 0 or Ch. 6, but this requires at least two different frequency components. The guide waves pictured so far are mono-chromatic and carry no information except a steady "hum" if they are classical waves, or a steady and uniform rain of random counts if we are describing a quantum wave. There is a $|cos(k y sin γ)|^2$ distribution of intensity, but otherwise it's smooth, featureless and motionless. (Quantum mechanics can be really dead, sometimes!)

To send "messages" or "wave-packets" it is necessary to have more than one frequency going. If the frequencies are close by then AM "lumps" (like Fig. 0.2 or Fig. 6.6) of increased photon counts will be observed moving down the hall at the velocity v_x *(group)* given by (6B.7d). As usual, you need many counts to make out even one "lump." (Low-quantum phenomena are elusive, to say the least!)

Evanescent waves

There is an important lower limit to frequency below which waves will not propagate. This happens just when the wave is too big in wavelength to fit even half of it in the wave guide. The limit is indicated in the Fig. 6B.2 at the bottom of the hyperbolic dispersion function (6B.5).

Consider angular frequency below the so-called *cut-off value* $ω_{cut}$ from (6B.5b).

$$ω_{cut} = π c/W \qquad (6B.8)$$

Then the wave vector k_x in (6B.5c) will go thru zero to becomes imaginary.

$$k_x = (ω^2 - π^2c^2 / W^2)^{1/2}$$

This affects the the usual *propagating* wave rather severely.

$$Ψ = exp i(k_x x - ω t) \qquad (6B.9)$$

Instead of propagating nicely, we get a so-called *evanescent* wave.

$$Ψ = exp(- μ_x x)exp i(- ω t) \qquad (6B.10a)$$

It decays exponentially with the distance *x* along the wave guide with the following decay rate constant.

$$μ_x = (π^2c^2/W^2 - ω^2)^{1/2}= ik_x , \qquad (6B.10b)$$

The decay increases as the frequency *ω* falls further below $ω_{cut}$. It is *huge* for *ω* =0. (Entry *verboten!*)

The cutoff $ω_{cut}$ in (6B.8) is the bottom of a band of allowed frequencies, and it is the bottom of the lowest of a series of bands labeled by a number n_y >1 of half waves that fit across the hall. We may generalize (6B.4b) to describe n_y half waves as follows.

$$k^{(+)}_y= k sin γ = n_y π /W \qquad (n_y = 1, 2,...) \qquad (6B.11a)$$

This leads to *multiple overlapping bands of dispersion function* $ω_{n_y}(k_x)$.

$$ω_{n_y}(k_x) =kc = c(k_x^2 + k_y^2 + k_z^2)^{1/2}= c(k_x^2 + n_y^2 π^2/ W^2)^{1/2} \qquad (6B.11b)$$

The lowest three of these overlapping hyperbolas (for n_y = 1, 2, and 3) are plotted in Fig. 6B.6.

After all this classical discussion, please note that each hyperbola is the bottom of a *quantum* stack of hyperbolas discussed around Fig. 4.2. The same applies to discrete mode frequency bands discussed in the following section.

Trapped waves and cavity modes: Discrete frequencies

When a wave is completely trapped in all the directions it can move, then its spectrum ceases to be continuous and becomes discrete or "quantized." This is what happens to the wave guide modes if the Hall of Mirrors is capped by a pair of doors at, say, $x=0$ and $x=L$, so it becomes a *wave cavity* of length L.

The doors demand the wave electric field be zero at x-boundaries as well as along the walls. The new boundary condition to go with (6B.11a) is the following.

$$k_x = k \cos \gamma = n_x \pi /L \ (n_x = 1, 2,...) \tag{6B.12a}$$

Now the frequency bands become broken into discrete "quantized" values $\omega_{n_x n_y}$, one for each pair of integers or "quantum numbers" n_x and n_y .

$$\omega_{n_x n_y} = kc = c(k_x^2 + k_y^2 + k_z^2)^{1/2} = c(n_x^2 \pi^2 / L^2 + n_y^2 \pi^2 / W^2)^{1/2} \tag{6B.12b}$$

The frequency values fall where the n_y -hyperbola intersects the n_x -value of k_x in (6B.12a) as shown in Fig. 6B.6. These correspond to *cavity modes*. Note: no zero or negative n_x or n_y are allowed.
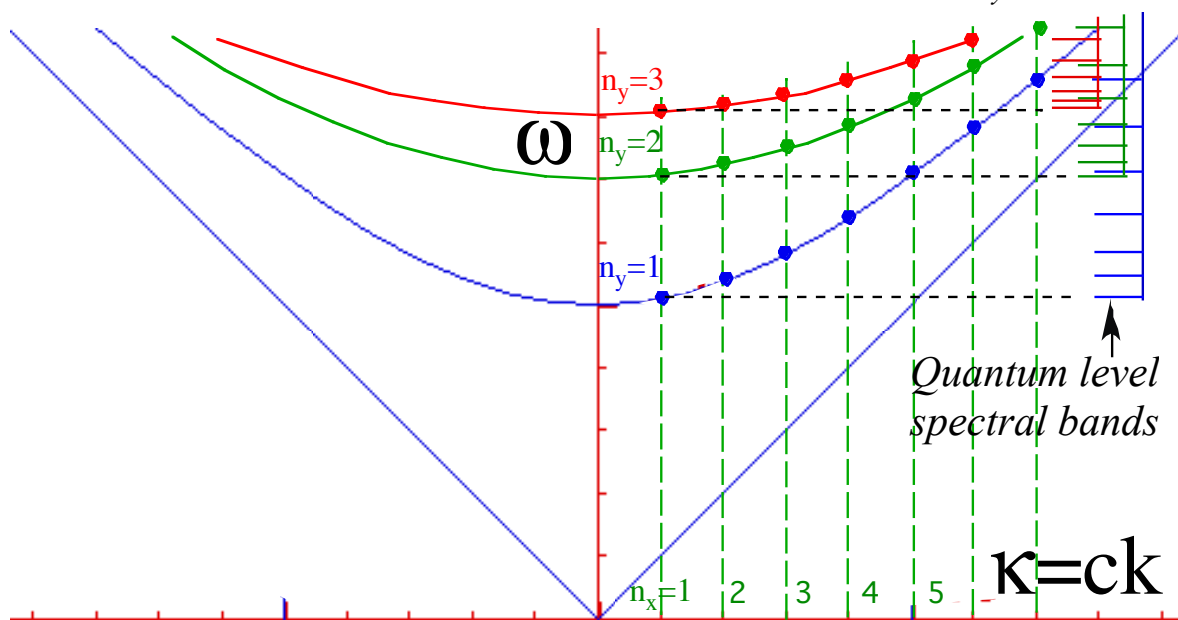

Fig. 6B.6 Cavity mode dispersion diagram showing overlapping and discrete ω and k values.

Three of the lowest cavity modes for the fundamental ($n_y=1$) dispersion curve corresponding to the x-quantum numbers $n_x= 1, 2$, and *3* are plotted in Fig. 6B.7 below. These are 2D standing waves. They can be thought of as interference patterns of four moving wave fronts, two oppositely moving pairs for each of the two wavefront lines intersecting at an antinode in each of the figures.

It should be noted that the Hall of Mirrors used in the preceding section is a tall hall indeed. It has no floor and no ceiling! Clearly, this is an impractical wave guide with infinite wavelength in the out-of-the-page direction z. The hall needs a floor and a ceiling separated by height H with boundary conditions.

$$k_z = n_z \pi /H \quad (n_z = 1, 2,...) \tag{6B.13a}$$

This gives new frequency bands corresponding to "quantized" values $\omega_{n_x n_y n_z}$.

$$\omega_{n_x n_y n_z} = kc = c(k_x^2 + k_y^2 + k_z^2)^{1/2} = c(n_x^2 \pi^2 / L^2 + n_y^2 \pi^2 / W^2 + n_z^2 \pi^2 / H^2)^{1/2} \tag{6B.13b}$$

Also, z-confinement has the effect of up-shifting the spectrum in (6B.11) due to the addition of the extra term $n_z^2 \pi^2 / H^2$ in (6B.13b). Since the lowest possible quantum number is $n_z = 1$, we cannot ever ignore it. However, for a tall hall *(H>>W or H>>L)* the resulting shift is small.

   The preceding formulae and figures are classical wave mechanics that provide the fundamental basis for a quantum electrodynamic (QED) field theory. Each classical "level" supports a quantum oscillator ladder of levels as mentioned before in Ch. 4. These will be developed in Unit 4 and beyond.
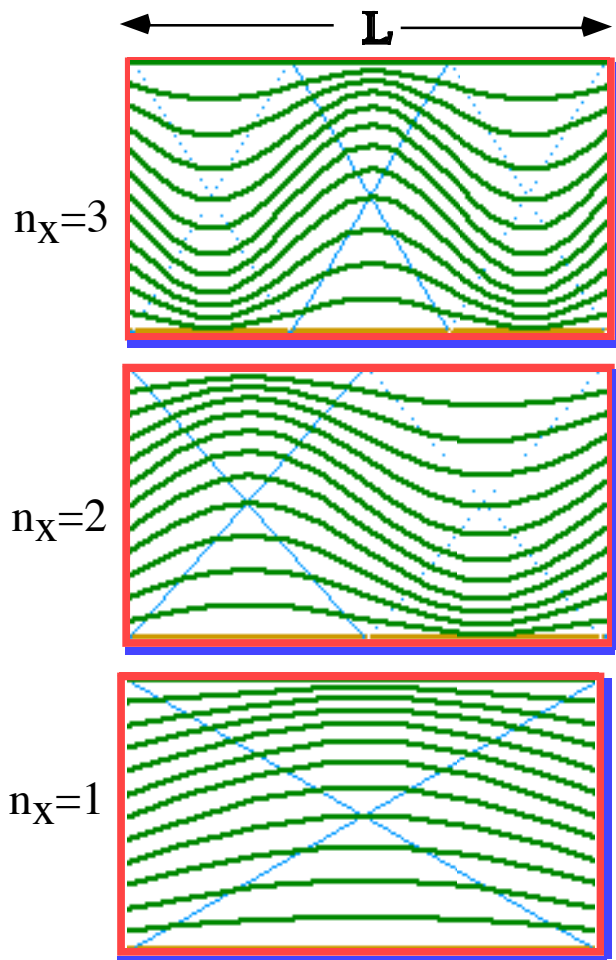

Fig. 6B.7 Cavity modes for three lowest quantum numbers

   The Thales stellar aberration angle geometry of a typical cavity mode shown in Fig. 6B.2 is developed in greater detail below in Fig. 6B.8. Many of the contacting tangents and intercepts that occupy Fig. 3.4, Fig. 5.1, Fig. 5.4, and Fig. 5.5 appear in Fig. 6B.8. This provides yet another view of beautiful relativistic relations between phase velocity and group velocity as they apply to waveguide and cavity modes. That this geometry ultimately applies to all matter in the universe, only makes each such representation and classical analogy all the more intriguing.
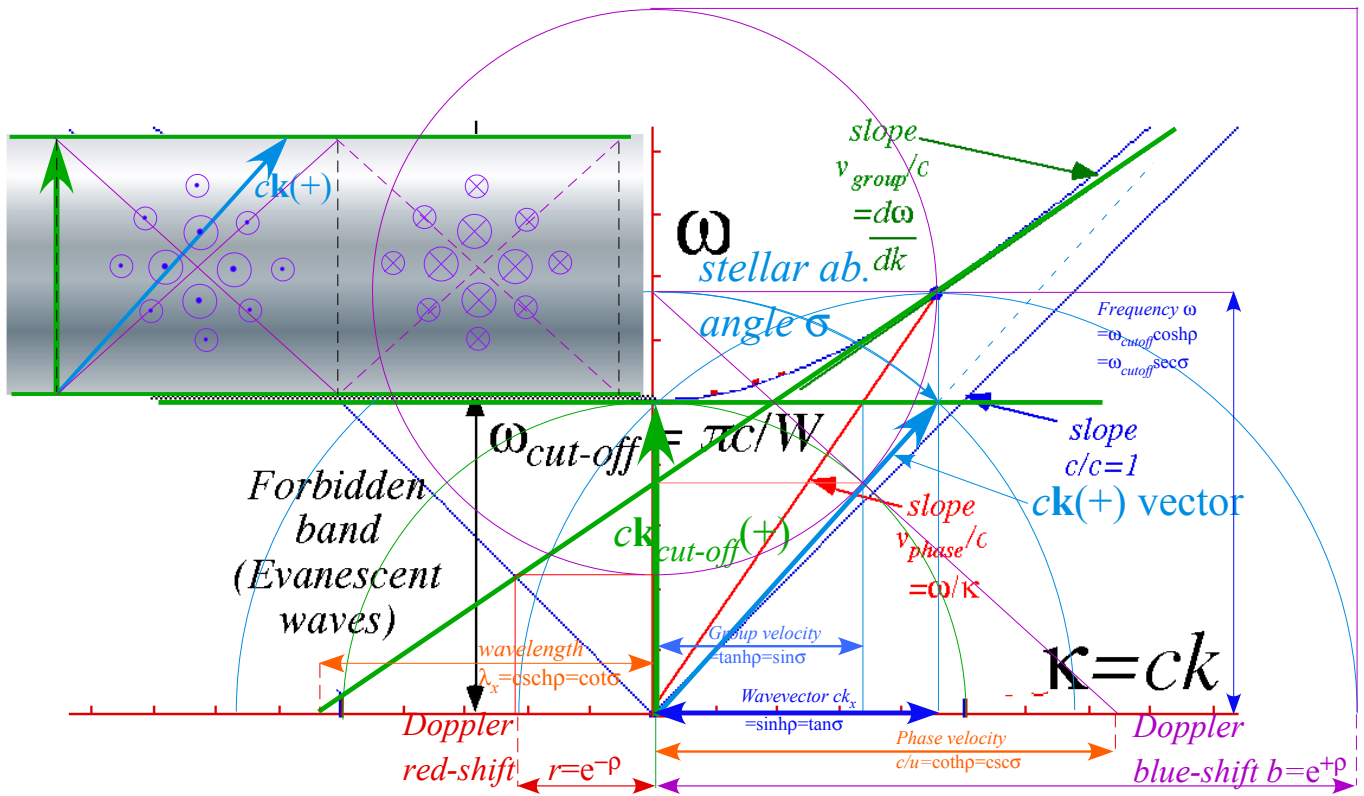
Fig. 6B.8 Thales geometry of cavity mode in Fig. 6B.8.

Chapter 7. Compton Effects and Optical Transitions

In Ch. 4-5 we found that space-time symmetry of a particle of mass M is like that of a 2-CW optical cavity wave of frequency $\omega = Mc^2/\hbar$. Here we relate 2-CW(k,ω) "baseball diamond" Doppler shifts from Ch. 2-3 to light-matter collisions and scattering by molecules, atoms or nuclei. Doppler shifts are related to recoil shifts in 1-photon emission, 1-photon absorption, and 2-photon Compton scattering.

1-photon kinematics for emission and absorption of light

Photo-emission and photo-absorption allow you to see. In order to read this page, dye molecules in your eye absorb light emitted by atoms in a computer screen or lamp or other source such as the sun if you're using daylight or moonlight. Without these processes we would all be blind.

There are several ways to describe and diagram emission and absorption by quantum levels. The first are Grotian level diagrams shown in Fig. 7.1a for a "quantum jump" between a molecular, atomic, or nuclear energy level-E_m and a lower level-E_ℓ. Each "jump" involves light at *transition frequency* $\omega_{m\ell}$ that is the *beat frequency* $\Delta\omega_{m\ell} = \omega_m - \omega_\ell$ between Planck frequency ω_m of level E_m and ω_ℓ of level E_ℓ.

$$E_m = \hbar\omega_m \quad (7.1a) \qquad\qquad\qquad\qquad E_\ell = \hbar\omega_\ell \qquad\qquad (7.1b)$$

Planck relation (4.5a) applies. We can only see beats or *relative differences* $\Delta\omega_{m\ell}$ as noted *vis-à-vis* (4.12).

$$E_{m\ell} = \hbar\ \Delta\omega_{m\ell} = \hbar\omega_m - \omega_\ell) = E_m - E_\ell \qquad\qquad (7.1c)$$

Beat-frequency light is indicated by a wave emerging from a line connecting the energy level E_m to E_ℓ in Fig. 7.1a. A wavy single arrow going out (or in) indicates output emission (or input absorption).

The kicker: Recoil shifts

Optical transitions have, quite literally, a "kicker." Due to Axiom-1 $(\omega = \pm ck)$, each 1-CW causing a frequency shift $\Delta\omega_{m\ell} = \omega_m - \omega_\ell$ must come with a "kick" due to k-vector shift $\Delta k_{m\ell} = (\omega_m - \omega_\ell)/c$. The kick or *recoil* by visible light is usually ignorable since $1/c$ is so tiny, but it is important for high-resolution spectra and for high-energy light such as γ-rays. Grotian diagrams in Fig. 7.1a tend to obscure or ignore recoil.

Feynman diagrams in Fig. 7.1b show atomic **K**-vectors $\mathbf{K} = (\omega, ck)$ being kicked into $\mathbf{K'} = (\omega', ck')$ as atoms emit (or absorb) photons with vector $\omega_{K'K} = \omega_{K'K}(\pm 1, 1)$. Baseball geometry in Fig. 7.2a fits vectors $\omega_{K'K}$ to connect low-level (ω_ℓ) and mid-level (ω_m) hyperbolas and conserve total **K**-vector consistent with translation symmetry conservation rules of (5.19). Fig. 7.2b shows head-to-tail vector sum triangles.

$$\mathbf{K'} = \mathbf{K} - \omega_{K'K} \quad [emission] \qquad\qquad\qquad \mathbf{K'} = \mathbf{K} + \omega_{K'K} \quad [absorption]$$

Vector $\mathbf{M'} = (\omega, ck) = \omega_m(\cosh\rho,\ \sinh\rho)$ on ω_m-hyperbola in Fig. 7.2a has recoil rapidity ρ and invariant ω_m and rest energy $E_m = \hbar\omega_m = M_m c^2$. Vector $\mathbf{L'}$ on lower ω_ℓ-hyperbola below $\mathbf{M'}$ has the same ρ but lower $E_\ell = \hbar\omega_\ell$. **K**-vector baseball diagram geometry follows directly from earlier Fig. 2.2 and Fig. 3.3.

This is not rocket science! (Or is it?)

Some quantum texts call photons "light bullets" since they have a "kick." Doppler redshift relation $\omega_\ell = e^{-\rho}\omega_m$ (top of Fig. 7.2a) shows atoms are like *light-rockets*. Consider invariant rest-mass ratio M_m/M_ℓ.

$$M_m/M_\ell = \omega_m/\omega_\ell = e^{+\rho} \quad (7.2a) \qquad\qquad c\cdot\rho = c\cdot\ln(M_m/M_\ell) \sim u \quad (7.2b)$$

At low recoil $(\rho \sim u/c << 1)$ this is rocket equation (8.8b Unit 1) if "exhaust velocity" is light-speed c. Given uncertainty relation $\Delta\upsilon\cdot\Delta t \sim 1$, we know high quality emission (low $\Delta\upsilon$) implies long time Δt to "exhaust" the light.

(a) Grotian 2-level diagrams

(b) Feynman (,ck) diagrams
(1-photon)

M-to-L′	*L′-to-M*	*L-to-M′*	*M′-to-L*
emission	*absorption*	*absorption*	*emission*

Fig. 7.1 Quantum optical transitions represented by (a) Grotian and (b) Feynman diagrams.

(a) 2-Level (ω,ck) "baseball" diamonds

(b) (ω,ck) vector sum (energy-momentum conservation)

Fig. 7.2 Optical transitions displayed on (a) "Baseball diamond" and (b) Vector conservation sums.

A typical atomic transition (such as we use to read by) has a huge *spectral quality (q) factor*.

$$q = \omega_0 / 2\Gamma = \text{(angular resonant frequency)/(transition decay rate)} = \omega_0 \cdot \Delta t = \omega_0 / \Delta\upsilon$$

Atomic q factors, discussed after (10.49) in Ch. 10 of Unit 1, range from 10^6 to over 10^8. The q qualifies a resonance by giving its amplification factor (over DC), its spectral purity, and its lifetime Δt in numbers of atomic beat periods or "heartbeats" it takes to complete a transition with 96% certainty. (Recall: $e^{-\pi} \sim 4\%$.)

High quality means a long "burn" to reduce an atomic mass energy from $E_m = M_m c^2$ to $E_\ell = M_\ell c^2$, so maybe a rocket formula $u \sim c \cdot \ln(M_m/M_\ell)$ makes sense. (Exact formula (7.2a) is $\rho = \ln(M_m/M_\ell)$.) Just saying quantum transitions are "jumps" misses a lot of physics. Getting there is (at least) half the fun!

2-photon processes: Rayleigh-Thompson-Compton scattering

Atomic 1-photon absorption shown in Fig. 7.1 is like an inelastic *("ka-runch")* SUV-VW collision in Fig. 1.1b or Fig. 2.1 of Unit 1. An atom (SUV) absorbs a photon (VW) to become more massive as it "jumps" from low level M_ℓ to a higher mass M_m. While we just write off lost energy in SUV-VW crashes, the energy of atom plus light is conserved and time reversible. An SUV-VW cannot *"uncrash"* but atoms may emit light as well as absorb it. Atomic emission equation (7.2) is analogous to rocket propulsion.

An atomic 2-photon process of *Compton scattering* is sketched in Fig. 7.3a. It is like an *elastic ("ka-bong")* SUV-VW collision in Fig. 2.2 of Unit 1. Atom-M_ℓ (SUV) briefly absorbs the $\omega_{K'K}$-photon (VW) but then just as quickly bounces it back as the atom recoils and returns to its initial M_ℓ-level after emitting the photon. Fig. 2.2 of Unit 1 is in Center-of-Momentum COM frame as are the process diagrams in Fig. 7.3 where Δk-component of total-$\Delta\mathbf{K}$ is zero. So, non-resonant Compton processes are a quick 1-2-punch.

Car 54 where are you?

An atomic *2-photon absorption* process sketched in Fig. 7.3a is somewhat analogous to a 3-car pile-up. (See car crash in Fig. 8.5 of Unit 1.) However, wave time-energy uncertainty fuzzes auto-analogies. Pure *(ω,ck)*-per-space-time pictures imply delocalization in classical space-time. CW *(ω,ck)* represented in Fig. 7.1 thru Fig. 7.4 make CW space-time grids everywhere and forever. Nevertheless, scaled CW *(ω,ck)* vectors overlap PW *(x,ct)*-paths as shown in Fig. 1.5 or Fig. 1.6 of Unit 1. Then Feynman *(ω,ck)*-diagrams mimic *(x,ct)*-diagrams and $\mathbf{K}$-arrows can represent PW *(x,ct)*-collision paths resembling car crashes.

However, with low-Δt PW paths comes fuzzy $\mathbf{K}$-conservation. Time interval Δt and space Δx is large for initial and final vectors in Fig. 7.3a but not so for mid lines $\mathbf{M}$ or $\mathbf{K}$. Thus intermediate *(ω,ck)* values must be fuzzy and include combinations of non-resonant values known as *virtual state sums*.

Suspended 2-photon diamonds

Photon lines in Fig. 7.3a arise from diamonds in Fig. 7.4 that resemble a $\pm 45°$ baseball diamond used in Fig. 2.1 to develop relativity. However, the general diamond example in Fig. 7.4b differs in that 1st and 3rd bases are not on the light-cone baselines but suspended by vectors $\mathbf{L}$ and $\mathbf{L'}$ like chopsticks pinch a piece of tofu. A new home plate lies at $\mathbf{K}(\omega_k)$ above origin and 2nd base is at $\mathbf{M}(\omega_m)$ above that. Pitcher's-mound lies at $\mathbf{L}(\omega_\ell)$ just below diamond center (as it does in regulation baseball). Half-sum-and-difference of *invariant* $[\omega_k, \omega_\ell, \omega_m]$ define a diamond with "rocket ratios" $\omega_m/\omega_\ell = \omega_\ell/\omega_k = e^\rho$ and geo-mean $\omega_\ell = \sqrt{(\omega_m \cdot \omega_k)}$.

Diamond center: $\frac{1}{2}(\omega_m + \omega_k) = \omega_\ell \cosh\rho$ (7.3a)   *Diamond radius:* $\frac{1}{2}(\omega_m - \omega_k) = \omega_\ell \sinh\rho$ (7.3b)

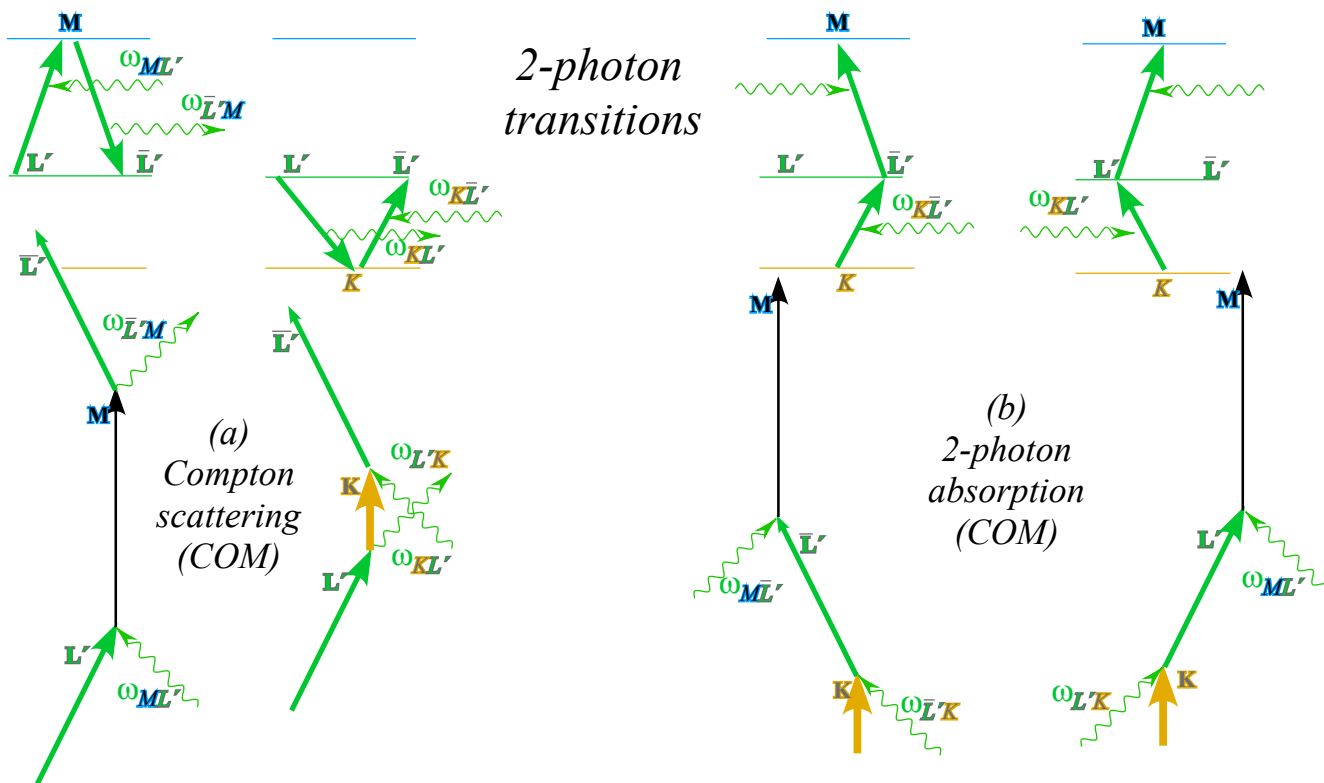One exponential e^ρ ratio defines a whole geometric series of hyperbola levels with equal recoil rapidity ρ.

2-photon transitions

Fig. 7.3 Level and Feynman diagrams of 2-photon processes: (a) COM Compton, (b) COM absorption.
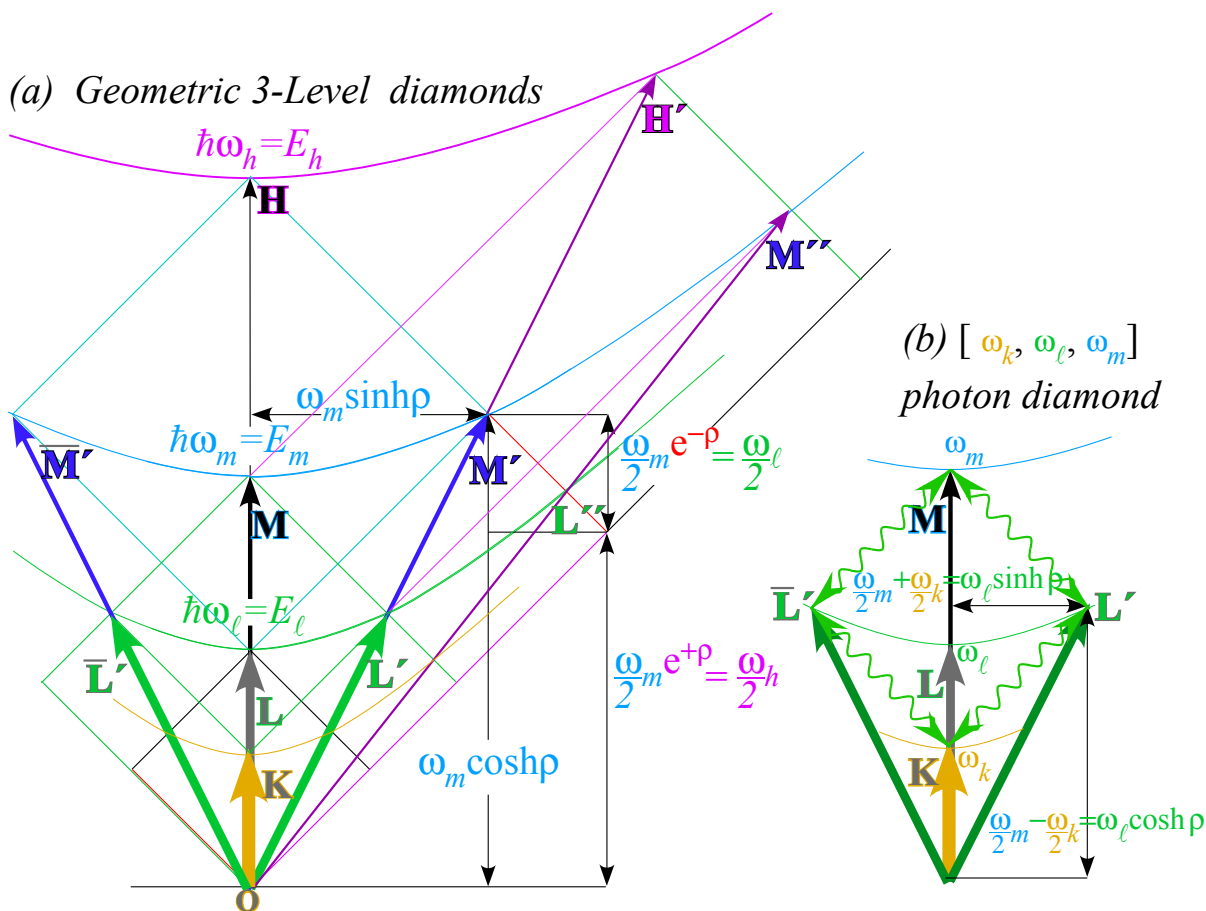
(a) Geometric 3-Level diamonds

Fig. 7.4 3-level diamond connection map in (ω,ck) per-spacetime. (b) COM example of "kite."

We now look at recoil effects in frames other than COM. We imagine we can "cut-and-paste" or create-and-destroy photon frequencies in the 2-CW cavity baseball diamond model of mass kinetics.

Feynman's Father's query

Right after Richard Feynman graduated from MIT his father asked a question, "Where is a photon before an atom emits it?" The question caught the new graduate off guard and it appeared that maybe a pricey MIT education was not worth all the money that his father had paid.[xx] Let us give a quantitative answer for Feynman's father's query using 2-CW optical analog for an atom that emits some of its "inner light" following its baseball-diamond geometry in Fig. 7.2.

To apply baseball diamonds of Fig. 7.2 to an atom, we say it has the *symmetry* of 2-CW cavity state represented by 2nd base $\mathbf{K}_2$ in the lower half Fig. 7.5a. A 1st base $\mathbf{K}_1=(\varpi,\varpi)$ and 3rd base $\mathbf{K}_3=(-\varpi,\varpi)$ sum to an atom's 2nd base $\mathbf{K}_2=(0,2\varpi)$ on a hyperbola of mass M_Q at Q.

$$M_Q = 2\hbar\varpi / c^2$$

The pitcher's mound P represents a 1-photon momentum-energy expectation value E_P at $\mathbf{K}_p = (1/2)\mathbf{K}_2$

$$E_P = \hbar\varpi / c^2$$

Point Q in Fig. 7.5a represents a 2-photon state of energy $M_Q=2E_P$.

In Fig. 7.5a an emitted photon $\omega_{QP'}$ is imagined being "cut" from 3rd base so $\omega_3 = \varpi$ shrinks by what we will call[xxi] a *father-Feynman factor ff* as 3rd base alone loses the outgoing $\omega_{QP'}$ photon energy.

$$\omega'_3 = ff\varpi = \omega_3 - \omega_{QP'} \qquad (ff=1/4 \text{ in Fig. 7.5a.})$$

If 1st base stays at its old value $(\omega'_1 = \varpi = \omega_1)$ the 2nd base moves from Q on its initial 2ϖ-hyperbola to P′ on its final $2\varpi'$ -hyperbola. Its new proper frequency ϖ' is a geometric mean of 3rd and 1st as in Fig. 3.3.

$$2\varpi' = 2\sqrt{\omega'_3\omega'_1} = 2\sqrt{ff}\,\varpi$$

(7.4a)

$$\omega'_3 = f\varpi' = ff\varpi \qquad\qquad (7.4b)$$

$$\omega'_1 = f^{-1}\varpi' = f^{-1}f\varpi = \omega_1 \qquad\qquad (7.4c)$$

The new 3rd base is a *Feynman*[xxii] *redshift* $f \equiv \sqrt{ff}$ of the new mean ϖ' and a *father-Feynman shift ff* of the old bases values $\omega_3 = \varpi = \omega'_1 = \omega_1$. They are each an inverse-shift f^{-1} of the new mean ϖ'. The *ff*-shift is a product of two *f*-shifts $ff=f^2$. This tricky notation is due to the Doppler derived group multiplication rule (3.5c) for an $f = b_{3'2'}$ and an equal $f = b_{2'1}$ to give composite $ff = b_{3'1} = b_{3'2'}b_{2'1} = f^2$.

In Fig. 7.5a old 1st base and new 3rd base span a diamond of rapidity ρ like Fig. 3.3b where $e^{-\rho} = \frac{1}{2}$. That redshift $\varpi' / \varpi = f = \frac{1}{2}$ in Fig. 7.5a-c is another example of "rocket" mass ratio introduced in (7.2).

$$e^{-\rho} = f \equiv \sqrt{ff} = \varpi' / \varpi = M_P / M_Q \qquad\qquad (7.5)$$

Photo-absorption and Compton effects

The factor $ff = \frac{1}{4}$, chosen in Fig. 7.5a, cuts a fraction $1 - ff = \frac{3}{4}$ off the 3rd base photon $\omega_3 = \varpi$ to emit $\omega_{QP'} = \frac{3}{4}\varpi$ and reduces mass M_2 by factor $f = \sqrt{ff} = \frac{1}{2}$ to M_1. Doppler factor $f^{-1}=2=e^\rho$ gives an atomic recoil

boost of $u = \frac{3}{5}c$. (Recall Fig. 2.2 where $b=2$ gives frame velocity $u = \frac{3}{5}c$.) Mass M_1 gets that boost by absorbing $\omega_{PQ'} = \frac{3}{2}\varpi$ to jump from P up to Q′ in Fig. 7.5b. Inverse $\omega_{QP'}$ cut falls from Q to P′ in Fig. 7.5a. Paste $\omega_{PQ'} = \frac{3}{2}\varpi$ onto 1st baseline in Fig. 7.5b ups M_1 to M_2 on ω′-axis P′Q′ in Fig. 7.5c.

Final ω′-frame shift is $b = e^\rho = 2$ of rapidity $\rho = \ln 2$ for either process. Emission $\omega_{Q'P''}$ is the final "cut" in a Compton "paste-and-cut" $P \to Q' \to P''$ process with the Feynman diagram in Fig. 7.6c. Its segments form an OPQ′P″O "kite" in Fig. 7.5c that is bent from a symmetric kite O$\overline{\text{P}}$′QP′O by the boost $\rho = \ln 2$ of the main kite OQ-axis relative to either of its wings O$\overline{\text{P}}$′ or OP′. Each kite is a suspended baseball diamond like Fig. 7.4b or a boosted ρ-warped version of one.

Both "paste-and-cut"($P \to Q' \to P''$) and reverse "cut-and-paste" ($P \to O' \to P''$) processes in Fig. 7.6 entail total recoil boost $2\rho = \ln 2^2$ from the lab ϖ axis to an ω″ axis of the Compton scattered atom in Fig. 7.5c. The latter first "cuts" down to point O′ on a $\frac{\sigma}{2}$-hyperbola by emitting photon $\omega_{PO'} = \frac{3}{8}\varpi$ before absorbing the $\omega_{O'P''} = \frac{3}{2}\varpi = \omega_{PQ'}$ photon that comes first in the former sequence.

An inverse Compton process ($Q \to P' \to Q''$) emits photon $\omega_{QP'} = \frac{3}{4}\varpi$ (as in Fig. 7.5a) then absorbs photon $\omega_{P'Q''} = 3\varpi$ that moves it from rapidity ρ on hyperbola-ϖ to rapidity 2ρ on hyperbola 2ϖ at point Q″ (upper right of Fig. 7.5c). Here a fixed mass $M_2 = 2\hbar\varpi$ emits $\frac{3}{4}\varpi$ to gain speed$(\frac{u}{c} = \frac{3}{5})$ by reducing its mass to $M_1 = \hbar\varpi$ then recovers mass by absorbing 3ϖ to end up at an even faster speed$(\frac{u}{c} = \frac{15}{17})$.

Photon **K**-vectors for any Compton process between *2:1*-rest mass hyperbolas make a ρ-warped baseball diamond with *ρ=ln2* according to (7.5) as shown in Fig. 7.5c and Fig. 7.6a. Like a *2:1*-Doppler diamond in Fig. 3.3b, it has an aspect ratio that is twice its blue-shift $b = e^\rho = 2$, that is $2e^\rho = 4$.

A *2:1*-rest mass drop shows geometry more clearly than a realistic ratio $10^{10}:10^{10}-1$ for an atomic transition that is about 10^{-10} of rest mass. Atomic rest-energy level ratios $E_m: E_h$ are close to unity and fortunately so for our health! Harmonic levels with integral *m:h* ratios used in Fig. 7.5 apply to optical-cavity models but *m* and *h* are small integers only for special spectra like Rydberg or rotor transitions.

Compton-Doppler staircase

In going from higher hyperbola $h\varpi$ to middle $m\varpi$ the lab recoil shift is $f_{hm} = e^{-\rho_{hm}} = \frac{m}{h}$ by (7.5), and its emitted frequency ω_{hm} is the altitude of a kite triangle, like $\overline{\text{P}}$′QP′ in Fig. 7.5c, given as follows.

$$\omega_{hm} = (1 - f_{hm}{}^2)\frac{h\varpi}{2} = \frac{h^2 - m^2}{2h}\varpi = m\varpi \sinh \rho_{hm} \qquad (7.6)$$

The example in Fig. 7.5a has $\omega_{QP'} = \frac{3}{4}\varpi = \omega_{2,1}$. Doppler shifts of $\omega_{2,1}$ by $f_{2,1} = \frac{1}{2}$ form a geometric series $(\cdots, \frac{3}{32}, \frac{3}{16}, \frac{3}{8}, \frac{3}{4}, \frac{3}{2}, 3, 6, 12, \cdots)\varpi$ of steps on a Compton staircase $PQ'P''Q''...$ between *(2:1)*-levels 2ϖ and 1ϖ in Fig. 7.5c. For any rational level ratio $e^{\rho_{hm}} = \frac{h}{m}$, each dilation factor γ_{hm}, recoil β_{hm}, or ratio ω_{hm}/ϖ is a rational ratio, too, and the Pythagorean sum $1 = \gamma_{hm}^{-2} + \beta_{hm}^2$ belongs to a rational triangle, $e.g., 1 = \frac{3^2}{5^2} + \frac{4^2}{5^2}$.
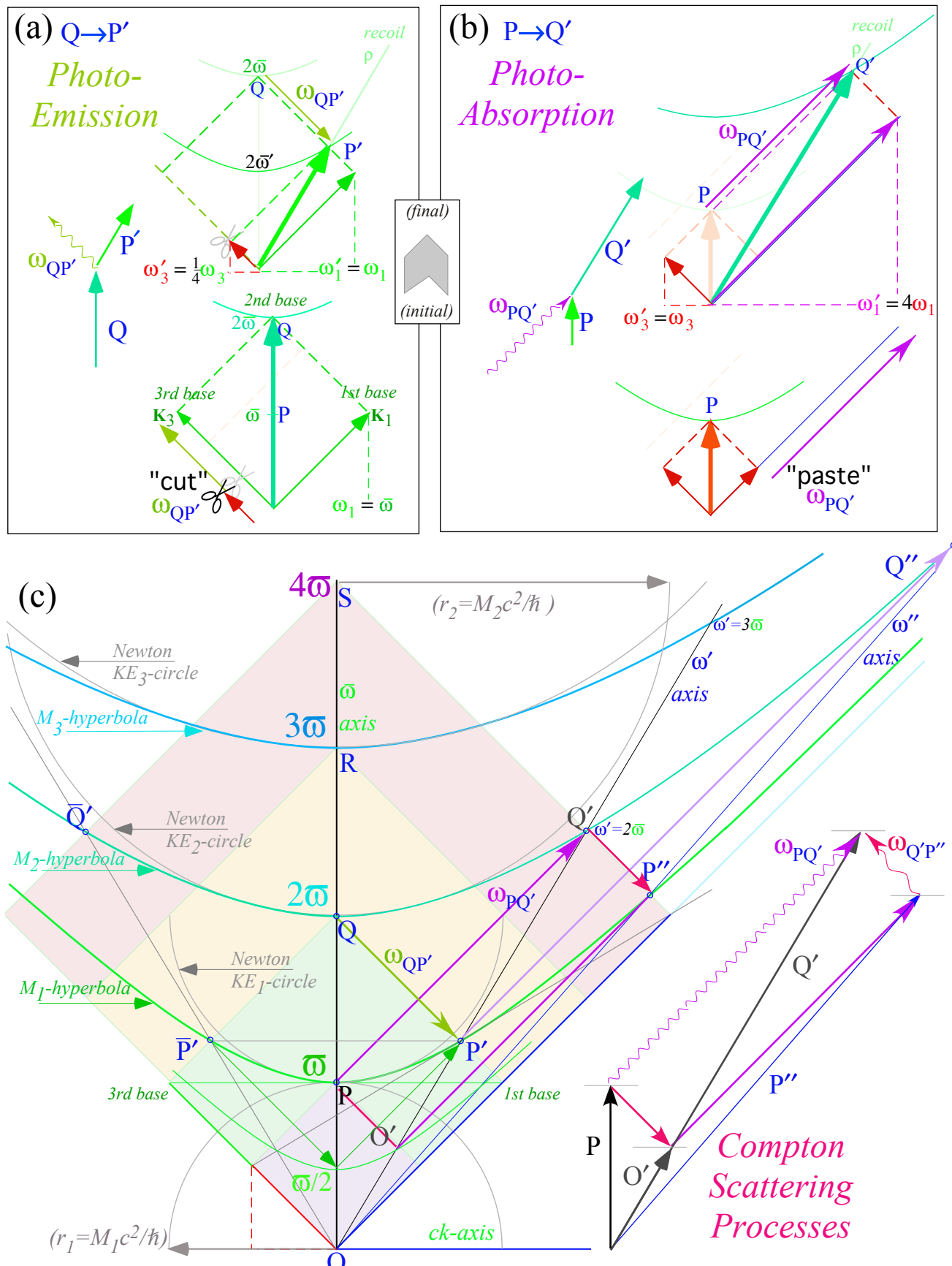
Fig. 7.5 Optical cavity model of (a) Emission, (b) Absorption, and (c) Compton scattering

$$\beta_{hm} = \frac{u_{hm}}{c} = \tanh \rho_{hm} = \frac{h^2 - m^2}{h^2 + m^2} \qquad (7.7a)$$

$$\gamma_{hm} = \cosh \rho_{hm} = \frac{h^2 + m^2}{2mh} \qquad (7.7b) \qquad\qquad \sinh \rho_{hm} = \frac{h^2 - m^2}{2mh} \qquad (7.7c)$$

Recoil trims emitted ω_{hm} below $\Delta = |h\text{-}m|\varpi$ by a factor $(h+m)/2h$ while absorption ω_{mh} costs more than Δ by a factor $(h+m)/2m$. Newtonian recoil $KE_h \cong M_h u^2 / 2$ is a circle of radius $M_h c^2$ in Fig. 7.5, so even low-u recoil costs a little. Photons, like money-changing tourists, get nicked coming and going.
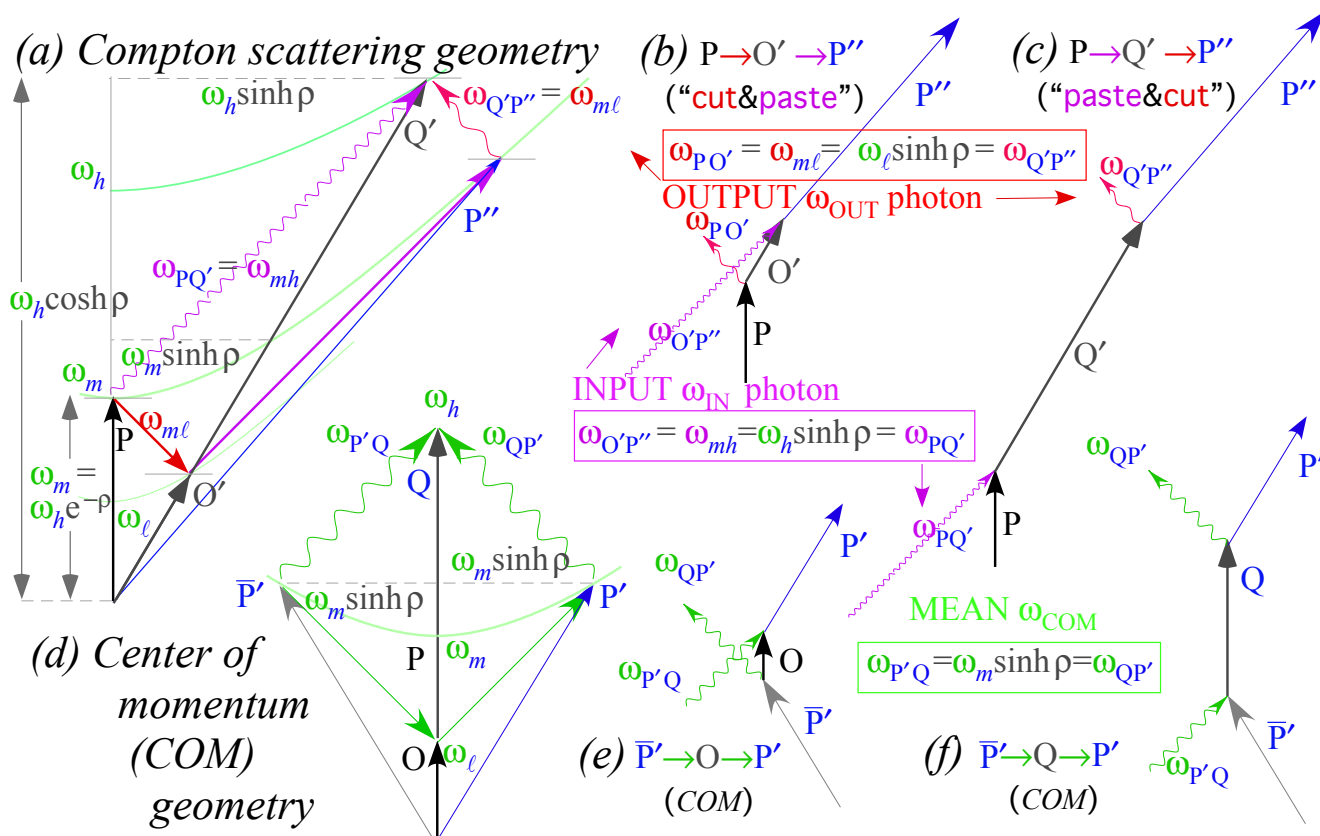
Fig. 7.6 Compton scattering. (a) Vector sums on mass hyperbolas of low ω_ℓ, medium ω_m, and high ω_h. (b-c) Feynman graphs. (d) Center of Momentum (COM) vector sums. (e-f) COM Feynman graphs.

An absorption ($m<h$) frequency $\omega_{mh} = \omega^{IN}$ is greater than emission ω_{hm} by a factor $f_{mh} = \frac{h}{m}$. A Compton ω^{OUT} due to ω^{IN} is less than ω_{hm} by the inverse factor $f_{mh}^{-1} = f_{hm} = \frac{m}{h}$. Hence a Compton output ω^{OUT} is less than its input ω^{IN} by the Doppler ratio-square $ff = f_{hm}^2 = (\frac{m}{h})^2$ as shown before.

$$\omega^{IN} = \omega_{mh} = \frac{h}{m} \omega_{hm} \ , \qquad\qquad \omega^{OUT} = \frac{m}{h} \omega_{hm} = (\frac{m}{h})^2 \omega^{IN} \qquad (7.8)$$

Compton processes in Fig. 7.6 start on middle $\omega_m = m\varpi$ hyperbola to do a 2-photon bounce off a lower $\omega_\ell = \ell\varpi$ or a higher $\omega_h = h\varpi$ hyperbola. An intermediate "bouncer" is said to be a *virtual* level if its ω_ℓ or ω_h values are integration variables being summed. A process $(m \to h \to m)$ or $(m \to \ell \to m)$ is said to be a

resonant Compton process if an *h*-state or *ℓ*-state exists. Whether numbers *m*, *h* , and *ℓ* are integers in a cavity model or real values for an atomic model, the results (7.6), (7.7), and (7.8) apply in any case.

Compton wavelength sum rule

Inverse frequencies $\omega^{-1} = (kc)^{-1} = \lambda(2\pi c)^{-1} \equiv \lambda\!\!\!^-/c$ give the famous Compton wavelength sum rule.

$$(\omega^{OUT})^{-1} = (\omega^{IN})^{-1} + 2(m\varpi)^{-1} \text{ , or: } \lambda\!\!\!^-^{OUT} = \lambda\!\!\!^-^{IN} + 2\lambda\!\!\!^-_C \text{ where: } \lambda\!\!\!^-_C = \frac{\hbar c}{m\varpi} = \frac{\hbar}{M_m c} . \qquad (7.9)$$

Compton radius $\lambda\!\!\!^-_C \equiv \lambda_C / 2\pi$ is a minimum cavity radius with a frequency equal to the "*zwitterbevegun*" of mass M_m. As input $\lambda\!\!\!^-^{IN}$ reflects from an M_m-cavity it picks up diameter $2\lambda\!\!\!^-_C$ to become $\lambda\!\!\!^-^{OUT}$. Size $\lambda\!\!\!^-^{OUT}$ depends on mass M_m of level-*m*, *not* on M_h or M_ℓ of higher level-*h* or lower level-*ℓ* that bounces level-*m*.

Compton radius $\lambda\!\!\!^-_C = \hbar / Mc$ is a curious inverse measure of mass size. Larger mass *M* has a *smaller* $\lambda\!\!\!^-_C$ size that recoils less and reflects photons more elastically. Elastic mirror reflection is what we expect in classical wave optics where light is assumed to be as "light" as anything can be.
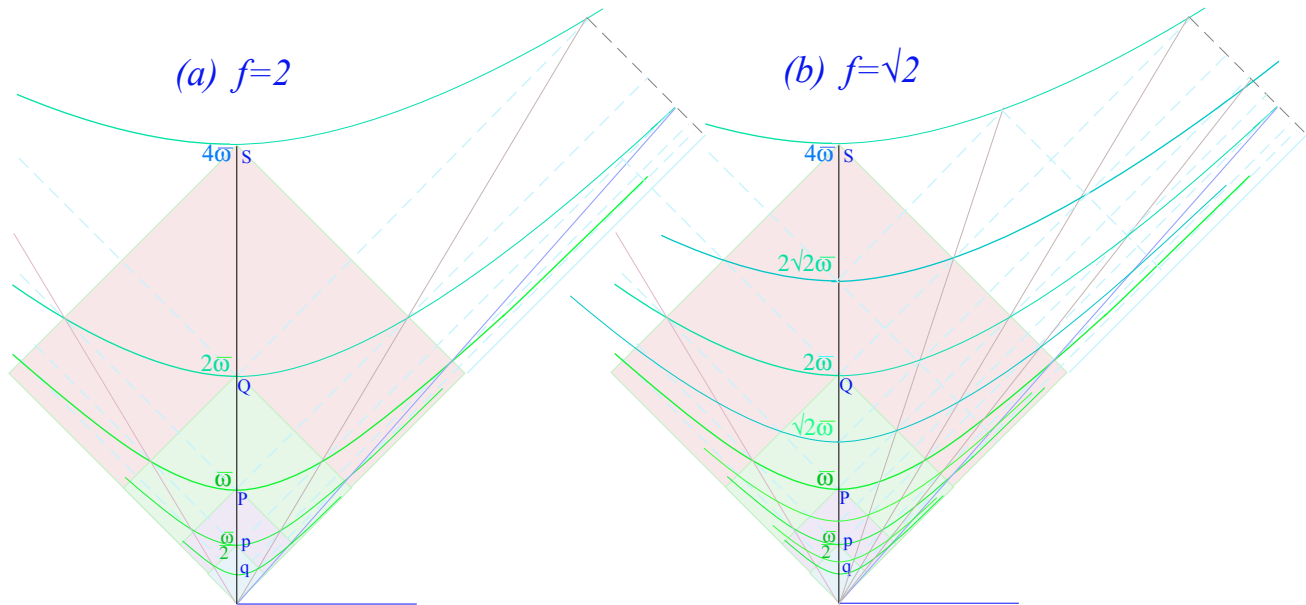

Fig. 7.7 Compton nets are congruent Compton staircases of transitions. (a) f=2:1 (b) f=√2 :1

Geometric transition series

A geometric ϖf^p -series $\varpi(...f^{-2}, f^{-1}, 1, f^1, f^2 ...)$ of *levels* also has a geometric series $f^p |f^2 - 1| \frac{\varpi}{2}$ of *transitions*. This gives Compton "nets" such as the $(f = 2)$ -net in Fig. 7.7a or a finer $(f = \sqrt{2})$ -net in Fig. 7.7b. Finer fractions $(f \to 1)$ give smaller jumps and acceleration that is more continuous and constant.

An acceleration of space-time frames by geometric or exponential frequency chirping is described in Chapter 8. Space-time grid in Fig. 8.2 has a geometric spacing like the Compton nets in Fig. 7.7 but with a $(\mathbf{P},\mathbf{G}) \rightleftarrows (\mathbf{P},\mathbf{G})$ axis switch and is an optical version of Einstein's famous thought experiment.

Optical PW bounce and accordian-like CW shifts

If the ω *vs ck* net plots in Fig. 7.7 were instead space-time *ct vs x* plots one could imagine each vertically sloping line is a path of an object moving at constant rapidity ρ away from the stationary *(ρ=0)* time *ct*-axis

of the lab frame. Each hyperbola in Fig. 7.7a crosses a path at proper times $\tau=...\ \tau,\ 2\tau,\ 4\tau,...$ that are local times on each object's ct'-axis given $e^\rho=f=2$. For general $f=e^\rho$, the times are $\tau=...\tau, f\tau, f^2\tau, f^3\tau, ...$

Imagine each $\pm 45°$ photon line is part of a PW light path reflecting back and forth between the lab ct-axis and the object ct'-axis. Let the lab and moving frame have reflecting mirrors to receive light of a certain frequency (for CW) or a band of frequencies (for PW) and reflect it back and forth between them.

If mirror-*1* sends out wavelength λ_0, mirror-*2* sees it as a Doppler red-shifted wavelength $\lambda_1=\lambda_0 e^\rho$ that it promptly returns to mirror-*1* who sees another red-shift factor e^ρ tacked on to give $\lambda_2=\lambda_1 e^\rho=\lambda_0 e^{2\rho}$. Locally observed reflection times τ_k and reflected wavelengths λ_k both form geometric series $...1, f, f^2, f^3,...$

$$\tau_k =(...\tau,\ \tau_1,\ \tau_2,\ \tau_3,\ ...) \quad =(...\tau,\ f\tau,\ f^2\tau,\ f^3\tau,\ ...) \quad =\tau(...1, f, f^2, f^3,\ ...) \qquad (7.10a)$$

$$\lambda_k =(...\lambda,\ \lambda_1,\ \lambda_2,\ \lambda_3,\ ...) \quad =(...\lambda,\ f\lambda,\ f^2\lambda,\ f^3\lambda,\ ...)=\lambda(...1, f, f^2, f^3,\ ...) \qquad (7.10b)$$

Resulting space-time zigzag paths in Fig. 7.8a have even "zig" reflections $(k=...0, 2, 4,...)$ off the stationary lab mirror-*1* and odd "zag" reflections $(k=...1, 3, 5,...)$ off mirror-*2*. Fig. 7.8b has added counter-propagating odd-time "zag" and even-time "zig" reflections to frame rectangular diamond-*k* whose 1st and 3rd bases lie at time τ_k for lab mirror-*1* and mirror-*2*. Its 2nd and home base lie on a line of rapidity half that of mirror-2 with red-shift $e^{\rho/2}=\sqrt{f}=2^{1/2}$ in Fig. 7.8b. Diamond-*k* 2nd-base is home base for diamond-*(k+1)*.

(a) PW bouncing ball (shift $e^\rho=2$)   (b) CW accordian node squeeze:

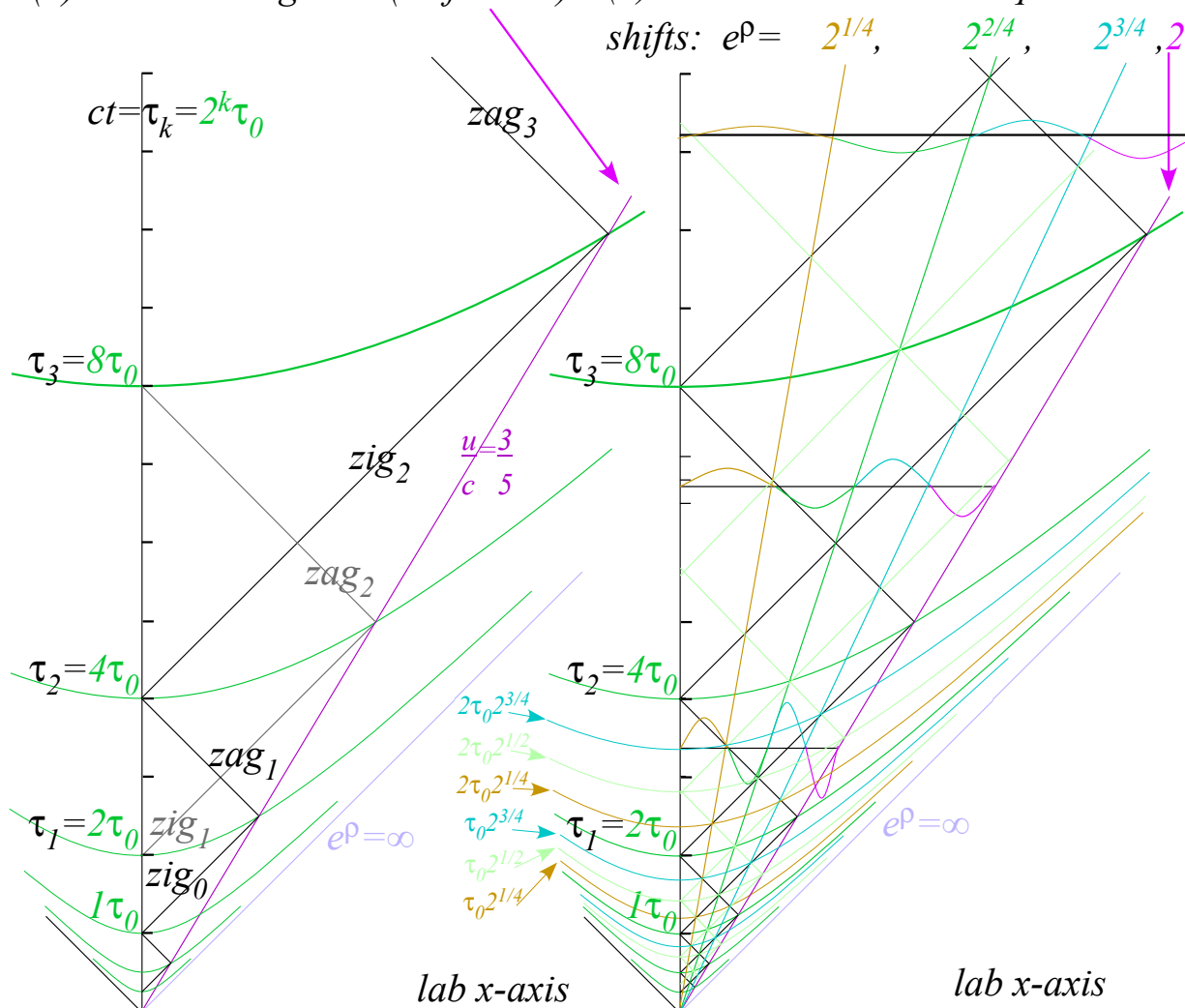*shifts: $e^\rho=$ $2^{1/4}$, $2^{2/4}$, $2^{3/4}$, 2*

Fig. 7.8 Space-time nets (a) PW zigzag paths bounce. (b) CW nodes squeeze like an accordian.

The space-time analog of "rocket" relations (7.2) is $\tau_{k+1}/\tau_k = e^{+\rho} = \tau_k/\tau_{k-1}$. Reflection path-nets also have half-sum-and-difference relations analogous to (7.3) and geometric mean relations $\tau_k = \sqrt{(\tau_{k+1} \cdot \tau_{k-1})}$. This is used to slice reflection time intervals into units of $2^{1/2}\tau_0$ or $2^{1/4}\tau_0$ as is done in Fig. 7.8b, and this gives lines of rapidity $\rho/4, 2\rho/4, 3\rho/4$, and ρ, with red-shifts $2^{1/4}$, $2^{2/4}$, $2^{3/4}$, and 2, respectively.

Ideal light bounces in Fig. 7.8 and mass bounces in Fig. 6.7 of Unit 1 share some key properties. While they change energy without limit, both conserve *action* perfectly. For a light cavity made of mirror-*1* and mirror-*2*, action is an integral number *n* of *1/2*-waves that is shown for *n=4* in Fig. 7.8b where CW nodes move ρ/n faster than the one behind and ρ/n slower than one ahead. Adiabatic *n* invariance is the rule for quantum wave systems and applies to photon number *N*, too. But, rules are made to be broken!

Chapter 8. Wave Frame Acceleration

Here we turn the hyperbola geometry of space-time Fig. 7.8 on its side to expose an accelerating wave frame made by CW, PW, or intermediate wave fields. This provides a coherent interference view of the Einstein elevator *gedankken* (thought) experiment. Like many such experiments of imagination, there are quite a few practical details left out. So it may be some time before we can actually *do* them!

Chirping and Einstein elevators

A spacetime version of Compton nets are curved coordinates for accelerated Einstein elevators and this helps to visualize equivalence principles for general relativity.[xxiii] Plots in Fig. 8.1 and Fig. 8.2 show waves from chirping tunable lasers forming colorful renderings of hyper-net coordinates.

A previous Fig. 2.2c plotted an atom *(x′,ct′)*-view of it running head-on at rapidity ρ into a green ϖ - beam that is blue ($\varpi\,e^{+\rho}$) shifted while the receding laser appears red ($\varpi\,e^{-\rho}$) shifted. The laser *(x, ct)*-grid then appears as a ρ-tipped Minkowski grid. If instead the lasers had been tuned to frequencies $\varpi\,e^{-\rho}$ and $\varpi\,e^{+\rho}$, respectively, the *(u=c*tanh ρ*)*-moving atom would see beams of green ϖ –light waves interfering to make a *square (ρ=0) Cartesian (x, ct)*-grid like Fig. 2.1c. (Amplitude would also be tuned along with frequency if we wanted to squelch the wave galloping shown in Fig. 6.2 and Fig. 6.3.)

Varying tuning parameter ρ of the lasers changes local grid rapidity ρ at the beams' spacetime intersection as sketched in Fig. 8.1a-b. This produces a curved space-time coordinate system of paths with rapidity changing just so *both* beams end up always the *same* color on any given trajectory.

Each trajectory plotted in Fig. 8.2 has its own constant proper acceleration *g* and local color ϖ . A mass *M* following such a *x(t)*-path has a **K** that follows its *M*-hyperbola in Fig. 7.7. The lasers each send waves that meet at each trajectory point *x(t)* and paint a local interference grid of varying rapidity ρ on a trajectory *x(t)* of varying velocity *u(t)* given by (6a) and sketched in Fig. 8.1a.

$$u = \frac{dx}{dt} = c\tanh\rho \qquad (8.1)$$

Setting *x′=0* and *t′=τ* in (2.21) relates proper time interval *dτ* to lab *dt* . This gives *x(t)* by τ-integrals.

$$\frac{dt}{d\tau} = \cosh\rho \qquad (8.2a) \qquad\qquad \frac{dx}{d\tau} = \frac{dx}{dt}\frac{dt}{d\tau} = c\tanh\rho\cosh\rho = c\sinh\rho \quad (8.2b)$$

$$ct = c\int\cosh\rho\ d\tau \qquad (8.2c) \qquad\qquad x = c\int\sinh\rho\ d\tau \qquad (8.2d)$$

Path *x(t)* depends on ρ(τ) variation in proper τ. Linear rate *u~gτ* or ρ=*gτ/c* gives a hyperbolic path in Fig. 8.1b of fixed proper acceleration *g* and a family of concentric paths of different *g* in Fig. 8.2.

$$ct = c\int\cosh\left(\frac{g\tau}{c}\right) d\tau = \frac{c^2}{g}\sinh\left(\frac{g\tau}{c}\right) (8.3a) \qquad x = c\int\sinh\left(\frac{g\tau}{c}\right) d\tau = \frac{c^2}{g}\cosh\left(\frac{g\tau}{c}\right) \qquad (8.3b)$$

Paths closer to the left hand blue-chirping laser have a higher *g* than flatter ones nearer the red-chirping right hand source. ρ-skewed baseball diamonds of PW and CW paths in lower Fig. 8.2 are spaced geometrically along the *x*-axis of a spaceship at a moment when its lab-relative rapidity is ρ=0.2.
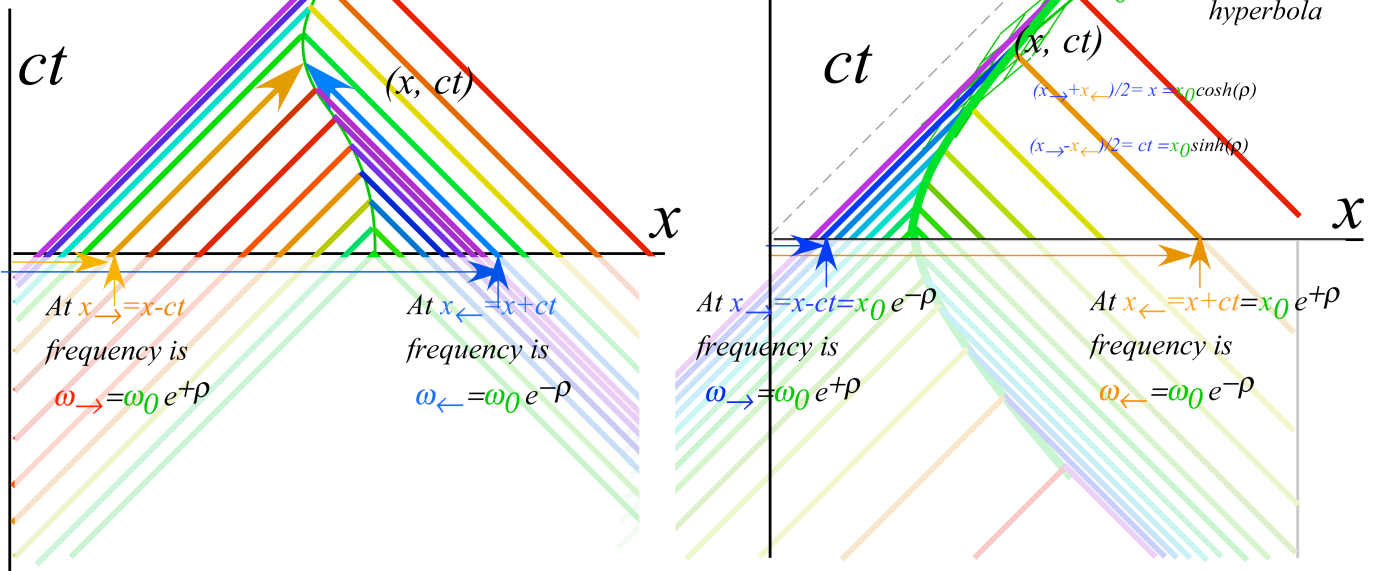
Fig. 8.1 Optical wave frames by red-and-blue-chirped lasers (a)Varying acceleration (b)Constant g.

Geometric $e^{\pm\rho}$-variation (8.3) of wave and coordinate spacing is due to a left-hand laser's right-moving wave of frequency $\omega_{\rightarrow}=\omega_0 e^{+\rho}$ on light cone $x_{\rightarrow}=x\text{-}ct=x_0 e^{-\rho}$ and a right-hand laser's left-moving wave of frequency $\omega_{\leftarrow}=\omega_0 e^{-\rho}$ on light cone $x_{\leftarrow}=x+ct=x_0 e^{+\rho}$. Wave interference does the rest.

Initial *(ρ=0)* position of hyperbola ω_0 is $\ell_0=x_0=c^2/g_0$. Each hyperbola has different but fixed location ℓ, color ω, and artificial gravity g that, by (8.3), are proper invariants of each path.

$$x^2\text{-}(ct)^2 = \ell^2 , \quad \text{where: } \ell=c^2/g \qquad (8.4)$$

Frequency ω and acceleration g vary inversely with the path's proper location ℓ relative to origin.

$$\omega\, \ell = \omega\, c^2/g = \omega_0\, c^2/g_0 = const. \qquad (8.5)$$

Rapidity $\rho=g\tau/c$ in (8.3) has proper time be a product of hyperbolic radius ℓ in (8.4) and "angle" ρ.

$$c\tau = \rho\, c^2/g = \ell\, \rho \qquad (8.6)$$

This is analogous to a familiar circular arc length formula $s = r\, \phi$. Both have a singular center.

The less familiar hyperbolic center *(x,ct)=(0,0)* here begins an elementary *event horizon*. The blue-chirp laser would need infinite frequency $\omega_0 e^{+\rho}$ at origin where $ct=e^{-\rho}$ goes to zero, so it gives up *before t=0*. After *t=0*, light from the laser to any path S or T given by (8.3) never arrives. Fig. 8.2 shows paths of a spaceship S and a "trailer" T trailing by invariant length $\ell_{ST}=\ell(S)\text{-}\ell(T)$ on an *x*-axis of rapidity ρ through origin *(x,ct)=(0,0)*. S and T always have the *same velocity* (8.1) relative to the lab, maintain proper interval ℓ_{ST}, but trailer T *feels greater g*. Lower parts of a rigid rod accelerate more, and this gives the lab-observed Lorentz length-contraction indicated at the top of Fig. 8.2.

In a Newtonian paradigm, asymmetric acceleration seems paradoxical, but if waves make a coordinate frame, asymmetry is a consequence of the DeBroglie relation (4.5b) between *k*-vector and momentum. Accelerating frames require shortening wavelength and this crowds waves.

Wave properties also manifest the accelerated frames' upstairs-downstairs disparity in proper time τ ("later" upstairs by (8.6)) and shift in frequency ω (lower or "red shifted" upstairs by (8.5)). Along nodal (white) lines that are the ship-trailer x-axis for a momentary rapidity ρ, wave phase is seen to be some constant $k\ell - \omega\tau = N\pi/2$. The Einstein equivalence of gravity to an accelerated elevator is manifested by a gravitational red shift and an increase of clock rates in the upstairs regions of a field.

A quantized version of Fig. 8.2 would be an atom with a transition at ω_I, undergoing a sequential *resonant* Compton scattering of exponentially chirped photons ω_I, $e^{\pm\rho}\omega_I$, $e^{\pm 2\rho}\omega_I$, $e^{\pm 3\rho}\omega_I,\dots$ between the *same* pair of hyperbolas in Fig. 8.2. The atom sees the *same* color and feels the *same* recoil rapidity at each step in the quantum version of constant acceleration.
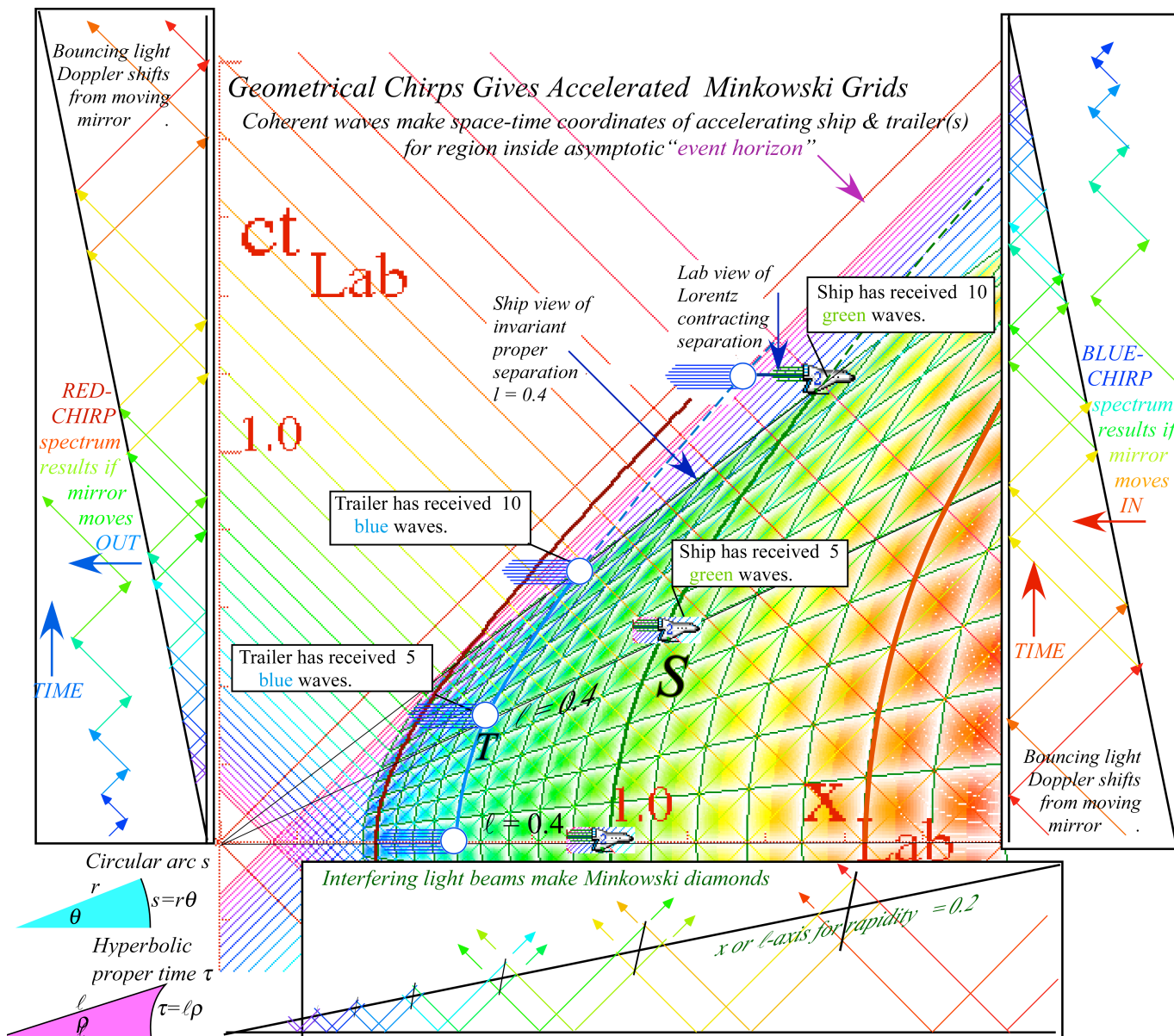

Fig. 8.2 Accelerated reference frames and their trajectories painted by chirped coherent light

Constant velocity gives constant acceleration

This leads one to ask if chirped light might be used for atomic or molecular acceleration. Logarithmic dependence ρ=*ln b* of rapidity on Doppler *b* favors ultra-precise *low* energy acceleration, more appropriate for nanotechnology than high-energy acceleration with its extreme bandwidth.

The flip symmetry between two sides of a light cone suggests optical cavities with a geometric chirp. If you flip the diamond sequence in lower Fig. 8.2 across the light cone to the sides of Fig. 8.2 you get spacetime light paths bouncing between mirrors moving relative to each other as analyzed in Fig. 7.8.

As mirrors close, trapped light blue-chirps exponentially as on the right side in Fig. 8.2. It red-chirps if the two mirrors separate as they do on the left side of Fig. 8.2 and in Fig. 7.8. Together, a desired $e^{\pm n\rho}$ spectrum could in principle be made by translating one etalon cavity at constant velocity relative to another stationary cavity that is enclosed by the translating one. In this way, light generated by mirrors of constant *velocity* provides the spectrum needed to make an interference net of constant *acceleration*. Coherent acceleration like Fig. 8.2 (but slower) might be done with precision needed for laser metrology.

Wave geometry vs. Newton

Wave geometry ought to make us more skeptical of the coordinate boxes and manifolds that have been our paradigm for centuries. A common image is the Newton-Descartes empty-box at some absolute time existing whether or not it contains any "particles." We first learn to picture spacetime coordinates as a giant metal frame of clocks like *Fig. 9* in Taylor and Wheeler's[xxiv] relativity text. That figure is more like a parody of common views of spacetime manifolds that remain with us to this day. Such a monstrosity of a framework is decidedly nonexistent and non-operational. Current metrology uses light waves.

A wave frame like Fig. 2.1, Fig. 2.2, or Fig. 8.2 is *physical* metrological coordinate system whose geometry and logic arises from the light that makes it. The things being coordinated (waves) have their own coordinates and dynamics built in. Einstein general theory of relativity trumped Newton's box by showing how it is affected (curved) by any energy or mass it holds. Quantum theory seems to go a step further by indicating that this box and its contents should be viewed as one and the same thing.

Pair creation and quantum frames.

Dirac, before others, realized that per-spacetime has the symmetry of spacetime. Past and future (time-reversal) symmetry demands *negative* frequency as well as positive. In order to visualize Dirac's pair-creation process we extend the playing field to back-to-back baseball-diamonds with *four* nets of invariant hyperbolas. Examples of pair-creation are sketched in Fig. 8.3 as seen from two different reference frames. Pair creation-destruction is then seen a strange sort of Compton process in which the "photon diamond" of Fig. 7.4 is centered at the light baseline intersection with 2nd base at $+mc^2$ and home base at $-mc^2$ and 1st and 3rd bases on $\pm$**G**-hyperbolas.

The Feynman graph of Compton scattering in Fig. 7.6c-d is turned on its side in Fig. 8.3 so it may start and end on different branches of the *m*-hyperbola corresponding to mass $\pm m$. Two photons, whose energy sum equals the energy gap $2mc^2$, appear to bounce off intermediate hyperbolas in Fig. 8.3 that are

conjugate hyperbolas defining group wavevectors $\mathbf{K_g}$ in Fig. 2.1 or 2.2. Such dispersion is said to belong to *instanton* or *tachyon* waves of imaginary frequency $\pm i\mu$ that entails a huge damping factor $e^{-mc^2\tau/\hbar}$ that proscribes their direct observation. They are said to be in the virtual or intermediate realm.
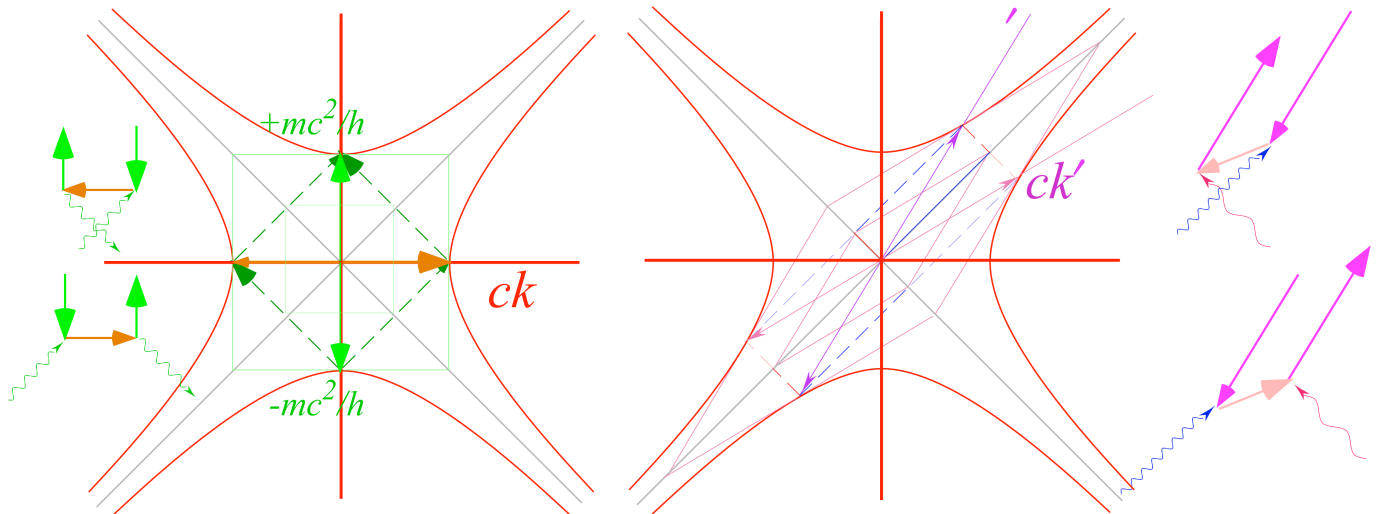

Fig. 8.3 Dirac matter-antimatter dispersion relations and pair-creation-destruction processes.

Dirac's is the first quantum theory to fully incorporate relativity. It introduces dual anti-worlds, in which all three mass definitions (3.6), (3.7), and (3.9) have negative values, but leaves many questions about their physical meaning. Analogies between the $(2\gamma \rightarrow e + \bar{e})$ process in Fig. 8.3 and exciton formation in the band theory of solids, shed some light on the physics. However, the exciton process is a straight-up 1-photon process whose momentum is tiny compared to the energy jump, and it lacks the world-anti-world symmetry of the Dirac exciton in which both the electron and an anti-electron have the same group velocity but opposite momentum. The Dirac model has duality of reversed energy (frequency), momentum ($\mathbf{k}$-vector), space, and time that is quite extraordinary.

A number of implications of Dirac's theory have been mostly ignored. There is an unwillingness to abandon vestigial concepts associated with absolute classical frames, manifolds, or "boxes." However, quantum frames are like all things quantum mechanical and have an intrinsic *relativity* associated with their wavelike interference. Quantum frames, as they are used in molecular and nuclear physics, are known to have internal or body-relative parts in addition to the more commonly known external or laboratory-relative parts. This inside-and-out duality is a deep quantum mechanical result arising first in the theory of quantum rotors by Casimir, but it also underlies Lorentz-Poincare symmetry that includes locally rotating frames as well as translating ones.

Indeed, the quantum theory of angular momentum has a built-in duality that is as fundamental as the left-and-right or bra-and-ket duality of the conjugate parts of Dirac's elegant quantum notation $\langle A|B \rangle$.

The Wigner $D^J_{m,n}$ –functions are quantum rotor wavefunctions $D^{J*}_{m,n}(\alpha\beta\gamma)$ that have their external laboratory *m*-quantum numbers on the left and their internal or body *n*-quantum numbers on the right. Their *J*-multiplicity is thus *(2J+1)-squared* and not simply the *(2J+1)* so familiar in elementary Schrodinger quantum theory of atomic angular momentum.

It took many years for classical physics to fully accept Einstein's translational relativity principles. Perhaps, if the wave nature of quantum physics had already been established, the relativistic axioms would have been seen as an immediate consequence of wave interference. Indeed, these two subjects are, perhaps, *too* closely related for that to have happened.

Now quantum theory demands a more general kind of relativity involving rotation and other accelerations that is a step beyond the special relativity of constant velocity. This brings up a quite controversial area first explored by Ernst Mach, the originator of *Mach's Principle*. Mach made the seemingly impossible proposal that centrifugal forces, the kind physicists assign the label *ficticious force*, are somehow due to their relativity to all matter in the universe.

Mach's idea may sound silly, but a kind of quantum Mach's Principle is needed to understand spectra and dynamics of quantum rotor $D^J_{m,n}$ waves even in the non-relativistic limit. We are unaware of any fully relativistic quantum treatment of such systems, and it is not clear what if anything would be the cosmological implication of such a grand relativistic quantum wave mechanics. Nevertheless, it seems that the dual 4-by-4 wave-anti-wave space of Dirac is one of the first to re-examine.

Physics is still at a stage where large-scale phenomena use Newton-Einstein particle-in-manifold theory while small-scale phenomena employ Planck-DeBroglie-Schrodinger wave field theory. However, both employ some form of space and time coordinates. In this they share an enigma whose existence is largely unquestioned. Supposed invariance to reference frame definition is taken to mean that underlying frames don't matter.

That leaves our fundamental metrology in a dysfunctional dysphoria of an ignored spouse, indispensable, but having only marginal identity. If Evenson and Einstein have taught us anything, it is that this has to be a mistake. Frames *do* matter! The results of Dirac and many others have shown they *make* matter and indeed *are* our matter.

References

Mark K. M. Evenson, J.S. Wells, F.R. Peterson, B.L. Danielson, G.W. Day, R.L. Barger and J.L. Hall, Phys. Rev. Letters 29, 1346(1972).

Mark Guinness Book of Records (1973).

Mark Glauber, Roy J., Hall, John L. and Hansch, Theodor W. *The Nobel Prize in Physics, 2005*. http://nobelprize.org/

Mark J. L. Hall and T. Hensch, Opt. Lett. 9, 502-504 (1984).

Mark N. Ashby, *Physics Today*, 55(5): 41 (May 2002).

Mark J. L. Hall, Laser Spectroscopy VII,(T. W. Hansch and Y. R. Shen, Eds., Springer-Verlag, 1985), pp. 393-394.

Mark William of Occam (1245-1326) *"Pluralitas non est ponenda sine neccesitate"* (Do not assume plurality without necessity.)

Mark A. Cho, Science 306, 1461 (2004).

Mark A. Einstein, Annalen der Physik 17,891(1905). (Translation by W. Perrett and G.B. Jeffery, *The Principle of Relativity*(with notes by A. Sommerfield) (Methuen, London 1923), (republished by Dover, London 1952).

Mark W. G. Harter, J. Mol. Spectrosc. 210, 166(2001).

Mark W. G. Harter, J. Evans, R. Vega, and S. Wilson, Am. J. Phys. 53, 671(1985).

Mark W.G. Harter and T. C. Reimer, //www.uark.edu/ua/pirelli/html/poincare_inv_2.htm

Mark D. E. Herschbach, (unpublished, 2005).

Mark H. Minkowski, *Mathematisch-Physikalische Klasse*, vol. 1, 53 (1908).

Mark H. A. Lorentz Koninklijke Akademie vanWetenschappen te Amsterdam. Section of Science. Proc. 6: 809-831 (1904).

Mark Albert Einstein *"Zur Elektrodynamik bewegter Korper."* Annalen der Physik 18,639 (1905); Annalen der Physik 17,891 (1905). (Translation: Perrett and Jeffery, *The Principle of Relativity*, (Methuen, London 1923), (Dover, 1952).

Mark Max Planck "*Zur Theorie des Gesetzes der Energieverteilung im Normal-spectrum.*" Deutsche Physikalische Gesellschaft. Verhandlungen 2: 237-245 (1900).

Mark Louis de Broglie, Nature 112, 540 (1923); Annalen der Physik (10) 2 (1923).

Mark P. A. M. Dirac, "Forms of Relativistic Dynamics" *Rev. Mod. Physics*, 21: 392 (1949).

Mark Albert Einstein "*Uber einen die Erzeugung und Verwandlung des Lichtes betreffenden heuristischen Gesichtspunkt.*" Annalen der Physik 17: 132-148 (1905). (Translation by A.B. Aarons and M.B. Peppard, Am. J. Phys. 33, 367(1965).)

Mark E. Schrodinger, Annalen der Physik (4) 79 361 and 489 (1923); 80, 437 (1926); 81,109 (1926).

Mark Schrodinger's protests about prevailing quantum mechanical interpretations are widely circulated. So far we have been unable to locate more solid references.

Mark N. Bohr, *Zeitschrift fur Physik*, 9, 1-2, (1922).

Mark W. Heisenberg, *The Physical Principles of the Quantum Theory*, (Dover, New York, 1930).

Mark P.A.M. Dirac, *Lectures on quantum mechanics*, (New York, Belfer Graduate School of Science, Yeshiva University, 1964). Dirac's first text in 1931 used α and β to denote bra-ket duality.

Mark A. Einstein, *"I shall never believe that god plays dice with the universe"* Albert Einstein Archives, The Jewish National & University Library, The Hebrew University of Jerusalem (www.albert-einstein.org), Einstein Archives Online, Volume 15, #294, Letter to Cornelius Lanczos, March 21, 1942,http://www.alberteinstein.info/db/ViewDetails.do?DocumentID=30893.

Mark R. Feynman, *The Pleasure of Finding Things Out*, (Perseus Publishing, Cambridge, MA,1999) p. 8.

Mark (unpublished) A huge energy shift is used for sake of geometric clarity. Atoms usually lose less than one part in 10^9 or 10^{10} of their rest mass in optical emission. The atom in the example loses rest mass $1/2\ M_2c^2$ emitting a $3/8\ M_2c^2$ photon.

Mark R. P. Feynman, R. Leighton, and M. Sands, *The Feynman Lectures* (Addison Wesley 1964) Our development owes a lot to Feynman's treatment cavity wave dispersion in Vol. II Ch. 24 and Vol. III Ch. 7.

Mark W. Rindler, *Essential Relativity-Special, General, and Cosmological*, Springer (New York 1977) p. 18. See also ref. 8, p. 111.

Mark E.F.Taylor and J.A. Wheeler, *Spacetime Physics* (W. H. Freeman San Francisco 1966) p. 18.

Acknowledgements

[i] A. Einstein, Annalen der Physik 17,891(1905). (Translation by W. Perrett and G.B. Jeffery, *The Principle of Relativity*(with notes by A. Sommerfield) (Methuen, London 1923), (republished by Dover, London 1952).

[ii] W. G. Harter, J. Mol. Spectrosc. 210, 166(2001).

[iii] W. G. Harter, J. Evans, R. Vega, and S. Wilson, Am. J. Phys. 53, 671(1985).

[iv] W.G. Harter and T. C. Reimer, //www.uark.edu/ua/pirelli/html/poincare_inv_2.htm

[v] D. E. Herschbach, (unpublished, 2005).

[vi] H. Minkowski, *Mathematisch-Physikalische Klasse*, vol. 1, 53 (1908).

[vii] H. A. Lorentz Koninklijke Akademie vanWetenschappen te Amsterdam. Section of Science. Proc. 6: 809-831 (1904).

[viii] Albert Einstein *"Zur Elektrodynamik bewegter Korper."* Annalen der Physik 18,639 (1905); Annalen der Physik 17,891 (1905). (Translation: Perrett and Jeffery, *The Principle of Relativity*, (Methuen, London 1923), (Dover, 1952).

[ix] Max Planck "*Zur Theorie des Gesetzes der Energieverteilung im Normal-spectrum.*" Deutsche Physikalische Gesellschaft. Verhandlungen 2: 237-245 (1900).

[x] Louis de Broglie, Nature 112, 540 (1923); Annalen der Physik (10) 2 (1923).

[xi] P. A. M. Dirac, "Forms of Relativistic Dynamics" *Rev. Mod. Physics*, 21: 392 (1949).

[xii] Albert Einstein "*Uber einen die Erzeugung und Verwandlung des Lichtes betreffenden heuristischen Gesichtspunkt.*" Annalen der Physik 17: 132-148 (1905). (Translation by A.B. Aarons and M.B. Peppard, Am. J. Phys. 33, 367(1965).)

[xiii] E. Schrodinger, Annalen der Physik (4) 79 361 and 489 (1923); 80, 437 (1926); 81,109 (1926).

[xiv] Schrodinger's protests about prevailing quantum mechanical interpretations are widely circulated. So far we have been unable to locate more solid references.

[xv] L. C. Epstein, *Relativity Visualized*. (Insight Press 1981)

[xvi] N. Bohr, *Zeitschrift fur Physik*, 9, 1-2, (1922).

[xvii] W. Heisenberg, *The Physical Principles of the Quantum Theory*, (Dover, New York, 1930).

[xviii] P.A.M. Dirac, *Lectures on quantum mechanics*, (New York, Belfer Graduate School of Science, Yeshiva University, 1964). Dirac's first text in 1931 used α and β to denote bra-ket duality.

[xix] A. Einstein, *"I shall never believe that god plays dice with the universe"* Albert Einstein Archives, The Jewish National & University Library, The Hebrew University of Jerusalem (www.albert-einstein.org), Einstein Archives Online, Volume 15, #294, Letter to Cornelius Lanczos, March 21, 1942,http://www.alberteinstein.info/db/ViewDetails.do?DocumentID=30893.

[xx] R. Feynman, *The Pleasure of Finding Things Out*, (Perseus Publishing, Cambridge, MA,1999) p. 8.

[xxi] (unpublished) A huge energy shift is used for sake of geometric clarity. Atoms usually lose less than one part in 10^9 or 10^{10} of their rest mass in optical emission. The atom in the example loses rest mass $1/2 \ M_2 c^2$ emitting a $3/8 \ M_2 c^2$ photon.

[xxii] R. P. Feynman, R. Leighton, and M. Sands, *The Feynman Lectures* (Addison Wesley 1964) Our development owes a lot to Feynman's treatment cavity wave dispersion in Vol. II Ch. 24 and Vol. III Ch. 7.

[xxiii] W. Rindler, *Essential Relativity-Special, General, and Cosmological*, Springer (New York 1977) p. 18. See also ref. 8, p. 111.

xxiv E.F.Taylor and J.A. Wheeler, *Spacetime Physics* (W. H. Freeman San Francisco 1966) p. 18.

Acknowledgements

Figure Captions

Fig. 1. Comparison of wave archetypes and related axioms of relativity.

   (a) Pulse Wave (PW) peaks locate where a wave is. Their speed is c for all observers.

   (b) Continuous Wave (CW) zeros locate where it is not. Their speed is c for all colors (or observers.)

Fig. 2. Pulse Wave (PW) as a sum of 12 Fourier CW's (a) PW parts: real ReΨ, imaginary ImΨ, and magnitude |Ψ|.

   (b) CW phasor clocks plot real vs. imaginary parts of wave amplitudeΨ .

Fig. 3. Wave addition of counter propagating Fourier components.

   (a) 2-PW Sum has binary sum has 4 values (0,0), (0,1), (1,0), (1,1) and diamond grid of peak paths on a plane of zeros.

   (b) 2-CW Sum and interference has value continuum and square grid of zeros.

Fig. 4. "Ficticious" sources and their wave coordinate lattices in (a) Spacetime and (b) Per-spacetime.

   CW lattices of phase-zero and group-node paths intermesh with PW lattices of "particle" or pulse wave paths.

Fig. 5. Co-propagating laser beams produce a collapsed wave lattice since all parts have same speed c.

Fig. 6. Laser lab view of 600Thz CW and PW light waves in per-space-time (a-b) and space-time (c-d).

Fig.7. Atom view of 600Thz CW and PW light waves in per-spacetime (a-b) and space-time (c-d) boosted to u=3c/5.

Fig. 8. Wave phasor addition. (a) Each phasor in a wave array is a sum (b) of two component phasors.

   (c) In phasor-relative views either A or else B is fixed. An evolving sum-and-difference rectangle is

   inscribed in the (dashed) circle of the phasor moving relative to the fixed one.

Fig. 9. Doppler shift b-matrix for a linear array of variously moving receiver-sources.

Fig. 10. (a) Euclidian mean geometry for counter-moving waves of frequency 1 and 4. (300THz units).

Fig. 10. (b) Geometry for the CW wave coordinate axes in Fig. 7.

Fig. 11. (a) Horizontal G-hyperbolas for proper frequency B=ν and 2B and vertical P-hyperbolas for proper wavevector k.

   (b) Tangents for G-curves are loci for P-curves, and vice-versa.

Fig. 12. Dispersion hyperbolas for 2-CW interference (a) Laser lab view. (b)Atom frame view.

Fig. 13. Geometry of contact transformation between relativistic (a) Hamiltonian (b) Lagrangian.

Fig. 14. "True" paths carry extreme phase and fastest phase clocks. Light-cone has only stopped clocks.

Fig. 15. Quantum waves interfere constructively on "True" path but mostly cancel elsewhere.

Fig. 16. Trigonometric geometry (a) Unit circular area ϕ=0.86. (b) Unit hyperbolic area ρ=0.99.

Fig. 17. Relativistic wave mechanics geometry. (a) Overview. (b) Details of contact transform tangents.

Fig. 18. Monochromatic (1-frequency) 2-CW wave space-time patterns.

Fig. 19. Dichromatic (2-frequency) 2-CW wave space-time patterns.

Fig. 20. (a-g) Elliptic polarization ellipses relate to galloping waves in Fig. 18. (h-i) Kepler anomalies.

Fig. 21. Cavity 2-CW modes. (a) Invariant "mass" hyperbolas. (b) COM frame. (c) ISOC frame.

Fig. 22. Optical cavity energy hyperbolas for mode number n=1-3 and photon number Nn=0, 1, 2,....

Fig. 23. Simulated spacetime photon counts for coherent (a-c) and photon-number states (d).

Fig. 24. Optical cavity model of (a) Emission, (b) Absorption, and (c) Compton scattering

Fig. 25. Compton scattering. (a) Vector sums on mass hyperbolas of low ω_ℓ , medium ω_m , and high ω_h.

   (b-c) Feynman graphs. (d) Center of Momentum (COM) vector sums. (e-f) COM Feynman graphs.

Fig. 26. Compton nets are congruent Compton staircases of transitions. (a) f=2:1 (b) f=√2 :1.